Synthesis and Properties of Donor-Acceptor Conjugated Macromolecules as N-Type Semiconductor for Organic Solar Cells

Abimbola Ololade Aleshinloye

Submitted to the
Institute of Graduate Studies and Research
in partial fulfillment of the requirements for the Degree of

Doctor of Philosophy
in
Chemistry

Eastern Mediterranean University
January 2015
Gazimağusa, North Cyprus

Approval of the Institute of Graduate Studies and Research

Prof. Dr. Serhan Çiftçioğlu
Director

I certify that this thesis satisfies the requirements as a thesis for the degree of Doctor of Philosophy in Chemistry.

Prof. Dr. Mustafa Halilsoy
Chair, Department of Chemistry

We certify that we have read this thesis and that in our opinion it is fully adequate in scope and quality as a thesis for the degree of Doctor of Philosophy in Chemistry.

Prof. Dr. Huriye İcil
Supervisor

Examining Committee

1. Prof. Dr. Huriye Icil
2. Prof. Dr. Okan Sirkecioğlu
3. Prof. Dr. Nurseli Uyanık
4. Asst. Prof. Dr. Nur Paşaoğullari Aydinlik
5. Asst. Prof. Dr. Hatice Nilay Hasipoğlu

ABSTRACT

The fabrication of novel molecular dyes with suitable absorptive properties for photon harvesting is an essential area to search on for efficient photovoltaic cells. Perylene diimides show vibronic absorption band at the middle of visible region of solar irradiation. Introduction of substituents onto the perylene bay region usually perturbs the orbital energy of the perylene π-π intermolecular system which eventually leads to shifting of the absorption maximum to longer wavelength. In this thesis, the electrochemical properties of chiral multichromophoric macromolecule (NPM) and its components were well studied. NPM exhibited low band gap energies of 2.25 V and 1.7 V in solution and solid-state, respectively. Also, three novel macromolecular bay-substituted perylene diimides have been synthesized successfully and photophsically characterized namely, *N*,*N'*-Di(dodecyl)-1,7-diphenoxylperylene-3,4,9,10-tetracarboxy diimide (BP-PDD), *N*,*N'*-Di(5-amino-3-pyrimidinethiol)-1,7-diphenoxyperylene-3,4,9,10-tetracarboxy diimide (BP-PPD) and *N*,*N'*-Di(2,2,4(2,4,4)-trimethyl-6-aminohexyl))-1,7-di(1-amino-4-ethanolpiperidyl)perylene-3,4,9,10-diimide (TPE-PDI). All the synthesized compounds possess appreciable longer wavelength comparing them with their parent perylene diimides with good solubility in several organic solvents. These compounds were characterized in detail by several techniques such as NMR, FT-IR, Elemental analysis; UV-visible, Fluorescence, TGA thermogram, DSC and the results were analyzed. These results showed an asset for construction of photovoltaic devices such as organic solar cells.

Keywords: Perylene, bay-substitution, absorptivity, macromolecule, solar cell

OZ

Verimli fotovoltaik hücre araştırmaları için uygun absorblama özelliklerine sahip foton toplayabilen yeni moleküler boyaların imalatı önemli bir araştırma alandır. Perylen diimidler güneş enerjisi görünür bölgenin ortasında titreşimsel absorpsiyon bandı göstermektedir. Perilen körfez bölgesi üzerine takılan sübstituentler genellikle perilen π-π molekküller arası sistemin orbital enerjisini bozmakta ve sonuç olarak absorpsiyonunun daha uzun dalga boyuna kaymasına neden olmaktadır. Bu tezde, kiral çok kromoforlu makromolekül (NPM) ve onun bileşenlerinin elektrokimyasal özellikleri iyice incelenmiştir. NPM, solüsyon ve katı halde, sırasıyla 2.25 V ve 1.7 V'luk düşük bant aralığı enerjisi sergilemektedir. Aynı zamanda, üç yeni makromoleküler körfez-sübstitüe perilen diimidler başarıyla sentezlenmiştir ve fotofiziksel olarak karakterize edilmiştir, *N*,*N'*-Di(dodesil)-1,7-difenoksiperilen-3,4,9,10-tetrakarboksidiimid (BP-PDD), *N*,*N'*-Di(5-amino-3-pirimidintiol)-1,7-difenoksiperilen-3,4,9,10-tetrakarboksidi- imid (BP-PPD) and *N*,*N'*-Di(2,2,4(2,4,4)-trimetil-6-aminohekzil))-1,7-di(1-amino-4-etanolpiperidil)perilen-3,4,9,10-diimid (TPE-PDI). Sentezlenen tüm bileşikler, ana perilen diimidlerle karşılaştırıldıklarında hatırı sayılır uzun dalga boyuna ve çeşitli organik çözücüler içinde iyi çözünürlüğe sahiptirler. Bu bileşikler, NMR, FT-IR, Elemental analiz, UV-görünür, Floresans, TGA termogramı, DSC teknikleri ile ayrıntılı bir şekilde karakterize edilmiştir. Bu sonuçlar, organik güneş pilleri gibi fotovoltaik cihazların yapımı için bir varlık göstermiştir.

Anahtar Kelimeler: Perilen, körfez-sübstitüsyon, absorptivite, makromolekül, güneş pili

DEDICATION

To

ALMIGTHY JEHOVAH

&

Damilare Aleshinloye

ACKNOWLEGMENT

"It is not in the pursuit of happiness that we find fulfillment, it is in the happiness of pursuit". **-Denis Waitley**

I give thanks to **GOD ALMIGHTY** for his grace and his mercies given to me.

I would like to say a big thank you to my advisor **Prof. Dr. HURİYE İCİL** for letting me pursue my PHD degree under her supervision and the privilege to work on this research area which is a major concern for humanity pertaining to energy. This thesis would not have been the way it is without the appreciated guidance, professional instructions and productive criticism from her.

To all the organic group members and students, I say a big thank you to you all for your moral support, friendliness and encouragement I received from you during the course of study.

My family, you mean the whole world to me. Kayode my darling husband, I cannot express my great appreciation enough but I will just say thank you my love. Daniella, Chelsea and my expecting baby, thank you for going through all the way with me. I love you all. To my mom, thank you for being a mother indeed because are the best. My siblings keep doing the good works. My mother-law, you are a certainly sweet mother. To friends and loved ones, I say thank you for all your prayers and support.

TABLE OF CONTENTS

LIST OF TABLES

LIST OF FIGURES

LIST OF ILLUSTRATIONS

LIST OF SYMBOLS/ABBREVIATIONS

Å	Armstrong
A	Absorption
A	Electron Acceptor
Anal.	Analytical
AU	Arbitrary unit
Avg.	Average
BP-PDD	*N*,*N'*-Di(dodecyl)-1,7-diphenoxylperylene-3,4,9,10-tetracarboxy diimide
BP-PPD	*N*,*N'*-bis-(5-amino-3-pyrimidinethiol)-1,7-diphenoxyperylene-3,4,9,10-tetracarboxy bisimide
c	Concentration
calcd.	Calculated
^{13}C NMR	Carbon-13 nuclear magnetic resonance spectroscopy
cm	Centimeter
$CDCl_3$	Deutero-Chloroform
$CHCl_3$	Chloroform
CV	Cyclic Voltammetry
^{o}C	Degree Celsius
δ	Chemical shift (ppm)
D	Diffusion Constant
D	Electron donor
DC	Dielectric constant
DCM	Dichloromethane

DMF	N,N’-dimethylformamide
DMSO	Dimethyl sulfoxide
DSC	Differential scanning calorimetry
DSSC	Dye sensitized solar cell
ε	Extinction coefficient
ε_{max}	Maximum extinction coefficient/Molar absorptivity
eV	Electron volt
$E_{1/2}$	Half-wave potential
E_g	Band gap energy
E_{ox}	Oxidation potential
E_p	Separation of peak potentials
E_{pa}	Anodic peak potential
E_{pc}	Cathodic peak potential
E_{red}	Reduction potential
E_s	Singlet state
f	Oscillator strength
F_c	Ferrocene
Fig.	Figure
FRET	Fluorescence resonance energy transfer
FT-IR	Fourier transform infrared spectroscopy
h	Hour
hν	Irradiation
Hz	Hertz
^{1}H NMR	Proton nuclear magnetic resonance spectroscopy
HOMO	Highest occupied molecular orbital

i_p	Peak current
i_{pa}	Anodic peak current
i_{pc}	Cathodic peak current
IR	Infrared spectrum/spectroscopy
ITO	Indium tin oxide
J	Coupling constant
kcal	Kilocalorie
kd	Rate constant of radiationless deactivation
k_f	Fluorescence rate constant
l	Path length
KBr	Potassium bromide
KOH	Potassium hydroxide
LED	Light emitting diode
LUMO	Lowest unoccupied molecular orbital
M	Molar concentration
M^+	Molecular ion peak
M_w	Weight average molecular weight
MHz	Megahertz
min	Minimum
mmol	Millimole
mol	Mole
MS	Mass spectrometry
n	Refractive index
n	Number of electrons (in the reduction process)
NDA	1,4,5,8-naphthalenetetracarboxylic dianhydride

NMI	N-(1-dehydroabietyl)-1,4,5,8-naphthalenetetracarboxylic-1,8-anhydride-4,5-imide
NMP	*N*-methylpyrrolidinone
NMR	Nuclear magnetic resonance spectroscopy
nm	nanometer
$NaBF_4$	Sodium tetrafluoroborate
NPM	N,N'-bis-{N-(3-[4-(3-amino-propyl)-piperazin-1-yl]-propyl)-N'-[1-dehdroabiety]-1,4,5,8-naphthalenetetracarboxydiimidly}-3,4,9,10-perylenebis(dicarboximide)
ns	nanosecond
Φ_f	Fluorescence quantum yield
PDA	Perlyene 3,4,9,10-tetracarboxylic dianhydride
PDI	Perlylene diimide
PET	Photoinduced electron transfer
ppm	Parts per million
PV	Photovoltaic
RT	Room temperature
SC	Solar cell
Std.	Standard
SWV	Square Wave Voltammetry
τ_o	Theoretical radiative lifetime
τ_f	Fluorescence lifetime
t	Time
$TBAPF_6$	Tetrabutylammoniumhexafluorophosphate
TGA	Thermogravimetric analysis

TPE-PDI	*N*,*N'*-bis-(2,2,4(2,4,4)-trimethyl-6-aminohexyl))-1,7-di(1-amino-4-ethanolpiperidyl)perylene-3,4,9,10-bisimide
u	Unknown
μ	Micro
UV	Ultraviolet
UV-vis	Ultraviolet visible light absorption
ν	Scan rate
ν	wavenumber
$\Delta\nu_{1/2}$	Half-width of the selected absorption
V	Volt
vs.	Versus
λ	Wavelength
λ_{exc}	Excitation wavelength
λ_{em}	Emission wavelength
λ_{max}	Maximum wavelength

Chapter 1

INTRODUCTION

1.1 Solar Cell Energy

Energy has become an important commodity in this our present world and even beyond our generation. As we know that energy remains constant, the challenge of energy is not its amount in existence but rather its quality. Therefore, we need to look for ways which are environmentally and economically friendly to convert the energy accessible on earth to forms beneficial to humankind. Fossil fuel which is currently the world's energy consumption, couple with the fact that it's finishing up it also causes a huge amount of pollution to the atmosphere. Unlimited source of energy we know of is that of sunlight which is from nature and could be converted to electricity. So photovoltaic technologies with the aid of sunlight as energy source, could be used in the manufacture of photovoltaic cells in medium and large scale production. This kind of solar cells are fabricated with ease and at low cost.

The firstborn of solar cell technology and obviously the known one is the crystalline silicon solar cells which are still in the market of today. Also the second-born of solar cells are the amorphous silicon (p-n heterojunctions) mostly used in calculators and many small electronic devices. Also nonsilicon-types such as cadmium telluride (CdTe), copper sulfide, gallium arsenide and copper indium gallium diselenide (CIGS) with more or less energy efficiencies of 20%. A good benefit of these thin layers of silicon is that the panels can be made malleable. These photovoltaics give

problems in their production, involves too much of energy to produce, harmful to health and also at a high cost but not so much as the crystalline silicon [1-2]. The third-born of solar cell are of different materials different from silicon and does not have problems related to that of silicon. Such kinds of solar cell are developed from organic dyes and are generally referred to as organic photovoltaics (PV cells). This dye-sensitized solar-cell (DSSC) widely known as Grätzel cell are very interesting to work with because of cheap manufacturing cost, structural modification, great εmax values for various devices, light-weight and malleable, also with different kind of charge separation mechanism [2-5].

The competences of PV cells made from organic materials are nevertheless still behind those from inorganic based photovoltaics. The formation of heterojunction with organic based PV devices by using a donor-acceptor (D-A) kind of organic compounds (materials) helps to detach the exciton into two different haulers. The haulers created are conveyed to the electrodes by these compounds which created the exciton. Thus, proves that organic compounds (materials) intended for PV products should own some notable light gathering and carriers transport characteristics nonetheless this is a difficult task to accomplish. In dye-sensitized solar cells (DSSCs), the charge creation is performed at the semiconductor-dye boundary and the movement of the charge is achieved via the semiconductor and the electrolyte. Modification of dye could lead to spectral property efficiencies and by improving the semiconductor and the electrolyte structure carriers transport properties can also be enhanced [1].

1.2 N-Type Semiconductors

Arylene diimides have shown to be a peculiar interesting type of organic n-type semiconductors because of their high electron affinities, huge εmax, brilliant self-organization potentials and creditable stability in their photochemical and thermal properties. Research has confirmed that various p-type organic semiconductors possess huge charge mobility in comparison with that of amorphous silicon. This made a great pathway for the study on n-type organic compounds (materials) due to their exceptional moderately less charge mobility and air stabilization [6-8].

Perylene diimides are appreciated n-type semiconducting compounds and they exhibit their usefulness in light emitting diode, OFET, photovoltaic etc. productions. Their extraordinary photophysical characteristics, thermal strength, ability of self-restructuring, electron acceptors and fast electron transporting properties have proved them to be so. Through modification of their structures with appropriate substituents which could be at the imide positions and /or at the bay sites, improves the effectiveness of their performance. To name one is their broadening of the absorption wavelength to the red-shift region which is very significant feature for solar cell production [7, 9-10]. Substitution using chiral compounds at the imides or the bay positions also makes them to be useful for active optical devices. Chirality could be shifted from low molecular weight to polymeric or supramolecular compounds that mostly display distinct optical properties and larger optical activity [11-12].

1.3 Bay-substituted Perylene Compounds

To what degree does substitution in the aromatic bay positions 1, 6, 7, and 12 (bay region) influence the π-electron delocalization in perylene compounds? It mainly affects both the photophysical and redox properties of such compounds. The

modification of the conjugated-system gives a significant influence on the intermolecular π-π assembling energy in solution as well as in solid state of these compounds [13-14]. Substitutions at bay positions enlarge the perylene core which is generally achieved beginning from the halogenated derivatives of these compounds mostly brominated ones.

Generally, this bromination method gives a mixture of di-, tri-, and tetra-brominated perylene compounds. The di-bromoperylene compounds contain 1,7 which is the main and 1,6 is the less regioisomers. The pureness of the 1,7 regioisomer has been achieved by repeated recrystallization or by column chromatography which has been reported in literature. 1,7-dibrominated perylene compounds are widely used as starting materials for the syntheses of extensive variety of perylene bisimides/dimides derivatives among its regioisomers. This is due to enhanced bathochromic shifts of the absorption and emission maxima also the high yield of the compounds with excellent electronic properties [15-21].

1.4 Supramolecules/Macromolecules

The development of novel materials with better-quality properties have been achieved by making use of supramolecular method (means) together with π-conjugated compounds making this one of the important approaches in the manufacturing of organic optoelectronic devices such as organic PV cells etc. as mentioned above [22-23]. In a supramolecular structure, intermolecular forces hold the components reversibly. Hydrogen bonding, van der Waals molecular interaction and electrostatic interaction are included in the molecular forces. Furthermore, supramolecule is mainly associated with units of greater complexity than the

individual molecules. Supramolecules are organizations apprehended together by intermolecular binding interactions. [24].

The supramolecular organization process involves molecular self- assemble by which individual molecules form definite aggregate and these aggregates produce greater-ordered compounds.

In a supramolecular-structure, the noncovalently bond assemblage possess characteristics which differ totally from their substituted monomers. This makes the joint characteristics prevailing with novel functions [25]. Good examples of self-assembly supramolecule are those of perylene diimide dyes.

1.4.1 Supramolecular Perylene Dyes

The fabrication of supramolecular systems centered on a particular intermolecular interaction makes it possible to generate active sites with several optical properties such as spectral region of absorption with different shapes, fluorescence spectra, intensities of electron transitions and much more. By these, supramolecules are synthesized based on the functionalities of the system for the manufacture of several supramolecular electronics and photonics. Perylene diimide dyes are functional supramolecular materials in relation to their brilliant photo/electronic properties which make them worthy compounds for supramolecular scheme of numerous devices [26- 28].

The architecture and fabrication of Donor-Acceptor (D-A) components with appropriate structural features has been acknowledged as a positive approach via the charge-transfer means between donor and acceptor materials for the synthesis of supramolecular systems [22]. Many works have been done and reported showing the significance of perylene supramolecules with brilliant applications [29, 30-31].

The investigation of a novel multichromophoric compound and bay substituted n-type semiconductors has directed this research on the electrochemical properties of a perylene based multichromophoric compound with distinctive and exceptional features for photovoltaic application followed by the syntheses and characterizations of three different bay-substituted perylene compounds. These compounds were fully analyzed using FTIR, UV-visible and fluorescence spectroscopy, thermal anaylses and electrochemical measurement.

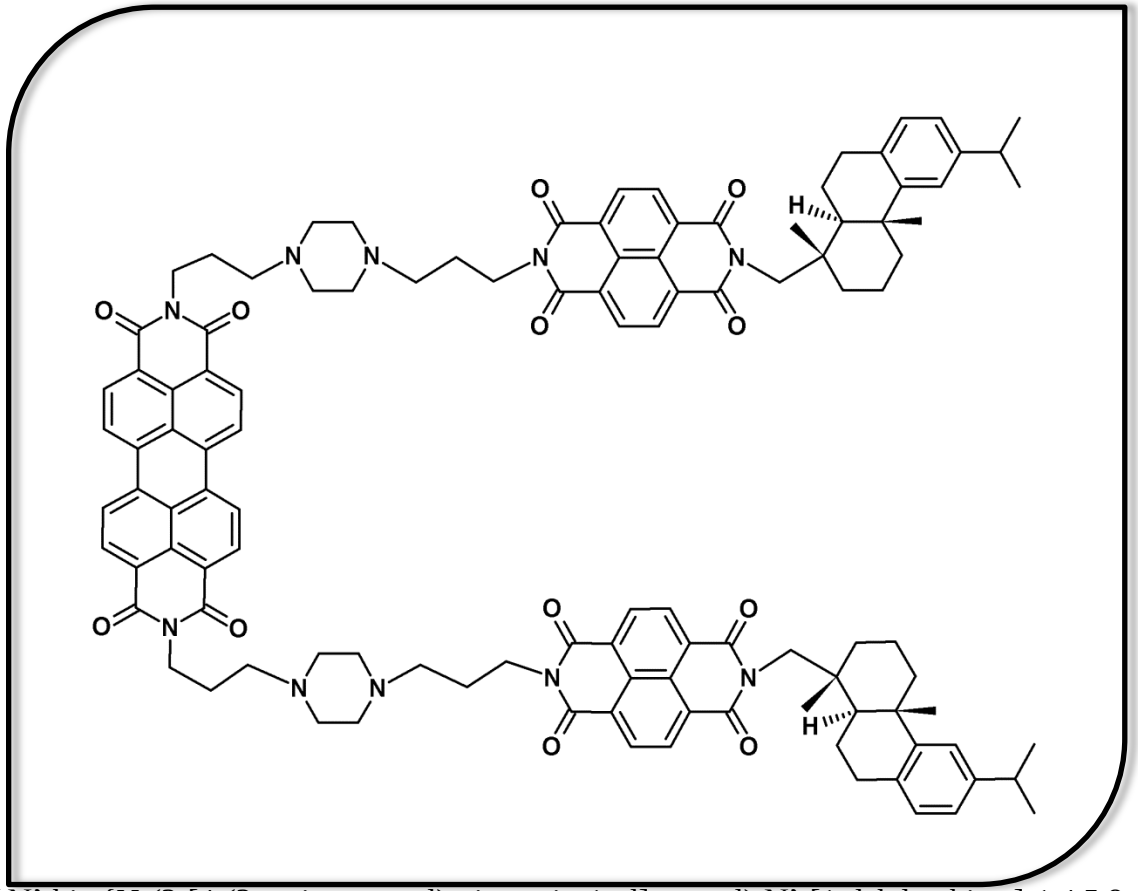

Figure 1.1: N,N’-bis-{N-(3-[4-(3-amino-propyl)-piperazin-1-yl]-propyl)-N’-[1-dehdroabiety]-1,4,5,8-naphthalenetetracarboxydiimidly}-3,4,9,10-perylenebis(dicarboximide) (NPM)

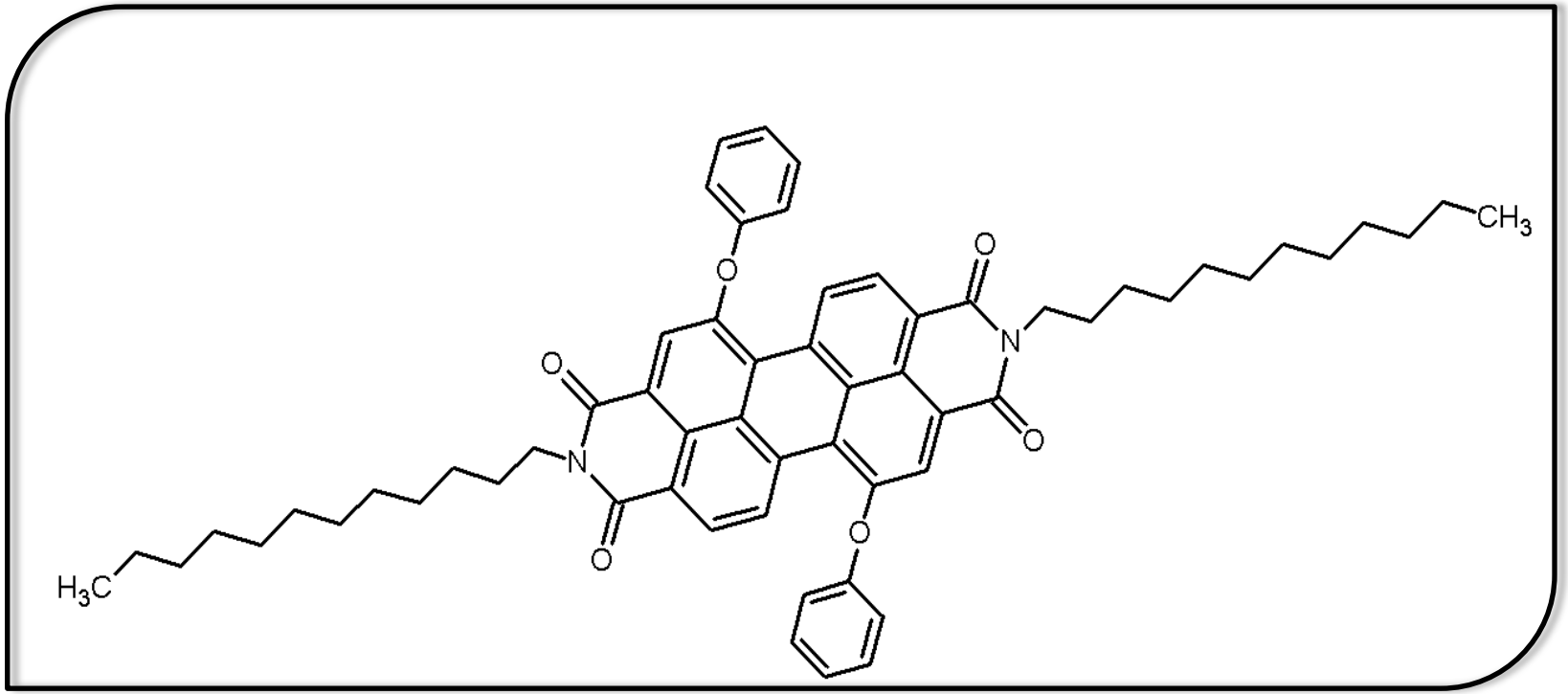

Figure 1.2: N'-Di(dodecyl)-1,7-diphenoxylperylene-3,4,9,10-tetracarboxy diimide (BP-PDD)

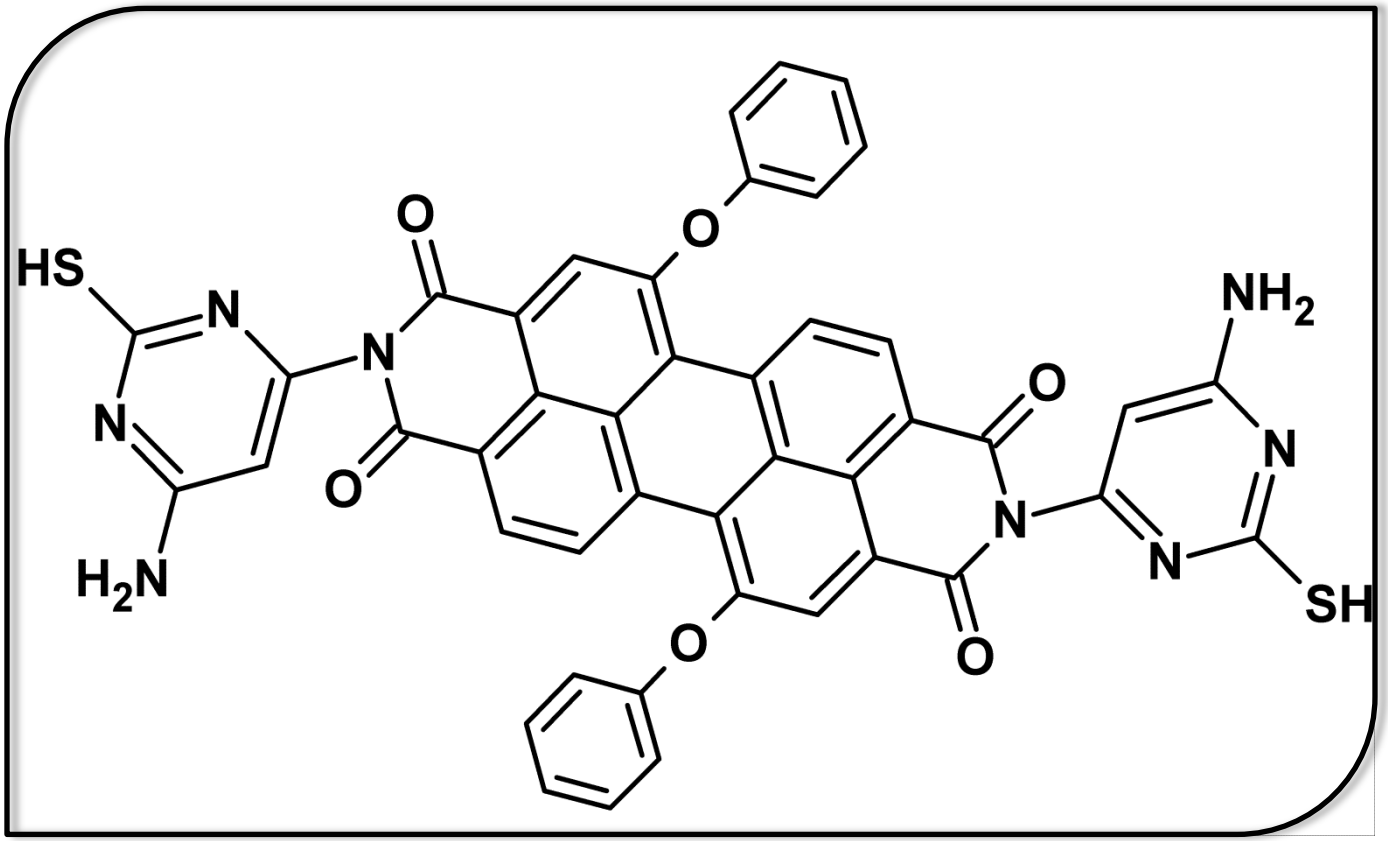

Figure 1.3: : N,N'-Di(5-amino-3-pyrimidinethiol)-1,7-diphenoxyperylene-3,4,9,10-tetracarboxy diimide (BP-PPD)

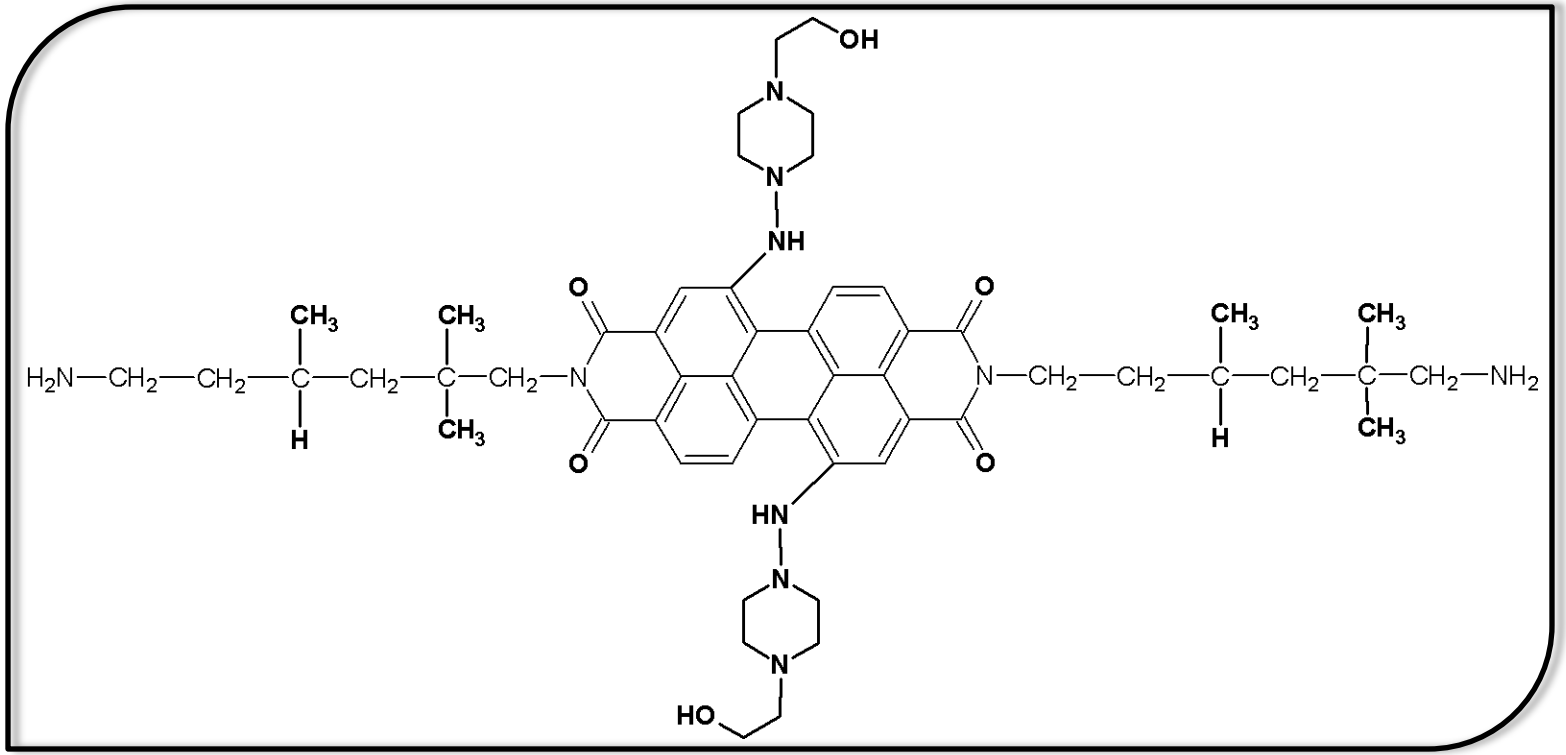

Figure 1.4: N,N'-Di(2,2,4(2,4,4)-trimethyl-6-aminohexyl))-1,7-di(1-amino-4-ethanolpiperidyl)perylene-3,4,9,10-diimide (TPE-PDI)

Chapter 2

THEORETICAL

2.1 Photovoltaic Cells

Various types of energy are available at present and in use. We have fossil fuel which is the most predominant amongst them all, hydroelectric power, wind power etc. Fossil fuel has we've all known that its diminishing that is coming to an end coupled with its environmental pollution problem has been a major concern to the whole scientist world. We therefore need a renewable energy source which is cheap and environmental friendly to replace it. Solar energy has been proved to have renewable energy source which is the sunlight and many research works are still going to make this energy available on a large scale with urge capacity for commercial use. Shown below is a typical example of a typical solar cell (Figure 2.1).

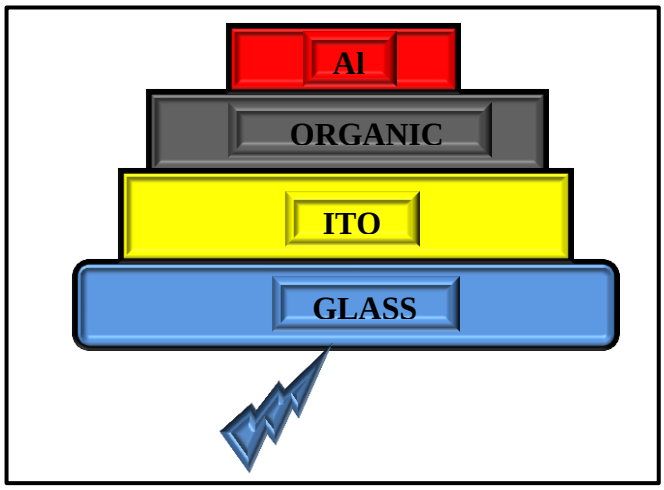

Figure 2.1: A Typical Photovoltaic cell

The firstborn and second-born of photovoltaics (Figure 2.2) are constructed on single junction devices. The thermodynamics calculation competence limits (Shockley) in single junction solar cells implies that absorbing a single photon gives the development of a single electron-hole pair also the total photon energy in surplus of the energy gap is evolved exothermically. The third-born of solar cell devices can overcome this limit. Examples of these types of such solar cells are DSSCs, molecular organic solar cells and many more. The main objective for the third-born solar cells is mainly for the production of electric power on a massive scale with cheap price. This will make the photovoltaic cells to be the lowest cost alternative for next generation in terms of energy.

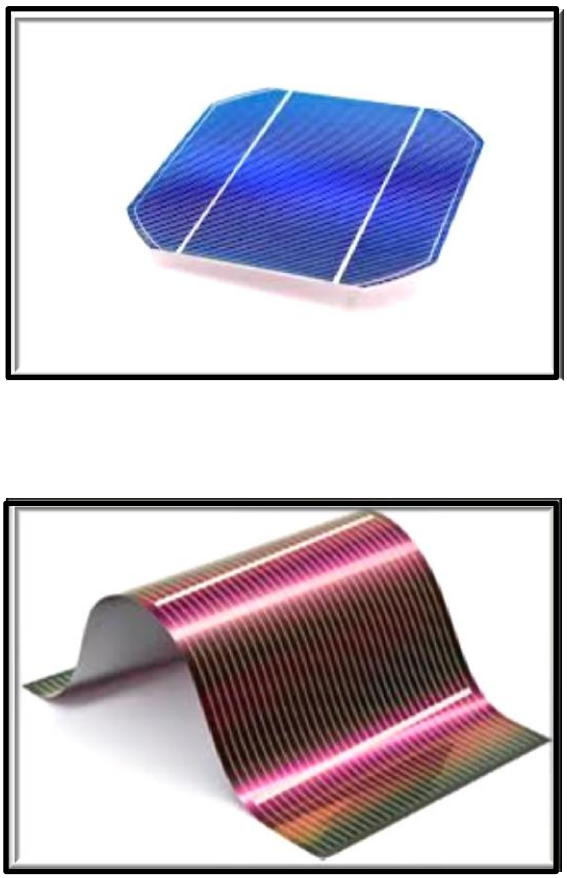

Figure 2.2: Images of the Firstborn and Second-born
of Photovoltaic Cells Respectively

2.2 Fabrication of Orthodox Photovoltaic Cells

Semiconductors for photovoltaic devices have been researched on rigorously. Crystalline silicon was primarily worked upon. The general technique for making silicon cells is through single-crystal cylinder technique whereby a single-crystal silicon seed crystal is touched to a smelted silicon melt and thereafter withdrawn to make available an elevated meniscus of smelted silicon with both the seed crystal and the container holding the melt rotated oppositely to improve radial growth. For making the cell to be an n-type or a p-type semiconductor, appropriate doping is required meaning silicon is doped with another material and upon slicing into a wafer of approximately hundred microns, hereby establishment of a junction will create a solar cell or photovoltaic device.

Different architectural structures have been achieved for different flux efficiency of photon to electric charge conversion. These are Single-layer, Bi-layer and bulk heterojunction layer solar cells

2.2.1 Single-Layer Cells

These single-layer cells (Figure 2.3) are the easiest photovoltaic cells fabricated. They are based on mono organic layer fitted into two metal electrodes of dissimilar work functions. An amendable characteristics of single-layer devices was accredited to the irregularity in the electron and hole injection into the molecular pie* and pie orbitals and to the development of a Schottky-type between the *p*-type (hole conducting) organic layer and the metal with the lesser work function. The power conversion productivities were recorded low approximately 10^{-2} %.

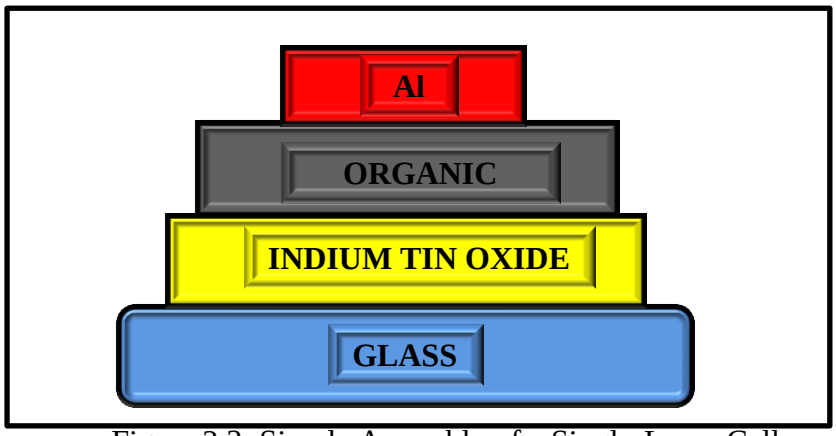

Figure 2.3: Simple Assembly of a Single-Layer Cell

2.2.2 Bi- Layer (D-A) Cells

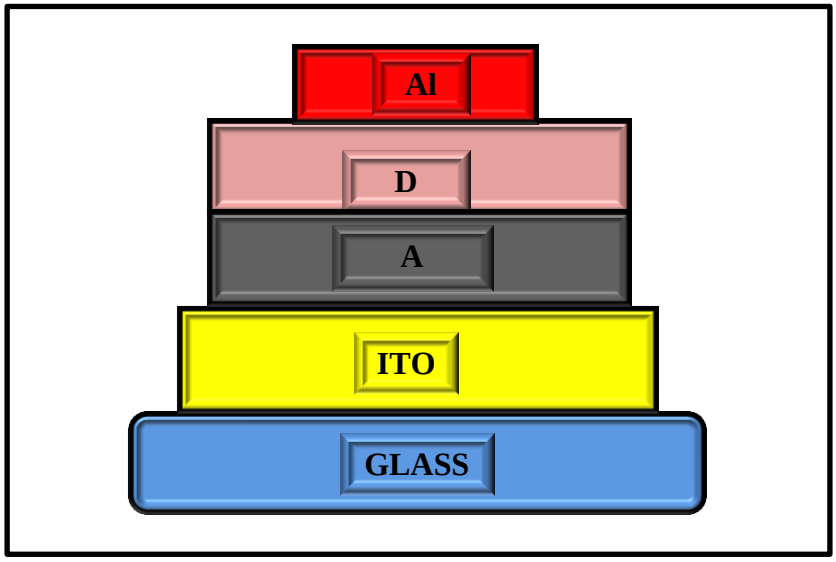

Figure 2.4: Simple Assembly of a Bi-Layer Cell

The introduction of bi-layer model (Figure 2.4) was the next step-forward in the fabrication of photovoltaic cells where by two organic layers with definite electron or hole transporting functionalities were fitted together between the electrodes. The heterojunction occurs when electron donor (D) and electron acceptor (A) contact one another. When a photon is taken in, an optical excitation (exciton) occurs which is a

coulombically bound electron-hole pair, and it distributes to the D/A interface and excitons are dispersed into open holes and electrons via the electrical field at this point. These excitons exhibit little diffusion length characteristics which make them to only absorb light at a very thin region around interfacial region which influences photovoltaic effect, thereby minimizes the effectiveness of bi-layer cells. Approximately 1% power conversion effectiveness for two organic compounds (a phtalocyanine compound as *p*-type (hole conducting) semiconductor and a perylene compound as *n*-type (electron conducting) semiconductor) fitted in-between a see-through conducting oxide and a translucent metal electrode was reported [19,32]. The organic dye (polymer) was thought of as a way to boost the lengthening of excitons diffusion length thus condensing the photoactive interfacial region.

2.2.3 Bulk Heterojunction Layer Cells

The notion of mixing (blend) p-type together with n-type semiconductors is identified as bulk heterojunction layer (Figure 2.5). This layer is related to the bi-layer device in reverence to the D-A model, however it displays an enlarged interfacial region where charge separation can occurs easily.

Blends are made up of the amalgamation of D and A moieties. The existence of the excitons produced is less and with reduced movement, the diffusion distance of excitons in organic dye (polymer) is < 10 nm, thus precaution should be observed that they are diffused in the interfacial region so that charge separation would take place. Within any region in the function phase, the excitons length is needed at the distance of the diffusive interface. Irrespective of their molar absorptivity, about 20 nm bi-layers of D/A moieties ought not to be optically condensed, letting the photons to travel effortlessly [32-33].

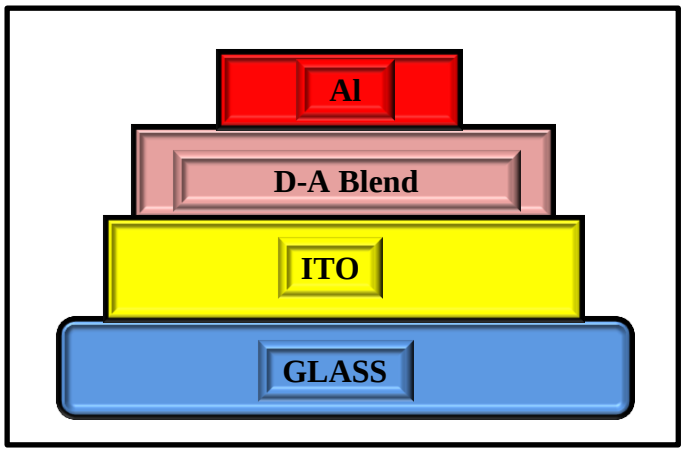

Figure 2.5: Simple Arrangement of a Bulk (Blend) Layer Cell

2.3 Organic Semiconductors

Talking sincerely, organic semiconductors are no more new in the research world. The 1st studies were the dim and photoconductivity of an aromatic compound called anthracene rock crystal (an archetype organic semiconductor) way back to the beginning of 20th century era. After that was the finding of electroluminescence around 1960, which made scientists to rigorously made their research more on molecular crystals. Their research works proved the fundamental processes which occur in optical excitation and charge carrier transport. The urge success in the syntheses of the conjugated polymers in which their doping were monitored also the organic photoconductors, were proved to be the 2nd group of organic semiconductors. These were achieved in the 1970s and were awarded with the noble prize in chemistry. Since then, organic semiconductors have been researched on for the reasons like reduced cost-price, photochemically stable and its high ε_{max} values. Besides these, the straightforwardness of their synthetic methods has proved additional benefit for different uses in various industries through modification of their properties. Their uses in are organic light emitting diodes production,

photoconductors production, chemical sensors fabrication, double layer organic solar cells construction, organic field effect transistors (OFET), photo-detectors, organic lasers, organic photovoltaic cells (OPVC) production [34-56].

These semiconductors primarily are divided into two classes, the materials made from polymers and low molecular weight materials. The common thing between these two classes is the conjugated π-electron system created by the p_z orbitals of sp^2-hybridized carbon atoms in the molecules. The major difference of these materials is mainly how they are fabricated into thin films that is, low molecular molecules are often deposited from the gas phase through an endothermic process called sublimation and then the polymeric materials solely fabricated from solution i.e. by spin-coating methods [57]. Organic semiconductors with fewer molecules can further be classified as linear joined cyclic compounds, two dimensional joined cyclic compounds and cyclic oligomers containing more than one atom/molecule.

Pentacene with the formula, $C_{22}H_{14}$ is a sample of linear joined cyclic compound. This compound functions as an organic semiconductor. Pentacene is known due to its utmost slim film flexibility in the mist of other organic semiconductors. It could be obtained commercially or could be easily synthesized [58]. This compound and its derivatives exhibit a band gap suitable for solar conversion and as imagers [59-61]. Due to its poor solubility, many studied has been made for its derivatives mostly to improve its solubility [62]. Thiophene and its derivatives are other good examples of this linear fused ring group [63]. Two- dimensional joined cyclic compounds are those of perylene and naphthalene. Oligomers of thiazolothiazole are classic samples

of heterocyclic oligomers of organic semiconductors which display good characterization and field-effect transistor performance [64].

2.3.1 Characteristics of Organic Semiconductors

Optical characteristics and charge carrier transport are the principal characteristics of organic semiconductors. Organic molecules are van-der-Waals-bonded meaning the intermolecular bonds are weak and comparing these to covalently bonded semiconductors like silicon and the likes, their mechanical and thermodynamic properties such as hardness and melting point are low. And in addition to these is the weakness in the delocalization of electronic wave functions amongst adjoining molecules, which influence their optical characteristics and charge hauler transport. As a result of this weak electronic delocalization, these types of semiconductors have two essential qualities in comparison with the inorganic semiconductors. The first is the presence of definite spin states which are the singlet and triplet states as in isolated molecules which has essential significances for the photo-physical properties of such molecules. The second essential quality attribute to the fact that excitons are frequently localized on one molecule and which make them exhibit substantial binding energy.

2.3.2 n-Type Organic Semiconductors

Organic semiconductors could function as p-type or n-type materials. P-type semiconductors are hole transporter while N-type electron transporters. These two types are necessary for the manufacture of diodes and transistors which create necessary devices. Various p-type organic semiconductors have been carefully synthesized and characterized but their n-types have been difficult to achieve. N-type semiconductors are a kind of extrinsic semiconductor that is, the semiconductor has

been doped where the dopant atoms are skilful enough to provide additional conduction electrons to the host material whereby generating surplus of negative (n-type) electron charge carriers. N-type organic semiconductors are synthesized from arylene diimide family (perylene, naphthalene, anthracene etc.) because they are not affected by heat and environmental pressures, great molar absorption coefficients, outstanding self-assembly ability and so on. There are other compounds that are used for synthesizing n-type organic semiconductors in the applications of organic field-effect transistors (OFET) devices, organic light emitting diodes or electronic paper displays [65]. Such compounds are fullerene and oligomers of thiophenes derivatives. Due to reduced temperatures for the synthesis of organic thin film transistors (OTFTs), this makes them to be deposited on thin plastic substrates without any destruction, making them to be thin and flexible devices. These compounds are therefore always thought-of for production in OFETs and OTFTs [66-68].

2.4 Organic/Polymer Photovoltaic Cells (PVC)

Organic/polymer photovoltaic cells have caught the attention of researchers mainly due to their exceptional stress-free processing, mechanical suppleness and reduced production price. During last decades, the innovation of novel organic materials that led to modern device constructions guaranteed an extremely rapid on rising organic photovoltaic cell performances, attaining approximately 11 % power conversion efficiency (PCE). Regardless of their weak PCE values in comparison with the conventional inorganic devices, organic/polymer photovoltaic cells have characteristic benefits such as high absorption coefficients, possibility to regulate electronic properties by chemical modifying as to regulate independently band gap,

valance and conduction energies [69-70], charge transport, flexibility, small production cost and ease processability in large capacity, environmental and thermal stability [71-75]

In organic/polymer photovoltaics, the transformation of light from the sun to electrical energy depends on the photoinduced electron transfer method concerning two materials, a donor and an acceptor with different ionization potential and electron affinity. The transformation of light from the sun to electrical power is a photovoltaic route showed below (Figure 2.6). The light being absorbed which could not be transformed to electricity is transformed to heat (thermal) which later-on disturbs the system [76-78].

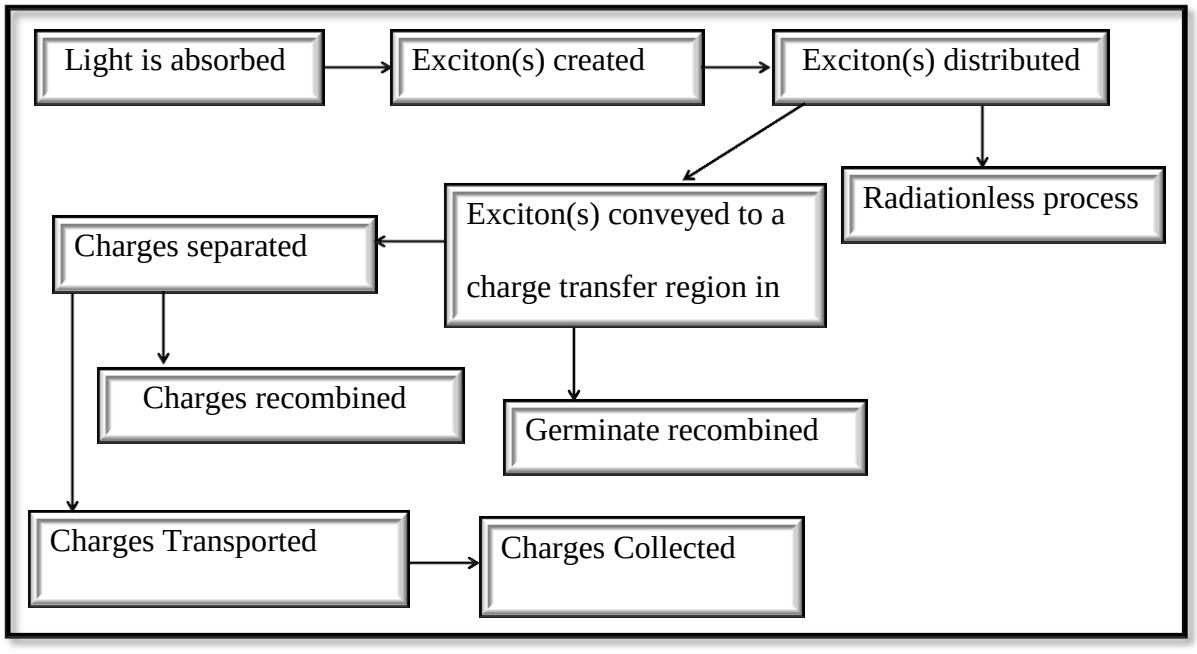

Figure 2.6: Conversion of Sunlight to Generate Electricity Processes

2.5 Dye Sensitized Solar Cells (DSSCs)

Now we are in the world of DSSCs which is the third-born of photovoltaic cells. Due to the disadvantages of the conventional PVs which we all know and has been stated in the literatures, scientists have being working so hard on how make this new innovation of photovoltaic cells to have high power conversion efficiency with ease in its fabrication which will make it available on a large scale for commercial use at reduced cost compared to those of their counterparts. The use of organic dye as the photon absorber instead of the traditional silicon is the major difference between these devices and the conventional ones. Ideally, absorption spectrum of photovoltaic cells ought to entirely cover solar irradiation range so as to obtain their full potentials. Thus, fabricating novel organic dye molecules/compounds materials that will possess full photon gathering properties throughout the absorption spectrum region has now become our major concern.

Dye-sensitized solar cells are generally made up of nano-crystalline films of TiO_2 and ZnO which are semiconductor oxides used as electron transporters and a film of dye placed to this semiconductor surface. Absorption of electrons inside the conduction band of the semiconductor takes place after photo-excitation of the dye, whereby the dye is being oxidized. This oxidized dye is renewed with the aid of the organic solvent which is the iodide/triiodide redox system in most cases. In conclusion, the iodide is restored through reduction of triiodide at the counter electrode also the electrons coming from the load of the circuit are donated to round up the circuit (Figure 2.7) [79-85].

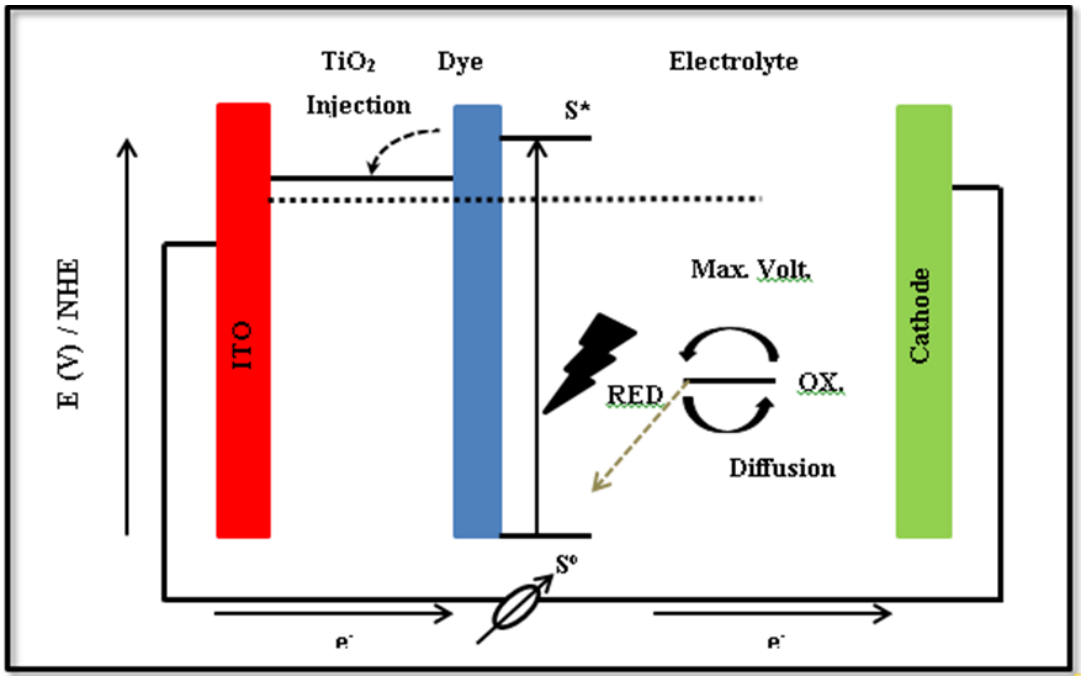

Figure 2.7: Common functioning basics of DSSCs

2.6 Chirality of Perylene Diimides and their Functionalities

The chiroptical functionalities of a single chiral molecule or supramolecular chiral assembly could be regulated by changing the structure or/and electronic state of such molecule or assemble [86-88]. Many studies have been carried out with different chiral compounds which could undergo chiroptical alterations in the presence of any external stimulant. Non-covalent synergies between chiral components are employed in the building of chiral environs also the bonded achiral chromophores may as well exhibit induced circular dichroism (CD) at their own absorption wavelengths in a chiral supramolecular system. Up till now, hardly there is UV-vis spectral region beyond 1000 nm for chiroptical switches [89-91]. Biological sensing, data storage and, optical communication are possible applications when the optical activities of chiral compounds could be adjusted in the near-IR spectral area, at the biowindow (800-1300 nm) also at telecom region (1310-1550 nm).). It is well acknowledged

that chiral perylene diimide syntheses have been greatly improved, the supramolecular synthesis possessing strong chiral properties is still challenging task [21, 89, 91]. Furthermore, the field where chiral molecules are employed to fabricate beneficial functionalities in nano-science materials is productive and thrilling, and signifies a remarkably great potential for further improvement. Different kinds of a-chiral, perylene diimides have been worked on, characterized possessing fascinating functionalities for photonic applications, molecular appliances and biological functions were researched on and stated in the literature [92–95]. Chiral perylene diimides are predominantly favorable group of organic dyes for chiral molecular switches because of the outstanding photochemical- electrochemical properties and thermal stability they possesses.

Chapter 3

EXPERIMENTAL

3.1 Materials

There was no extra purification carried out on the chemicals used; however some of the solvents used were distilled using the standard literature procedures [96]. Perylene dianhydride, naphthalene dianhydride, 1,4-bis(3-aminopropyl)piperazine, dehydroabietylamine, phenol, 4,6-diamino-2-pyrimidinethiol, 1-amino-4-piperidieneethanol, dodecylamine, 2,2,4(2,4,4)-trimethyl-1,6-hexane diamine, zinc acetate, bromine, iodine, potassium hydroxide, potassium carbonate, sodium chloride, sodium sulphate are all from Sigma Aldrich.

3.2 Instrumentation

IR spectra of all the compounds were analyzed by Mattson Satellite FTIR spectrometer using KBr pellets. Elemental analyses of compounds were gotten from Carlor Erba-1106 Carbon, Hydrogen, Nitrogen analyzer. NMR spectra were well-noted in Fourier Transform mode on Bruker/XWIN – NMR (400 MHz for ^{1}H NMR, 100.6 MHz for ^{13}Carbon NMR). The chemical shift values are provided in δ units (ppm) with Tetramethyl silane (TMS) as internal standard. All coupling constants, *J*, are given in Hertz (Hz). UV-Visible spectra in solutions were detailed with a Varian Cary – 100 spectrophotometer. Emission and excitation spectra and Q_f values of the synthesized compounds were properly worked on via Varian Cary Eclipse Fluorescence Spectrometer and determined at excitation, λ_{exc} = 485 nm for perylene

compounds. Electrochemical properties in solution and solid-state were studied using Gamry instruments workstation equipped with a PC computer monitoring Reference 600 Potensiostat/Galvanostat/ZRA system. CV of the compounds in solution was done via a three-electrode cell with a polished 2 mm glassy carbon as working electrode, Pt as counter electrode Ag/AgCl reference electrode. $1.76x10^{-5}$ M concentrated solutions in electro-active material and supporting electrolyte (0.1 M $NaBF_4$ in dimethyl sulfoxide (DMSO)) were used. The internal reference used was Ferrocene. Solid-state redox potentials of the compounds were detailed in 1 M HCl solution by immobilized microparticles voltammetry technique. The scan rate of 50-1000 (mVs^{-1}) and 60-150 Hz as frequency were applied for the measurements. Mass spectra were detailed out on a Finnigan MAT 311 A instrument at 70 eV ionization energy. Thermogravimetric analyses (TGA) were obtained from Perkin Elmer, TGA, Model, Pyris 1. All heated compounds were at 10 ^{o}C / minutes in Oxygen. Thermal analyses were measured using a Perkin Elmer, DSC Model, Jade DSC apparatus. The compounds were heated at 10 ^{o}C / minutes temperature increment under nitrogen atmosphere.

3.3 Synthetic Methods

To begin with, a chiral multichromophoric system based perylene bisimide containing two chiral naphthalene monoimides was synthesized, purified and analyzed (Aleshinoye, Bodapati and Icil, 2015).

Then three bay substituted perylene supramolecules using two different methods of synthesis with one perylene-naphthalene multichromophoric compound were

differently prepared. These compounds possess high stability with excellent photophysical and electrochemical properties.

Method A:

(i) A dibrominated perylene dianhydride mixture of 1,7- and 1,6-regioisomers along with a small amount of 1,6,7-regioisomer was synthesized in accordance to the literature procedure [98, 99].

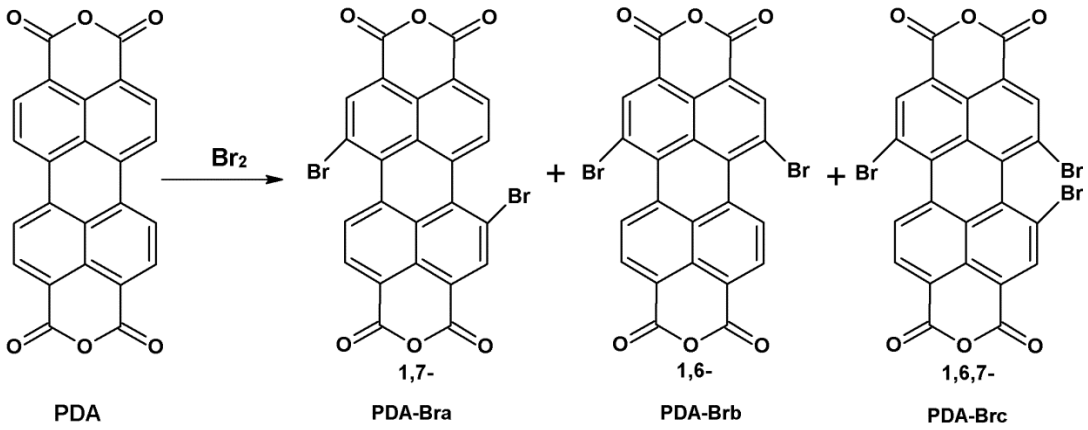

Scheme 3.1: Synthesis of Brominated Perylene Dianhydride

(ii) Due to isomeric-mixture insolubility in common organic solvents, a portion of the mixture was directly reacted with phenol thereby, substituting bromine atoms at the bay positions with this alcohol. Neither recrystallization nor column chromatography techniques could separate the isomers.

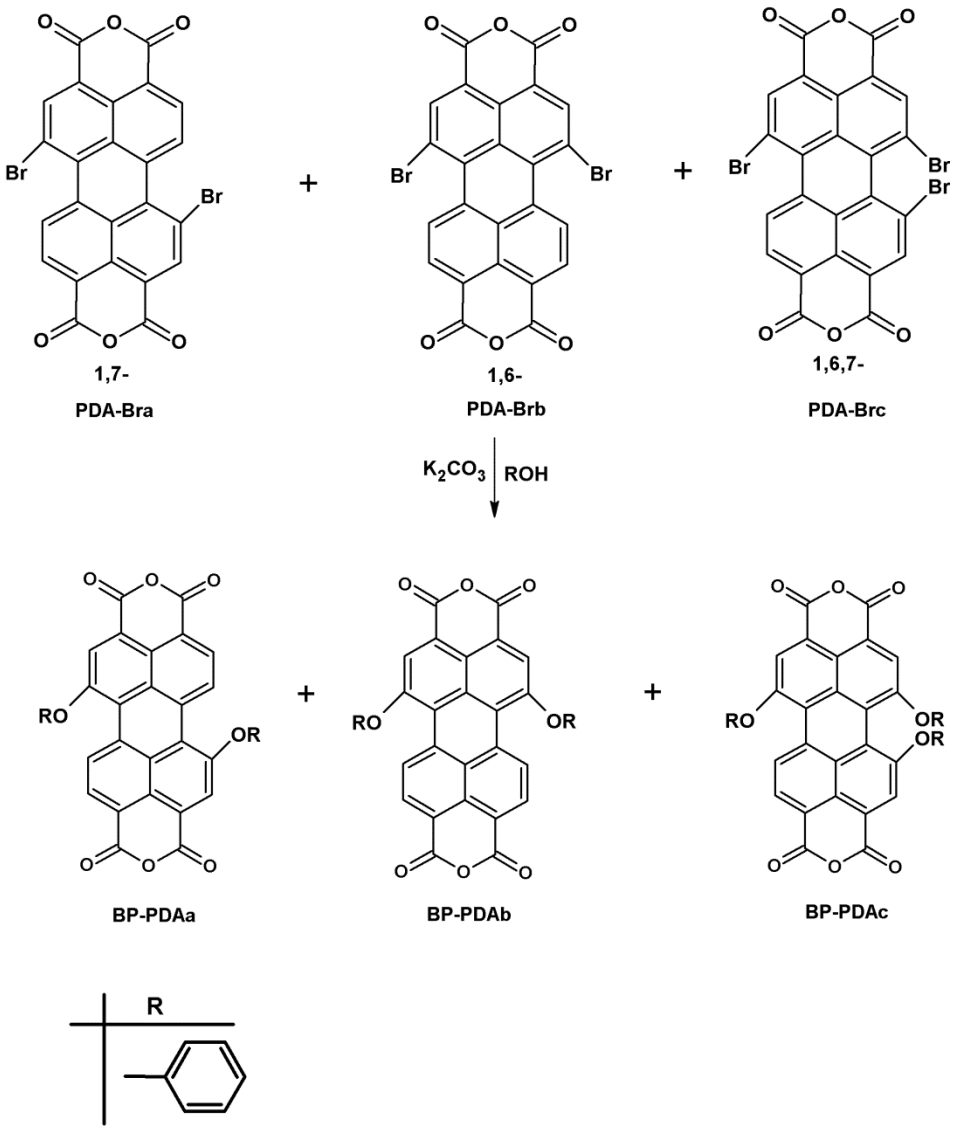

Scheme 3.2: Synthesis of Bay-substituted Perylene Dianhydride

(iii) Subsequent reaction with amine groups were carried out on the isomeric mixtures transforming the dianhydride into diimides. 1,6,7-regioisomer was separated as discussed in the literature [98]. 1,7-regioisomer was collected at high yield alongside with little amount of 1,6- regioisomer..

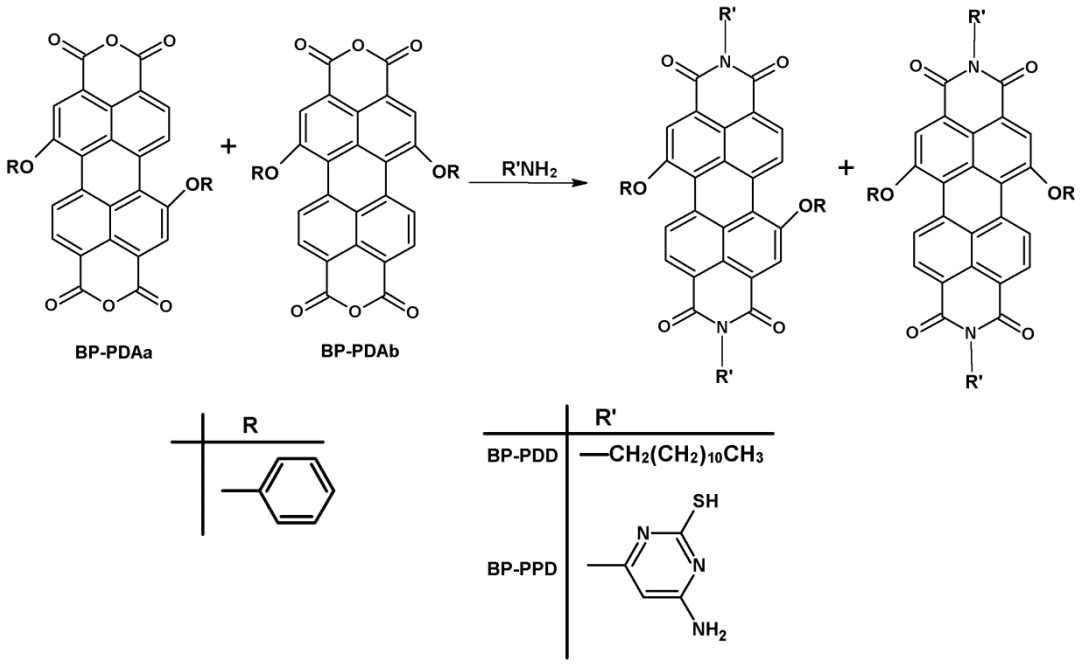

Scheme 3.3 Synthesis of Bay-substituted Perylene Diimide, Method A

Method B:

Another perylene diimide was prepared and purified according to the literature [100]. This compound was reacted with bromine orienting its substitution at 1,7- bay position. The bromine atoms were further removed and substituted with an amine compound.

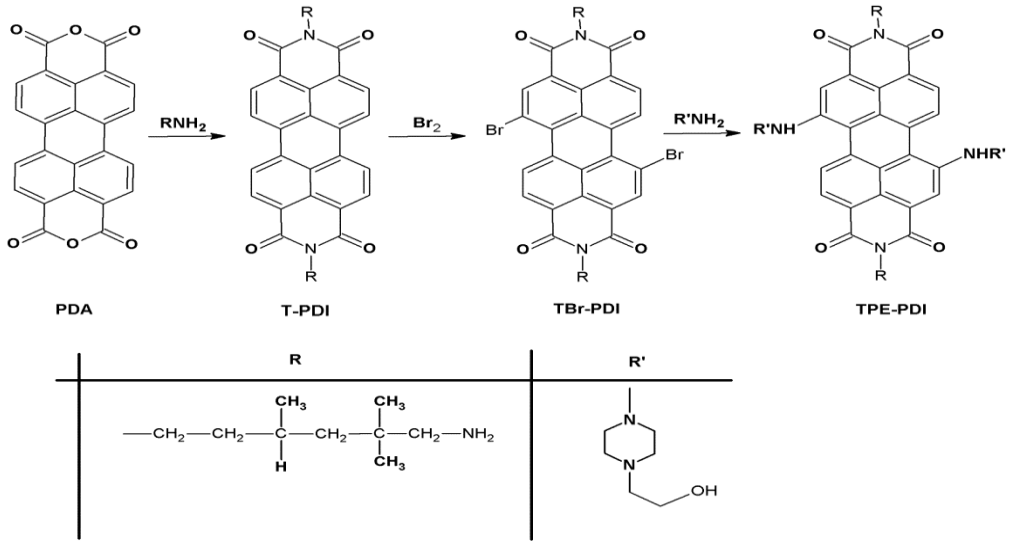

Scheme 3.4: Synthesis of Bay-substituted Perylene Diimide, Method B

The bay-substituted compounds were characterized by various analytical methods such as ^{1}HNMR, ^{13}CNMR, FT-IR, and elemental analysis. The photochemical and thermal properties of these perylene compounds were also studied in details.

3.4 Electrochemical Properties of Chiral Multichromophoric System Based Perylene Bisimide Containing Two Chiral Naphthalene Monoimides

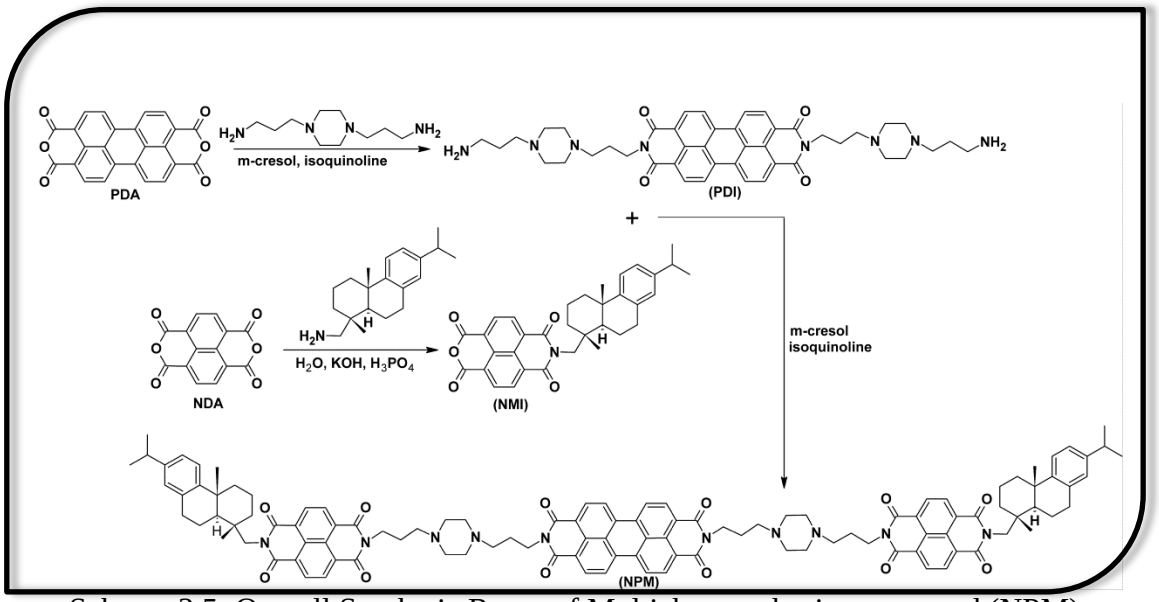

Scheme 3.5: Overall Synthetic Route of Multichromophoric compound (NPM) which Exhibits Excellent Electrochemical Properties

The multichromophoric compound **NPM** was synthesized using perylene bisimide containing two chiral naphthalene monoimides at the imide positions. The prework of this compound has been done (synthesis and analysis); only the electrochemical information is discussed in this thesis (Aleshinloye, Bodapati and Icil, 2015).

3.5 Synthetic Route of *N,N'*-Di(dodecyl)-1,7-diphenoxylperylene-3,4,9,10-tetracarboxy diimide (BP-PDD)

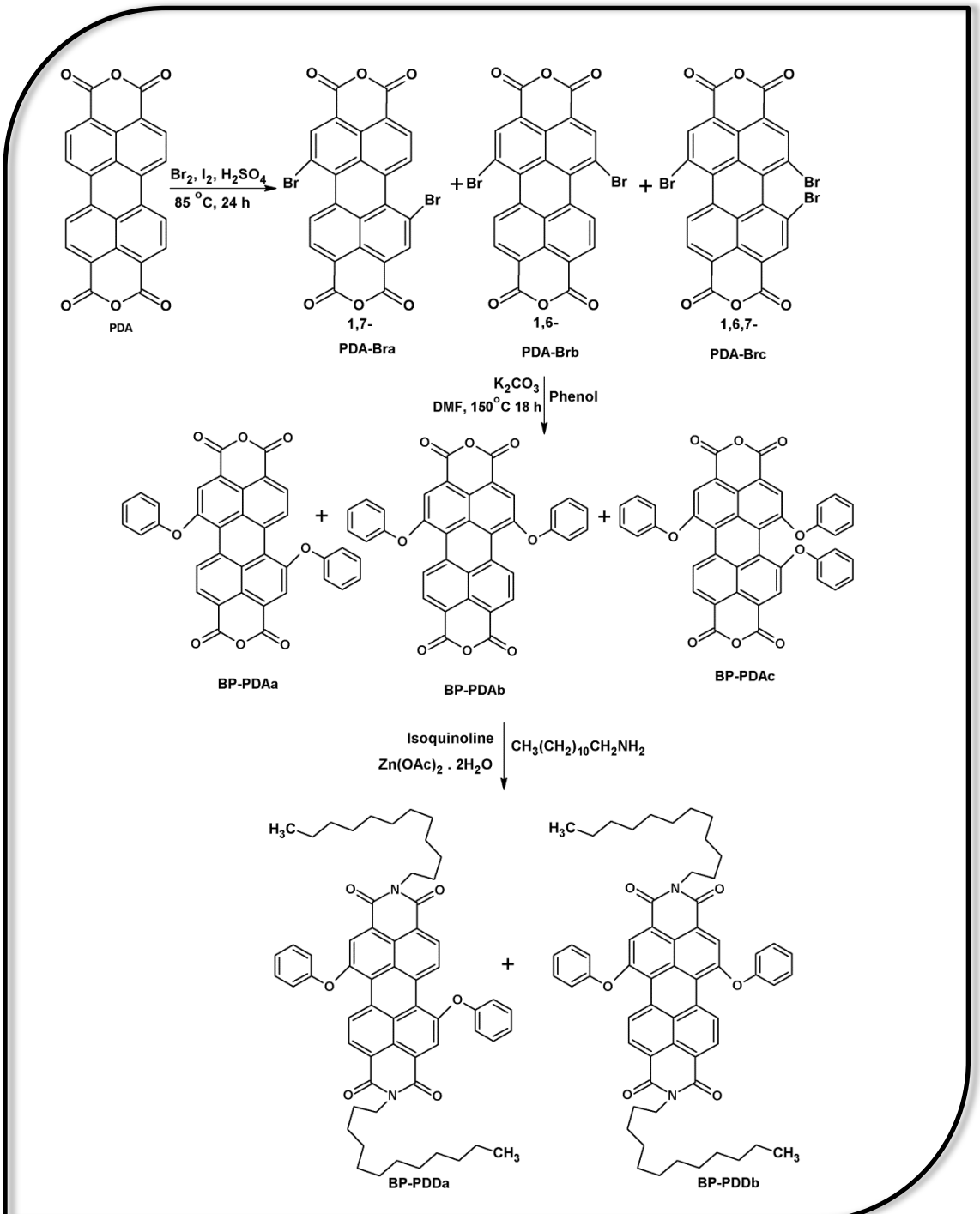

Scheme 3.6: Overall Synthetic Route of BP-PDD starting from Bromination of Perylene dianhydride to the final product, Bay-substituted Perylene diimide, Method A

3.5.1 Synthesis of Brominated Perylene dianhydride (PDA-Br)

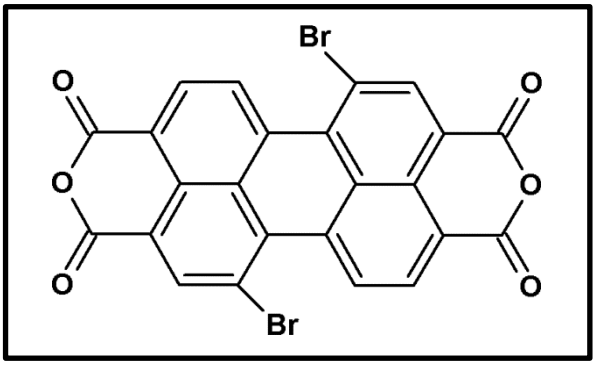

Figure 3.1: 1,7-Dibromoperlyene 3,4,9,10-tetracarboxylic dianhydride (PDA-Br)

Iodine-catalyzed bromination of PDA was synthesized in accordance to the literature [98]. PDA (2 g, 5.10 mmol) was added to 30 mL concentrated sulphuric acid and stirred at 25 ^{o}C, then at 60 ^{o}C for 24 h. Iodine (0.06 g, 0.236 mmol) was added with the reaction mixture and first stirred at 25 ^{o}C, then at 55 ^{o}C for 5 h later at 80 ^{o}C for another 5 h. Bromine (0.8 mL, 15.61 mmol) was put in dropwise to the reaction flask over the course of 1 h at 25 ^{o}C and with stirring for 22 h at 85 ^{o}C and 2 h at 100 ^{o}C. Excess bromine was displaced with argon gas. Water (20 mL) was put in dropwise to the cooled mixture then the precipitate was collected was retrieved by filtration. The unpurified product was cleansed with 86 % sulphuric acid followed by 100 mL distilled water to afford products, **PDA-Br** (Figure 3.1, as major product) and dried under reduced pressure at 110 ^{o}C. Yield (2.54 g, 91 %); Brownish-red color.

FTIR (cm^{-1}): 3058cm^{-1} (aromatic C-H stretch), 1771cm^{-1}and 1725 cm^{-1} (anhydride C=O), 1596 cm^{-1} and 1497 cm^{-1} (C=C stretch), 1374 cm^{-1} (C-O-C stretch), 803 cm^{-1} and 733 cm^{-1} (C-H bend), 692 cm^{-1} (Br). UV-vis (λ_{max}) (DMF): 425, 488, 517 nm. Fluorescence (λ_{max}) (DMF): 552, 584 nm.

3.5.2 Synthesis of 1,7-Diphenoxylperylene-3,4,9,10-tetracarboxylic dianhydride (BP-PDA)

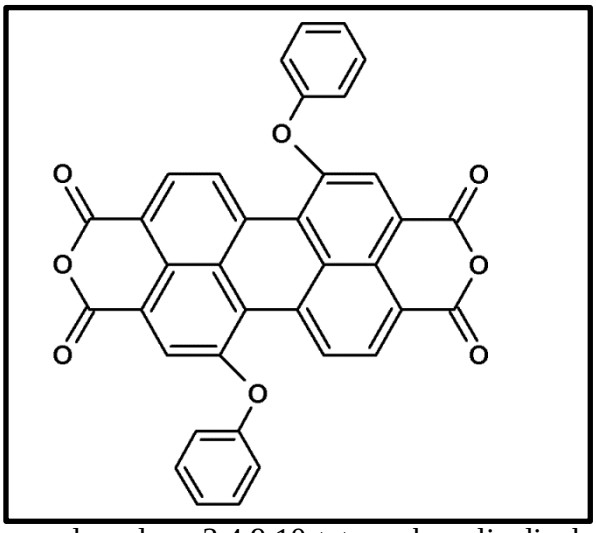

Figure 3.2: 1,7-Diphenoxylperylene-3,4,9,10-tetracarboxylic dianhydride (BP-PDA)

PDA-Br (1 g, 1.82mmol) was added to 20 mL dried DMF. K_2CO_3 (0.622 g, 4.50mmol) and phenol (0.424 g, 4.43mmol) were mixed with the solution. The reaction temperature was elevated to reflux for 18 h in the presence of argon with nonstop stirring. At the end of the reaction, the solution was added in a mixture of 50 mL acetic acid + 50 mL cold water and allowed to cool to 0 ^{o}C all through the night. The mixture was filtered-out to get the crude product, **BP-PDA** (Figure 3.2, as major product) **.** It was first purified with water Soxhlet then with methanol Soxhlet to eliminate the unreacted phenol and later dried in vacuum oven. Yield (0.90 g, 85 %); Dark-red color. FTIR (cm^{-1}): 3060cm^{-1} (aromatic C-H stretch), 1762cm^{-1} and 1735 cm^{-1} (anhydride C=O), 1593 cm^{-1} and 1513 cm^{-1} (C=C stretch), 1387 cm^{-1} (C-O-C stretch), 1262 cm^{-1} (C-O-C ether), 805 cm^{-1} and 737 cm^{-1} (C-H bend). UV-vis (λ_{max}) (TCE): 382, 518, 541 nm. Fluorescence (λ_{max}) (TCE): 525, 575 nm. ^{1}H NMR, δ_H (ppm) (500 MHZ, DMSO):

8.53 (d, *J*=5.0 Hz, 2 Ar-H; H-C(6), H-C (12)), 8.31 (d, *J*=5.0 Hz, 2 Ar-H; H-C (5), H-C (11)), 8.22 (s, 2 Ar-H; H-C(2), H-C (8)), 8.02 (m, 10 Ar-H; H-C (17-21), H-C (17'-21')).

3.5.3 Synthesis of *N,N'*-Di(dodecyl)-1,7-diphenoxylperylene-3,4,9,10-tetracarboxy diimide (BP-PDD)

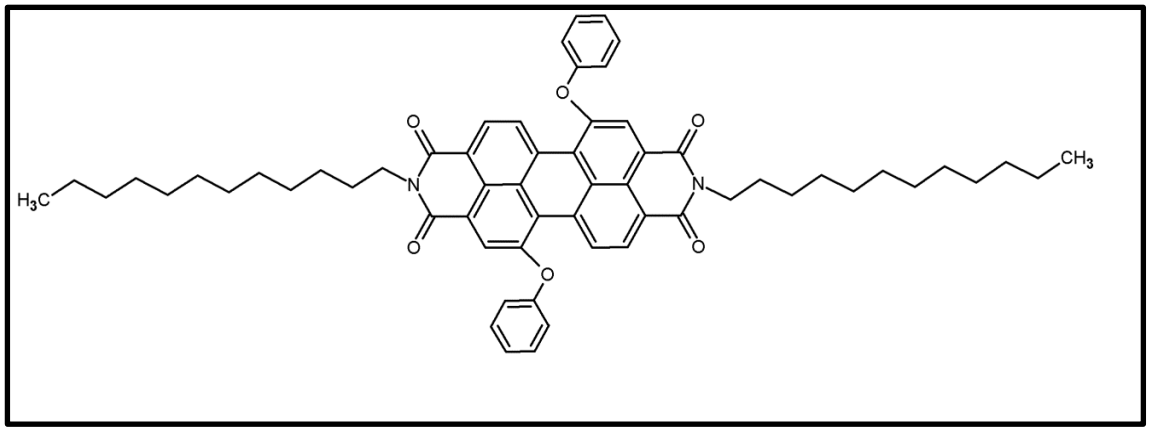

Figure 3.3: N,N'-Di(dodecyl)-1,7-diphenoxylperylene-3,4,9,10-tetracarboxy diimide (BP-PDD)

Using the procedure from the literature (101), BP-PDA (0.20 g, 0.346 mmol), dodecylamine (0.32 g, 1.726 mmol) and zinc acetate (0.076 g, 0.346 mmol) reacted in dried isoquinoline (5 mL) in nitrogen atmosphere at 80 ^{o}C for 3 h, at 120 ^{o}C for 4 h, at 160 ^{o}C for 8 h, at 180 ^{o}C for 4 h and lastly at 200 ^{o}C for 2 h. The solution was cooled to room temperature and added into 50 mL methanol. The precipitate was collected and washed using ethanol Soxhlet used for 2 day to eliminate all impurities, dried at 110 ^{o}C under vacuum and then purified by recrystallization to obtain product, **BP-PDD** (Figure 3.3)**.** Yield (0.27 g, 75 %); Violet color.

3.5.4 *N,N'*-Di(dodecyl)-1,7-diphenoxylperylene-3,4,9,10-tetracarboxy diimide (BP-PDD)

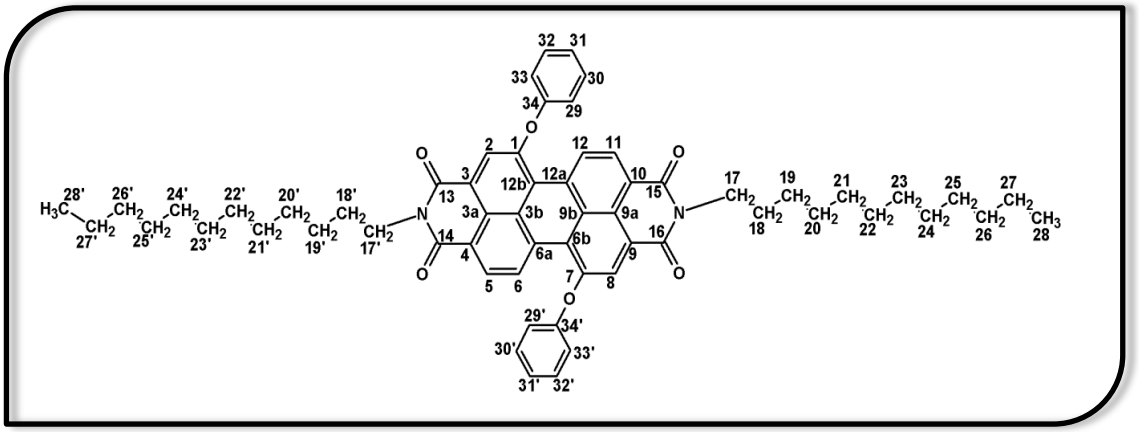

Figure 3.4: Carbon Numbering of N,N'-Di(dodecyl)-1,7-diphenoxylperylene-3,4,9,10-tetracarboxy diimide (BP-PDD)

^{1}H NMR, δ_H (ppm) (500 MHz, DMSO + $CDCl_3$): 7.97 (d, *J* = 5.0 Hz, 4 Ar-H, H-C (5), H-C (6), H-C (11), H-C (12)), 7.32 (s, 2 Ar-H; H-C (2), H-C(8)), 7.12 (b, d, 10 Ar-H, H-C (29-33, 29'-33')), 3.75 (b, 2 CH_2, H-C (17), H-C (17')), 1.19 (d, *J* = 13.50 Hz, 20 CH_2, H-C (18-27, 18'-27')), 0.79 (s, 2 CH_3, H-C (28), H-C (28')). FTIR (cm^{-1}): 3057 (Ar C-H), 2921 and 2850 (Al C-H), 1697 and 1656 (imide C=O), 1590 and 1510 (Ar C=C), 1262 (C-O-C ether). UV-vis (λ_m(TCE): 390, 515 and 543 nm. Fluorescence (λ_{max}) (TCE) = 578 nm. Φ_f = 41 %, $\lambda_{excit.}$ = 485 nm. Anal. Calcd $_{ax}$). for $C_{60}H_{66}N_2O_6$: C: 79.09%; H: 7.73 %; N: 3.07 %, found: C: 78.85 %; H: 7.87 %; N: 3.40 %

3.6 Synthetic Route of *N, N'*-Di(5-amino-3-pyrimidinethiol)-1,7-diphenoxylperylene-3,4,9,10-tetracarboxydiimide (BP-PPD)

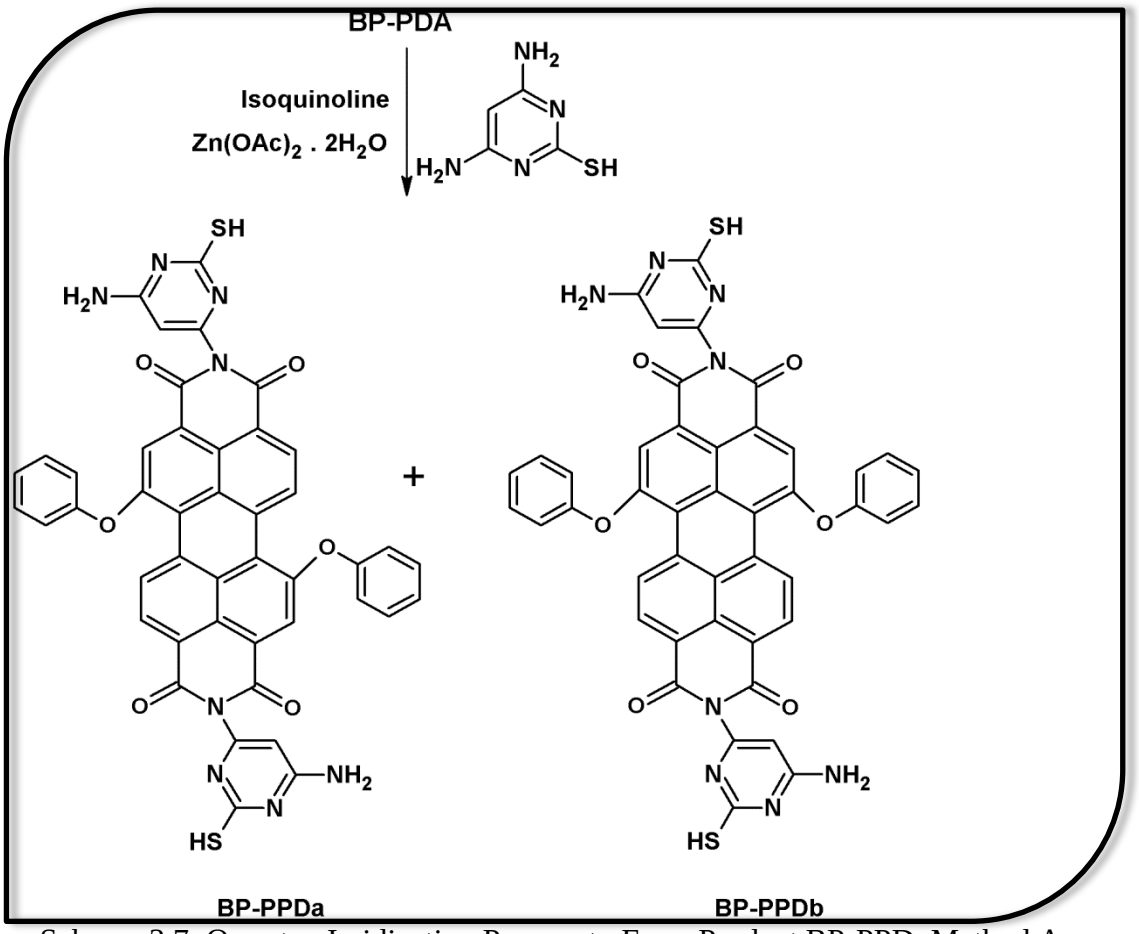

Scheme 3.7: One step Imidization Process to Form Product BP-PPD, Method A

3.6.1 Synthesis of *N, N'*-Di(5-amino-3-pyrimidinethiol)-1,7-diphenoxylperylene-3,4,9,10-tetracarboxy diimide (BP-PPD)

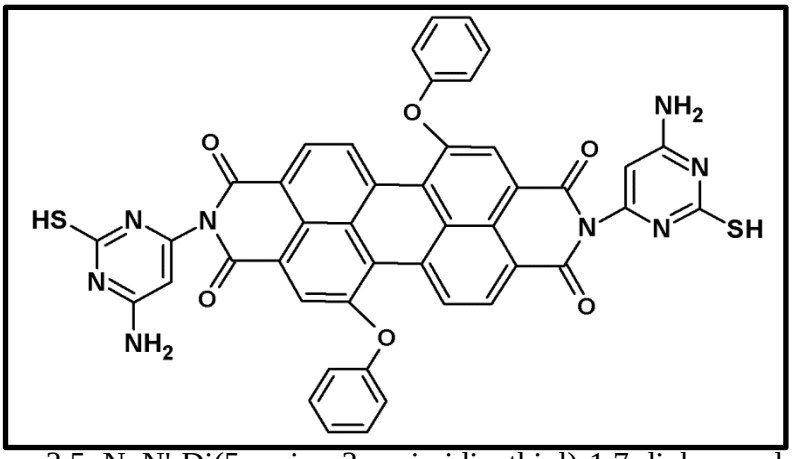

Figure 3.5: N, N'-Di(5-amino-3-pyrimidinethiol)-1,7-diphenoxylpery lene-3,4,9,10-tetracarboxy diimide (BP-PPD)

Using the procedure from the literature (101), BP-PDA (0.60 g, 1.04 mmol), 4,6-Diamino-2-pyrimidinethiol (0.44 g, 3.12 mmol) and zinc acetate (0.23 g, 1.04 mmol) reacted in dried isoquinoline (20 mL) in nitrogen atmosphere at 80 ^{o}C for 3 h, at 120 ^{o}C for 4 h, at 160 ^{o}C for 8 h, at 180 ^{o}C for 4 h and lastly at 200 ^{o}C for 2 h. The solution was cooled to room temperature and added into 50 ml methanol. The precipitate was collected and washed with methanol Soxhlet for 2 day in eliminate impurities, dried at 110 ^{o}C under vacuum and then purified by recrystallization to obtain product, **BP-PPD** (Figure 3.4). Yield 83 % (0.707 g, 83 %); Violet color.

3.6.2 *N, N'*-Di(5-amino-3-pyrimidinethiol)-1,7-diphenoxylperylene-3,4,9,10-tetracarboxy diimide (BP-PPD)

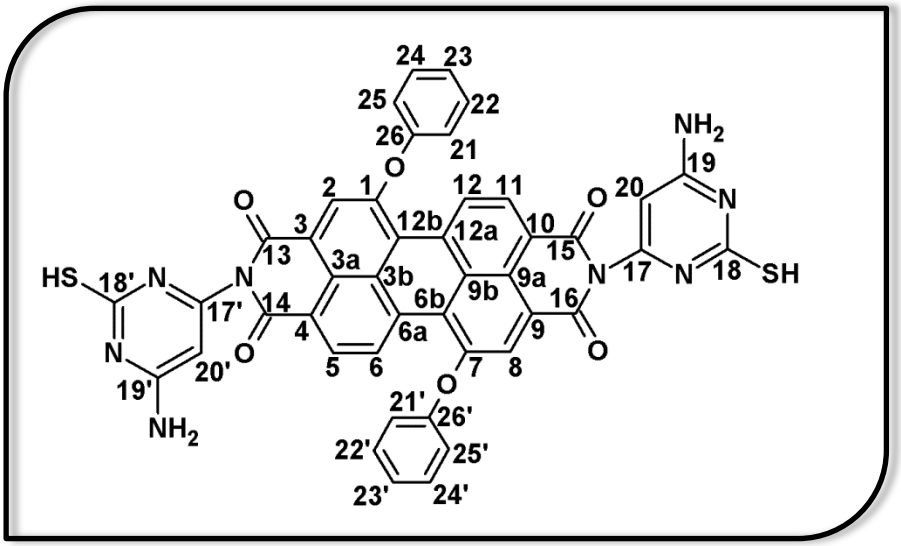

Figure 3.6: Carbon Numbering of N, N'-Di(5-amino-3-pyrimidinethiol)-1,7-diphenoxylperylene-3,4,9,10-tetracarboxy diimide (BP-PPD)

^{1}H NMR, δ_H (ppm) (400 MHz, DMSO): 8.27 - 7.96 (b, 8 Ar-H, H-C (5), H-C (6), H-C (11), H-C (12), H-C (2), H-C (8), H-C (20), H-C (20')), 7.62 - 7.27 (b, d, 12 Ar-H, H-C (21-26), H-C (21'-26')), 2.90 (s, 4H, SH-C(18,18')), 2.75 (s, NH_2-C s, 2H, (19, 19')).

^{13}C NMR, δ_C (ppm) (100 MHz, DMSO): 157.79-158.94 (4 C=O, 8 C, C(13-16), C(17-20), C(17'-20')), 119.28-110.69 (20 Ar–C, C(1-12), C(3a), C(3b), C(6a), C(6b), C(9a), C(9b), C(12a), C(12b)). FTIR (cm^{-1}): 3440, 3328 and 3200 (N-H str.), 3063 (Ar C-H), 2852 (S-H), 1703 and 1672 (imide C=O), 1622 (N-H bend), 1588 and 1542 (Ar C=C), 1339 (C-N str.), 1252 (C-O-C ether), 1196 (C-N amine), 804, 754 (C-H bend). UV-vis (λ_{max}) (DMF): 435, 503 and 525 nm. Fluorescence (λ_{max})

(DMF) = 535, 572 nm. Φ_f = 11 %, $\lambda_{excit.}$ = 485 nm. Anal. Calcd. for $C_{44}H_{24}N_8O_6S_2$: C: 64.07 %; H: 2.93 %; N: 13.58 %, found: C: 63.45 %; H: 2.87 %;N: 13.94 %

3.7 Synthetic Route of *N,N'*-Di(2,2,4(2,4,4)-trimethyl-6-aminohexyl)-1,7-di(1-amino-4-ethanolpiperidyl)perylene-3,4,9,10-diimide (TPE-PDI)

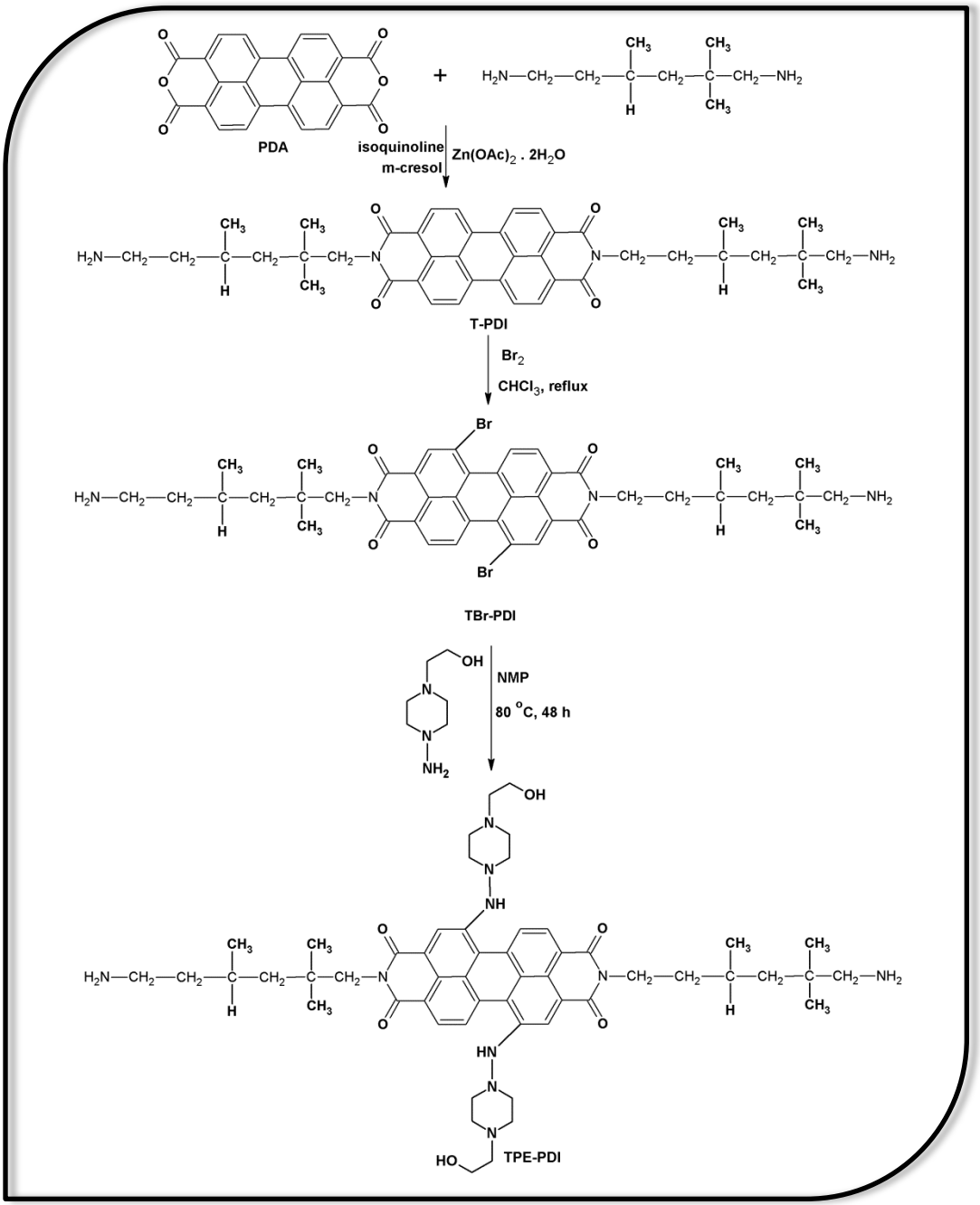

Scheme 3.8: Overall Synthetic Route of TPE-PDI starting from Imidization of PDA followed by its Bay-substitution, Method B

3.7.1 Synthesis of *N,N'*-Di(2,2,4(2,4,4)-trimethyl-6-aminohexyl)perylene-3,4,9,10-diimide (T-PDI)

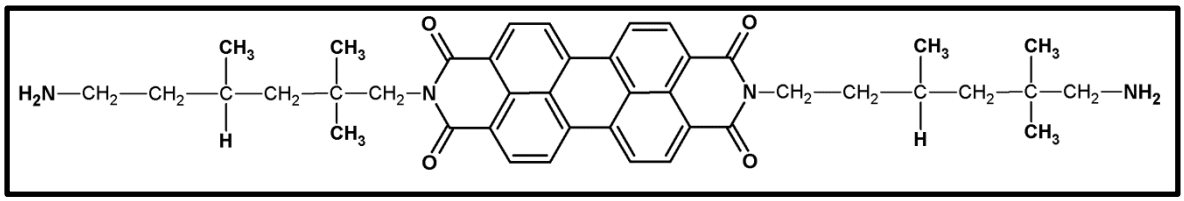

Figure 3.7: N,N'-Di(2,2,4(2,4,4)-trimethyl-6-aminohexyl)perylene-3,4,9,10-diimide (T-PDI)

Following the procedure from the literature [101] PDA (2.0 g, 5.10 mmol), 2,2,4(2,4,4)-trimethyl-1,6-hexane diamine (3.22 g, 20.40 mmol) and zinc acetate (1.20 g, 5.10 mmol) reacted in dried solvent mixture (60 ml m-cresol and 10 ml isoquinoline) in nitrogen atmosphere at 80 ^{o}C for 4 h, at 120 ^{o}C for 4 h, at 160 ^{o}C for 8 h and lastly at 200 ^{o}C for 4 h. The solution was cooled to room temperature and added 400 ml methanol. The precipitate was collected and dried at 110 ^{o}C under vacuum-oven. The untreated product, **T-PDI** (Figure 3.5) was washed in ethanol Soxhlet apparatus for 2 days to eliminate impurities. Yield: (3.307 g, 96 %); Dark red color. FTIR (cm^{-1}): 3384 (N-H), 3077 (Ar C-H), 2954, 2926 and 2850 (Al C-H), 1694 (imide C=O), 1654 (N-H bending), 1593 (Ar C=C), 1342 (C-O-C), 806 and 746 (C-H). UV-vis (λ_{max}) ($CHCl_3$): 459, 490 and 527 nm. Fluorescence (λ_{max}) ($CHCl_3$) = 536, 579, 624 nm. Φ_f = 35 %, $\lambda_{excit.}$ = 485 nm. Anal. Calcd. for $C_{42}H_{48}N_4O_4$: C: 74.97 %; H: 7.19 %; N: 8.33 %, found: C: 74.93 %; H: 7.05 %; N: 7.95 %

3.7.2 Synthesis of *N,N'*-Di(2,2,4(2,4,4)-trimethyl-6-aminohexyl)-1,7-dibromoperylene-3,4,9,10-diimide (TBr-PDI)

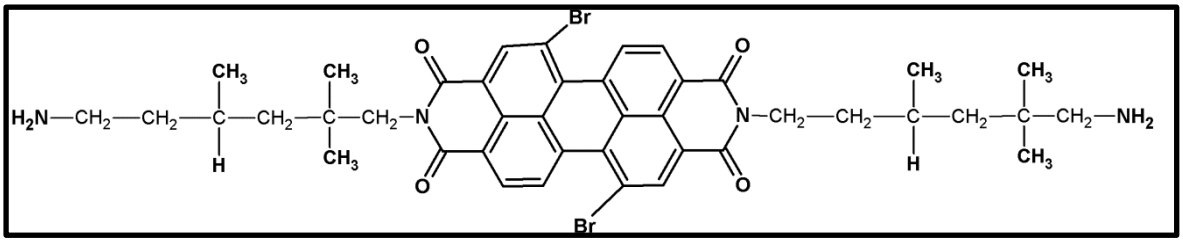

Figure 3.8: : N,N'-Di(2,2,4(2,4,4)-trimethyl-6-aminohexyl)-1,7-dibromoperylene-3,4,9,10-diimide (TBr-PDI)

Following the procedure from the literature [102] T-PDI (0.5 g, 0.74 mmol) and Br_2 (0.12 g, 2.37 mmol) in 30 mL of chloroform, temperature was elevated to reflux in an enclosed system for two days. The bromine excess was displaced by bubbling of argon gas, the solvent was removed by drying and product **TBr-PDI,** (Figure 3.6) was obtained. Since the product is not completely soluble in any organic solvent, it was used for the subsequent synthesis without further purification. Yield (0.657 g, 97 %); Brownish red color. FTIR (cm^{-1}): 3505 (N-H), 3087 (Ar C-H), 2957, 2928 and 2870 (Al C-H), 1693 (imide C=O), 1652 (N-H bending), 1593 (Ar C=C), 1342 (C-O-C), 1044 (C-Br), 810 and 746 (C-H).

3.7.3 Synthetic of *N,N'*-Di(2,2,4(2,4,4)-trimethyl-6-aminohexyl)-1,7-di(1-amino-4-ethanolpiperidyl)perylene-3,4,9,10-diimide (TPE-PDI)

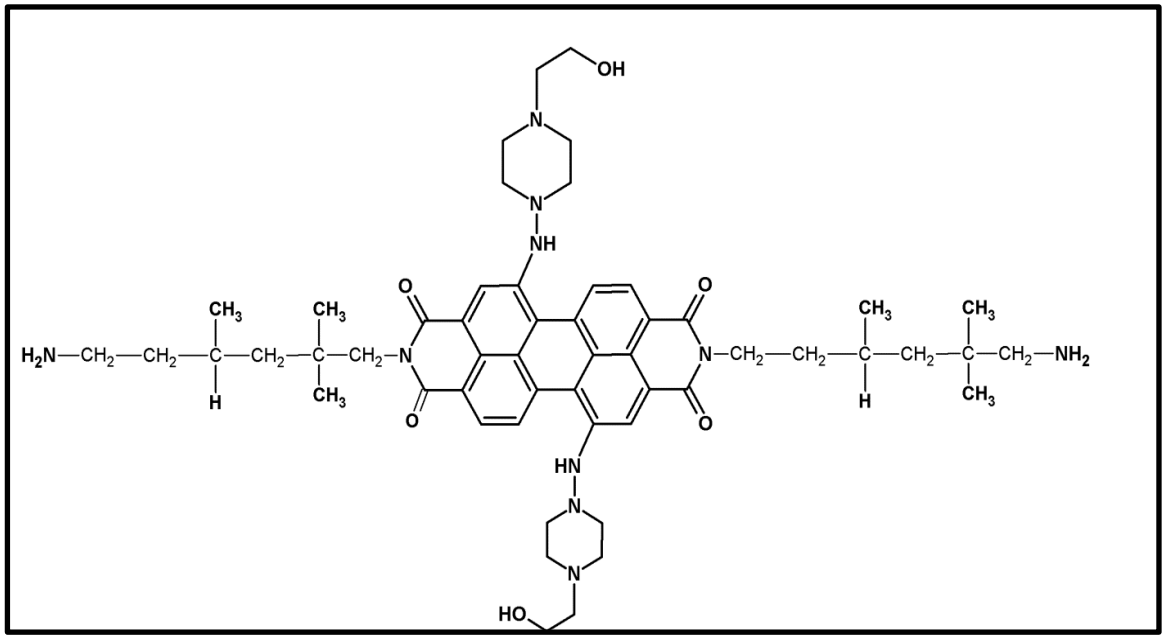

Figure 3.9: N,N'-Di(2,2,4(2,4,4)-trimethyl-6-aminohexyl)-1,7-di(1-amino-4-ethanolpiperidyl)perylene-3,4,9,10-diimide (TPE-PDI)

Following the procedure from the literature [103] TBr-PDI (0.5 g, 0.602 mmol) was added into dried NMP (25 mL) under argon atmosphere with continuous stirring. 1-amino-4-piperidieneethanol (0.262 g, 1.81 mmol) was mixed with the solution and the temperature was elevated to 80 ^{o}C for 48 h. The reaction was cooled to room temperature, it was emptied into a separatory funnel containing 100 mL CH_2Cl_2, water (1 L), and saturated NaCl solution (100 mL). The organic layer, **TPE-PDI** (Figure 3.7) was collected and small amount of sodium sulphate was added into it to remove traces of water. It was further purified by recrystallization and dried under reduced pressure at 110 ^{o}C. Yield (0.050 g, 8.7 %); Orange color.

3.7.4 *N,N'*-Di(2,2,4(2,4,4)-trimethyl-6-aminohexyl)-1,7-di(1-amino-4-ethanolpiperidyl)perylene-3,4,9,10-diimide (TPE-PDI)

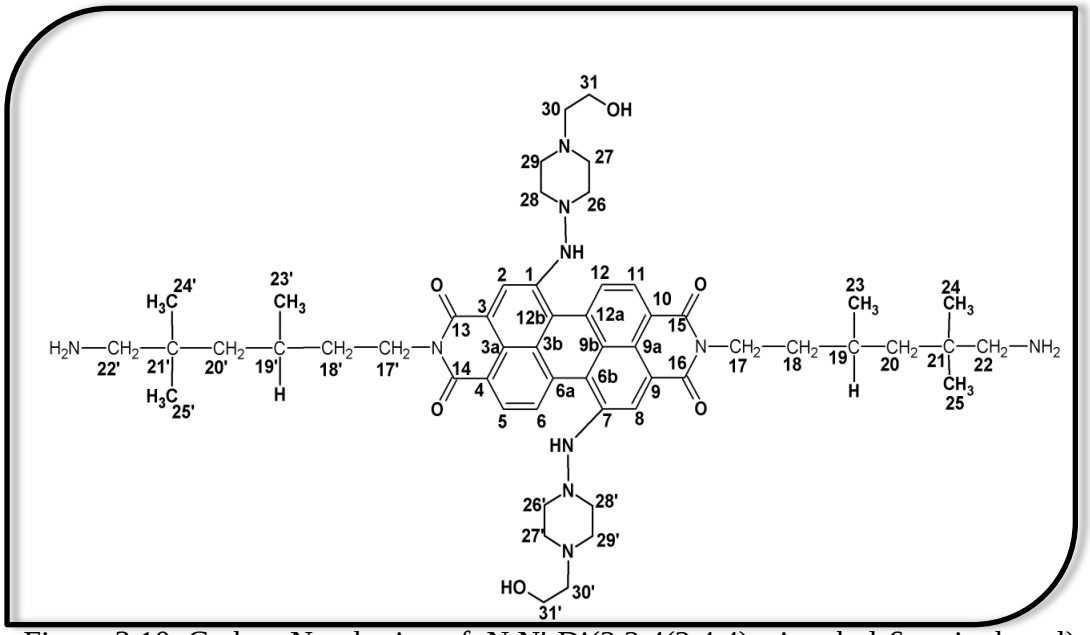

Figure 3.10: Carbon Numbering of N,N'-Di(2,2,4(2,4,4)-trimethyl-6-aminohexyl)-1,7-di(1-amino-4-ethanolpiperidyl)perylene-3,4,9,10-diimide (TPE-PDI)

^{1}H NMR, δ_H (ppm) (400 MHZ, $CDCl_3$): 8.49 (b, d, , *J*=36.0 Hz 6 Ar-H, H-C (2), H-C (5), H-C (6), H-C (8), H-C (11), H-C (12)), 4.14 (m, 2 CH_2, H-C (31), H-C (31')), 3.56 (t, 2 CH_2, H-C (17), H-C (17')), 3.23 (s, NH-C (7)), 2.78 (t, 2 CH_2, H-C (30), H-C (30')), 2.60 (s, 2 CH_2, H-C (22), H-C (22)'), 2.28 (t, J=8.0 Hz, 2 CH_2, H-C (18), H-C (18')), 1.97 (m, 2 CH, H-C (19), H-C (19')), 1.59 (s, 2 OH, HO-C (31), HO-C (31')), 1.35 (d, J=8.0 Hz, 2 CH_2, H-C (20), H-C (20')), 1.18 (s, 4 CH_3, H-C (24), H-C (25), H-C (24'), H-C (25')), 1.02 - 0.81 (m, 10 CH_2, H-C (26-29), H-C (26'-29'), NH_2-C(22), NH_2-C(22'), H-C (23), H-C (23')). ^{13}C NMR, δ_C (ppm) (100 MHz, $CDCl_3$): 166.66 (4C=O, C(13), C(14), C(15), C(16)), 147.01-118.56 (20 Ar–C, C(1-12), C(3a), C(3b), C(6a), C(6b), C(9a), C(9b), C(12a), C(12b)), 60.85 (2 OH–C, C(31), C(31'), 52.97 (2CH_2, C(22), C(22')), 46.97 (2CH_2, C(20), C(20')), 44.67 (2CH_2,

C(17), C(17')), 38.50 ($3CH_2$, C(18), C(18')), 34.67 (2(C), C(21), C(21')), 28.69 (2CH, C(19), C(19')), 27.0 ($4CH_3$, C(24), C(25), C(24'), C(25')), 23.08 ($8CH_2$, C(26), C(27), C(28), C(29), C(26') C(27'), C(28'), C(29')), 21.06 ($2CH_2$, C(30), C(30')) 19.46 ($2CH_3$, C(23), C(23')). FTIR (cm^{-1}): 3546 (OH), 3505, 3467 (N-H), 3087 (Ar C-H), 2958, 2928, 2872 and 2852 (Al C-H), 1695 (imide C=O), 1654 (N-H bending), 1594 (Ar C=C), 1355 (C-O-C), 810 and 746 (C-H).UV-vis (λ_{max}) ($CHCl_3$): 371, 439, 467, 490 and 526 nm. Fluorescence (λ_{max}) ($CHCl_3$) = 538, 577, 625 nm. Φ_f = 48 %, $\lambda_{excit.}$ = 485 nm. Anal. Calcd. for $C_{54}H_{74}N_{10}O_6$: C: 67.62%; H: 7.77 %; N: 14.60 %, found C: 66.62%; H: 7.47 %; N: 14.40 %.

Chapter 4

DATA AND CALCULATIONS

4.1 Electrochemical Parameters

Cyclic voltammetry was used in the thorough study for the electrochemical characterizations of NPM in DMSO solvent containing 0.1 M $NaBF_4$ (supporting electrolyte) and in solid state was recorded in I M HCl solution.

4.1.1 Redox Potentials / Half-Wave Potentials ($E_{1/2}$)

Redox Potential is an extent at which chemical species gain electrons and can as well be reduced which is a reversible process. This can be calculated from a cyclic voltammogram agreeing with the internal reference used by using equation (4.1) [106].

$$E_{1/2} = \frac{Epc + Epa}{2} \quad (4.1)$$

$E_{1/2}$: Half-wave potential (V)

E_{pc}: Cathodic peak potential (V)

E_{pa}: Anodic peak potential (V)

Redox Potentials of NPM

The cyclic voltammograms of NPM (Figure 4.83) showed one reversible redox process in solution and two reversible processes in solid state. The redox potential in solution is calculated relative to the reference electrode below.

$$\boldsymbol{E_{red1/2}\ vs.Ag/AgCl = \frac{Epc+Epa}{2} = \frac{(-0.819)+(-0.289)}{2} = -0.554\ V}$$

The peak potentials separations where n is the number of electrons is calculated by the equation below (Equation 4.2)

. $$\Delta E_p = E_{pa} - E_{pc} = \frac{0.059}{2}\ V \qquad \textbf{(4.2)}$$

Peak Potentials Separations of NPM

$\Delta E_p = E_{pa} - E_{pc}$

$\Delta E_p = (-0.819) - (-0.289) = 0.530$ V

ΔE_p = 530 mV

Ferrocene was used as internal reference and its oxidation potential was estimated as 0.534 V therefore, *E*ox = 0.534 V

The calculation of redox potential in relation to internal reference is as follows,

$E_{red1/2}$ vs. Fc = ($E_{red1/2}$ vs.Ag/AgCl) – (E_{ox}vs.Ag/AgCl)

$E_{red1/2}$ vs. Fc = (–0.554) – (0.534) = –1.088

$E_{red1/2}$ vs. Fc = –1.088 V

In the same manner, the redox potentials of NPM, PDI and NMI in solution and in solid state were calculated, results were shown in Table 1.1

Table 1.1: Electrochemical information of NPM, PDI and NMI in solution and solid-state

compound	E_{pc} [a] / V	E_{pa} [b] / V	$E_{1/2}$ [c] *vs.* (Ag/AgCl) [d]	ΔE_p [e] / mV	E_{Fc} [f] *vs.* (Ag/AgCl) / V	$E_{1/2}$ *vs.* Fc / V	LUMO [g]	$E_{g,opt}$ [h] / eV	HOMO [i] / eV
NPM in DMSO	–0.819	–0.289 0.718	–0.554	530	0.534	–1.088	–3.712	2.252	–5.963
NPM in solid-state	–0.399 0.349	–0.189 0.709	–0.294 0.523	210 360	0.270 0.270	–0.564 0.253	–4.254	1.700	–5.954
PDI in DMSO	–0.658	–0.499 0.651	–0.578	159	0.534	–1.112	–3.687	2.252	–5.939
PDI in solid-state	–0.369 0.329	–0.139 0.739	–0.254 0.534	230 410	0.270 0.270	–0.524 0.264	–4.276	1.790	–6.066
NMI in DMSO	–0.370 –0.769	–0.241 –0.649	–0.306 –0.709	129 120	0.534 0.534	–0.840 –1.243	–3.556	3.000	–6.556

[a] E_{pc}: cathodic potential.
[b] E_{pa}: anodic potential.
[c] $E_{1/2}$: half wave potential.
[d] Ag/AgCl: silver/silver chloride reference electrode.
[e] ΔE_p: peak potential separations
[f] E_{Fc}: oxidation potential of ferrocene (internal reference).
[g] LUMO: lowest unoccupied molecular orbital.
[h] E_g: energy gap,. [i] HOMO: highest occupied molecular orbital.

4.1.2 LUMO Level Energies

Lowest unoccupied molecular orbital energy level is calculated relating to the vacuum level. The redox data are standardized to the ferrocene/ferricenium couple with energy calculation of – 4.8 eV [105].

$$E_{LUMO} = -(4.8 + E_{1/2}) \quad (4.3)$$

E_{LUMO}: LUMO energy level (eV)

$E_{1/2}$: Half-wave potential (V)

E_{LUMO} of NPM

$E_{LUMO} = -(4.8 + E_{1/2})$

$$E_{LUMO} = -(4.8 + (-1.088)) = -3.712 \text{ V}$$

$$E_{LUMO} = -3.712 \text{ V}$$

In the same manner, the LUMO values for NPM, PDI and NMI were calculated and the results were tabulated in Table 1.1

4.1.3 Optical Band Gap Energies (E_g)

The optical band gap energy values for NPM, PDI and NMI were calculated using equation 4.4 and the results were tabulated in Table 1.1

$$E_g = \frac{1240\ eV\ nm}{\lambda} \quad (4.4)$$

E_g: band gap energy (eV)

λ: cut-off wavelength of the absorption band (nm)

E_g of NPM

$$E_g = \frac{1240\ eV\ nm}{\lambda} = \frac{1240\ eV\ nm}{550.62} = 2.252$$

$$E_g = 2.252$$

4.1.4 HOMO Level Energies

The calculations for highest occupied molecular orbital energy were done using equation 4.5 for NPM, PDI and NMI compounds and the results were tabulated in Table 1.1

$$E_{HOMO} = E_{LUMO} - E_g \quad (4.5)$$

E_{HOMO}: energy of HOMO level (eV)

E_{LUMO}: energy of LUMO level (eV)

E_g: band gap energy (eV)

HOMO Level Energy of NPM

$E_{HOMO} = E_{LUMO} - E_g$

$E_{HOMO} = -3.712\ V - 2.252\ V$

$E_{HOMO} = -5.963\ V$

4.1.5 Diffusion Constants (D)

Randles-Seveik equation (Equation 4.6) explains the outcome of scan rate on the peak current (i_p) [105].

$$i_p = (2.69 \times 10^5)\, n^{3/2}\, v^{1/2}\, D^{1/2}\, A\, c \quad (4.6)$$

To make the Diffusion constant, D subject of the formula, equation 4.15 is rearranged.

$$D = \frac{(\frac{i_{pc}}{v^{1/2}})^2}{[(2.69\times10^5\, A s mol^{-1} v^{-1/2})^2 \times (n^{3/2})^2 \times (Ac)^2]}$$

$i_p = i_{pc}$: Cathodic peak current from the cyclic voltammogram of the compounds

$\nu^{1/2}$: Scan rate used to record the cyclic voltammogram of the compound

n: Number of electrons

D: Diffusion constant in $cm^{2/}s$

A: Area of working electrode in cm^2

c: Concentration of the electroactive species (mol / cm^3)

$A = \pi r^2 = 0.0314\ cm^2$

$\boldsymbol{c} = 1.76\times10^{-8}$ mol / cm^3

n = 2

Table 1.2: Diffusion constants data of NPM, PDI and NMI

Compound	**D (cm^2s^{-1})**
NPM in DMSO	1.65×10^{-6}
NPM in solid state	1.10×10^{-8}
PDI in DMSO	6.14×10^{-9}
PDI in solid state	5.82×10^{-10}
NMI in DMSO	7.45×10^{-8}

4.2 Calculations of Optical Parameters

4.2.1 Maximum Extinction Coefficients (ε_{max})

The $\boldsymbol{\varepsilon_{max}}$ is a quantity for measuring the extent at which a chemical substance takes in light at a known wavelength. This is a characteristic of a chemical substance that is independent of the amount of the substance present. It is calculated using Beer-Lambert's Law,

$$\varepsilon_{max} = \frac{A}{cl} \qquad (4.7)$$

A: absorbance

ε_{max}: molar extinction coefficient at the selected absorption wavelength ((L / mol . cm))

c: concentration (mol / L)

l: pathlength (cm)

ε_{max} Calculation of BP-PDD:

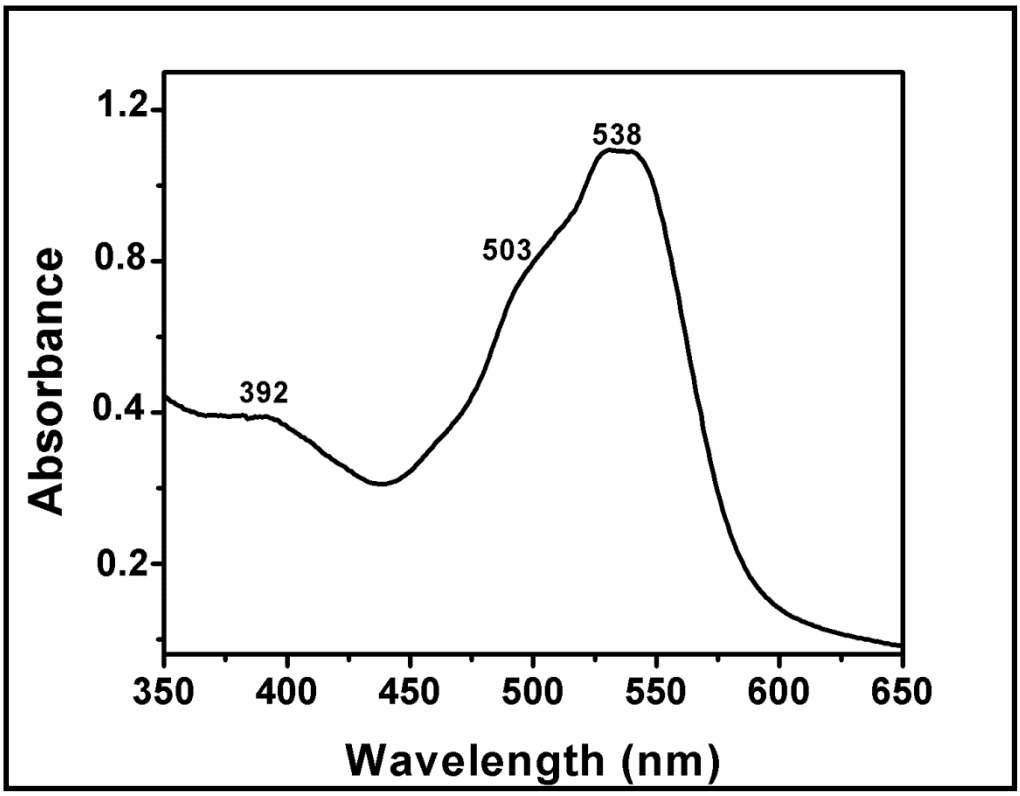

Figure 4.1: Absorption Spectrum of BP-PDD in Chloroform at 1 x 10-5 M

The absorption spectrum of BP-PDD showed the absorption at 1.129 for the concentration of 1 x 10^{-5} M at the wavelength, (λ_{max}) 538 nm.

$$\varepsilon_{max} = \frac{1.129}{1 \times 10^{-5}\ M \times 1\ cm} = 112900\ L\ /\ mol.\ cm$$

$$\varepsilon_{max} = 112900\ L\ /\ mol.\ cm$$

The molar absorptivity for other synthesized compounds were calculated in the same manner and the results were tabulated in the table below (Table 1.3).

Table 1.3: Molar absorptivity data of BP-PDD, BP-PPD and TPE-PDI

Compound	Concentration	Absorbance	λ_{max}	ε_{max} (L / mol . cm)
BP-PDD	1 x 10^{-5} M	1.129	538 nm	112900 (133300)*
BP-PPD	1 x 10^{-4} M	0.166	528 nm	6390 (7142)*
TPE-PDI	1 x 10^{-5} M	1.700	526 nm	170000 (183330)*

* : The results were calculated from the slope of the graphs plotted for each compound

Using the plot of absorbance versus concentration to calculate ε_{max}, five different concentrations of the compound's solutions were prepared and their maximiun absorbances were determined (Table 1.4). Then the graph was plotted and its slope was calculated which is the maximum extinction coefficient of the compound.

Table 1.4: Concentrations with their absorbances of BP-PDD, λmax = 538 nm

Concentration (M)	Absorbance
3 x 10^{-6}	0.352
4 x 10^{-6}	0.414
6 x 10^{-6}	0.787
8 x 10^{-6}	0.920
1 x 10^{-5}	1.129

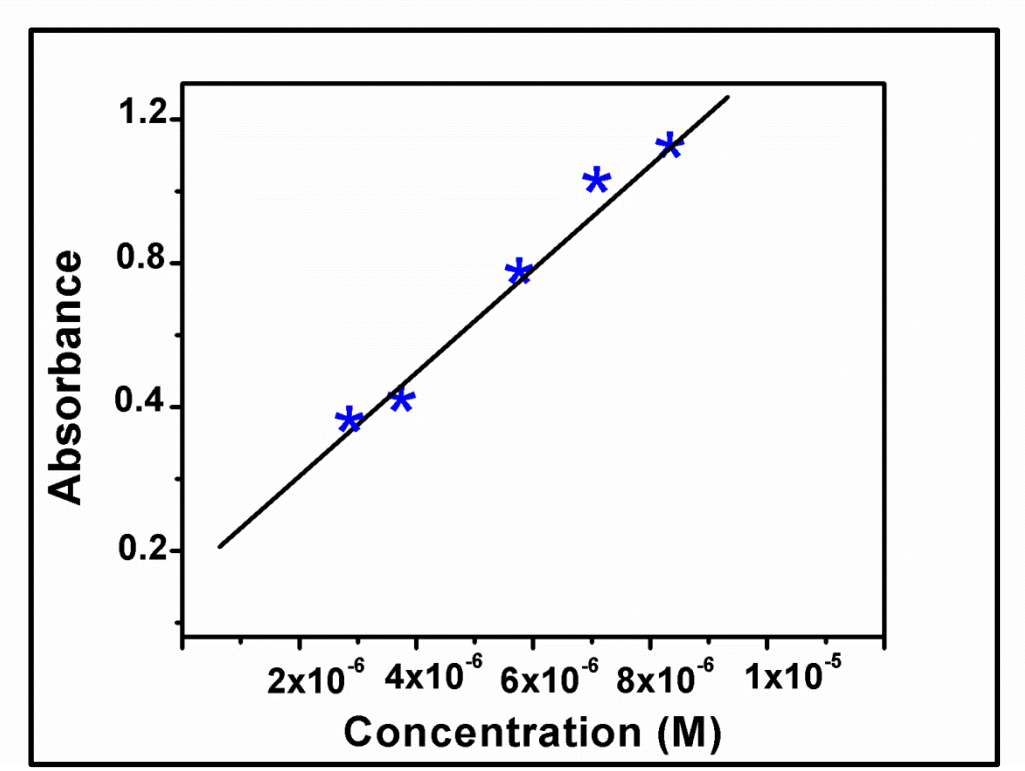

Figure 4.2: Graph of Absorbance versus Concentration of BP-PDD in Chloroform

The slope of the graph, ε_{max}, is 133300 L/mol.cm

In the same manner, ε_{max} of other two compounds were determined in several solvents, calculating their slopes from the plots of different concentrations versus absorbances and and the results are shown in the Tables 1.5-1.7. These results were used for further calculations.

Table 1.5: Molar absorptivity data of BP-PDD in several solvents

Solvent	**λ_{max}**	**ε_{max} (L / mol . cm)**
TCE	543	145000
$CHCl_3$	538	133300
DCM	532	107000
EtOH	523	31500
MeOH	516	9120
DMF	527	80000
DMSO	524	71000

Table 1.6: Molar absorptivity data of BP-PPD in several solvents

Solvent	**λ_{max}**	**ε_{max} (L / mol . cm)**
TCE	532	3610
$CHCl_3$	528	1660
DCM	519	947
EtOH	532	2170
MeOH	550	3240
DMF	524	7142
DMSO	525	3850

Table 1.7: Molar absorptivity data of TPE-PDI in several solvents.

Solvent	λ_{max}	ε_{max} **(L / mol . cm)**
TCE	529	176800
$CHCl_3$	526	183330
DCM	524	162900
EtOH	520	16310
MeOH	516	15770
NMP	525	161100
DMF	524	123000
DMSO	526	122000

4.2.2 Fluorescence Quantum Yields (Φ_f)

When a substance or compound absorb light or other electromagnetic radiation and later emits such light, this process is called fluorescence. The **(Φ_f)** provides the information about the effectiveness of the fluorescence process. It can be explained as the ratio of the number of photons released to the number of photons or light taken in.

$$\phi_f = \frac{A_{std}}{A_u} \times \frac{S_u}{S_{std}} \times \left[\frac{n_u}{n_{std}}\right]^2 \times \phi_{std} \qquad \textbf{(4.8)}$$

Φ_f (U): Fluorescence quantum yield of unknown

A_{std}: Absorbance of the reference at the excitation wavelength

A_u: Absorbance of the unknown at the excitation wavelength

S_{std}: The integrated emission area across the band of reference

S_u : The integrated emission area across the band of unknown

n_{std} : Refractive index of reference solvent

n_u : Refractive index of unknown solvent

Φ_{std} : Fluorescence quantum yield of reference [104]

The N,N'-bis(dodecyl)-3,4,9,10-perylenebis(discarboximide) in chloroform (Φ_f = 1) [104] was used as standard for Φ_f measurements of the compounds synthesized . The excitation wavelength, λ_{max} used for synthesized compounds was 485 nm so was the standard. Since the measurements were taken in different solvents, it is necessary to use refractive indexes of solvents used. Refractive index correction is used mainly because as irradiation passes from solution into the atmosphere which is from upper to lower index area, its intensity changes due to refraction.

Φ_f Calculation of BP-PDD :

Φ_{std} = 1 when the solvent is chloroform

A_{std} = 0.1009

A_u = 0.1010

S_{std} = 3096.3 counts / (cm.sec)

S_u = 1505.9 counts / (cm.sec)

n_{CHL} = 1.4458

From Equation 4.2;

$$\boldsymbol{\Phi_f(\text{BP PDD}) = \frac{0.1009}{0.1010} \times \frac{1505.9}{3096.3} \times \left[\frac{1.4458}{1.4458}\right]^2 \times 1 = 0.49}$$

Φ_f of BP-PDD = 0.49

The **Φ_f** values of BP-PDD, BP-PPD and TPE-PDI were calculated in several solvents, shown in the table given below (Table 1.8).

Table 1.8: Φf of BP-PDD, BP-PPD and TPE-PDI in several solvents

Solvent	BP-PDD	BP-PPD	TPE-PDI
	Φ_f	Φ_f	Φ_f
TCE	0.41	0.25	0.43
$CHCl_3$	0.49	0.087	0.48
DCM	0.50	0.099	0.61
EtOH	0.09	0.067	0.54
MeOH	0.04	0.14	0.42
NMP	-	-	0.18
DMF	0.20	0.11	0.33
DMSO	0.06	0.098	0.08

4.2.3 Half-width of the Selected Absorption ($\Delta\bar{\nu}_{1/2}$)

The $\Delta\bar{\nu}_{1/2}$ is generally considered as whole width at half maximum absorption which is defined as full or half-width of the curve at half of a maximum intensity [105].

$$\Delta\bar{\nu}_{1/2} = \bar{\nu}_I - \bar{\nu}_{II} \qquad \textbf{(4.9)}$$

$\bar{\nu}_I, \bar{\nu}_{II}$: The frequencies from the absorption spectrum in cm^{-1}

$\Delta\bar{\nu}_{1/2}$: Half-width of the selected maximum absorption in cm^{-1}

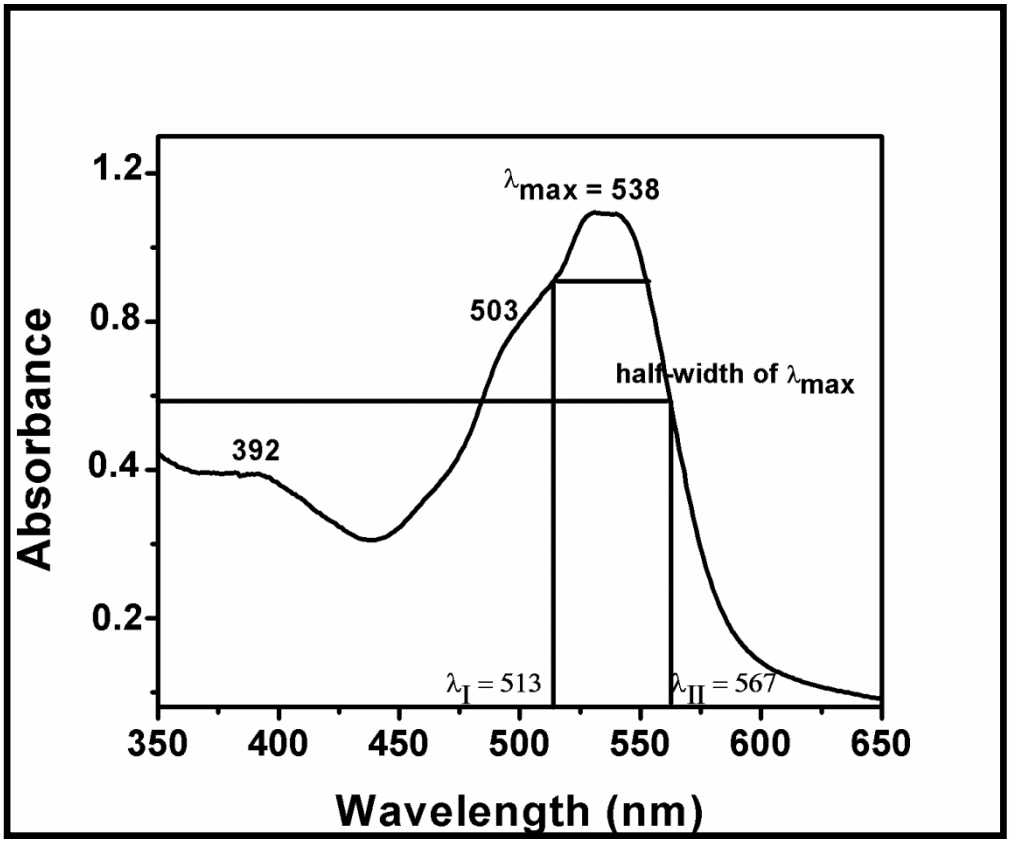

Figure 4.3: Representative Figure on how to Calculate the Half-width of BP-PDD in $CHCl_3$

Calculating the $\Delta\overline{\nu}_{1/2}$ of BP-PDD in $CHCl_3$

λ_{max} = 538 nm

$$\lambda_{max=} 538\ nm \times \frac{10^{-9}}{1\ nm} \times \frac{100\ cm}{1\ m} = 5.38 \times 10^{-5}\ cm$$

$$\overline{V}_{\max} = \frac{\mathbf{1}}{\boldsymbol{\lambda_{max}}} = \frac{\mathbf{1}}{5.38 \times 10^{-5}\ cm} = 18587.36\ cm^{-1}$$

λ_I = 513 nm

$$\lambda_{I=} 513\ nm \times \frac{10^{-9}}{1\ nm} \times \frac{100\ cm}{1\ m} = 5.13 \times 10^{-5}\ cm$$

$$\overline{V}_I = \frac{\mathbf{1}}{\boldsymbol{\lambda_I}} = \frac{\mathbf{1}}{5.13\times 10^{-5}\ cm} = 19493.18\ cm^{-1}$$

λ_{II} = 567 nm

$$\lambda_{II=} 567\ nm \times \frac{10^{-9}}{1\ nm} \times \frac{100\ cm}{1\ m} = 5.67 \times 10^{-5}\ cm$$

$$\bar{\nu}_{II} = \frac{1}{\lambda_{II=}} = \frac{1}{5.67\times 10^{-5}\ cm} = 17636.68\ cm^{-1}$$

From Equation 4.3,

$$\Delta\bar{\nu}_{1/2} = \bar{\nu}_I - \bar{\nu}_{II}$$

$$\Delta\bar{\nu}_{1/2} = 1856.5\,\text{cm}^{-1}$$

4.2.4 Theoretical Radiative Lifetimes (τ_o)

Theoretical radiative lifetime is the lifetime of an excited molecule or compound where there is no radiationless transition. The following equation 4.10 was used to calculate the theoretical radiative lifetimes [104].

$$\tau_0 = \frac{3.5\times 10^8}{\bar{\nu}_{\max}^2 \varepsilon_{\max} \Delta\bar{\nu}_{1/2}} = \frac{3.5\times 10^8}{\lambda_{\max}^2 \varepsilon_{\max} \Delta\bar{\nu}_{1/2}}$$

(4.10)

τ_o : Theoretical radiative lifetime (ns)

$\bar{\nu}_{\max} = \lambda_{\max}$: Wavenumbers (cm^{-1})

ε_{max} : The maximum extinction coefficient at the maximum absorption wavelength

$\Delta\bar{\nu}_{1/2}$: Half-width of the selected absorption (cm^{-1})

τ_o of BP-PDD:

Using Equation 4.10, theoretical radiative lifetime of BP-PDD in $CHCl_3$ was calculated.

$$\tau_0 = \frac{3.5\times 10^8}{\lambda_{\max}^2 \varepsilon_{\max} \Delta\bar{\nu}_{1/2}}$$

$$\tau_0 = \frac{3.5\times 10^8}{(18587.36)^2 \times 133300 \times 1856.5}$$

$$\tau_0 = 2.23 \times 10^{-9} \text{ sec} \times \frac{1 \text{ ns}}{10^{-9} \text{sec}} = 2.23 \text{ ns}$$

$$\boldsymbol{\tau_o = 2.23 \text{ ns}}$$

The theoretical radiative lifetimes of BP-PDD, BP-PPD and TPE-PDI were calculated from equation 4.4 in several solvents and tabulated in Tables 1.9 – 1.11.

Table 1.9: Theoretical radiative lifetimes of BP-PDD in several solvents

BP-PDD

Solvent	λ_{max} (nm)	ε_{max} (L / mol . cm)	$\bar{\nu}^2_{max} (cm^{-2})$	$\Delta\bar{\nu}_{1/2} (cm^{-1})$	τ_o (ns)
TCE	543	145000	3.39 x 10^8	5223.73	1.36
$CHCl_3$	538	133300	3.45 x 10^8	3415.95	2.23
DCM	532	107000	3.53 x 10^8	5320.92	1.74
EtOH	527	31500	3.60 x 10^8	4961.25	6.21
MeOH	519	9120	3.71 x 10^8	5529.65	18.72
DMF	527	80000	3.60 x 10^8	5060.41	2.40
DMSO	524	1000	3.60 x 10^8	5215.17	2.59

Table 1.10: Theoretical radiative lifetimes of BP-PPD in several solvents

BP-PPD

Solvent	λ_{max} (nm)	ε_{max} (L / mol . cm)	$\bar{\nu}^2{}_{max}\,(cm^{-2})$	$\Delta\bar{\nu}_{1/2}(cm^{-1})$	τ_o (ns)
TCE	532	3610	3.53×10^8	7255.38	38.04
$CHCl_3$	528	1660	3.59×10^8	5613.49	106.06
DCM	519	947	3.71×10^8	4368.71	233.33
EtOH	532	2170	3.53×10^8	5640.41	81.40
MeOH	550	3240	3.31×10^8	5833.89	55.56
DMF	525	7142	3.63×10^8	3741.54	36.08
DMSO	524	3850	3.64×10^8	5340.39	46.67

Table 1.11: Theoretical radiative lifetimes of TPE-PDI in several solvents

TPE-PDI

Solvent	λ_{max} (nm)	ε_{max} (L / mol . cm)	$\bar{\nu}^2{}_{max}\,(cm^{-2})$	$\Delta\bar{\nu}_{1/2}(cm^{-1})$	τ_o (ns)
TCE	529	176800	3.57×10^8	4757	1.16
$CHCl_3$	526	183330	3.61×10^8	3772	1.40
DCM	524	162900	3.64×10^8	4874	1.21
EtOH	516	16310	3.76×10^8	3768	15.22
MeOH	520	15770	3.70×10^8	6718	8.93
NMP	525	161100	3.63×10^8	5511	1.09
DMF	524	123000	3.64×10^8	4772	1.64
DMSO	526	122000	3.61×10^8	5068	1.57

4.2.5 Theoretical Fluorescence Lifetimes (τ_f)

Theoretical fluorescence lifetime is the average period a molecule stays in an excited state prior to going back to the ground state (emitting a photon). $\boldsymbol{\tau_f}$ were calculated via the equation 4.11 presented below.

$$\boldsymbol{\tau_f = \tau_0 \text{ x } \Phi_f} \qquad \textbf{(4.11)}$$

τ_f : Fluorescence lifetime (ns)

τ_o : Theoretical radiative lifetime (ns)

Φ_f : Fluorescence quantum yield

τ_f of BP-PDD

The τ_f of the compounds were calculated using the results from the theoretical radiative lifetimes and fluorescence quantum yields and tabulated in Table 1.12. For compound BP-PDD, ($CHCl_3$)

τ_f = 2.23 ns x 0.49 = 1.09 ns

Table 1.12: Theoretical fluorescence lifetimes of BP-PDD, BP-PPD and TPE-PDI in several solvents

Solvent	BP-PDD (ns)	BP-PPD (ns)	TPE-PDI (ns)
TCE	0.56	9.51	0.50
$CHCl_3$	1.09	9.23	0.67
DCM	0.87	23.10	0.74
EtOH	0.57	5.45	8.22
MeOH	0.75	7.78	3.75
DMF	0.48	3.97	0.52
NMP	-	-	0.20
DMSO	0.16	4.57	0.13

4.2.6 Theoretical Fluorescence Rate Constant (k_f)

The fluorescence rate constant is the speed of impulsive emission of radiation of a molecule [105].

$$k_f = 1/\tau_0 \qquad (4.12)$$

k_f: Fluorescence rate constant (s^{-1})

$\tau_{0:}$ Theoretical radiative lifetime (s)

k_f of BP-PDD

The k_f of compounds were calculated using the results from the theoretical radiative lifetimes and tabulated in Table 1.13. For compound BP-PDD, ($CHCl_3$)

$k_f = 1/2.23 \times 10^{-9}\ s^{-1} = 4.50 \times 10^{8}\ s^{-1}$

Table 1.13: Fluorescence rate constant data of BP-PDD, BP-PPD and TPE-PDI in several solvents

Solvent	BP-PDD (s^{-1})	BP-PPD (s^{-1})	TPE-PDI (s^{-1})
TCE	7.35×10^8	0.26×10^8	6.06×10^8
$CHCl_3$	4.50×10^8	0.09×10^8	7.14×10^8
DCM	5.75×10^8	0.04×10^8	8.26×10^8
EtOH	1.61×10^8	0.12×10^8	0.66×10^8
MeOH	0.53×10^8	0.18×10^8	1.12×10^8
DMF	4.17×10^8	0.28×10^8	6.34×10^8
NMP	-	-	9.17×10^8
DMSO	3.86×10^8	0.21×10^8	6.10×10^8

4.2.7 Radiationless Deactivation Rate Constants (k_d)

The radiationless deactivation rate constant of the synthesized compounds were calculated by the formula,

$$k_d = (k_f / \Phi_f) - k_f \quad \textbf{(4.13)}$$

k_d: Rate constant of radiationless deactivation (s^{-1})

k_f: Fluorescence rate constant (s^{-1})

Φ_f: Fluorescence quantum yield

k_d of BP-PDD

The k_d of compounds were calculated using the results from the fluorescence rate constant and fluorescence quantum yield and tabulated in Table 1.14. For compound BP-PDD, ($CHCl_3$)

$k_d = (4.50 \times 10^8 / 0.49) - 4.50 \times 10^8$

$k_d = 4.68 \times 10^8\ s^{-1}$

Table 1.14: Radiationless deactivation rate constant data of BP-PDD, BP-PPD and TPE-PDI in several solvents

Solvent	BP-PDD (s^{-1})	BP-PPD (s^{-1})	TPE-PDI (s^{-1})
TCE	10.58×10^8	0.78×10^8	8.03×10^8
$CHCl_3$	4.68×10^8	0.94×10^8	7.74×10^8
DCM	5.75×10^8	0.36×10^8	5.28×10^8
EtOH	16.28×10^8	1.67×10^8	0.56×10^8
MeOH	12.72×10^8	1.10×10^8	1.55×10^8
DMF	16.68×10^8	2.27×10^8	12.87×10^8
NMP	-	-	41.77×10^8
DMSO	60.47×10^8	1.93×10^8	70.15×10^8

4.2.8 Oscillator Strength (*f*)

The dimensionless quantity, oscillator strength, describes the strength of an electronic transition and the equation below is used for its calculation.

$$f = 4.32 \times 10^{-9} \Delta \bar{\nu}_{1/2}\ \varepsilon_{max} \qquad (4.14)$$

f: Oscillator strength

$\Delta \bar{\nu}_{1/2}$: Half-width of the selected absorption (cm^{-1})

ε_{max}: The maximum extinction coefficient in L /mol · cm at the maximum absorption wavelength, λ_{max}

f of BP-PDD

The f of compounds were calculated using the results from the half-width of the selected absorption and tabulated in Table 1.15. For compound BP-PDD, ($CHCl_3$)

$$f = 4.32 \times 10^{-9} \times 3415.95 \times 133300 = 1.97$$

$$f = 1.97$$

Table 1.15: Oscillator strength data of BP-PDD, BP-PPD and TPE-PDI in several solvents

Solvent	BP-PDD	BP-PPD	TPE-PDI
TCE	3.26	0.11	3.63
$CHCl_3$	1.97	0.040	2.99
DCM	2.46	0.018	3.43
EtOH	0.68	0.059	0.27
MeOH	0.22	0.082	0.46
DMF	1.75	0.12	2.54
NMP	-	-	3.82
DMSO	1.60	0.088	2.67

4.2.9 Singlet Energies (E_s)

Singlet energy (E_s) is the least energy needed for a fluorophore to become excited from S_0 which is the ground state to the S_1 which is the first excitation energy state.

$$E_s = \frac{2.86 \times 10^5}{\lambda_{max}} \quad \textbf{(4.15)}$$

E_s: Singlet energy (kcal mol^{-1})

λ_{max}: Maximum absorption wavelength (Å)

E_s of BP-PDD

The **E_s** of compounds were calculated using the results from the maximum absorption wavelength and tabulated in Table 1.16. For compound BP-PDD, ($CHCl_3$)

$$\lambda_{max=} 538\, nm \times \frac{10^{-9} m}{1\, nm} \times \frac{1\, Å}{10^{-10} m} = 5380\, Å$$

$$\boldsymbol{E_s = \frac{2.86 \times 10^5}{5380} = 53.16\ kcal\ /\ mol}$$

Table 1.16: Singlet Energy Data of BP-PDD, BP-PPD and TPE-PDI in several solvents (kcal / mol)

Solvent	BP-PDD	BP-PPD	TPE-PDI
TCE	52.67	53.76	54.06
$CHCl_3$	53.16	54.17	54.37
DCM	53.76	55.11	54.80
EtOH	54.68	53.76	55.00
MeOH	55.43	52.00	55.43
DMF	54.27	54.58	54.58
NMP	-	-	54.48
DMSO	54.58	54.48	54.37

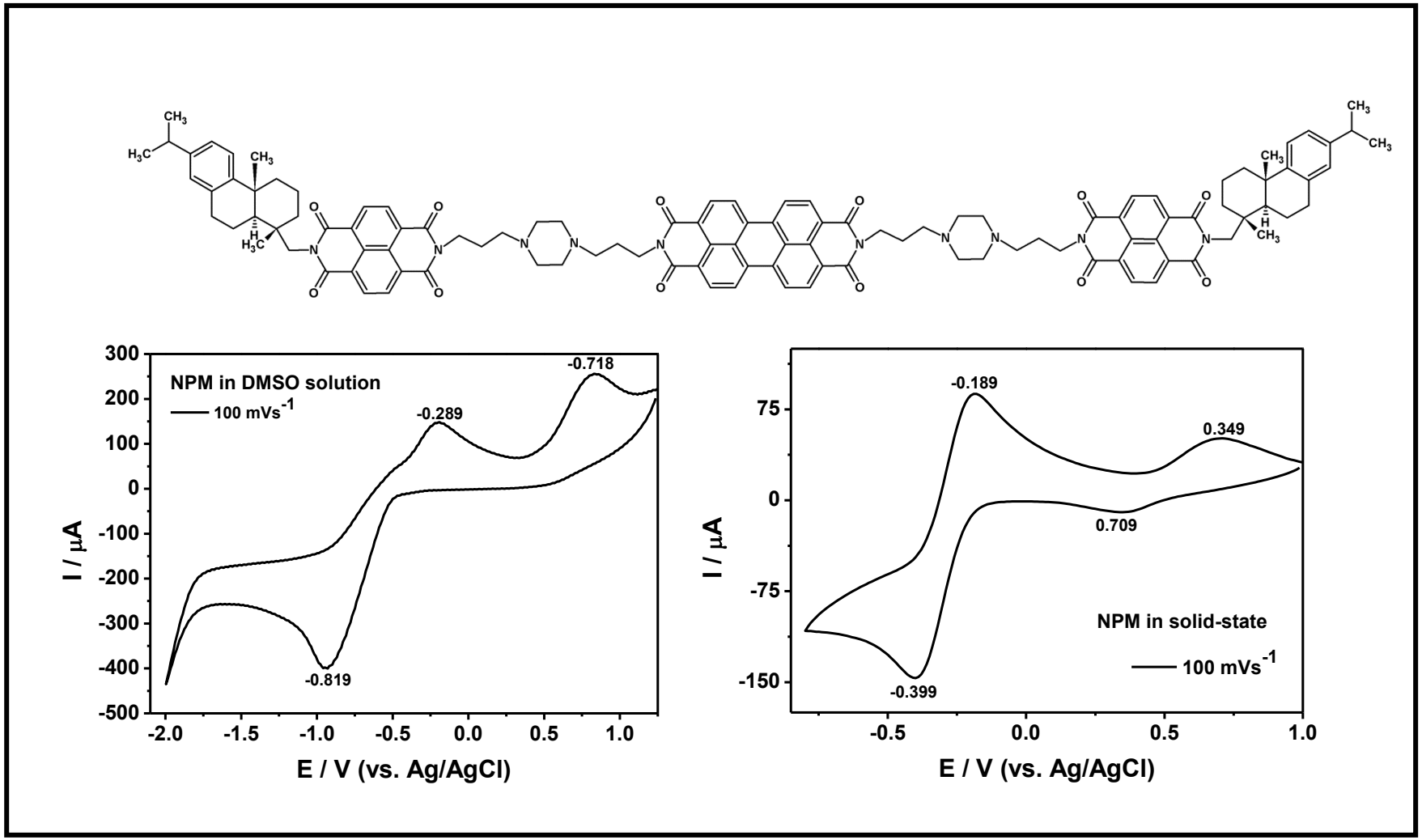

Figure 4.4: Cyclic Voltammogram of NPM at 100 mVs−1 Scan Rate in DMSO and in Solid State

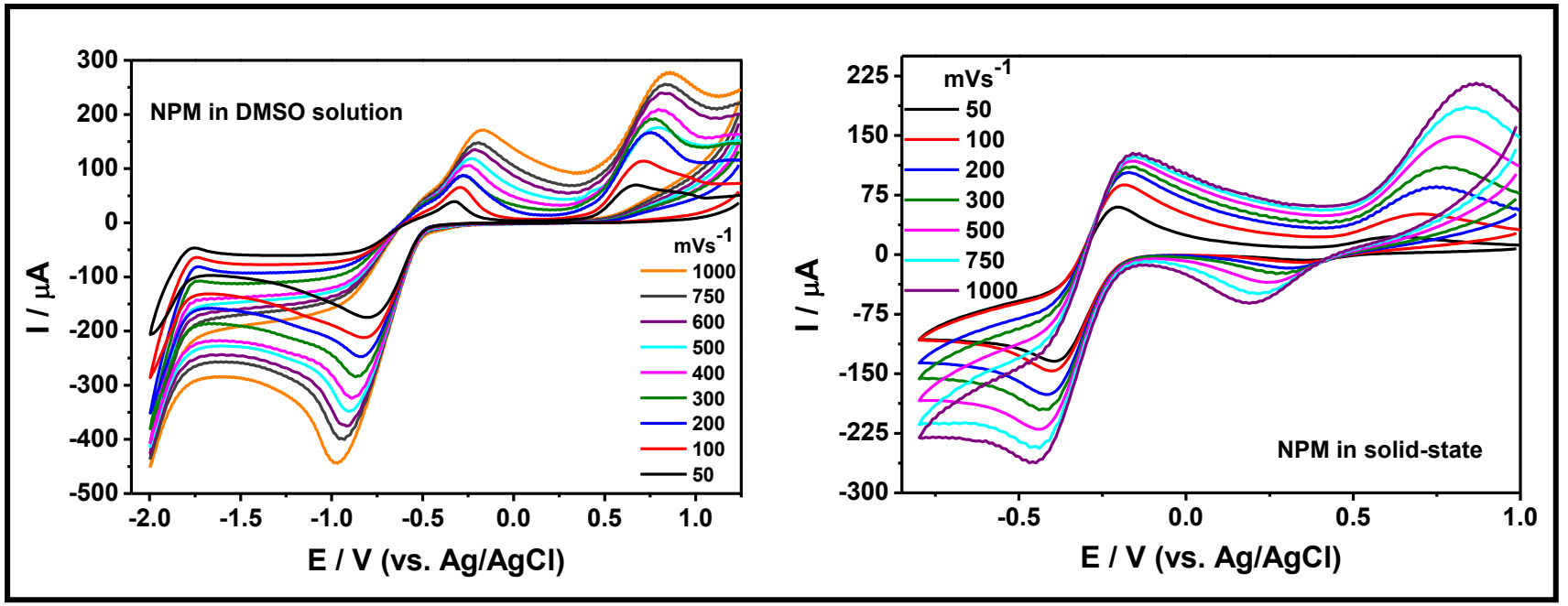

Figure 4.5: Cyclic Voltammogram of NPM at Different Scan rates (50 -1000 (mVs-1)) in DMSO and in Solid State

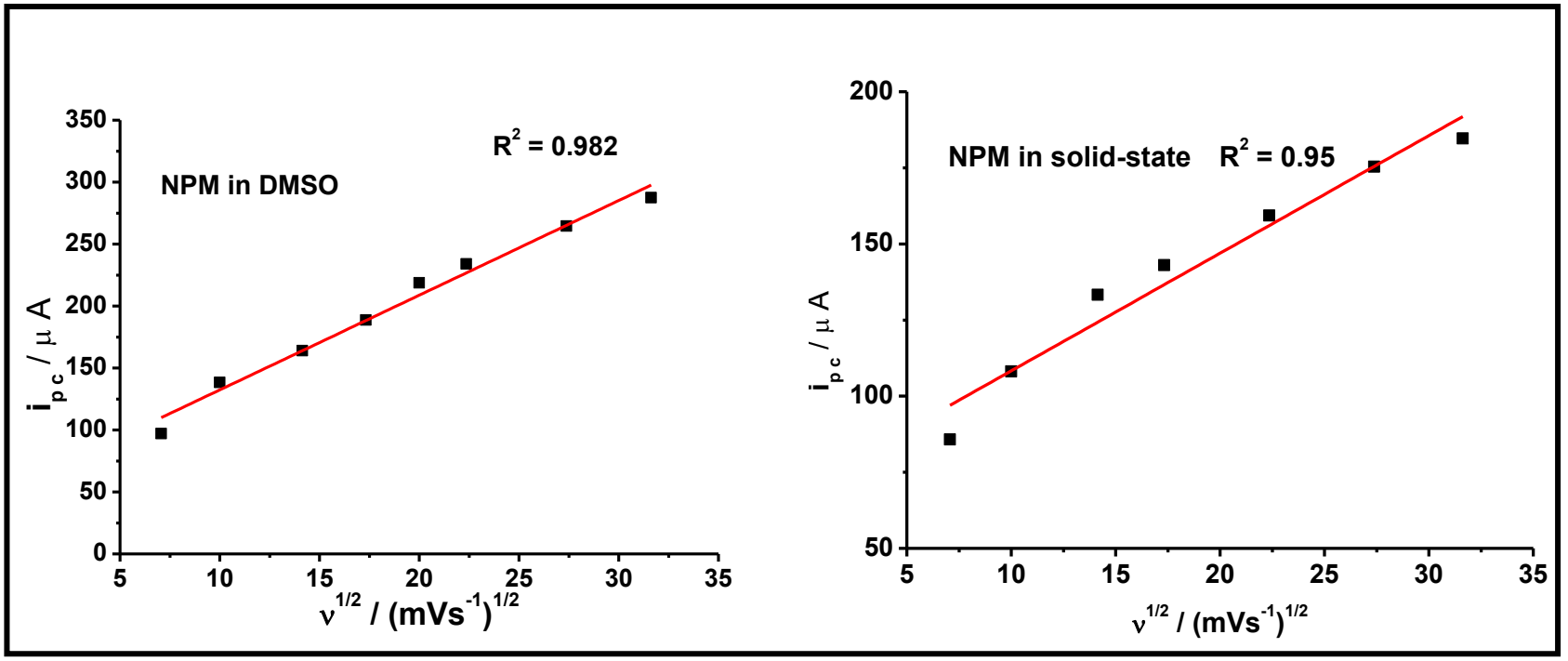

Figure 4.6: Result of Variation of Scan Rate on the ipc of NPM, Plot of ipc versus Square Root of Scan Rate in DMSO and in Solid State

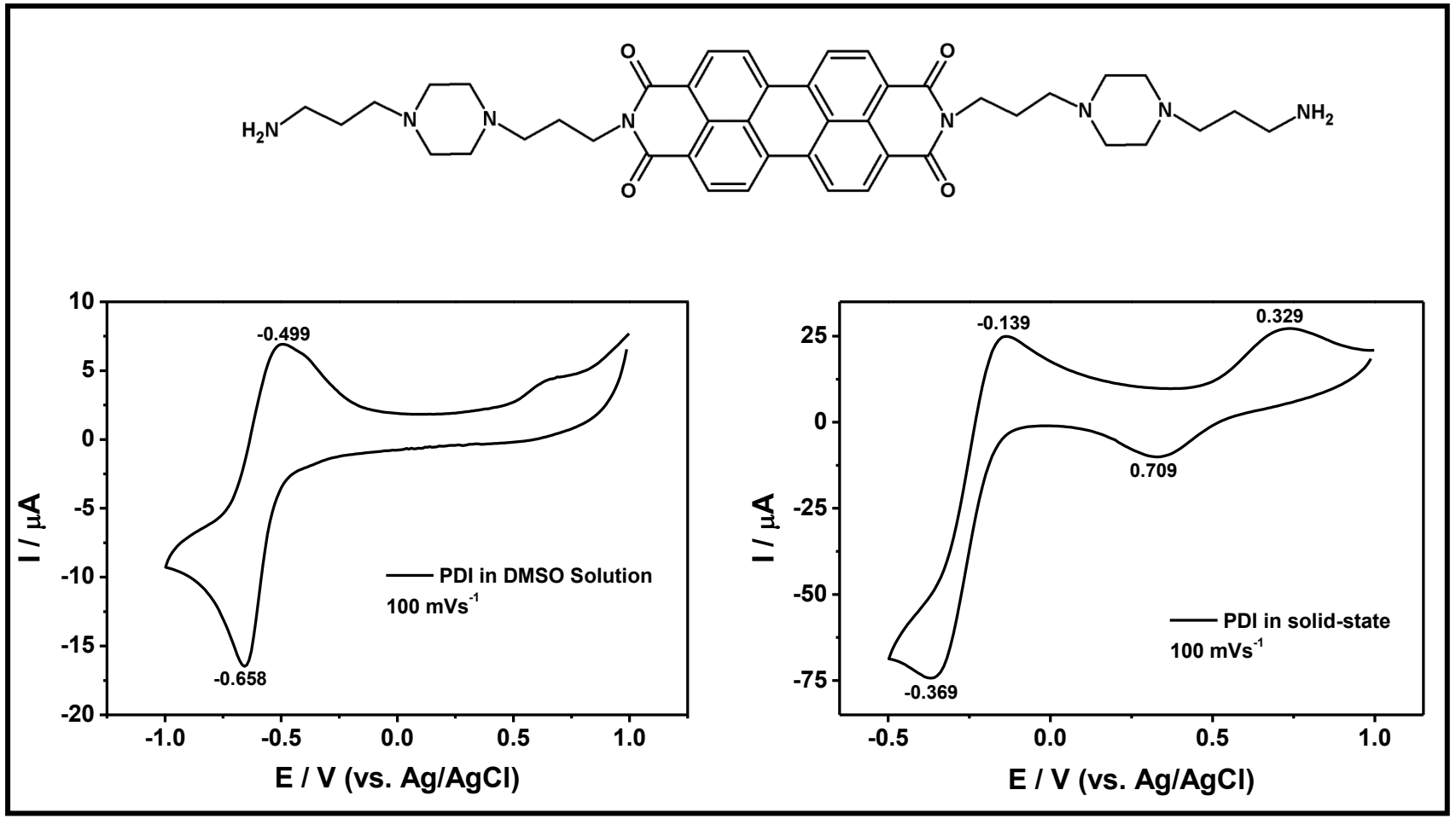

Figure 4.7: Cyclic Voltammogram of PDI at 100 mVs−1 Scan Rate in DMSO and in Solid State

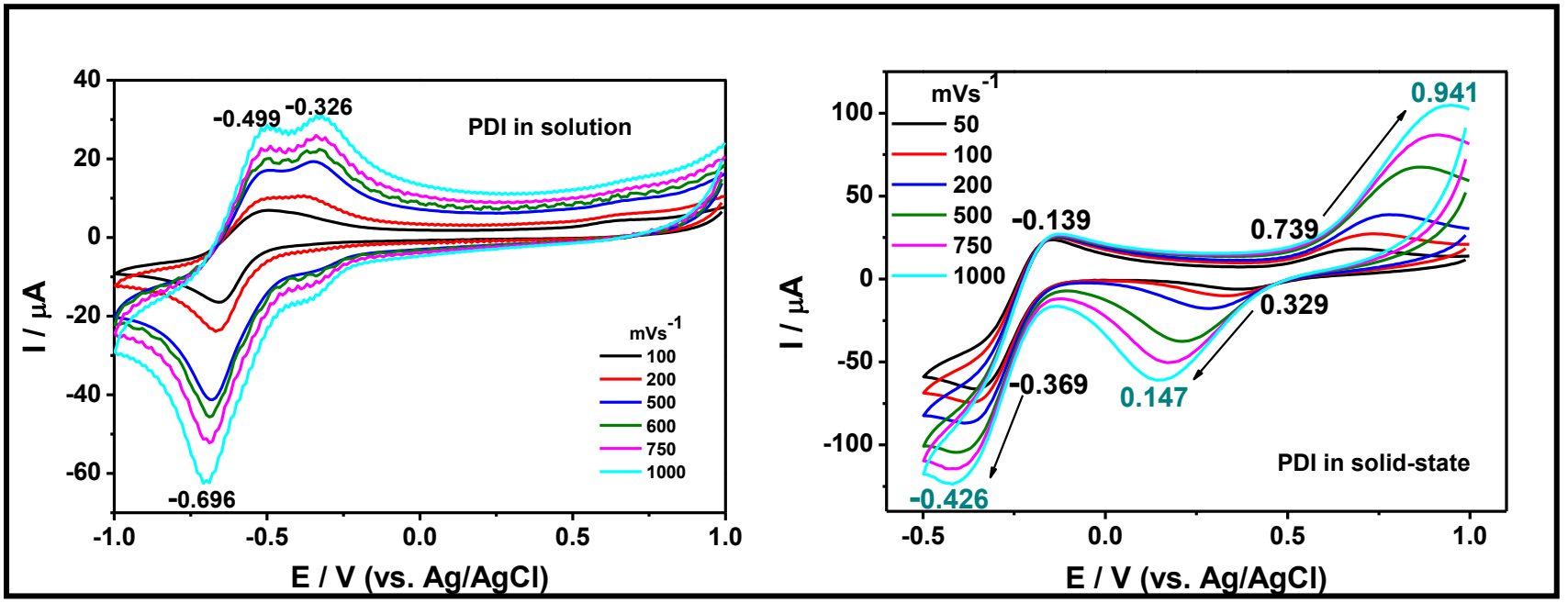

Figure 4.8: Cyclic Voltammogram of PDI at Different Scan rates (50 -1000 (mVs-1)) in DMSO and in Solid State

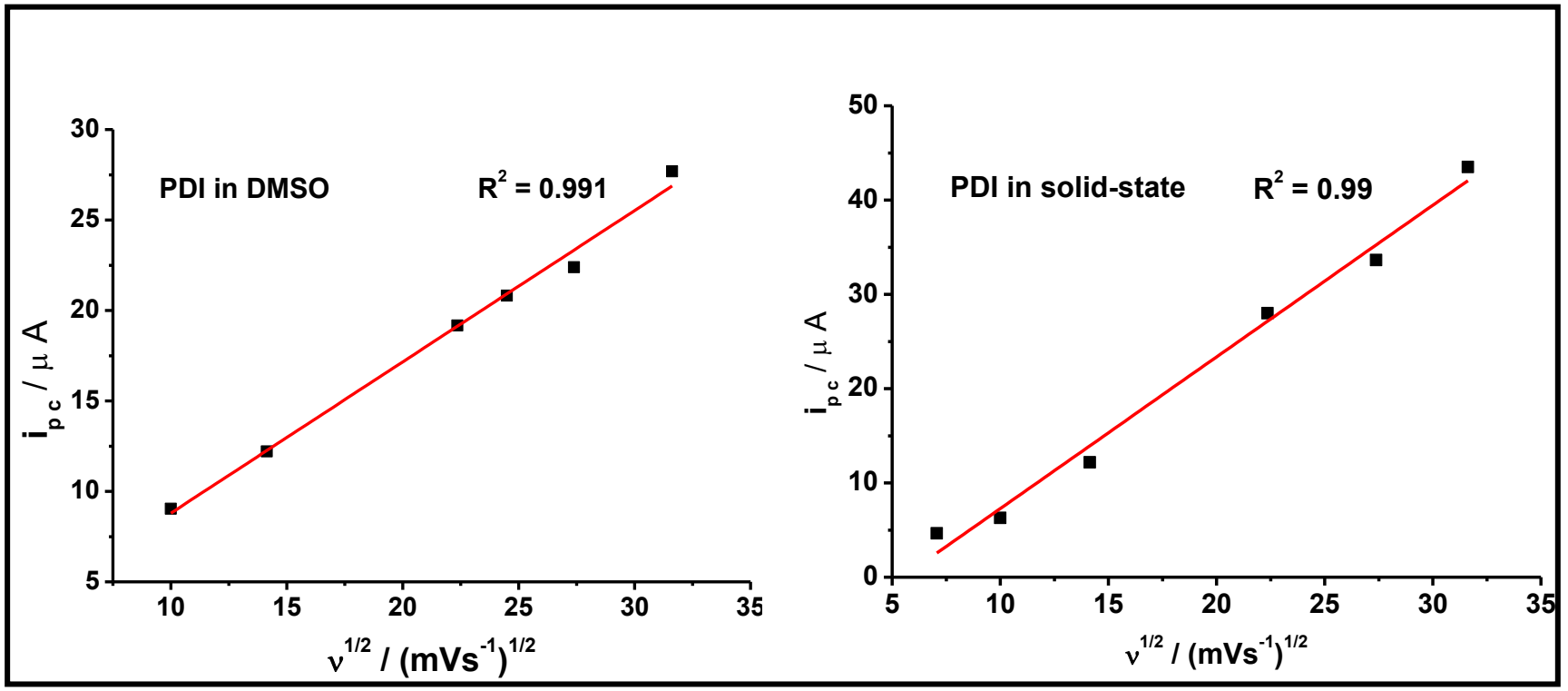

Figure 4.9: Result of Variation of Scan Rate on the ipc of PDI, Plot of ipc versus Square Root of Scan Rate in DMSO and in Solid State

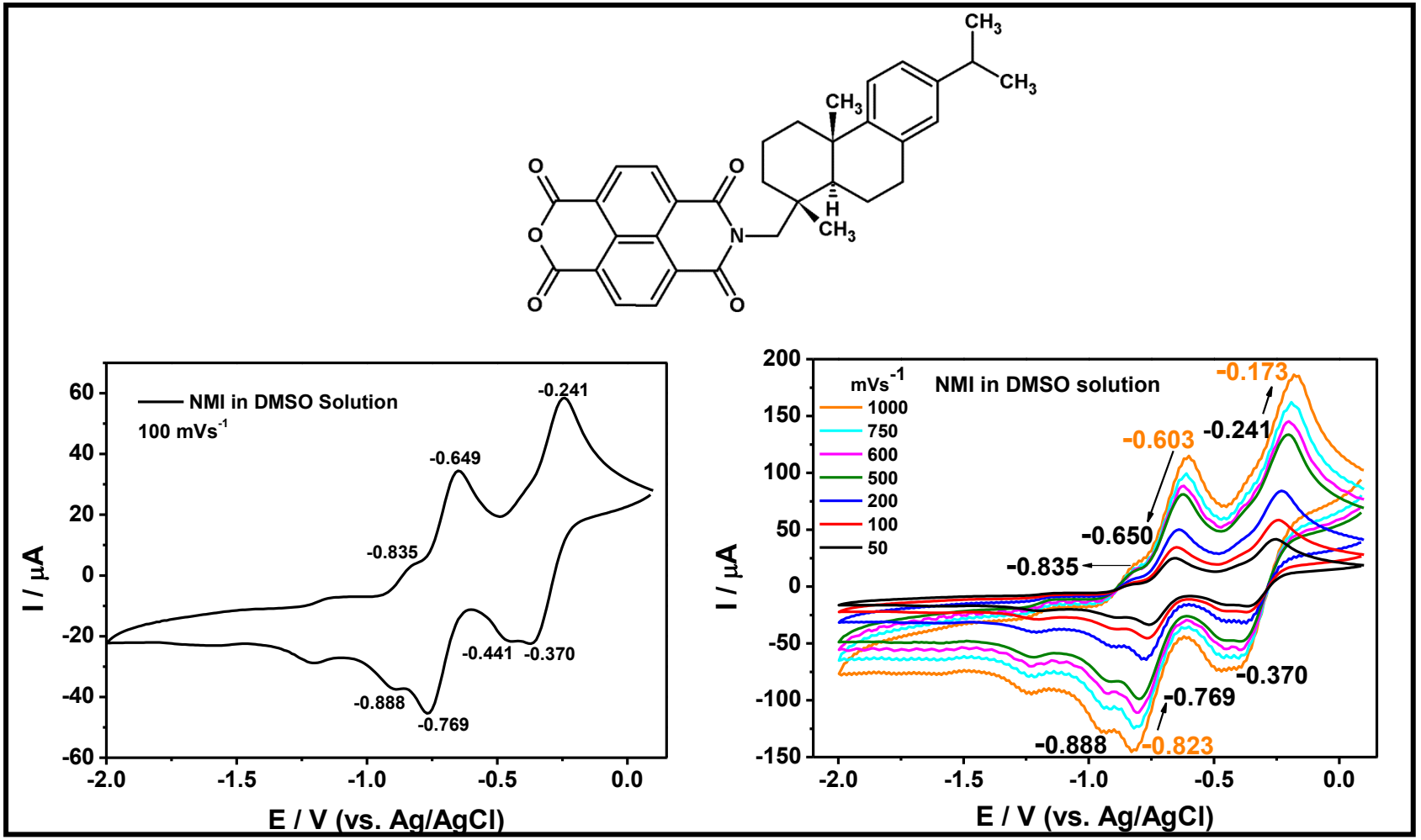

Figure 4.10: Cyclic Voltammogram of NMI, on the Left Only at 100 mVs-1 and on the Right at Different Scan rates (50 -1000 (mVs-1)) in DMSO

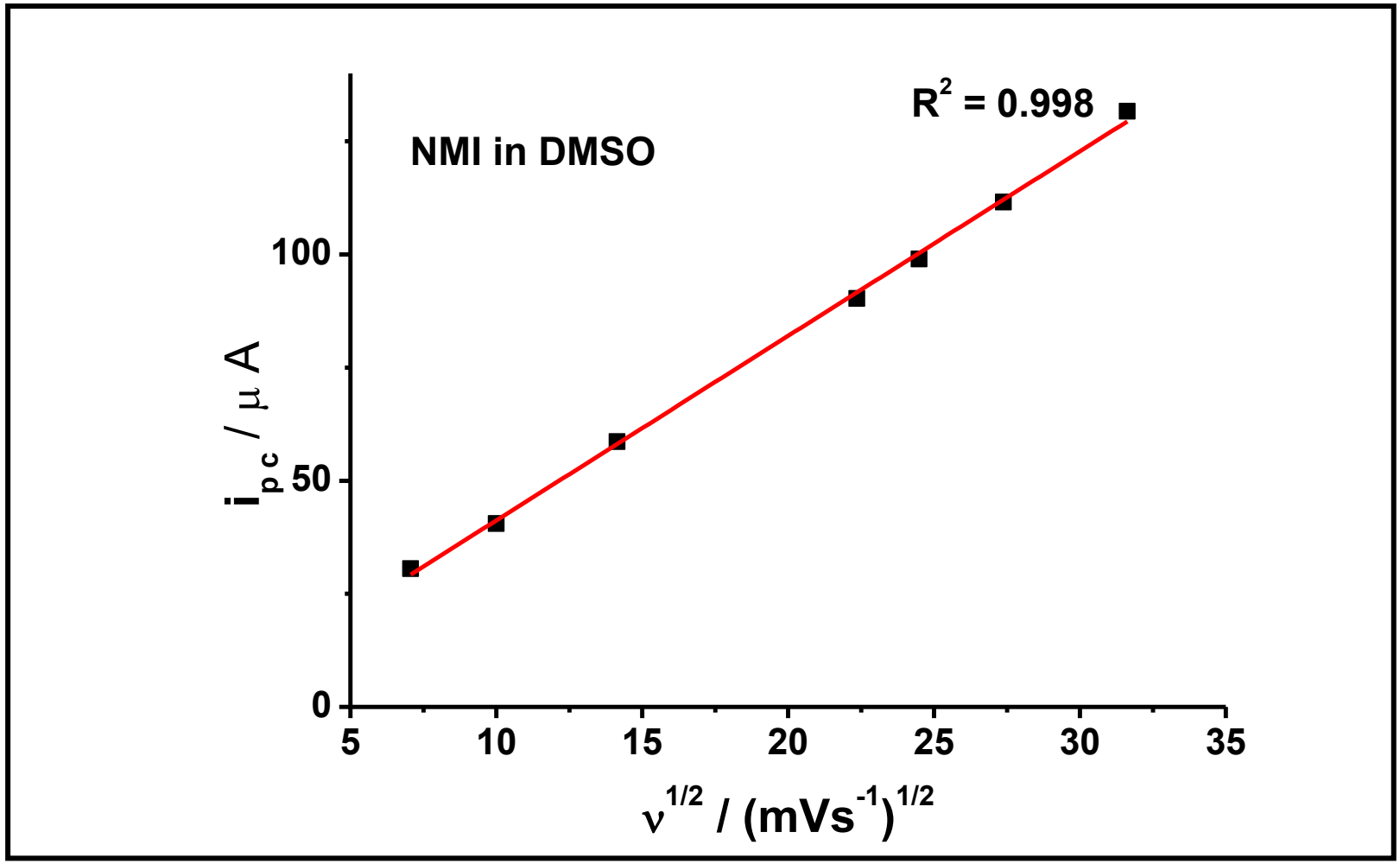

Figure 4.11: Result of Variation of Scan Rate on the ipc of NMI, Plot of ipc versus Square Root of Scan Rate in DMSO

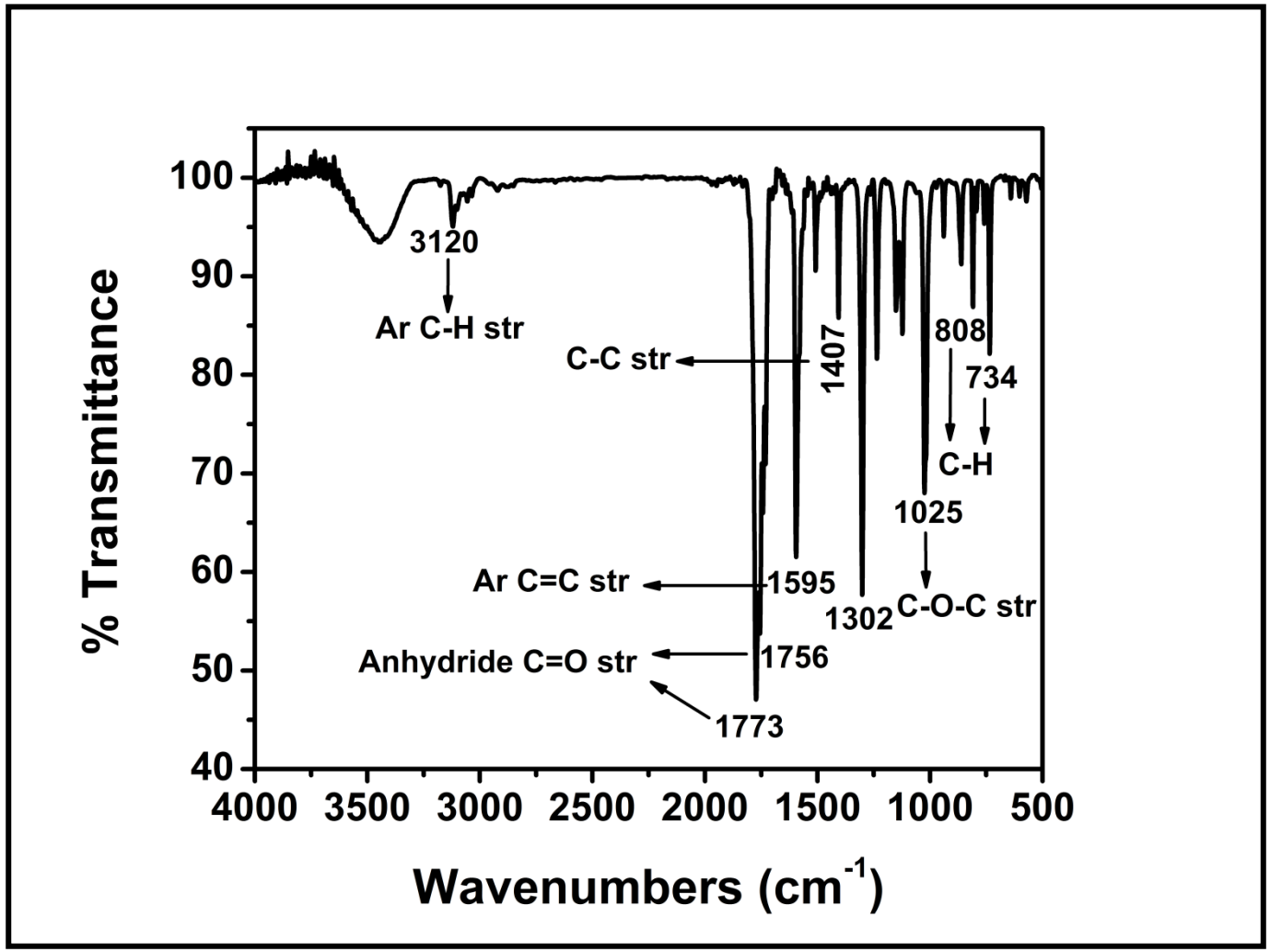

Figure 4.12: FT-IR Spectrum of PDA, (KBr Film)

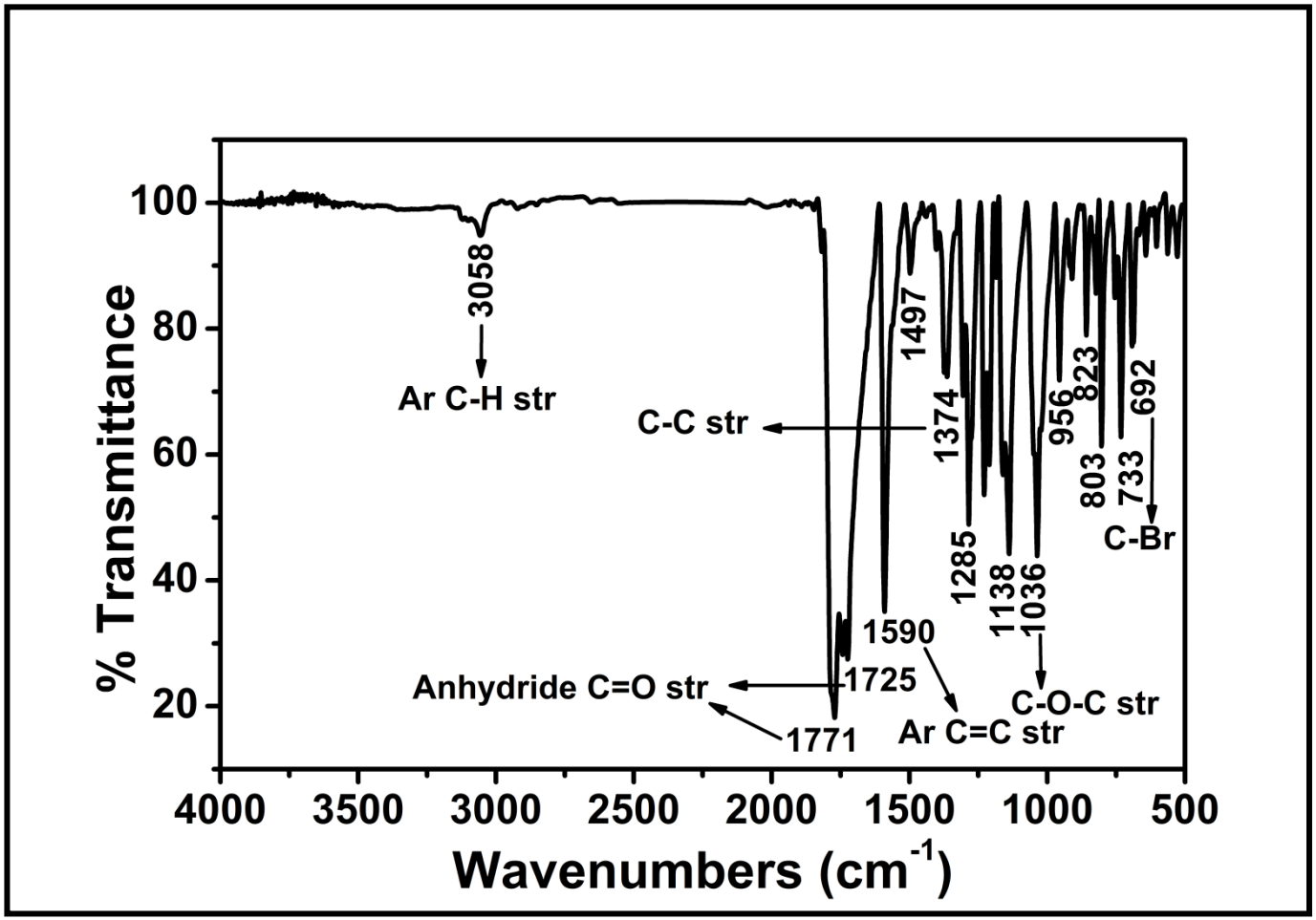

Figure 4.13: FT-IR Spectrum of PDA-Br, (KBr Film)

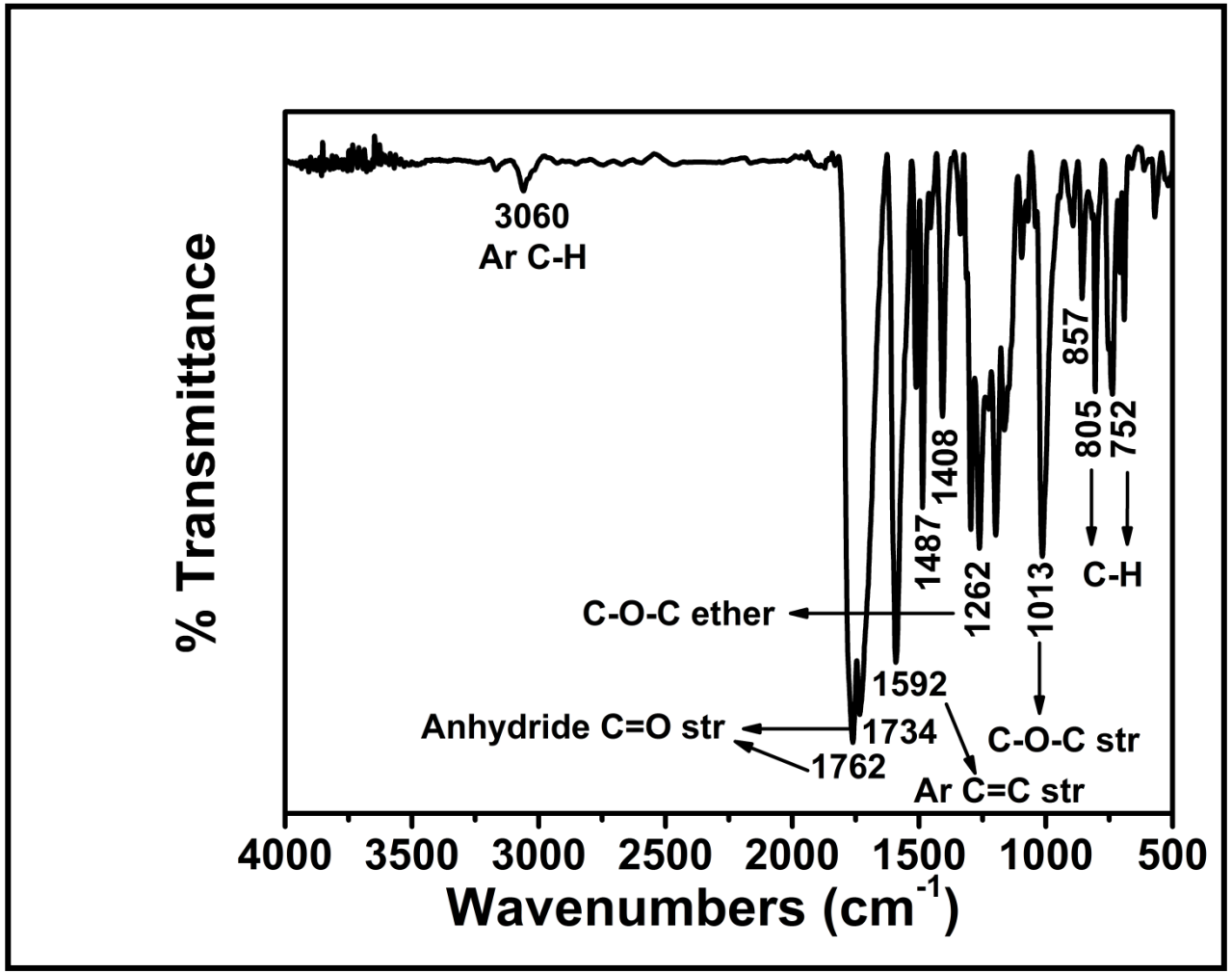

Figure 4.14: FT-IR Spectrum of BP-PDA, (KBr Film)

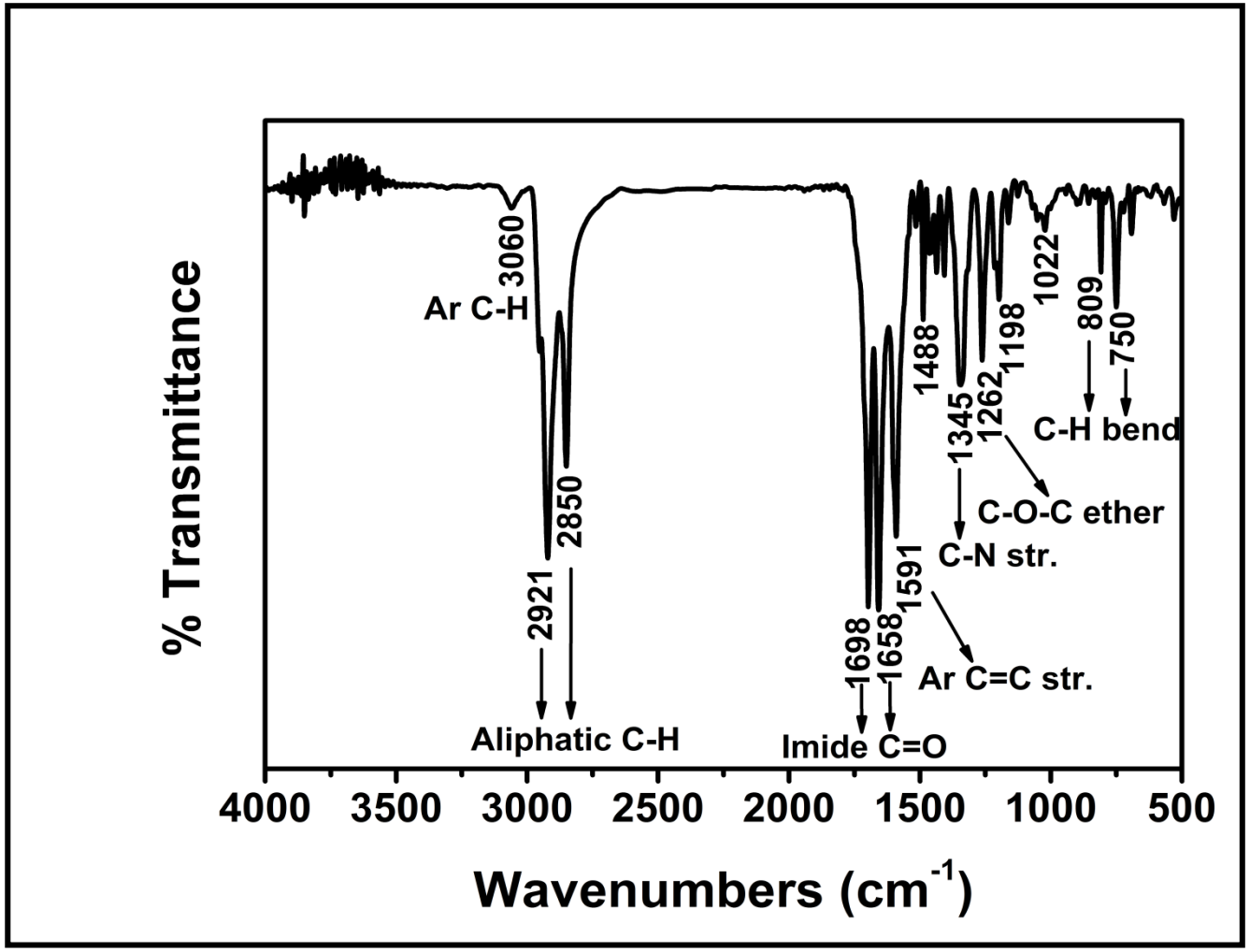

Figure 4.15: FT-IR Spectrum of BP-PDD, (KBr Film)

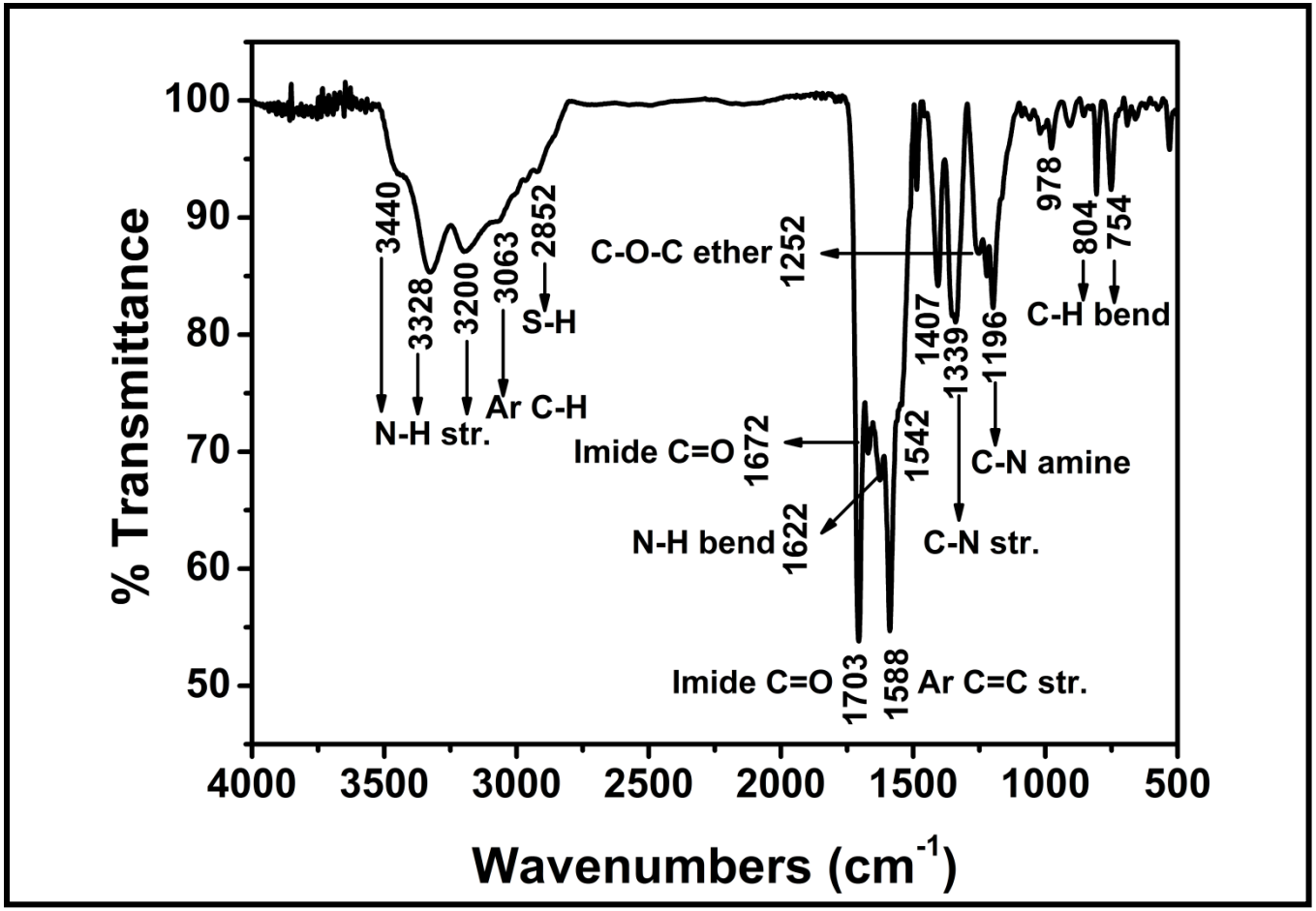

Figure 4.16: FT-IR Spectrum of BP-PPD, (KBr Film)

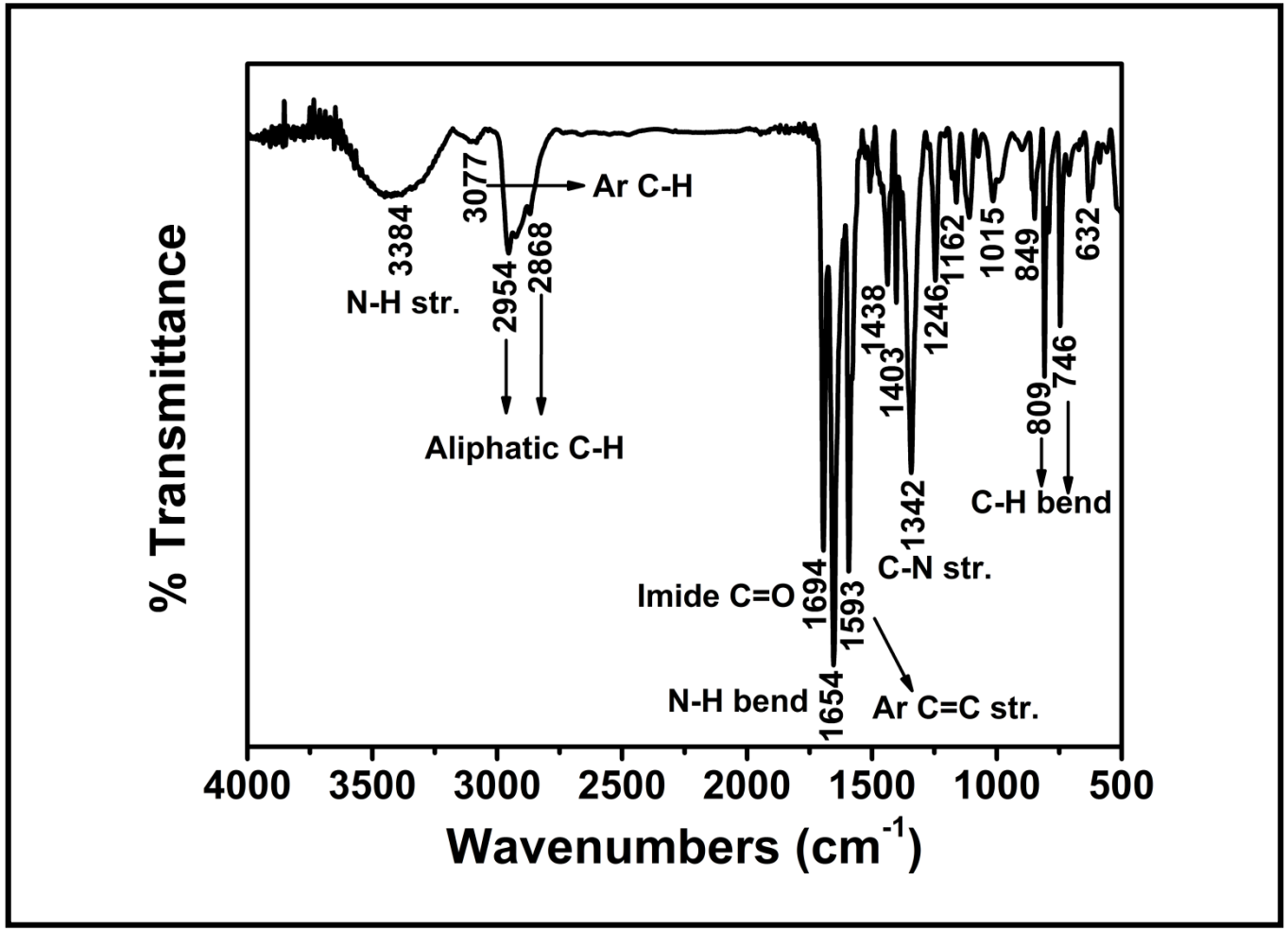

Figure 4.17: FT-IR Spectrum of T-PDI, (KBr Film)

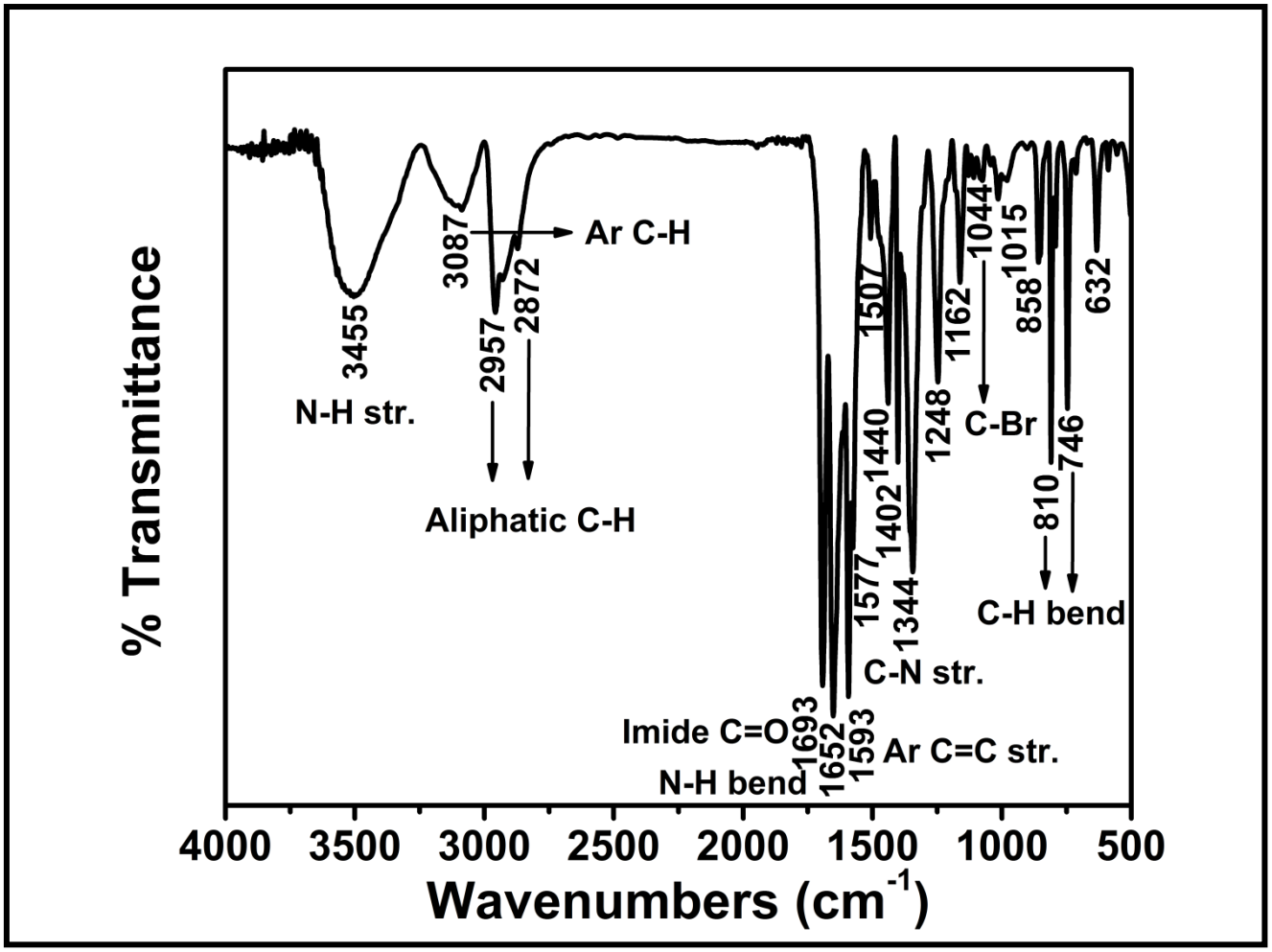

Figure 4.18: FT-IR Spectrum of TBr-PDI, (KBr Film)

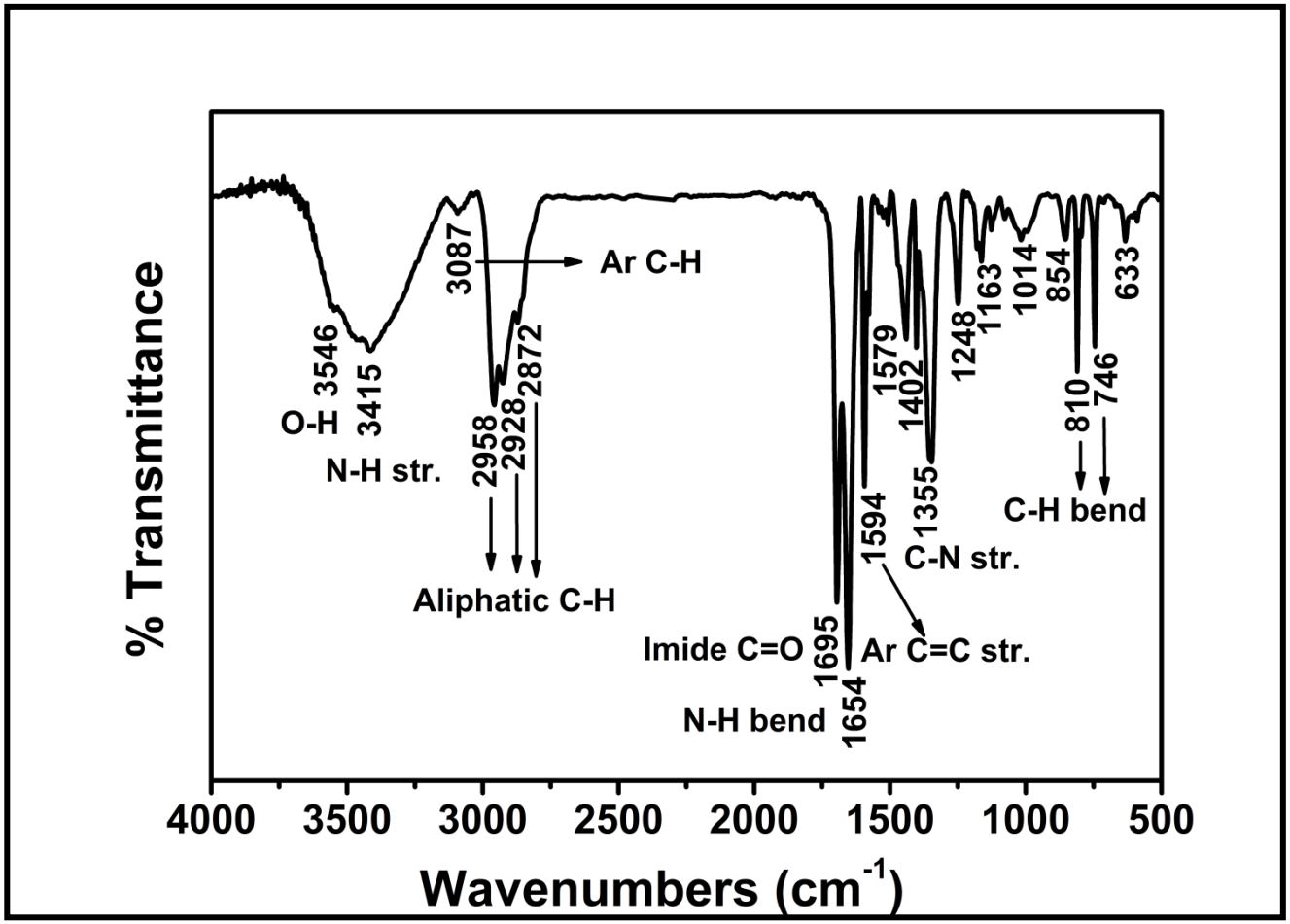

Figure 4.19: FT-IR Spectrum of TPE-PDI, (KBr Film)

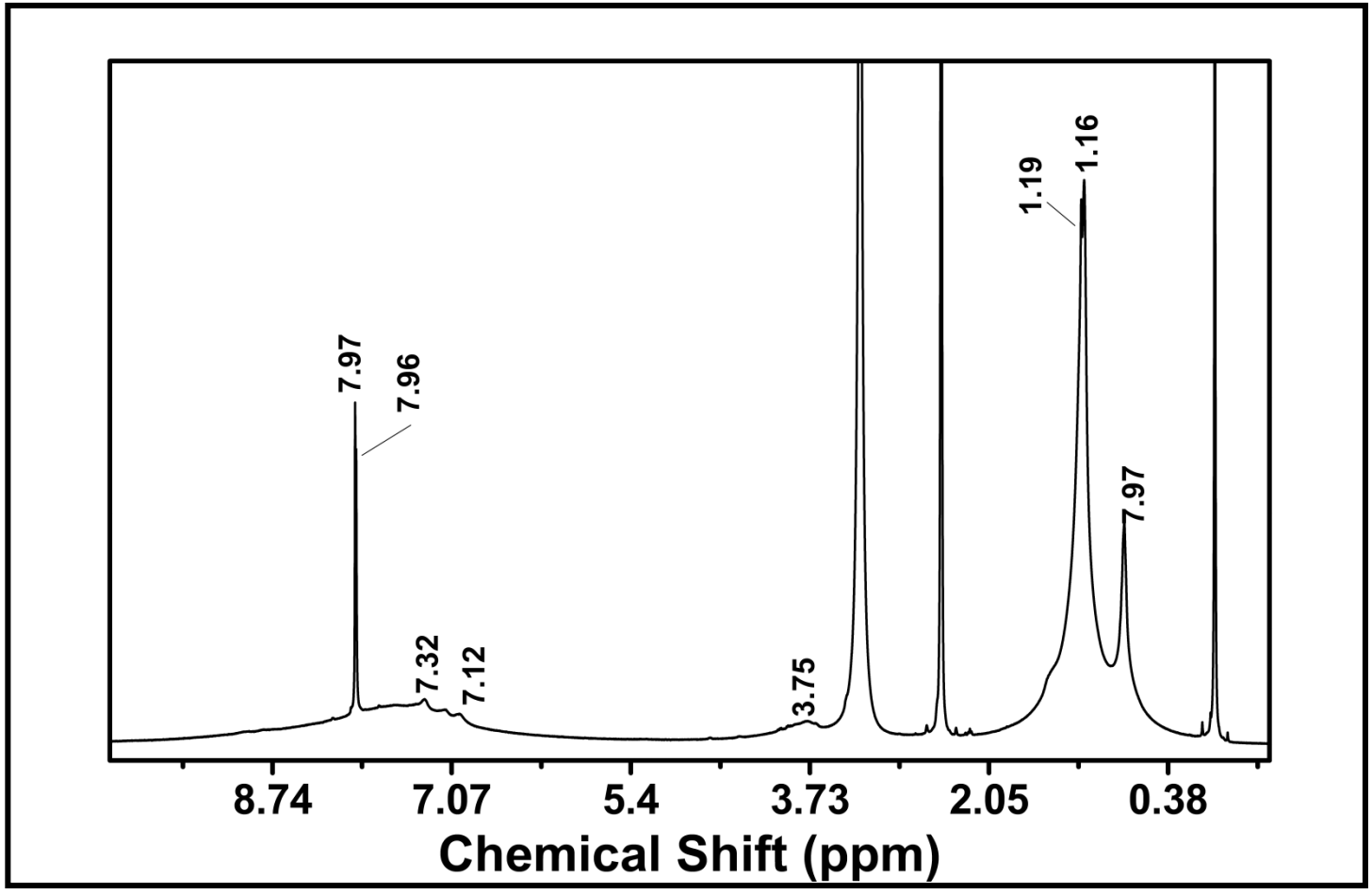

Figure 4.20: 1H-NMR Spectrum of BP-PDD in Deuterated DMSO

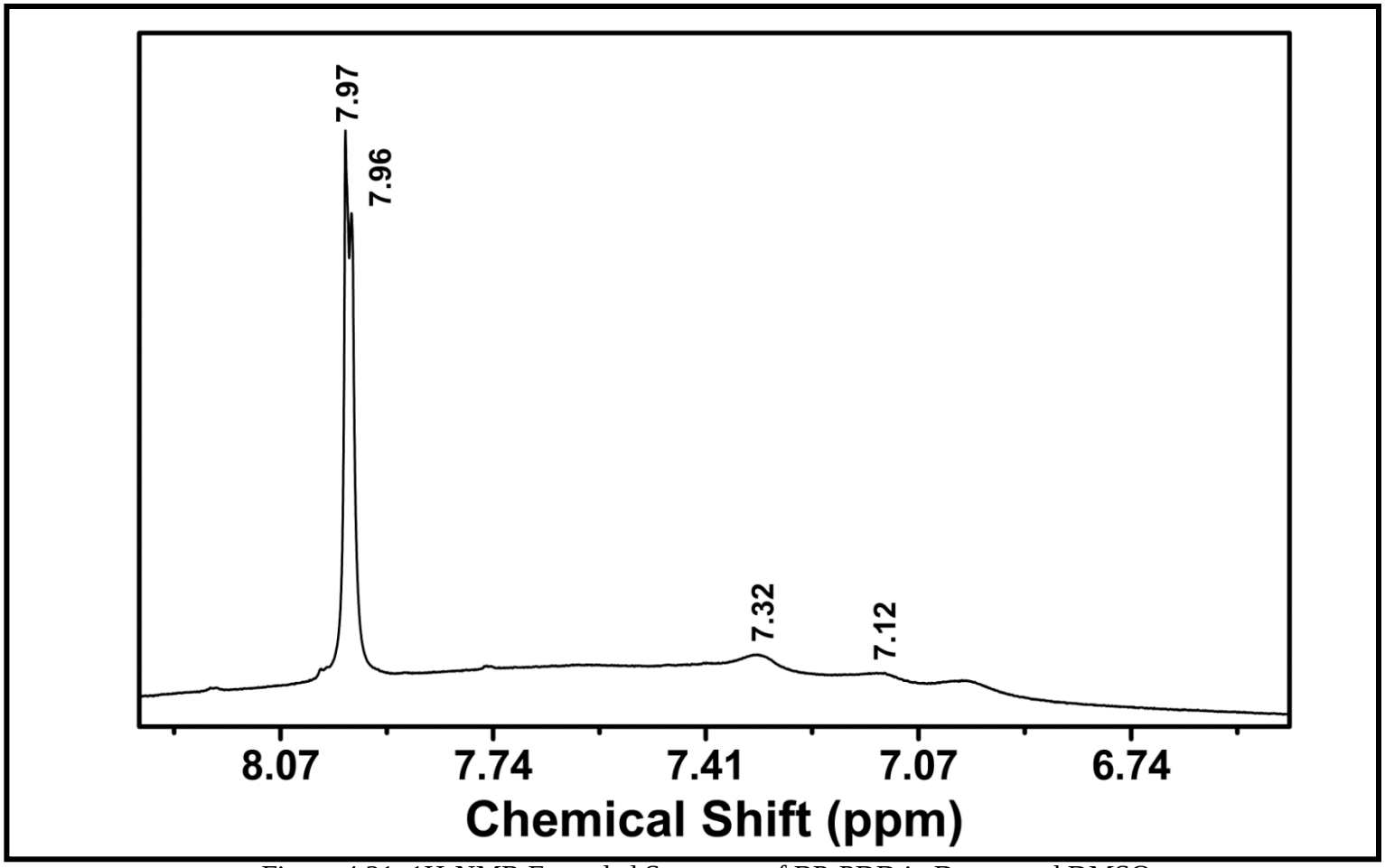

Figure 4.21: 1H-NMR Extended Spectrum of BP-PDD in Deuterated DMSO

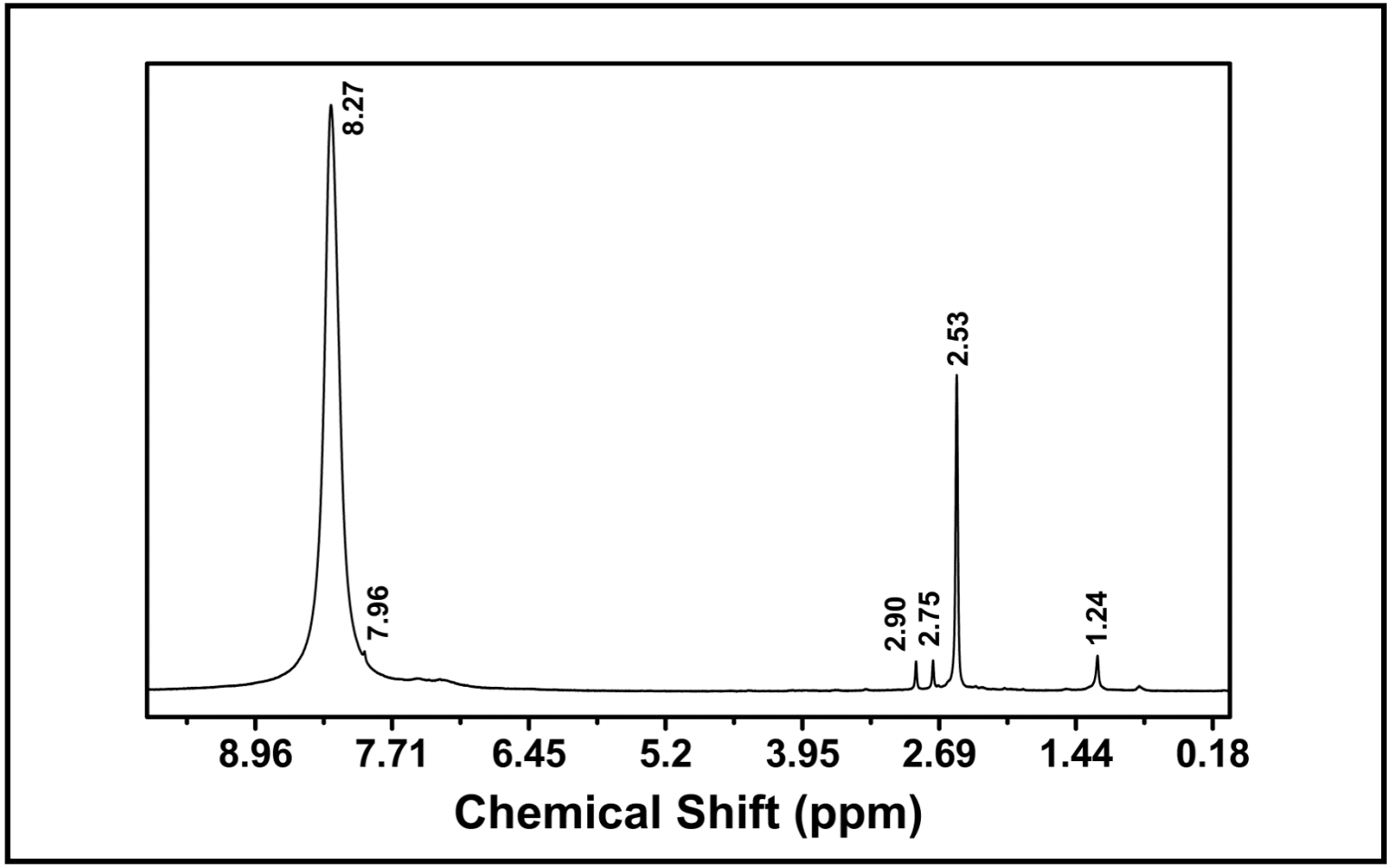

Figure 4.22: 1H-NMR Spectrum of BP-PPD in Deuterated DMSO

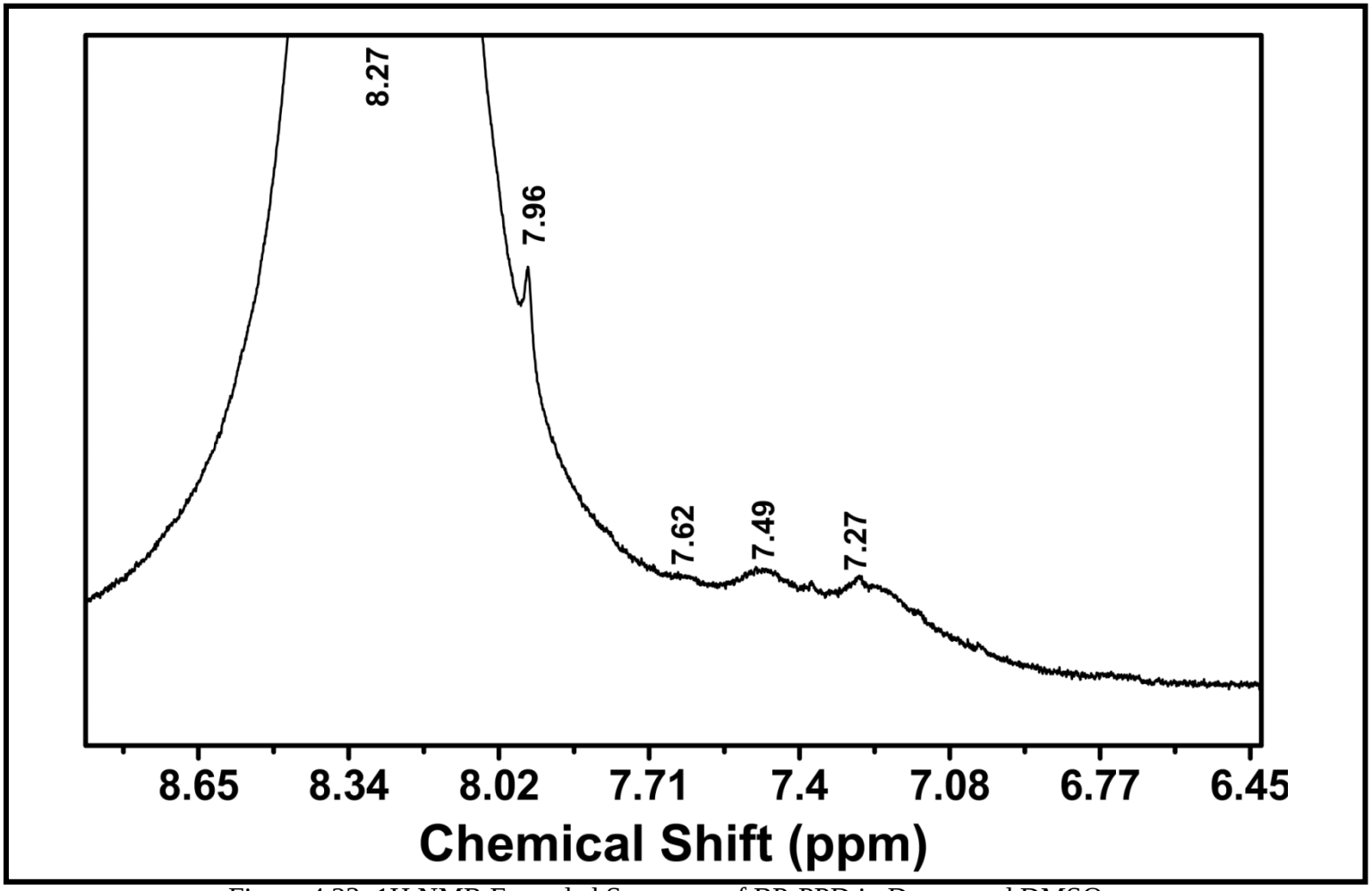

Figure 4.23: 1H NMR Extended Spectrum of BP-PPD in Deuterated DMSO

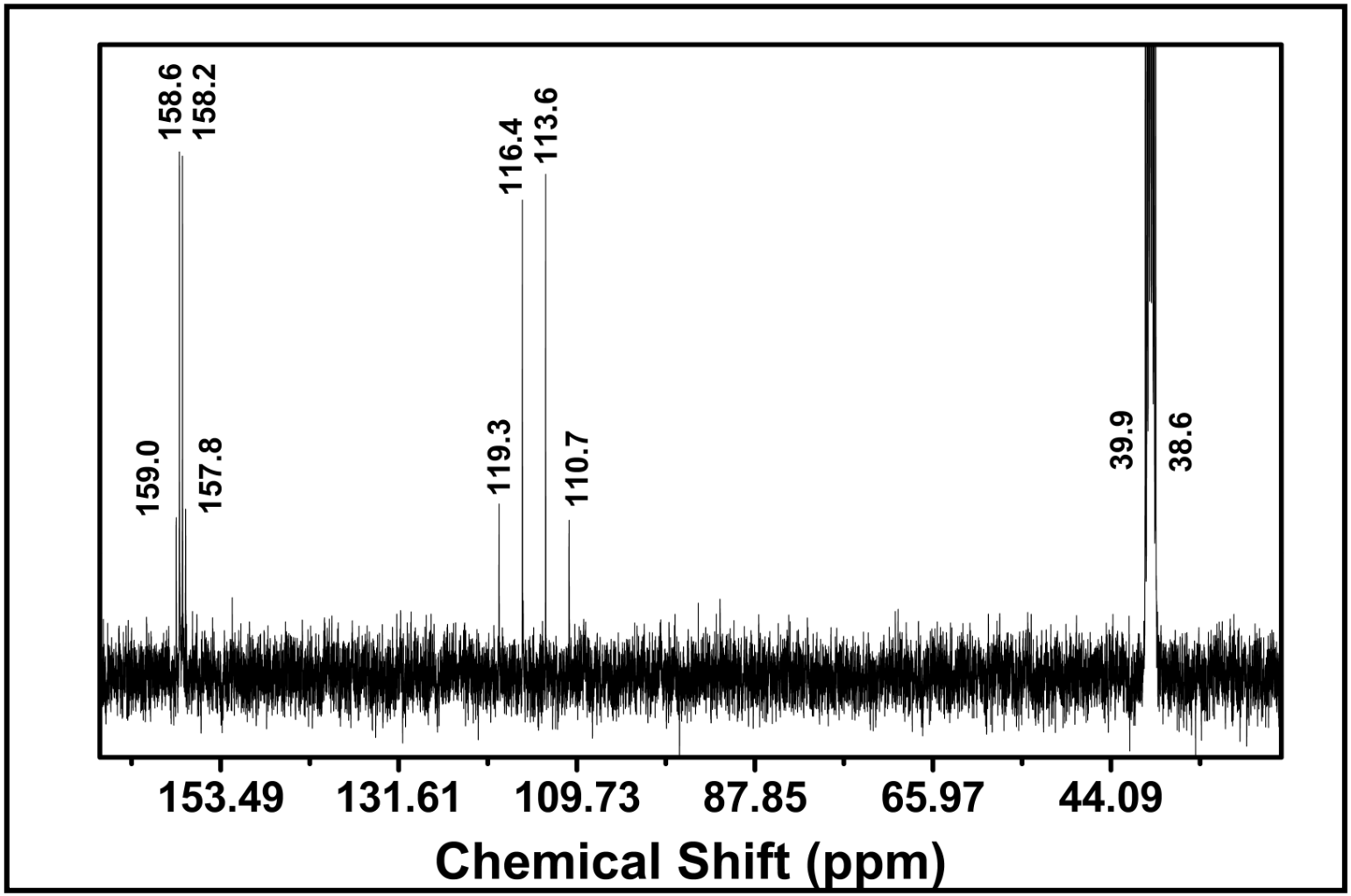

Figure 4.24: 13C-NMR Spectrum of BP-PPD in Deuterated DMSO

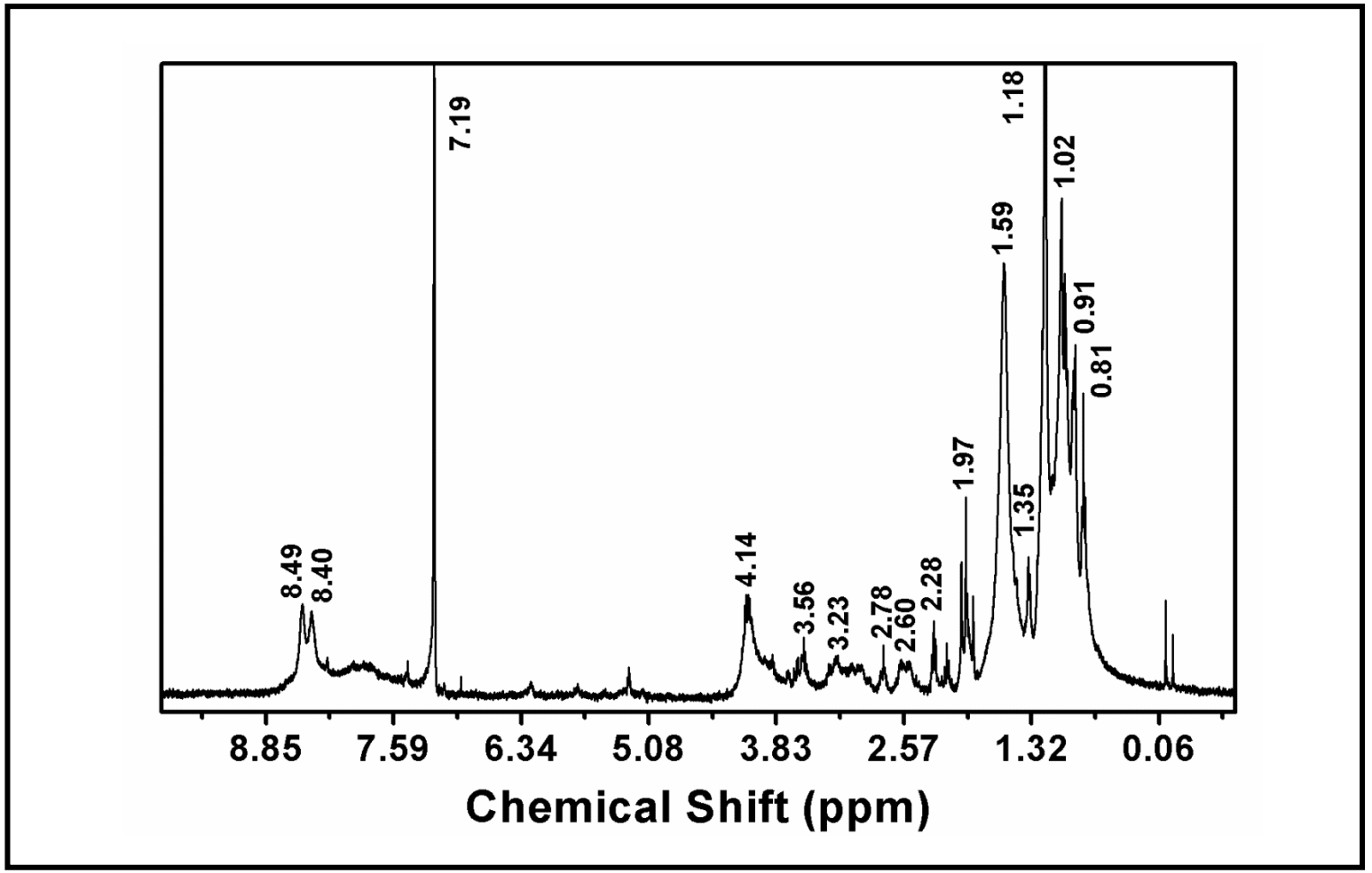

Figure 4.25: 1H-NMR Spectrum of TPE-PDI in $CDCl_3$

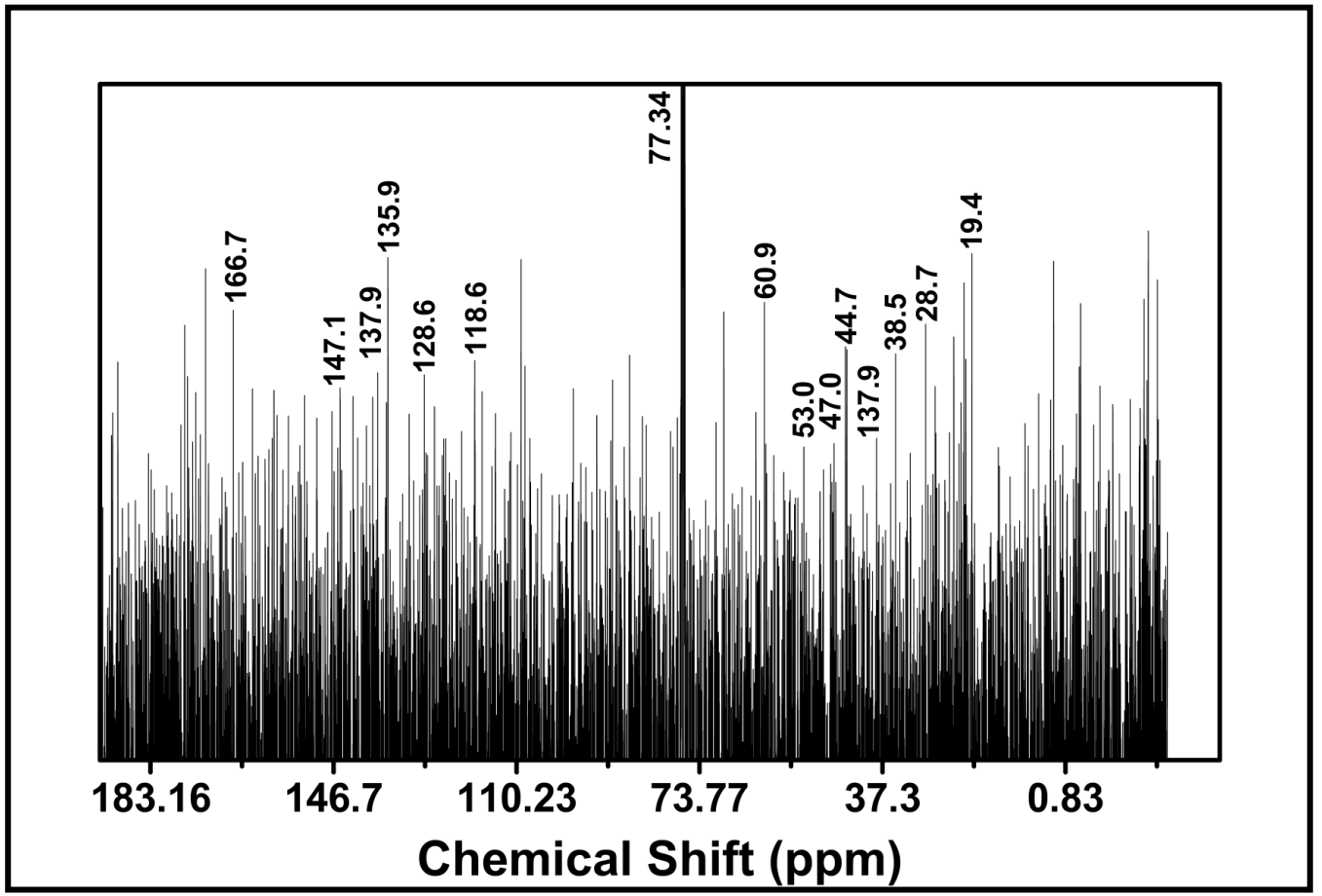

Figure 4.26: 13C-NMR Spectrum of TPE-PDI in $CDCl_3$

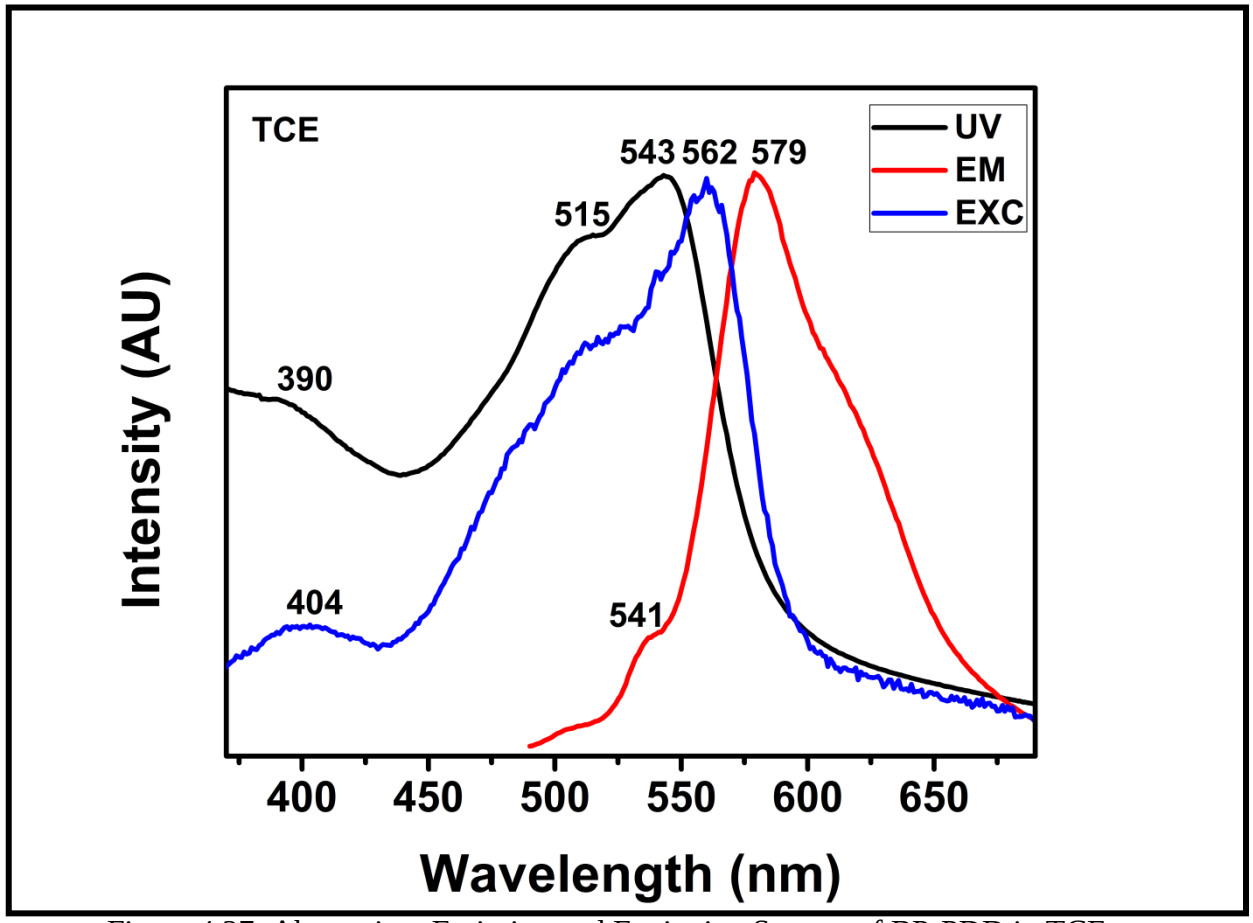

Figure 4.27: Absorption, Emission and Excitation Spectra of BP-PDD in TCE

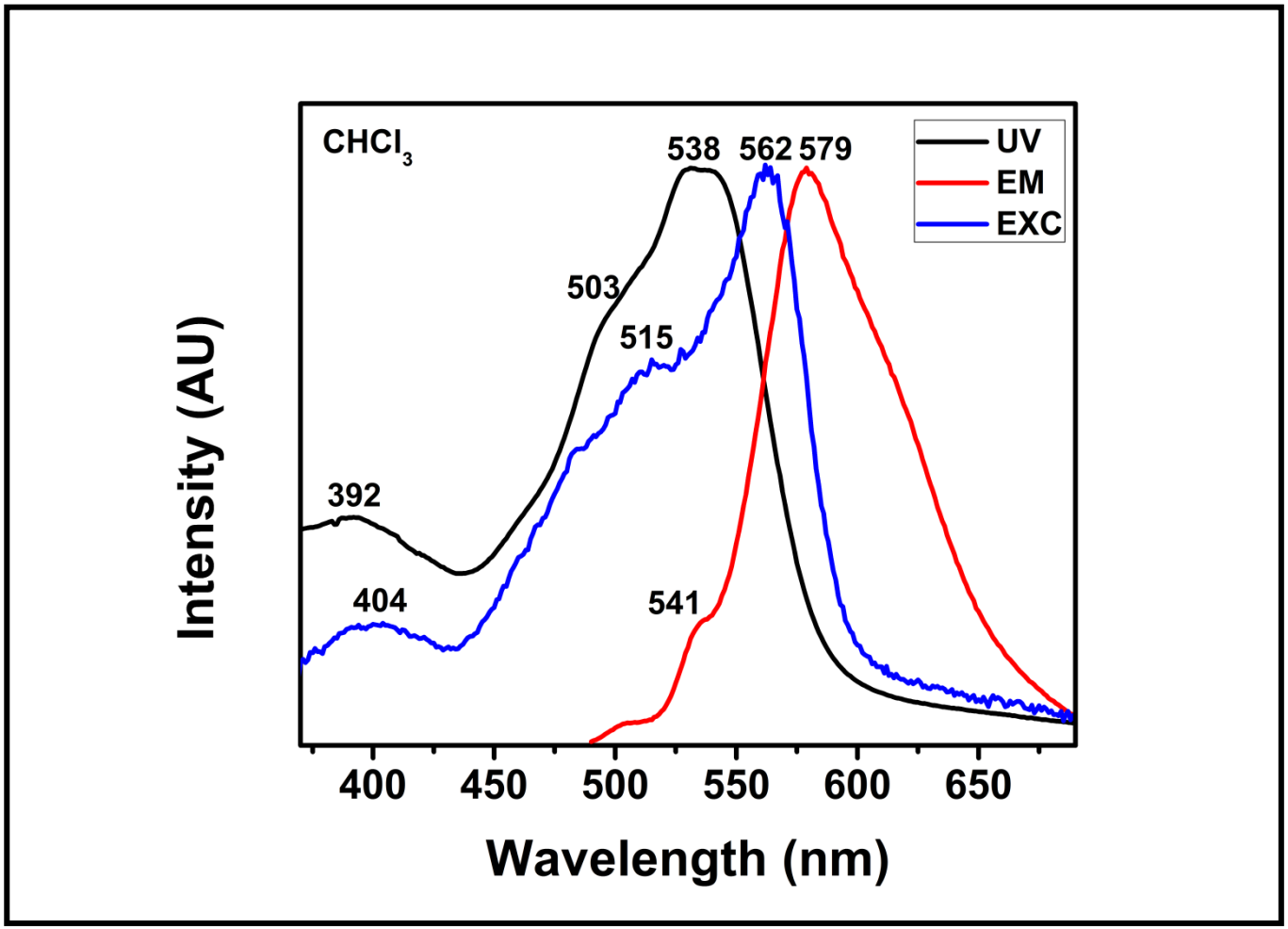

Figure 4.28: Absorption, Emission and Excitation Spectra of BP-PDD in $CHCl_3$

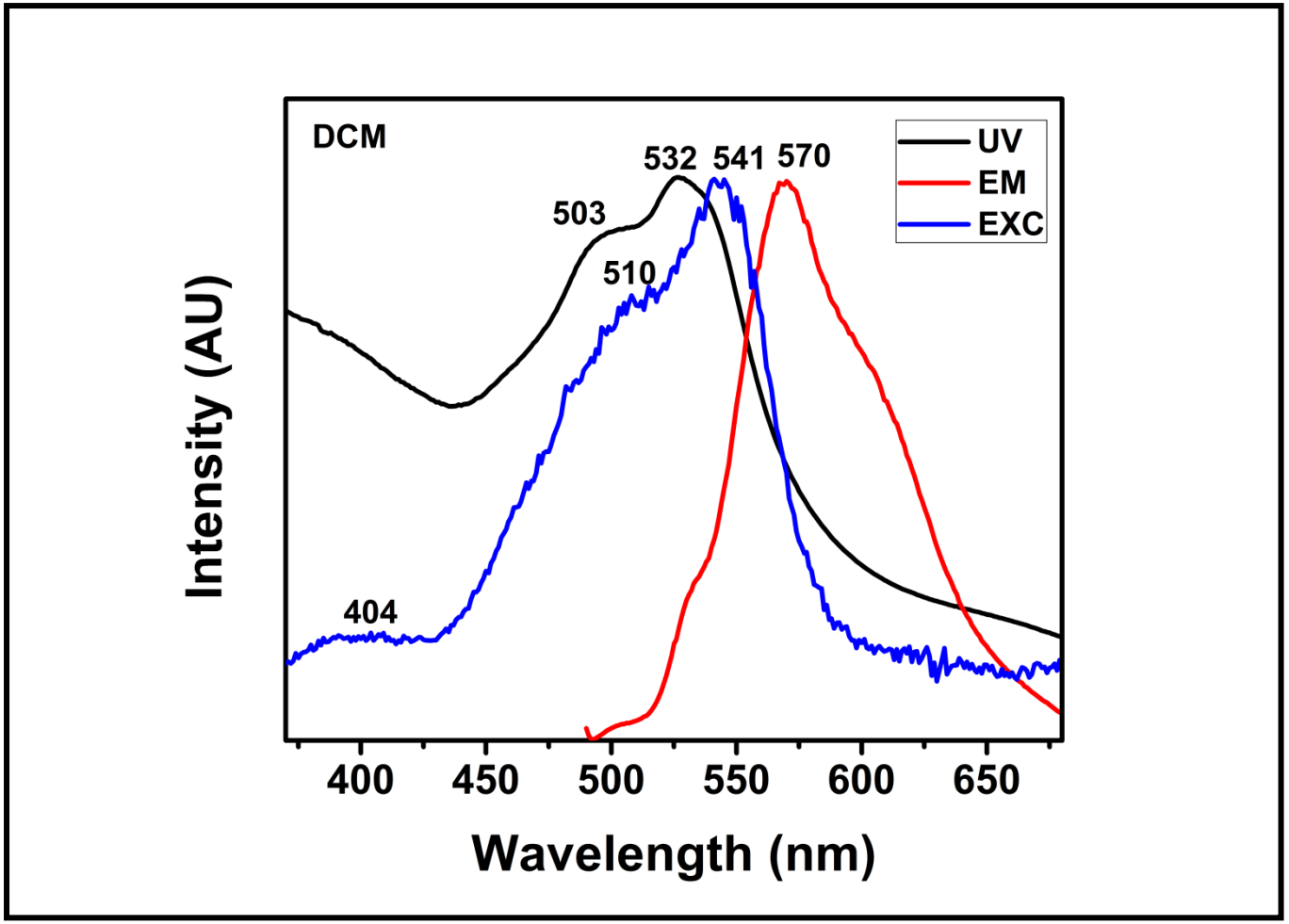

Figure 4.29: Absorption, Emission and Excitation Spectra of BP-PDD in DCM

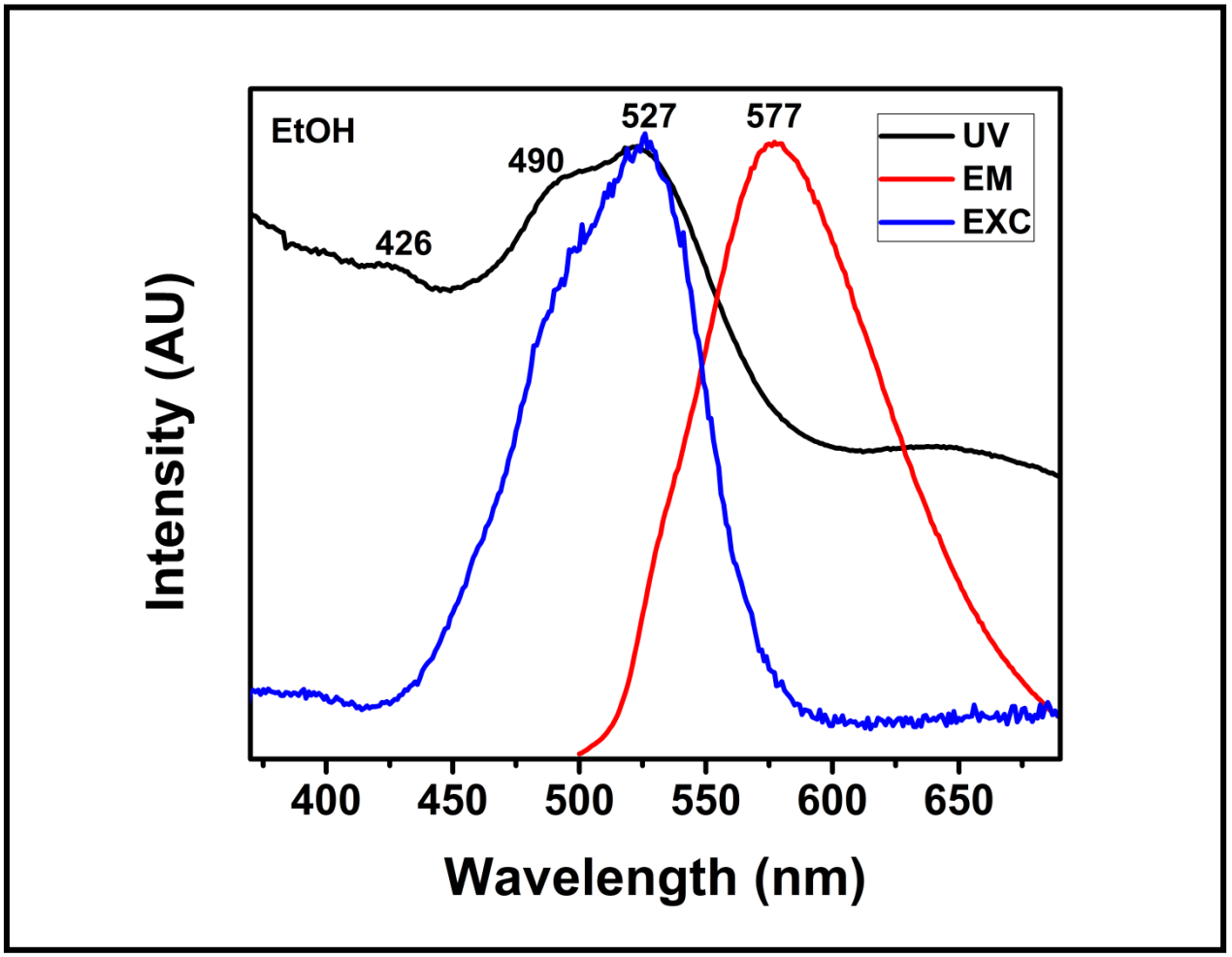

Figure 4.30: Absorption, Emission and Excitation Spectra of BP-PDD in EtOH

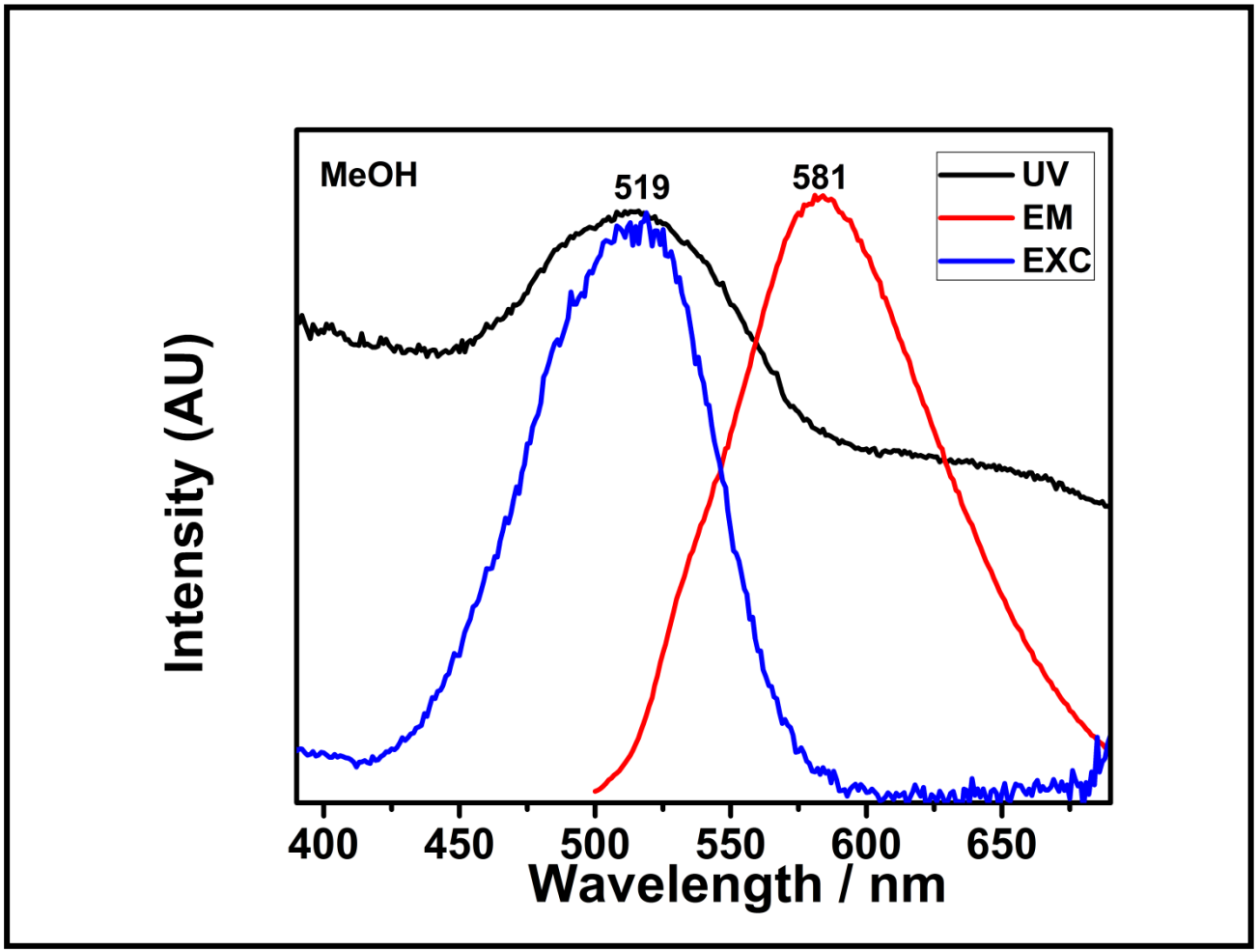

Figure 4.31: Absorption, Emission and Excitation Spectra of BP-PDD in MeOH

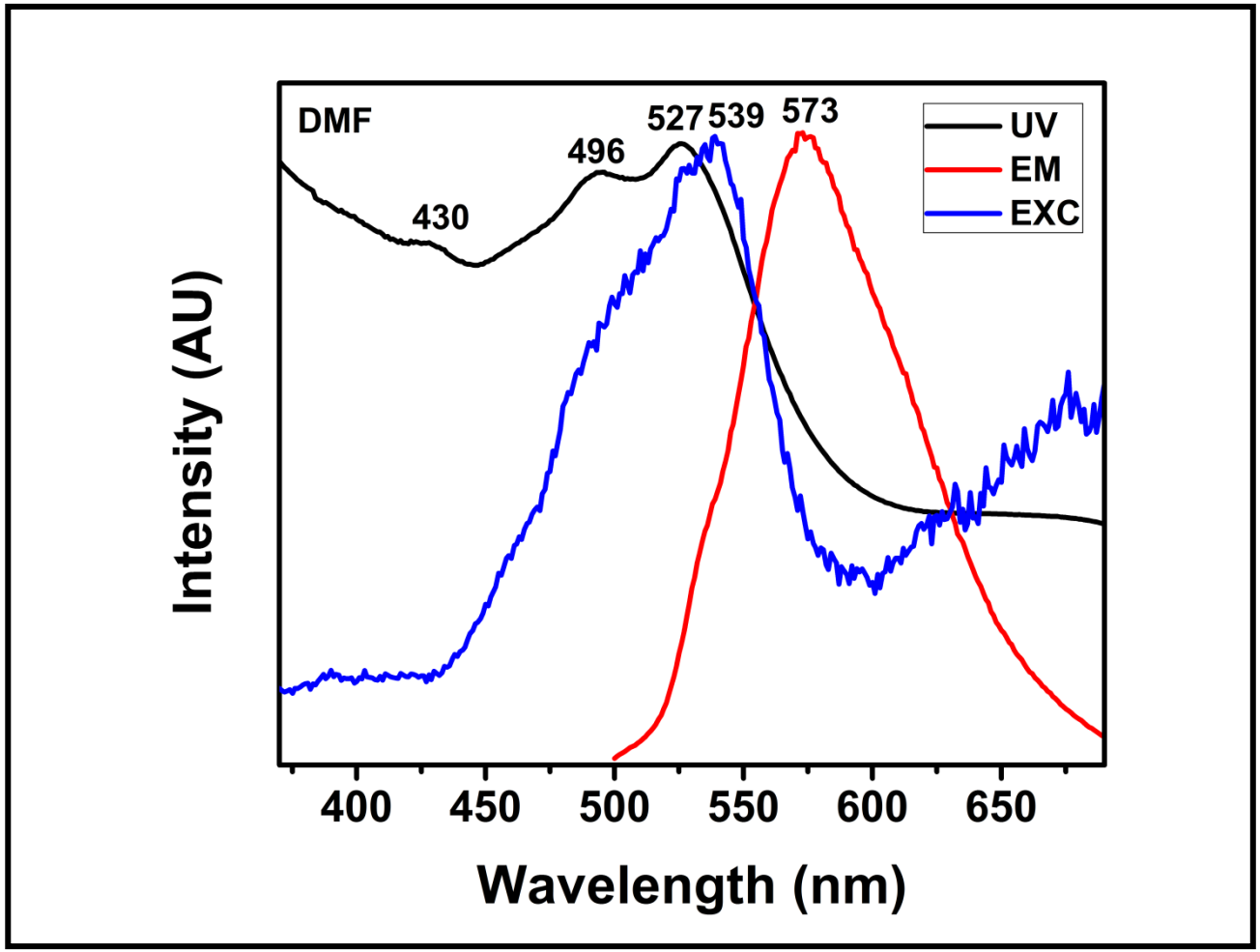

Figure 4.32: Absorption, Emission and Excitation Spectra of BP-PDD in DMF

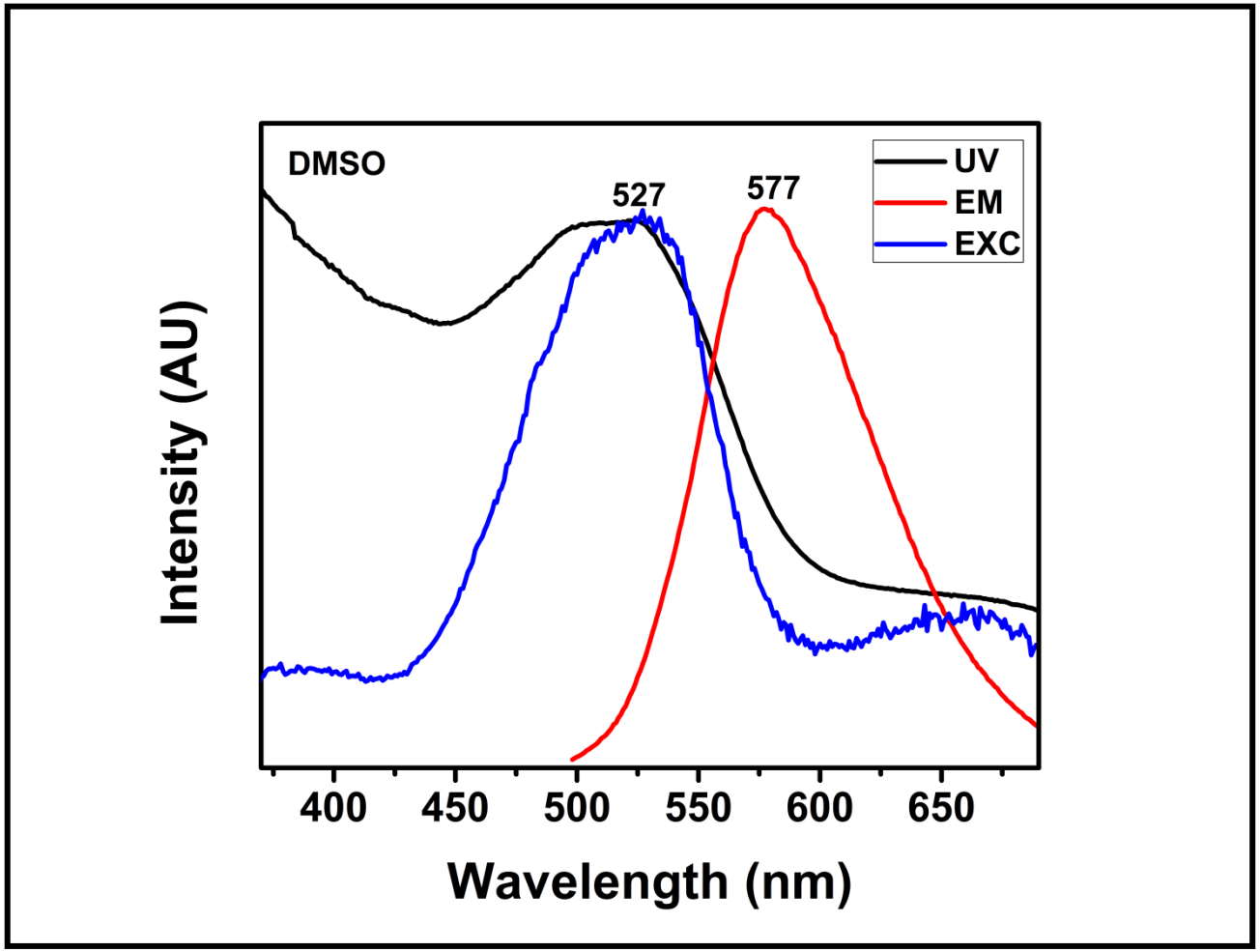

Figure 4.33: Absorption, Emission and Excitation Spectra of BP-PDD in DMSO

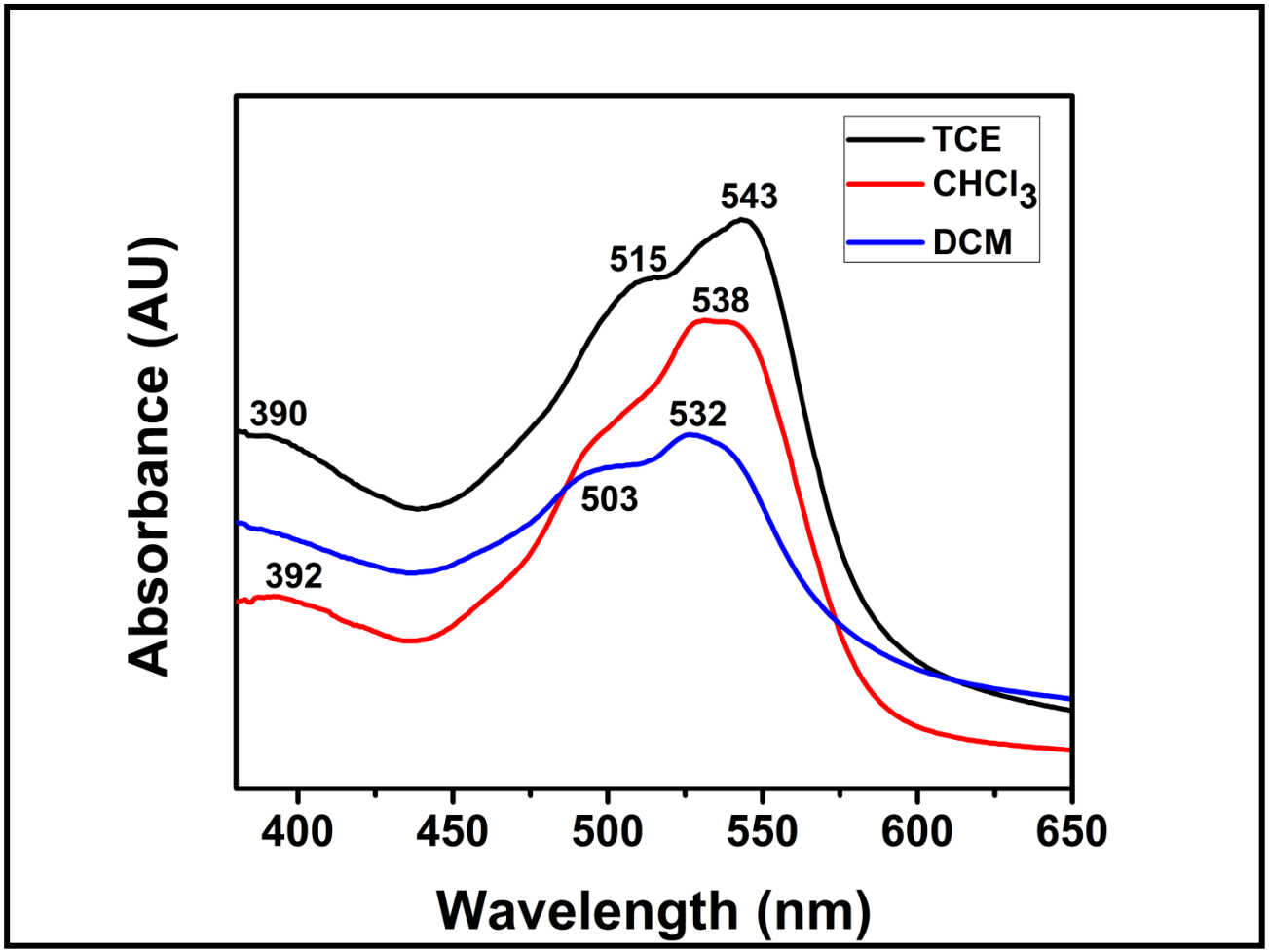

Figure 4.34: UV-visible Absorption Spectra of BP-PDD in Non-polar Solvents

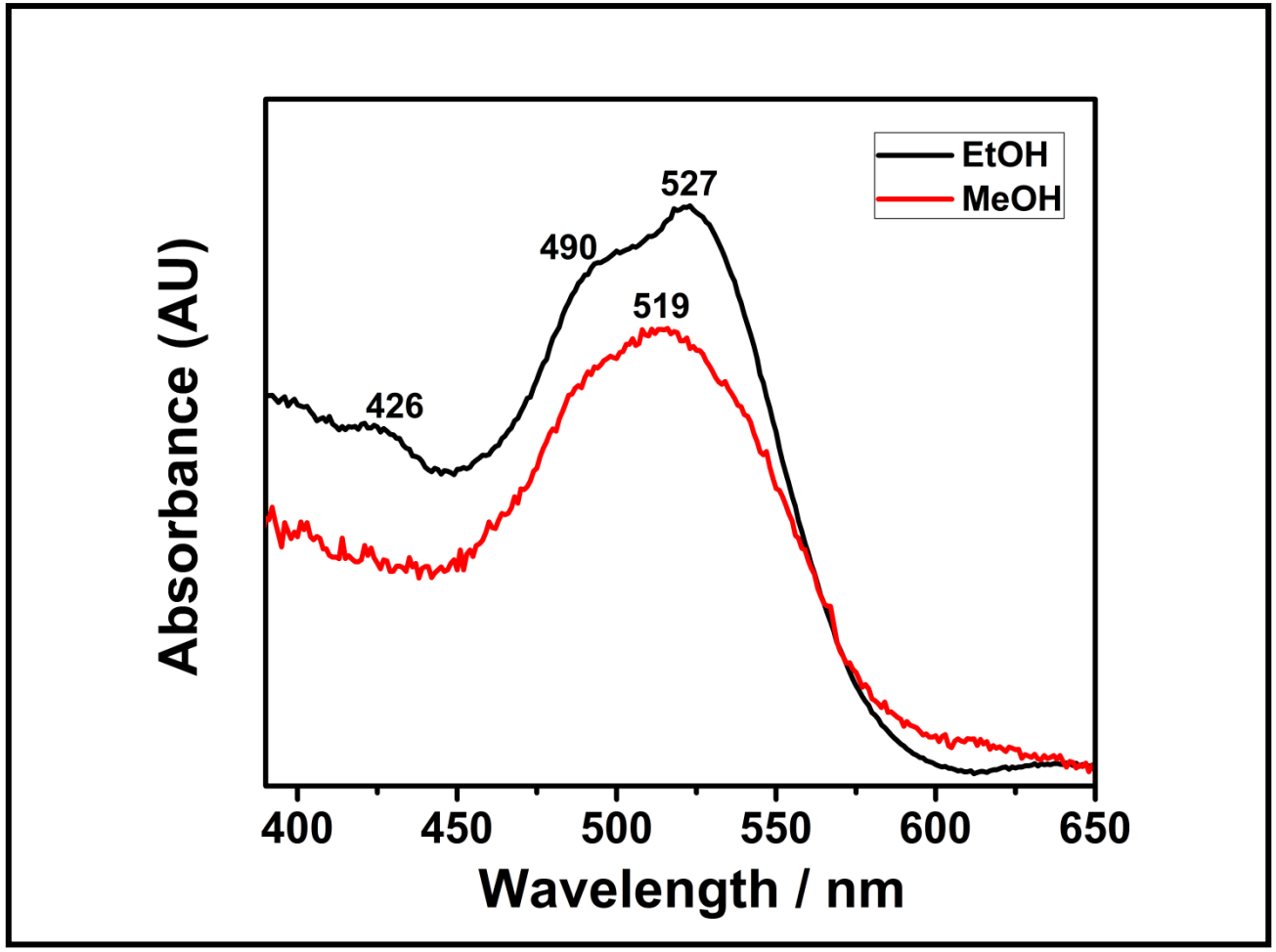

Figure 4.35: UV-visible Absorption Spectra of BP-PDD in Protic Solvents

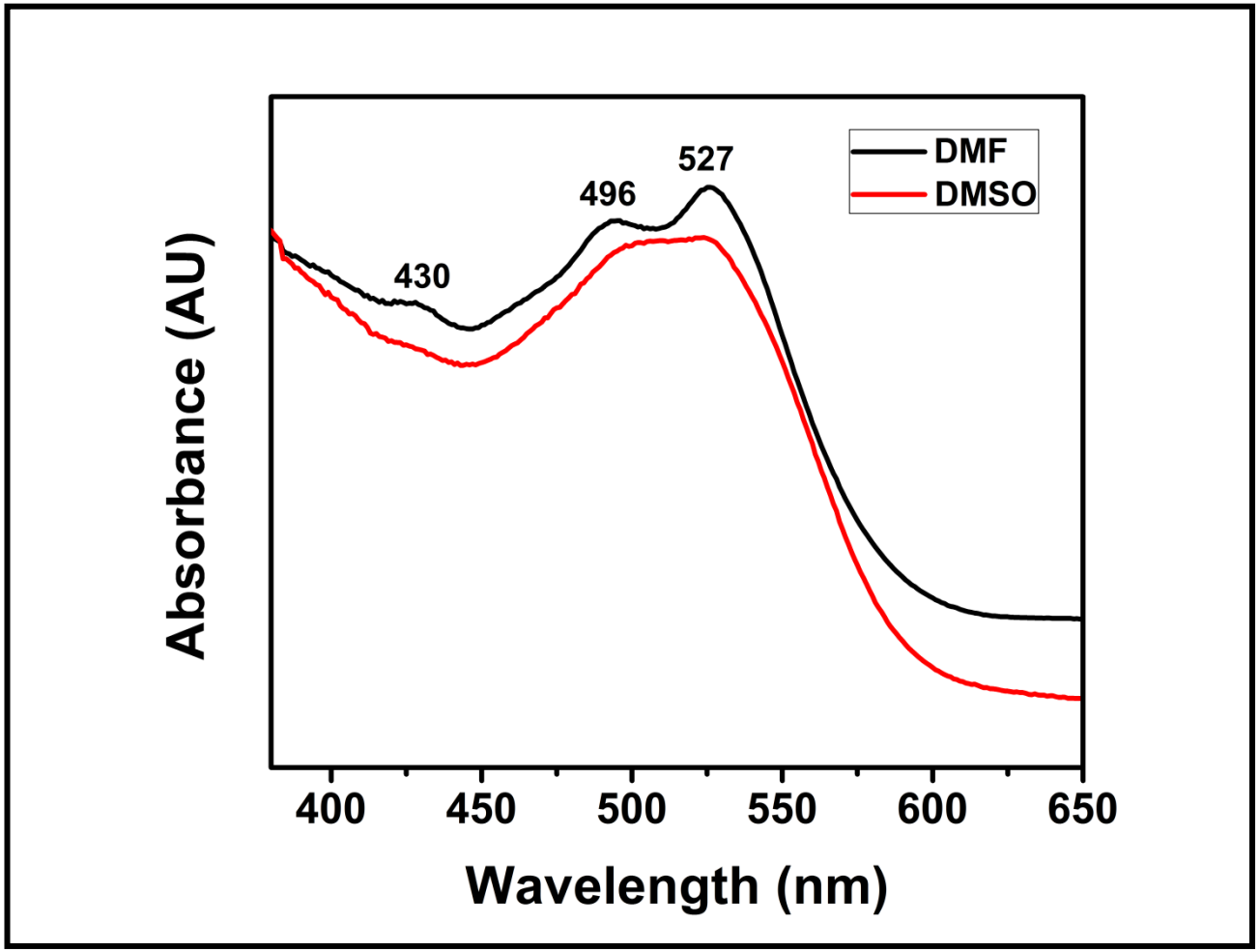

Figure 4.36: UV-visible Absorption Spectra of BP-PDD in Aprotic Solvents

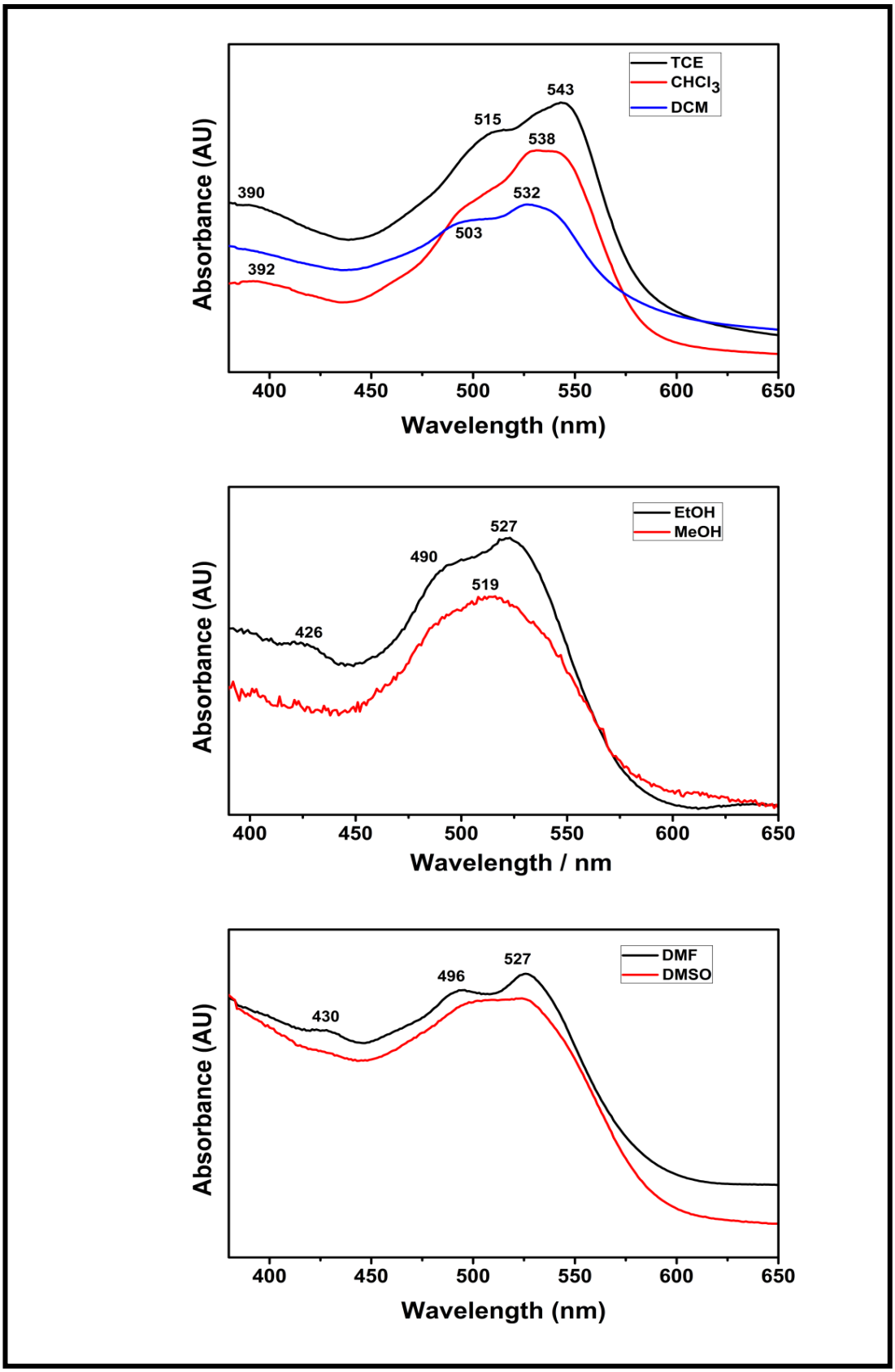

Figure 4.37: UV-visible Absorption Spectra of BP-PDD Several Organic Solvents

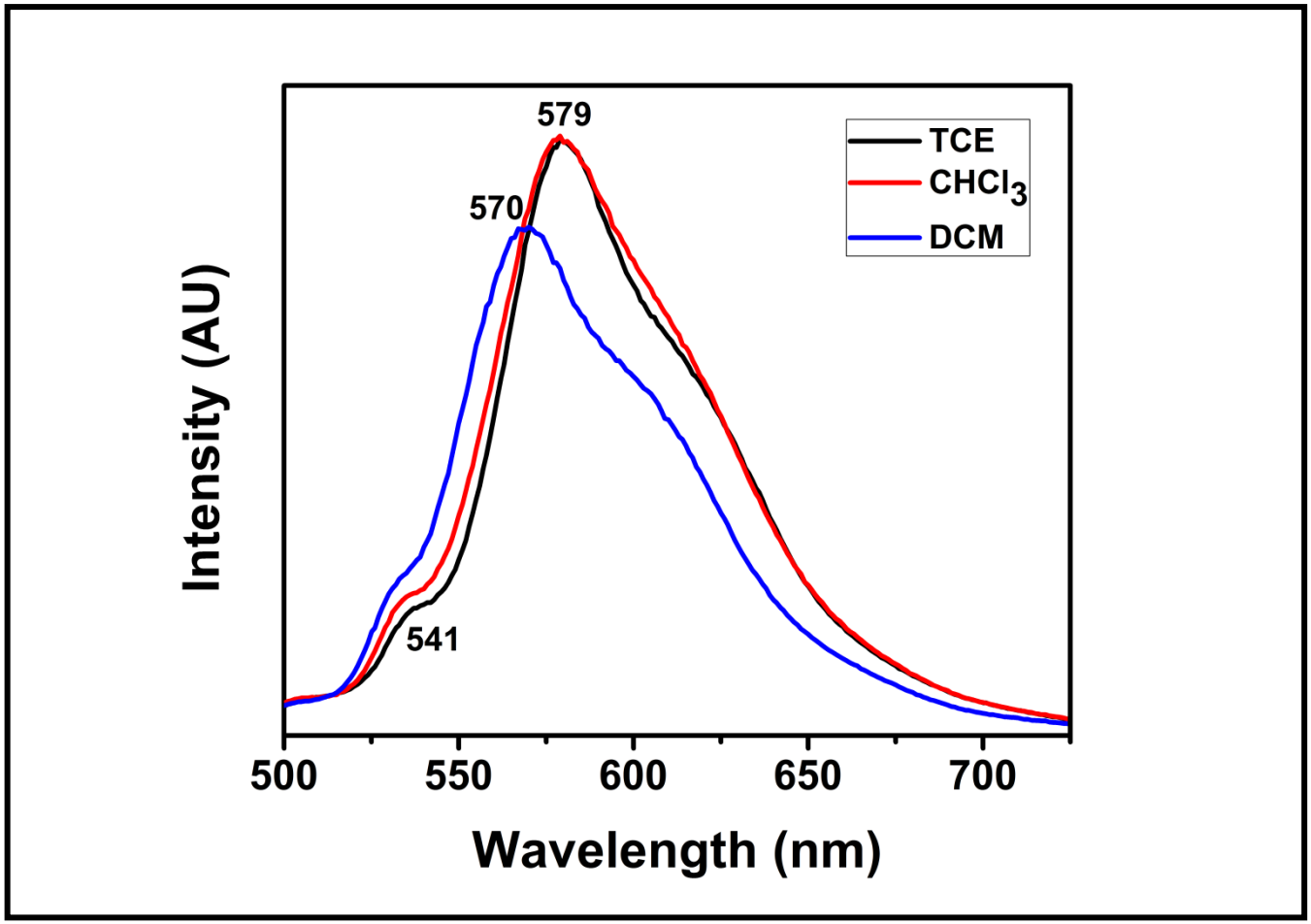

Figure 4.38: Emission Spectra of BP-PDD in Non-polar Solvents

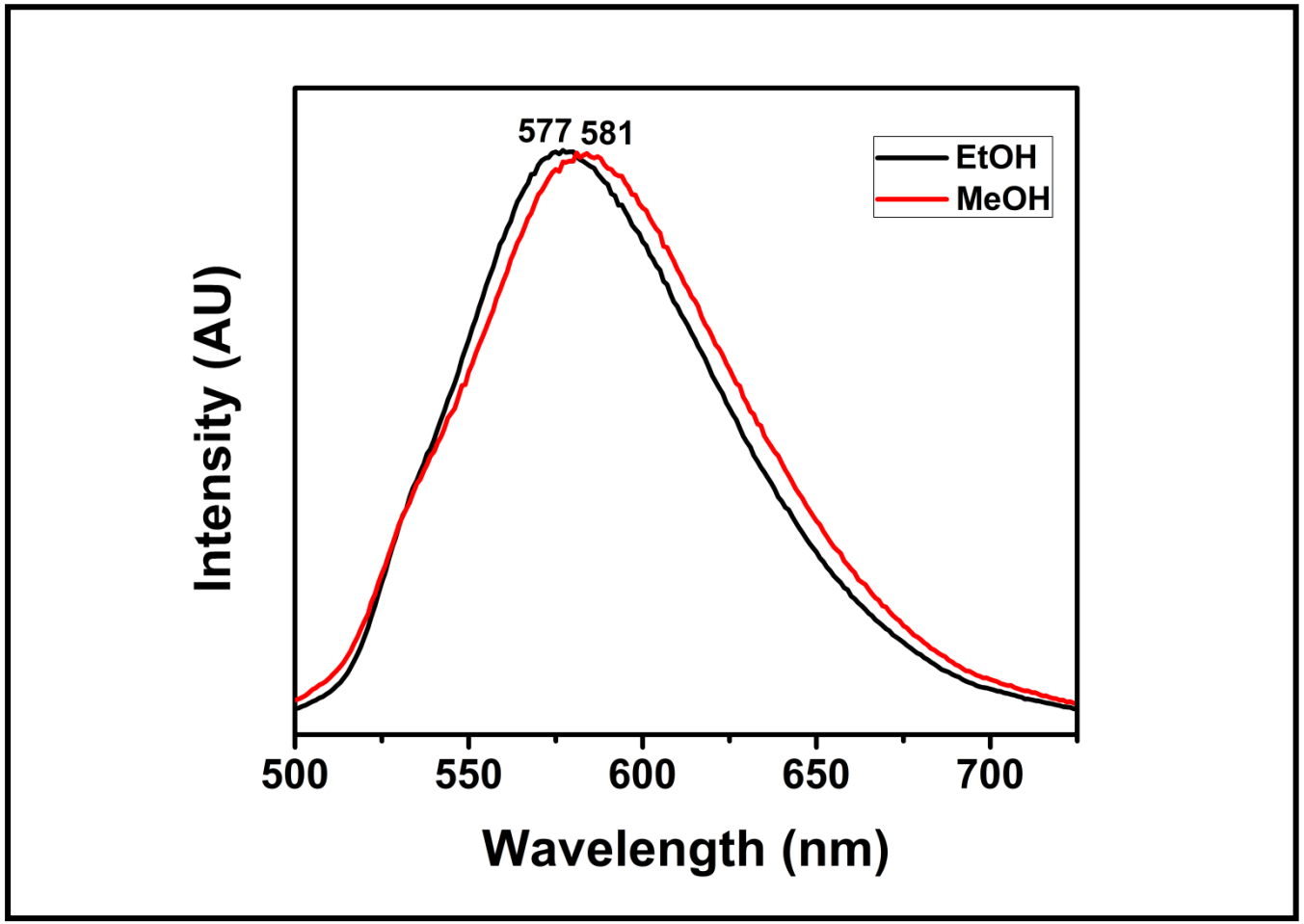

Figure 4.39: Emission Spectra of BP-PDD in Protic Solvents

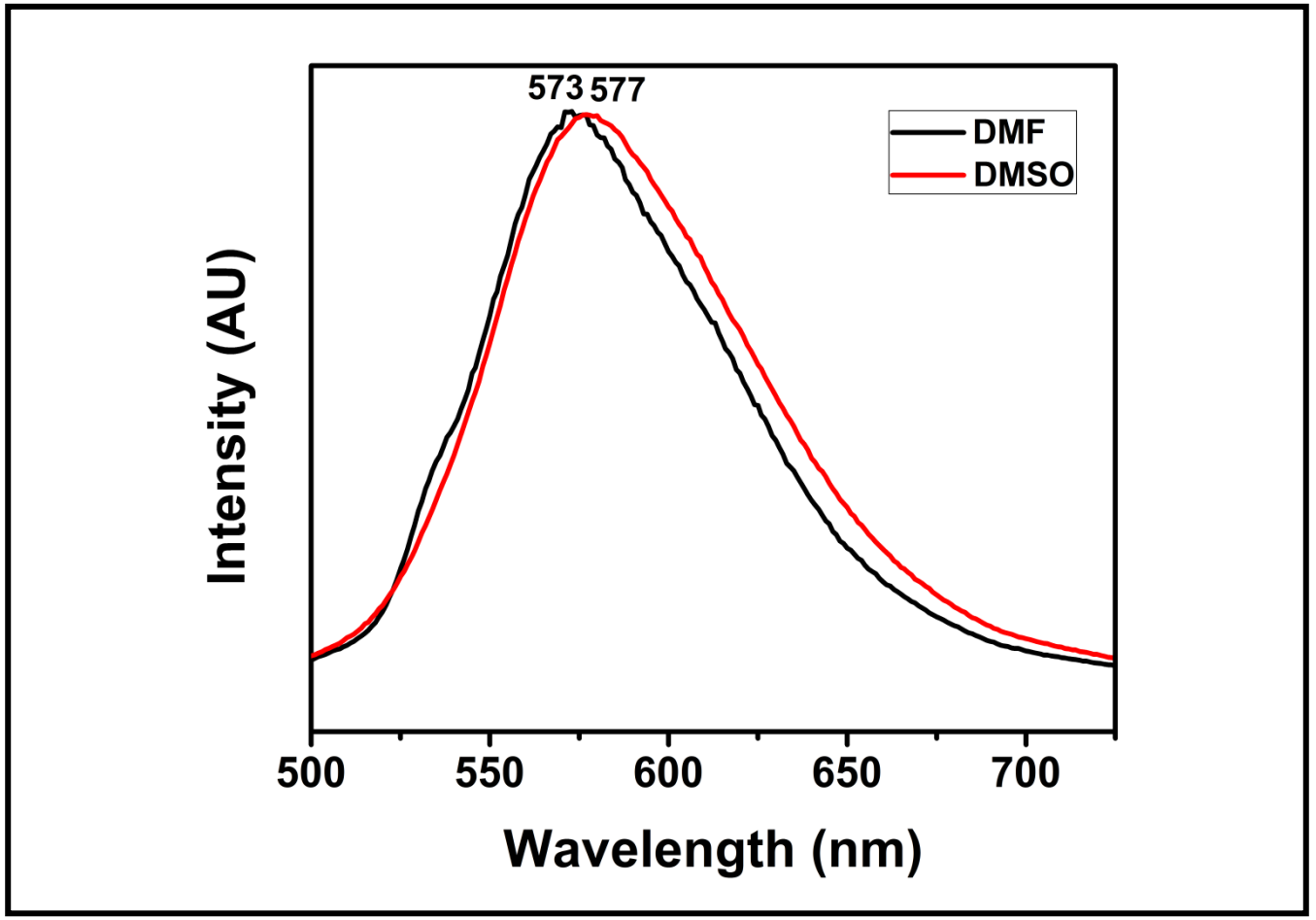

Figure 4.40: Emission Spectra of BP-PDD in Aprotic Solvents

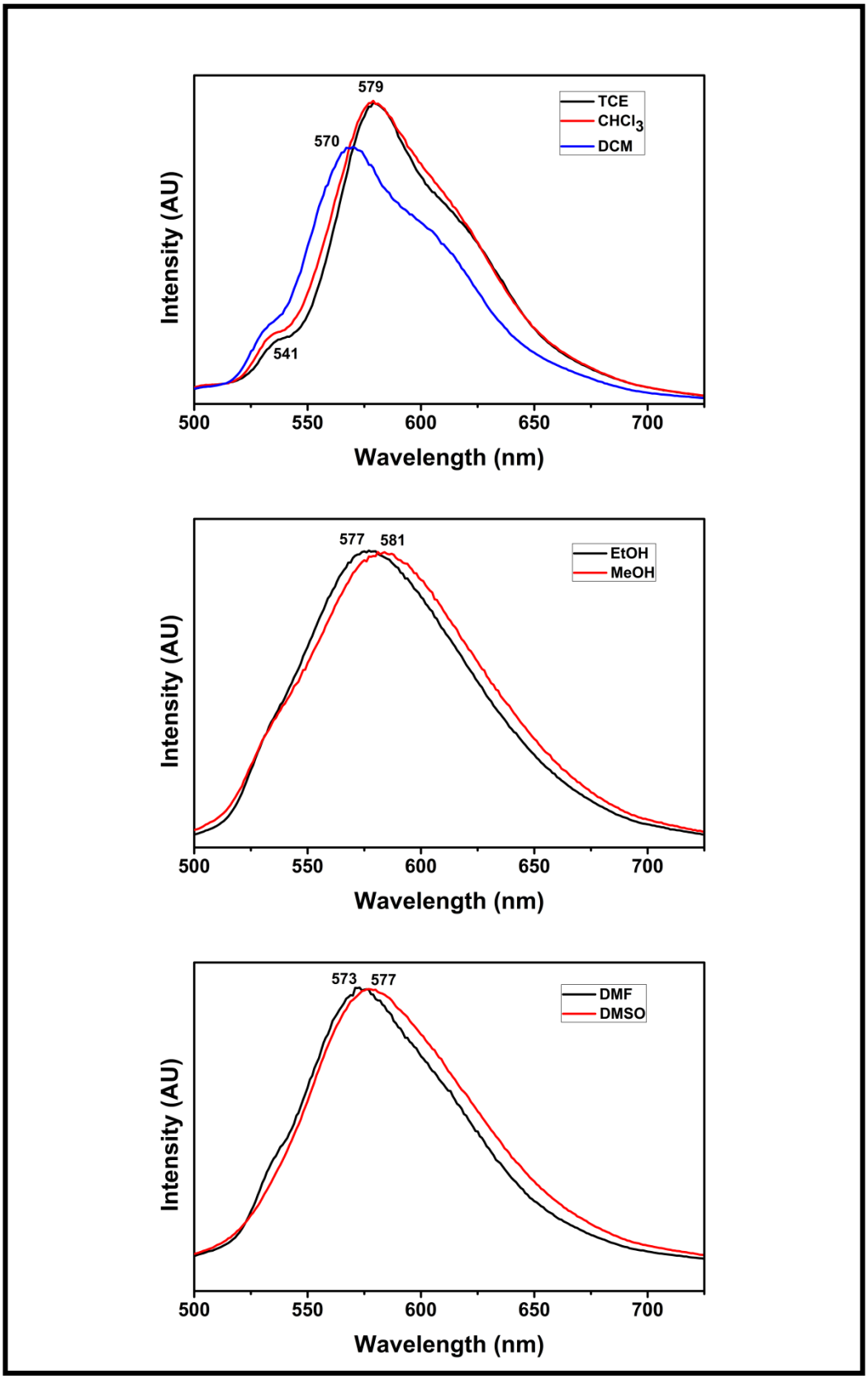

Figure 4.41: Emission Spectra of BP-PDD in Several Organic Solvents

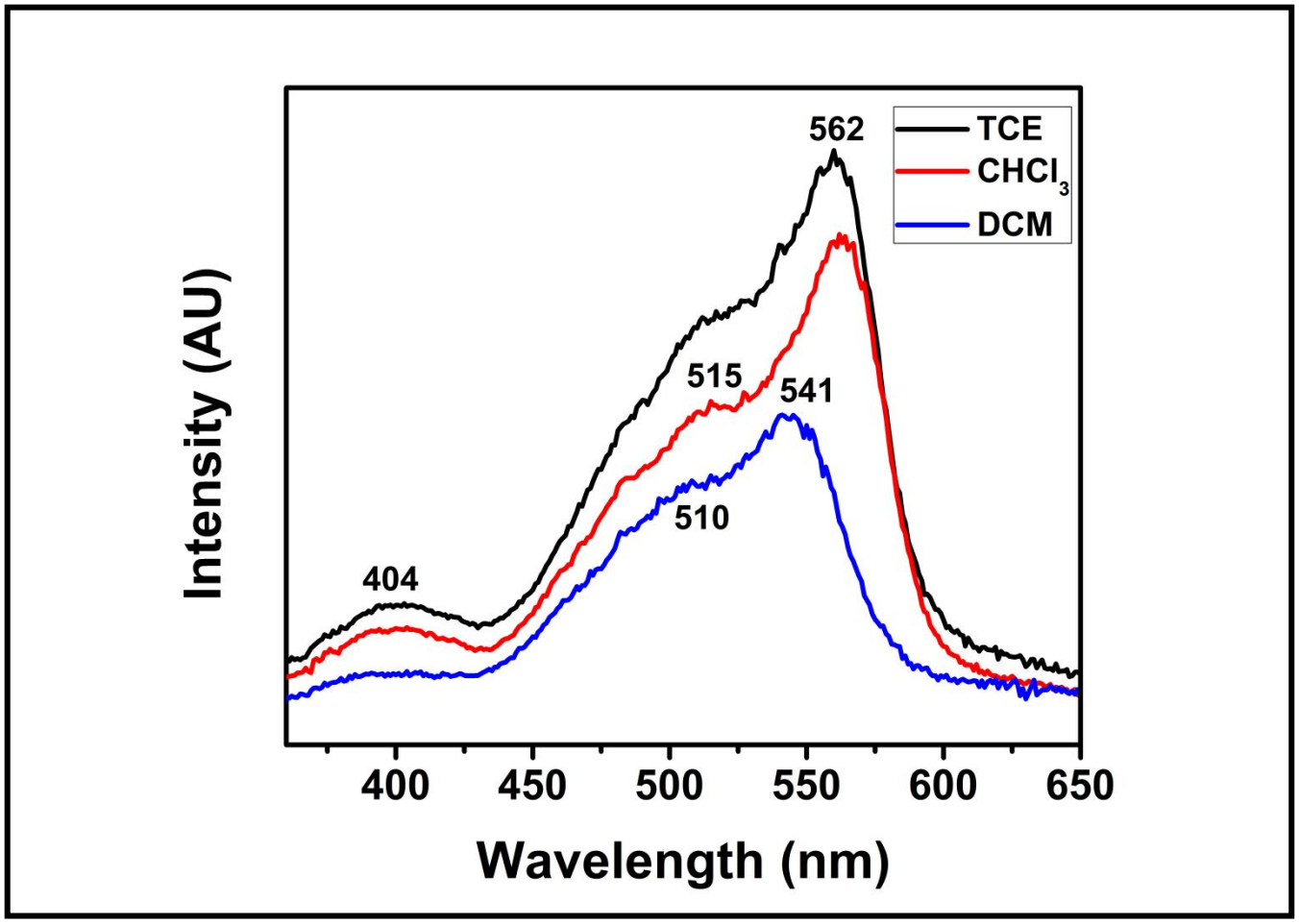

Figure 4.42: Excitation Spectra of BP-PDD in Non-polar Solvents

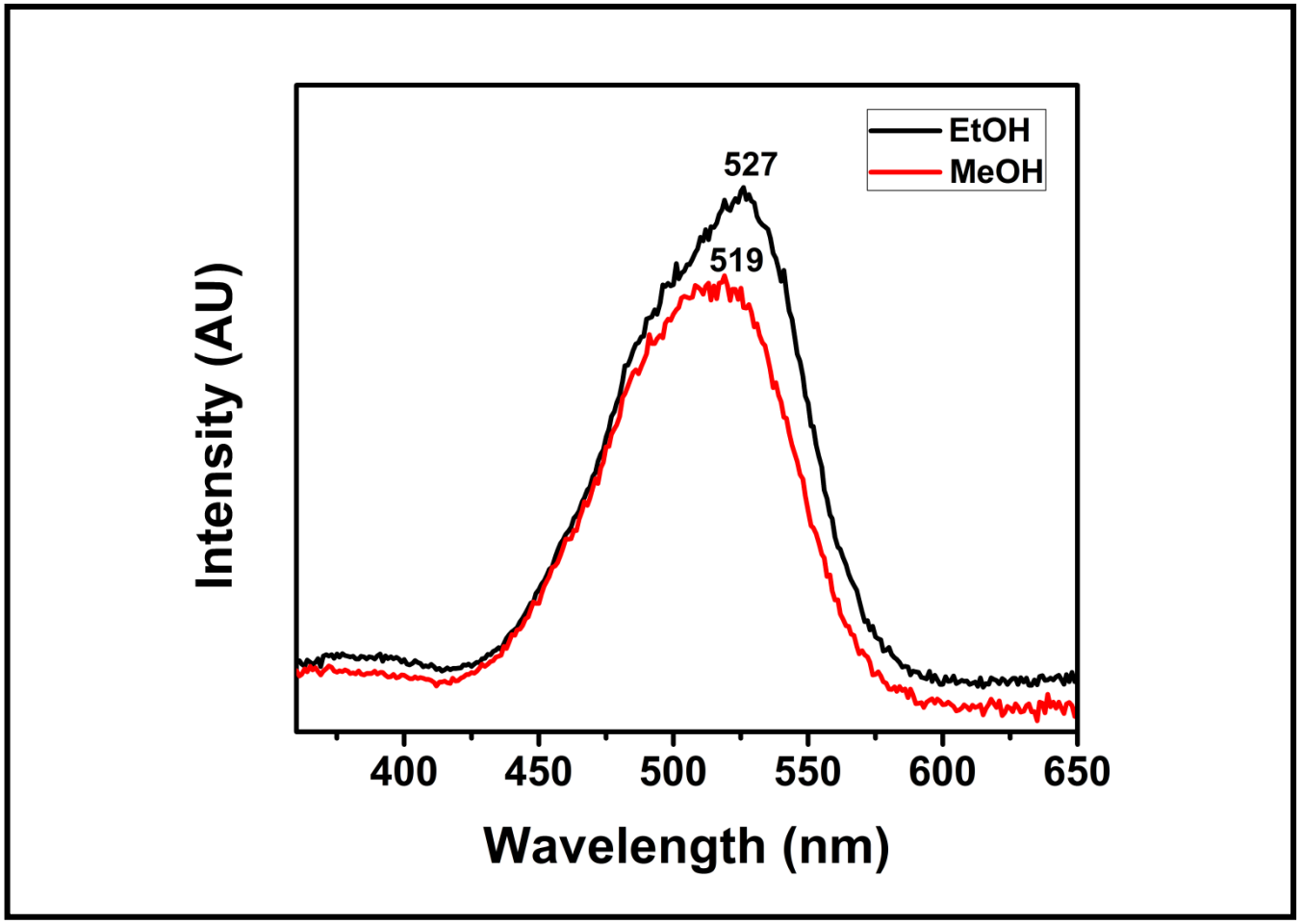

Figure 4.43: Excitation Spectra of BP-PDD in Protic Solvents

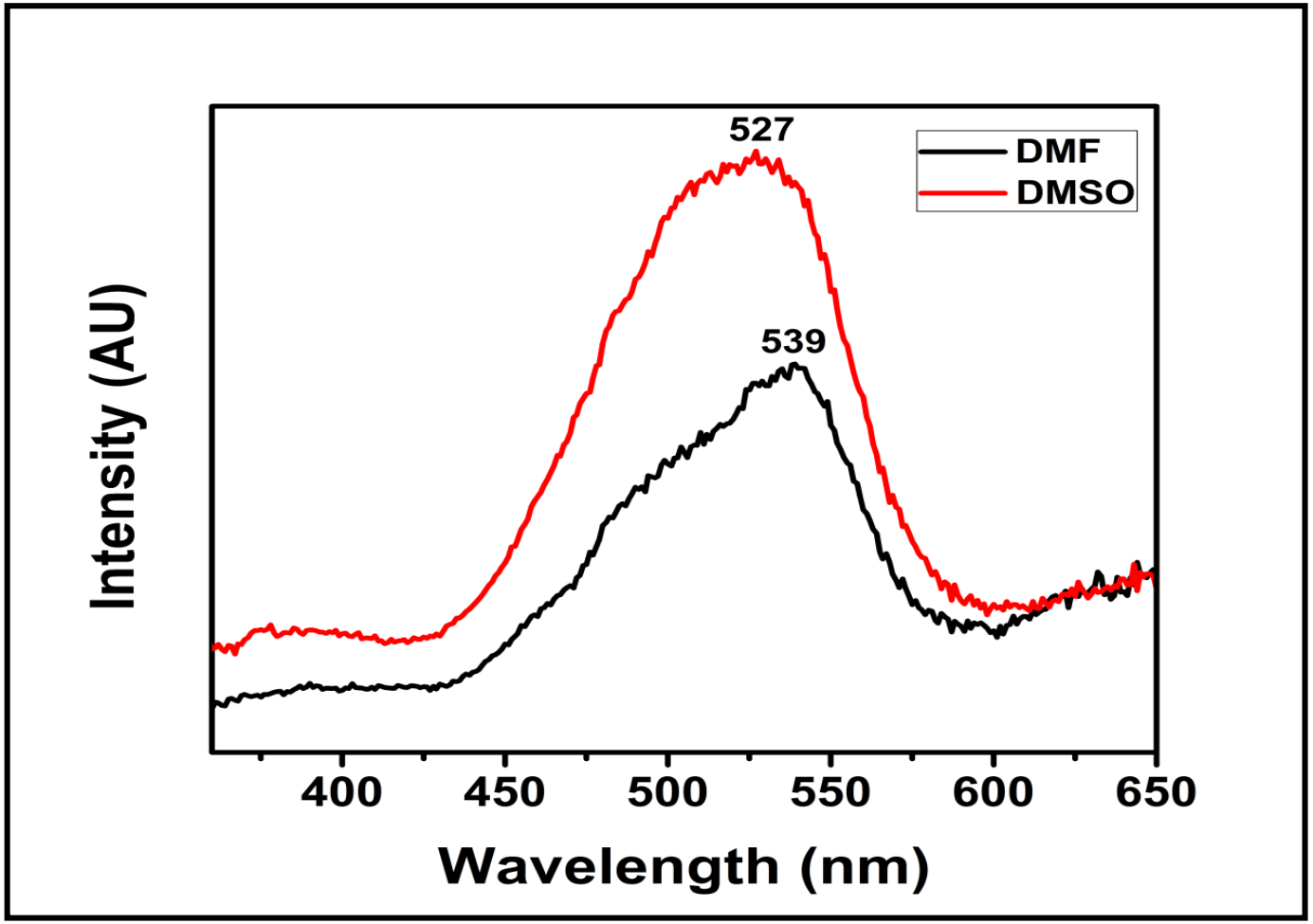

Figure 4.44: Excitation Spectra of BP-PDD in Aprotic Solvents

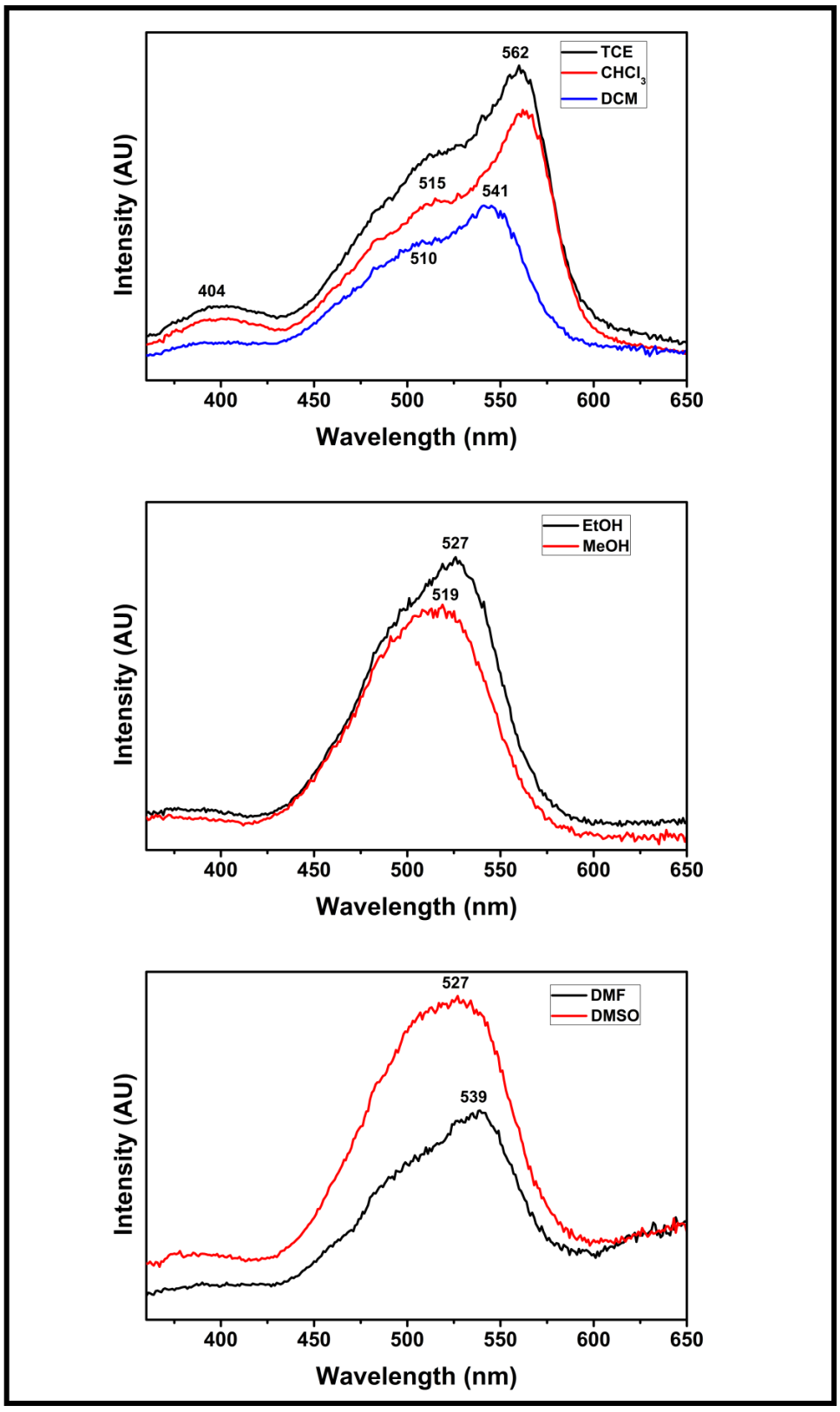

Figure 4.45: Excitation Spectra of BP-PDD in Several Organic Solvents

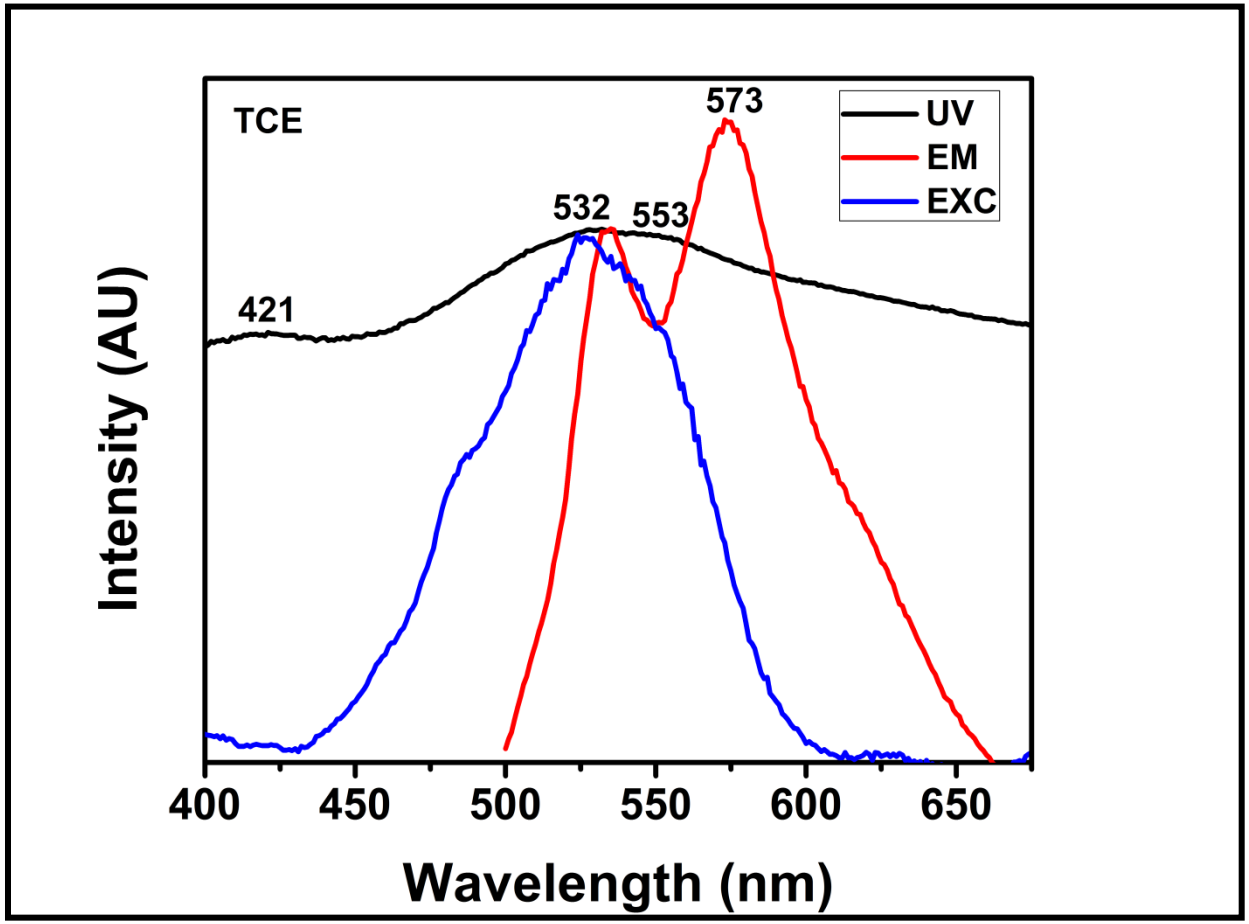

Figure 4.46: Absorption, Emission and Excitation Spectra of BP-PPD in TCE

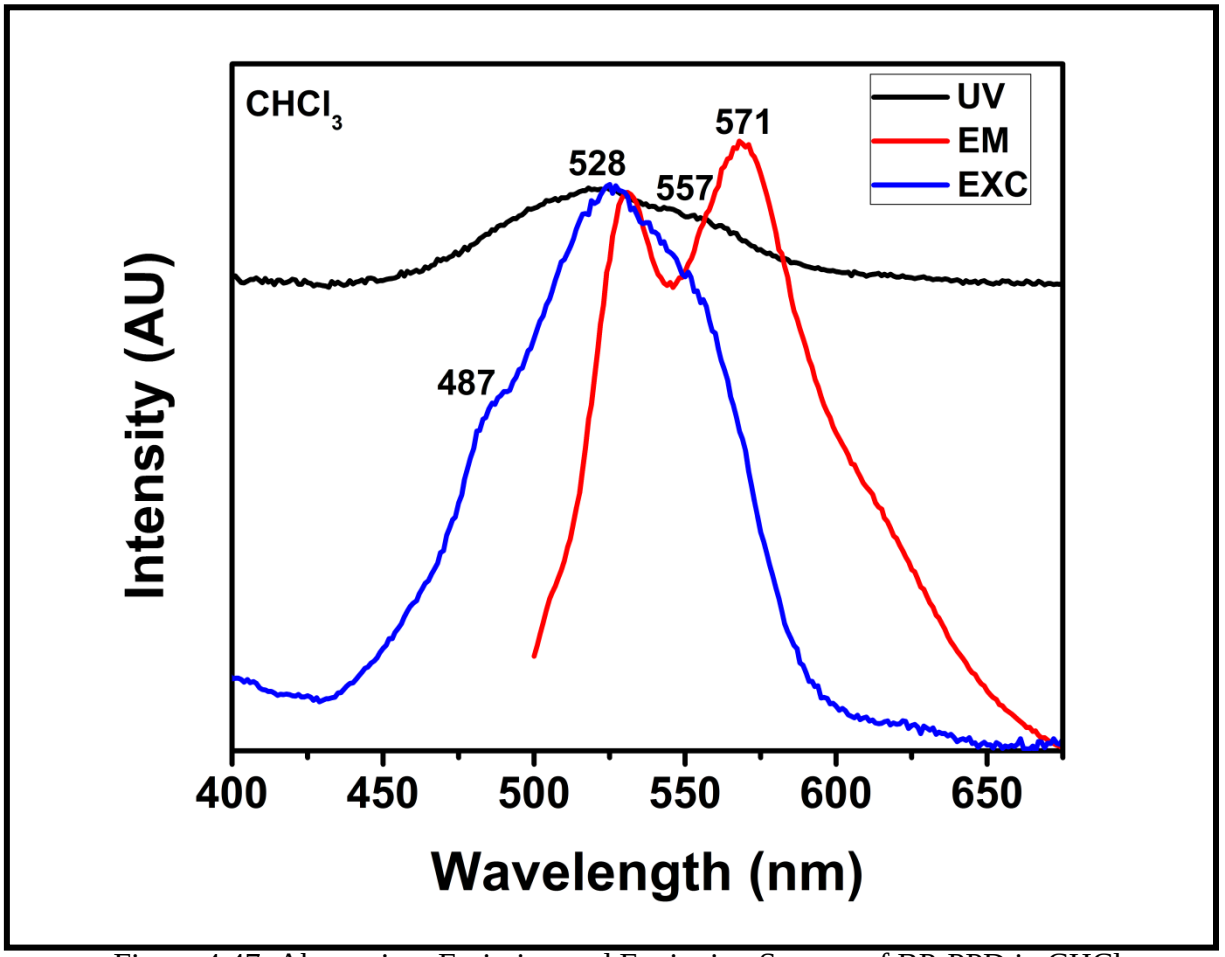

Figure 4.47: Absorption, Emission and Excitation Spectra of BP-PPD in $CHCl_3$

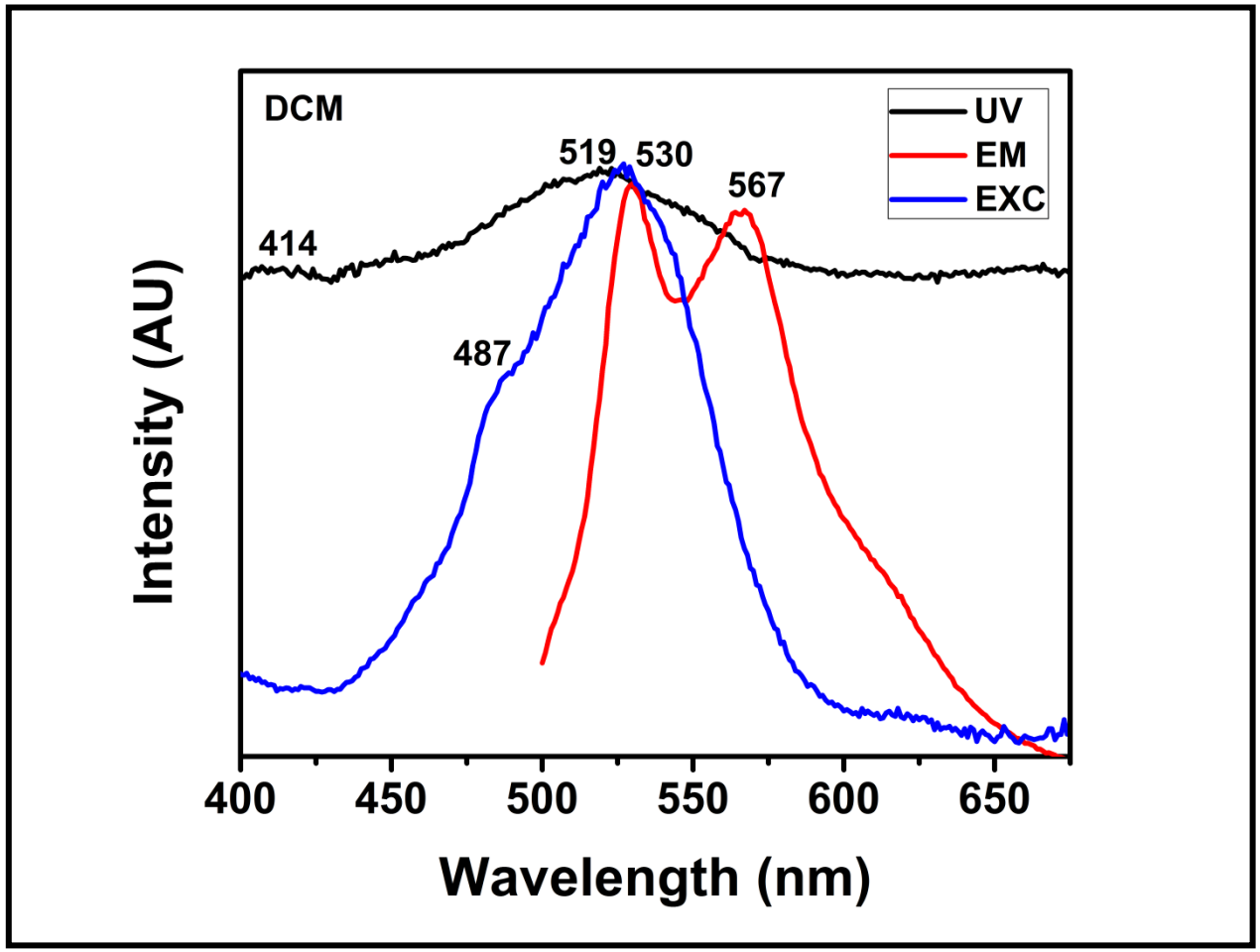

Figure 4.48: Absorption, Emission and Excitation Spectra of BP-PPD in DCM

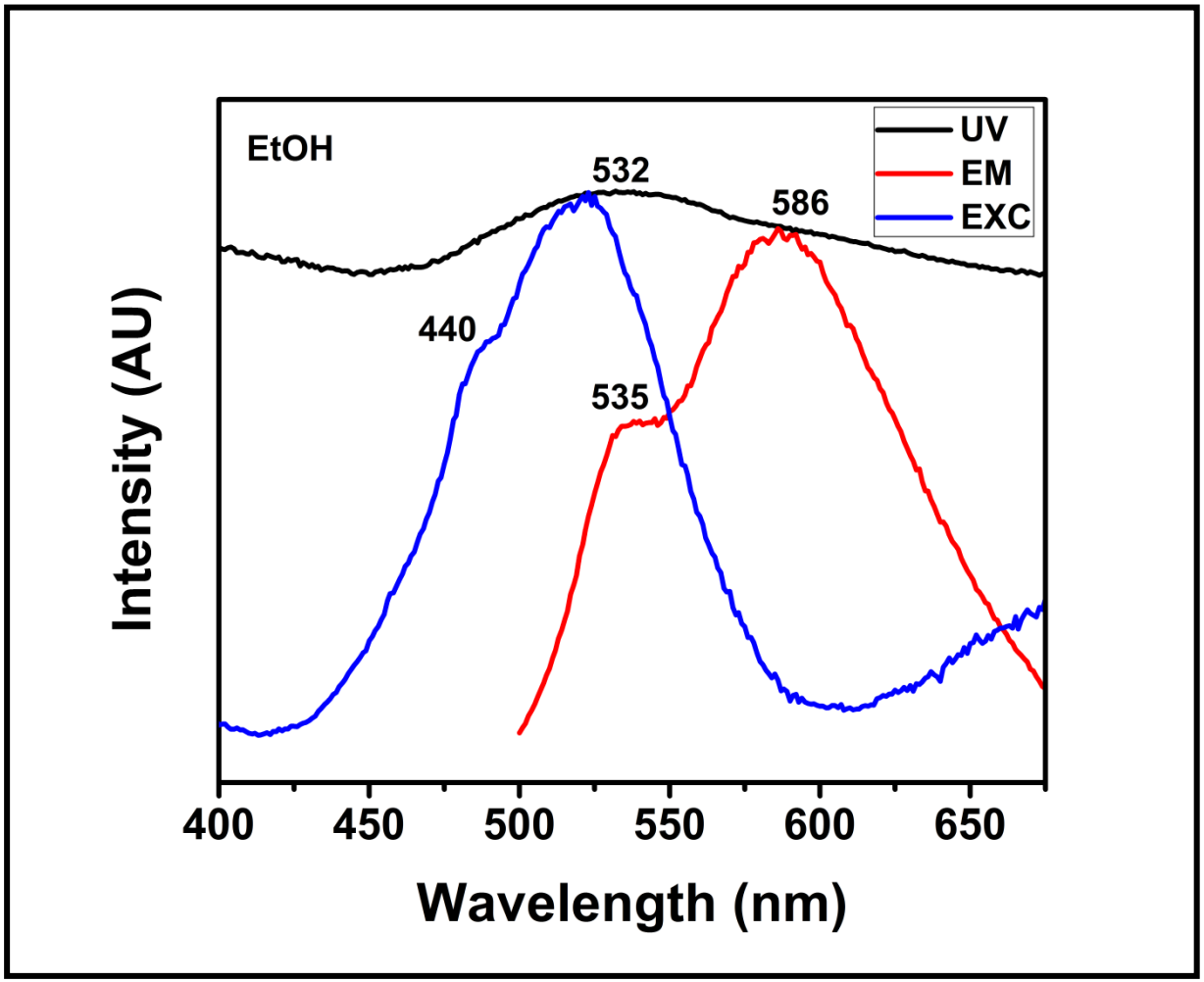

Figure 4.49: Absorption, Emission and Excitation Spectra of BP-PPD in EtOH

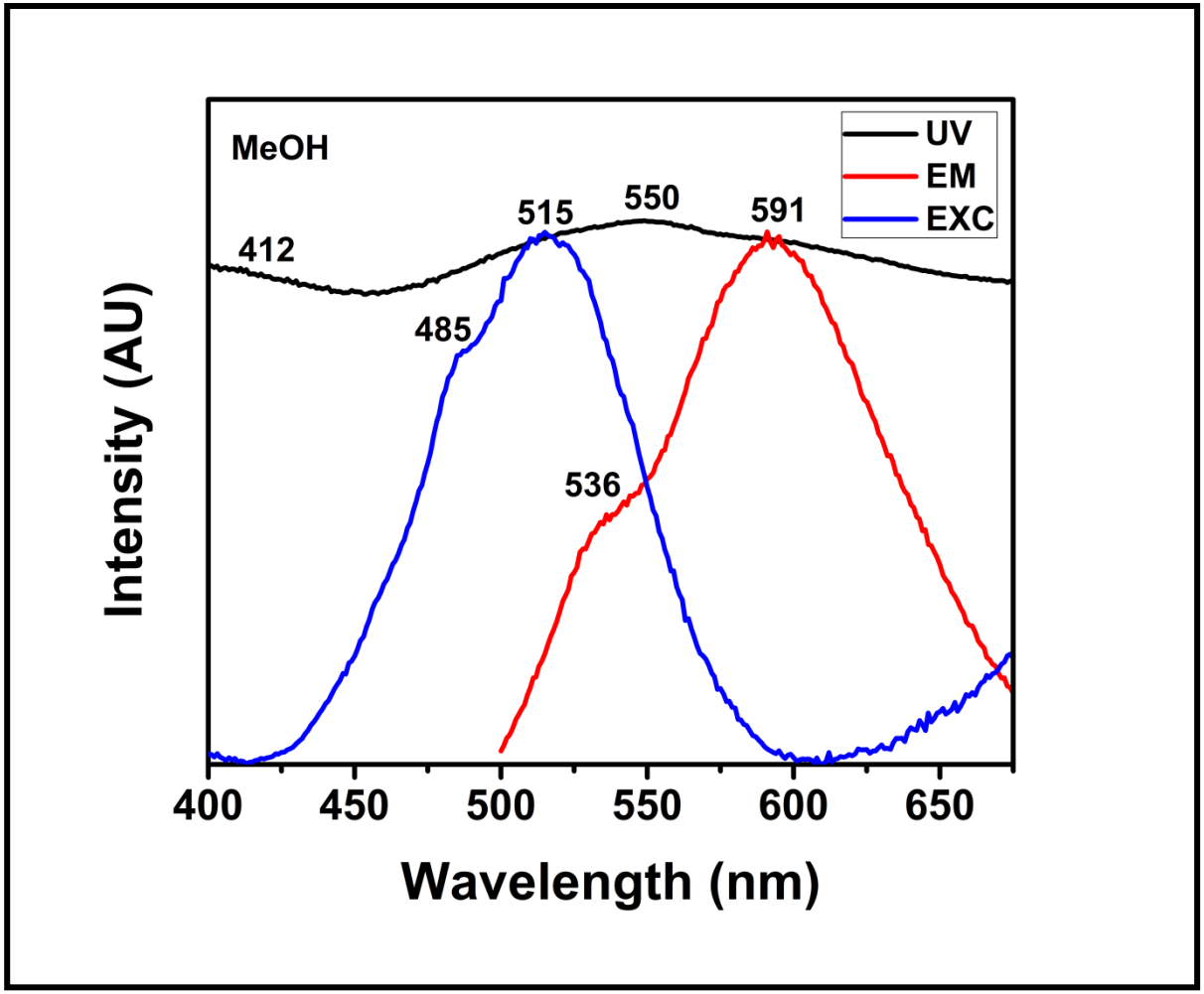

Figure 4.50: Absorption, Emission and Excitation Spectra of BP-PPD in MeOH

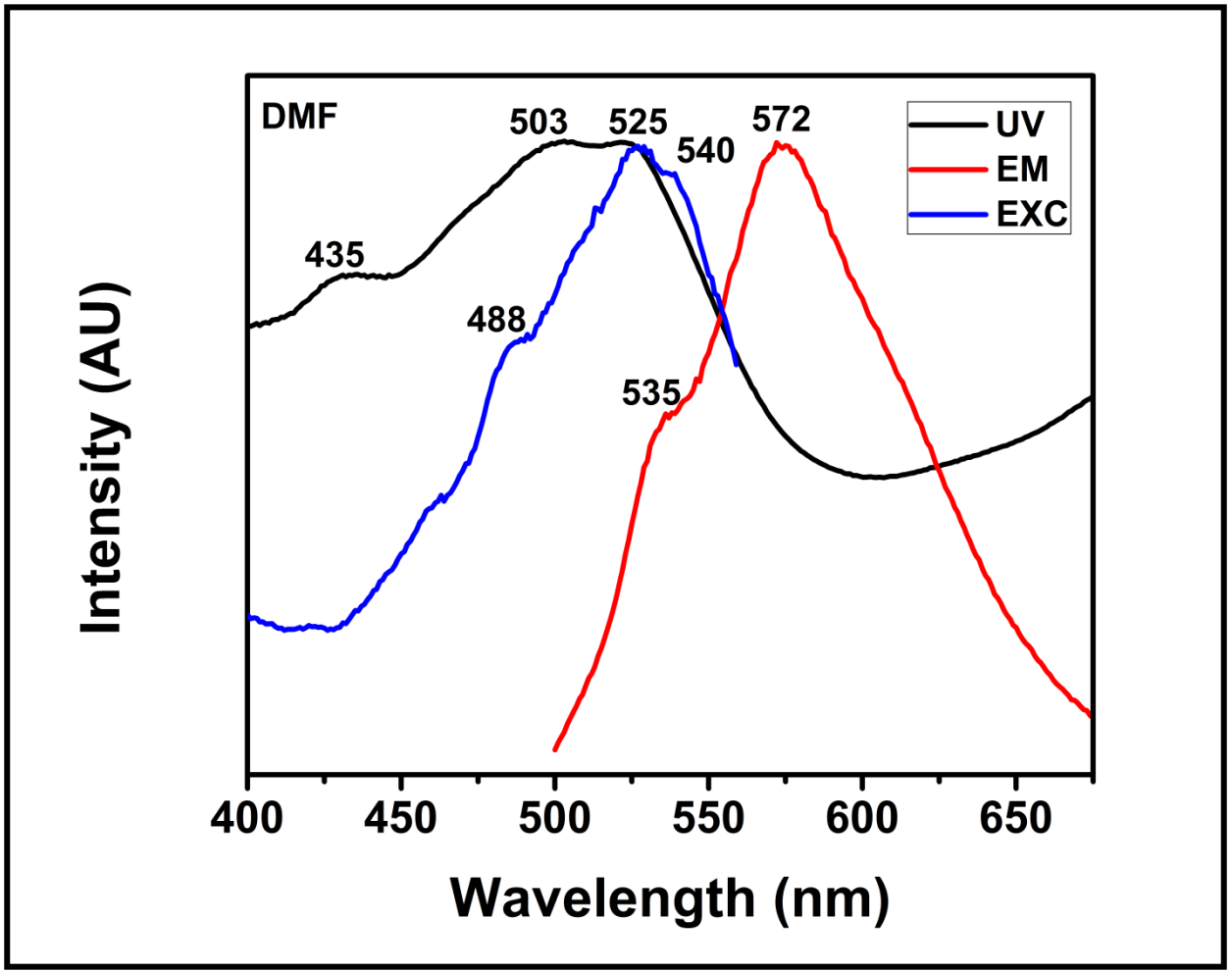

Figure 4.51: Absorption, Emission and Excitation Spectra of BP-PPD in DMF

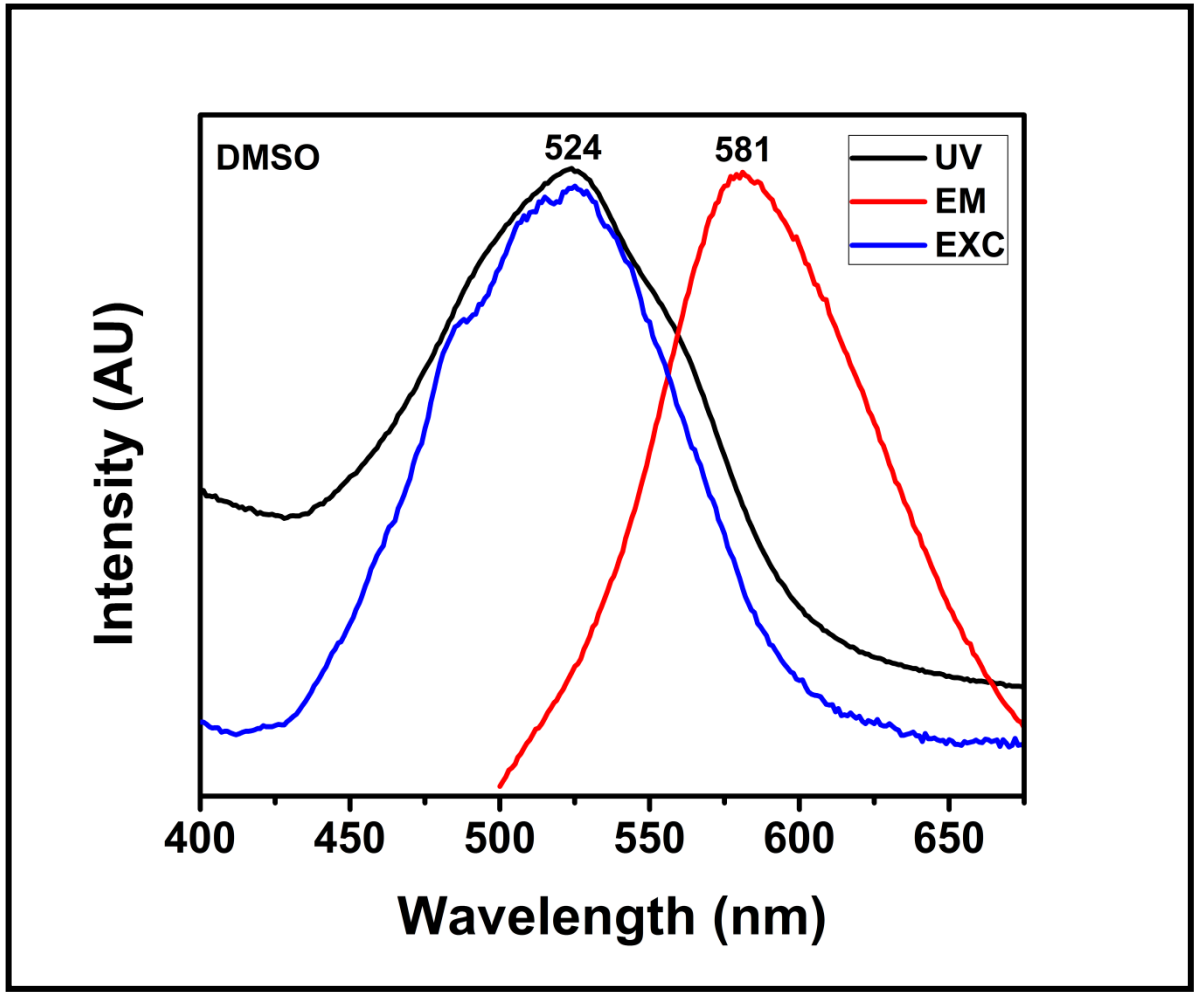

Figure 4.52: Absorption, Emission and Excitation Spectra of BP-PPD in DMSO

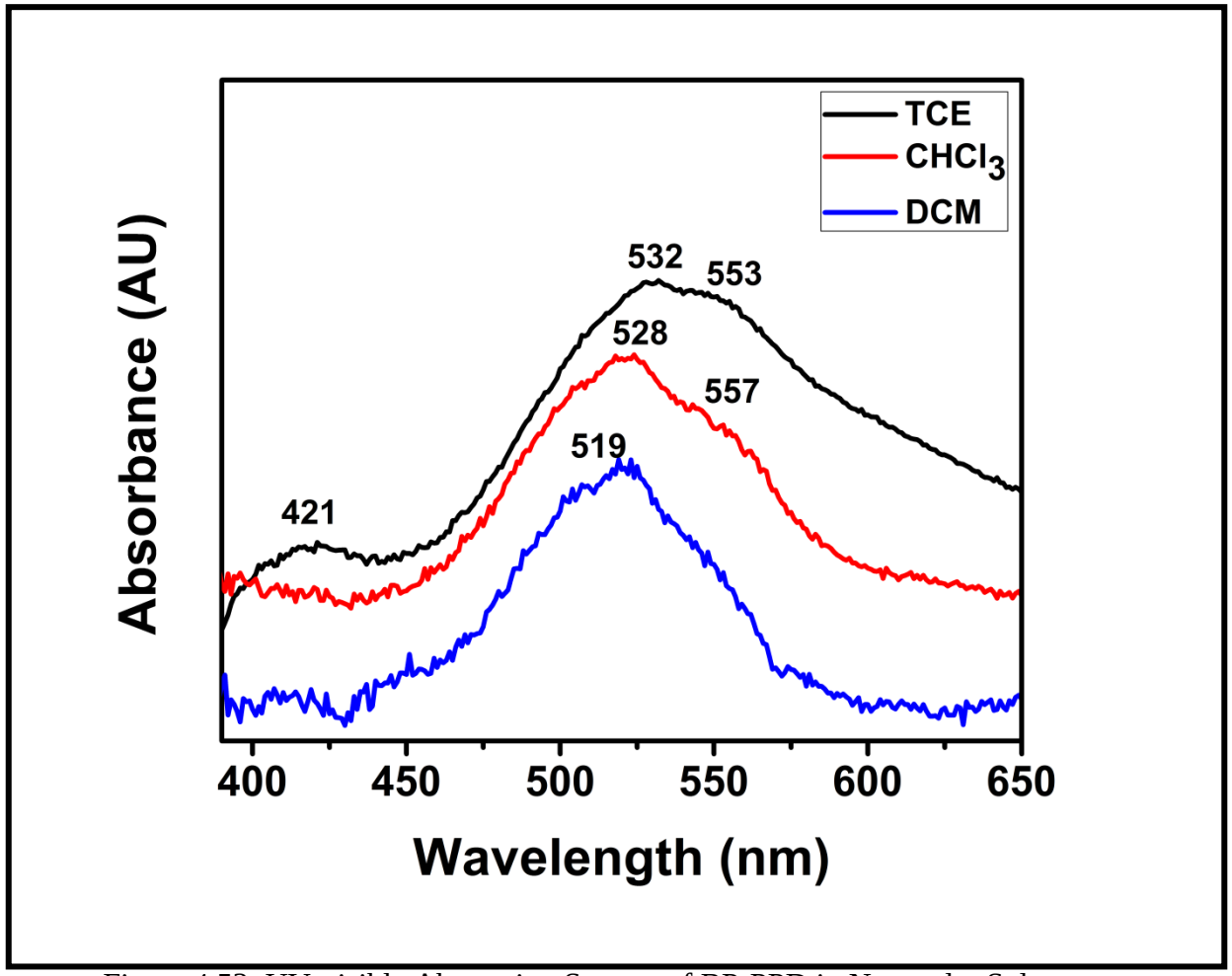

Figure 4.53: UV-visible Absorption Spectra of BP-PPD in Non-polar Solvents

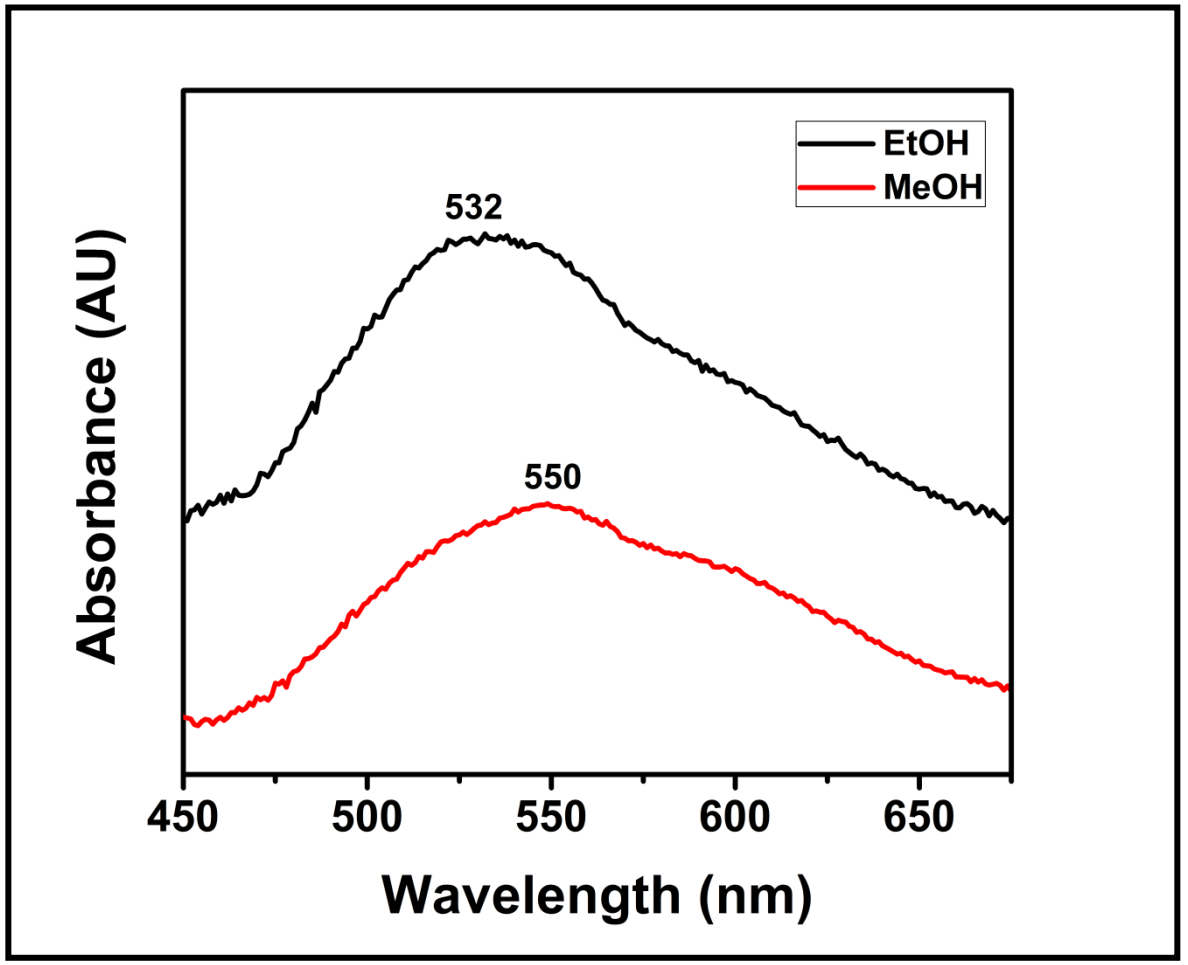

Figure 4.54: UV-visible Absorption Spectra of BP-PPD in Protic Solvents

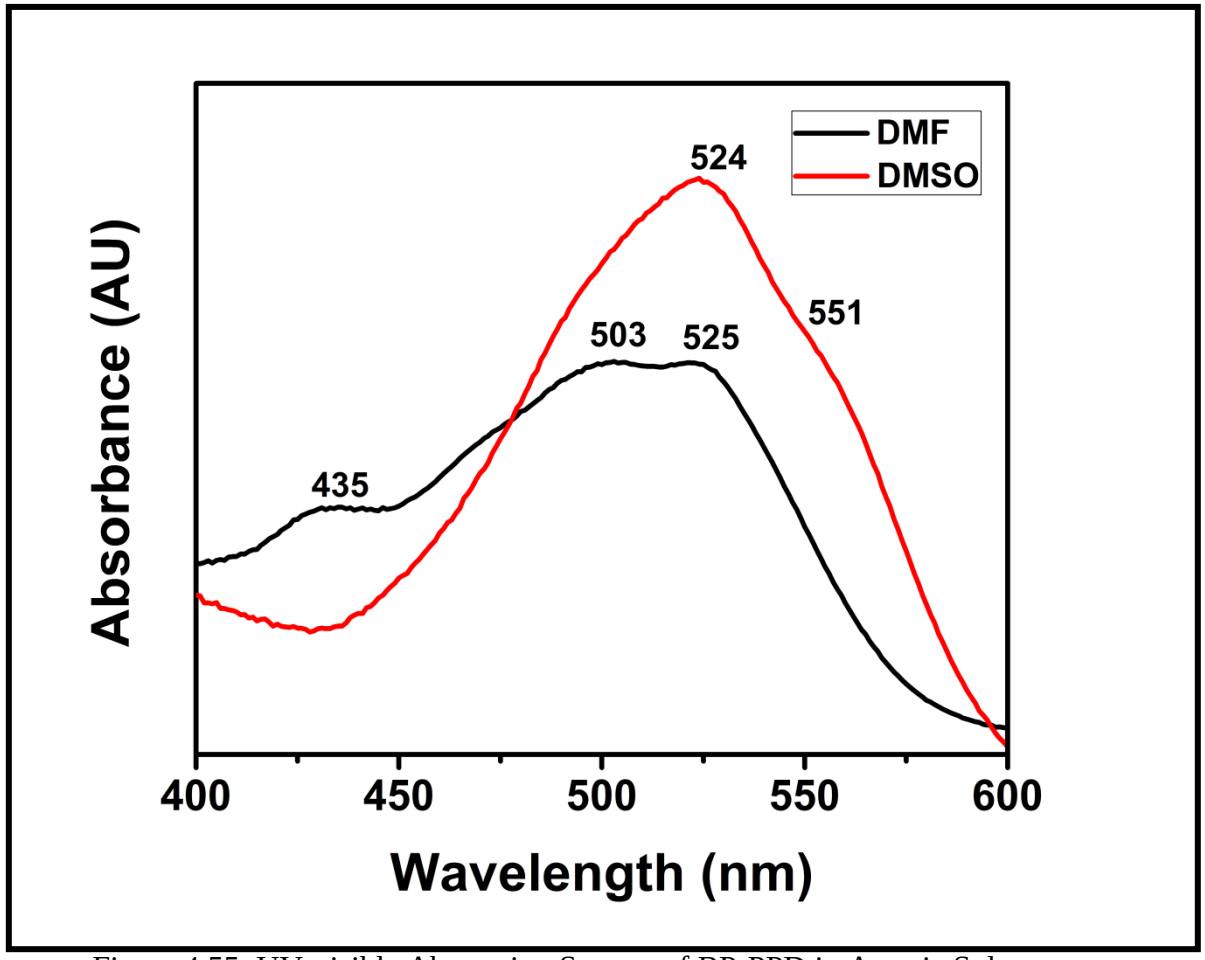

Figure 4.55: UV-visible Absorption Spectra of BP-PPD in Aprotic Solvents

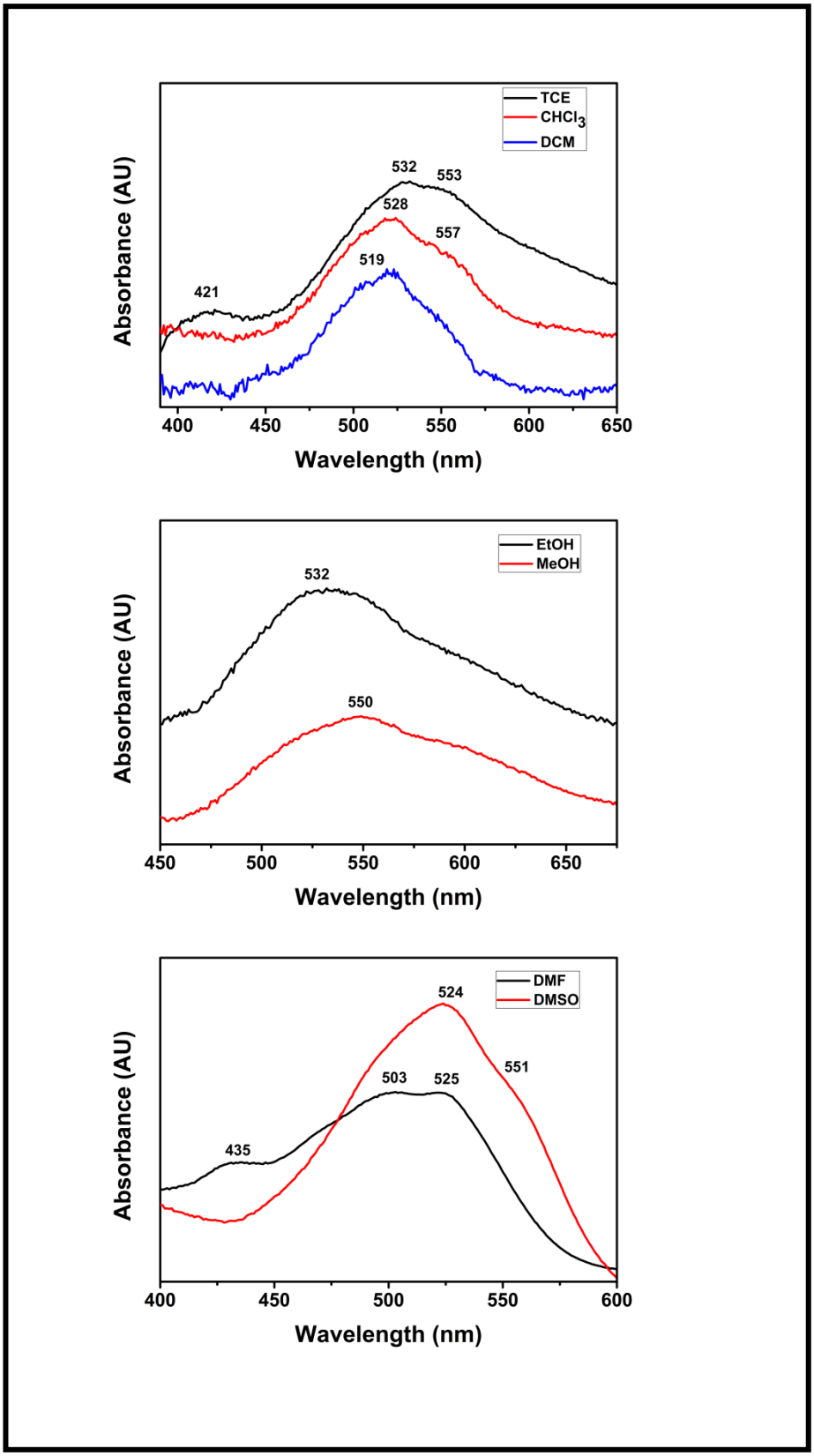

Figure 4.56: UV-visible Absorption Spectra of BP-PPD in Several Organic Solvents

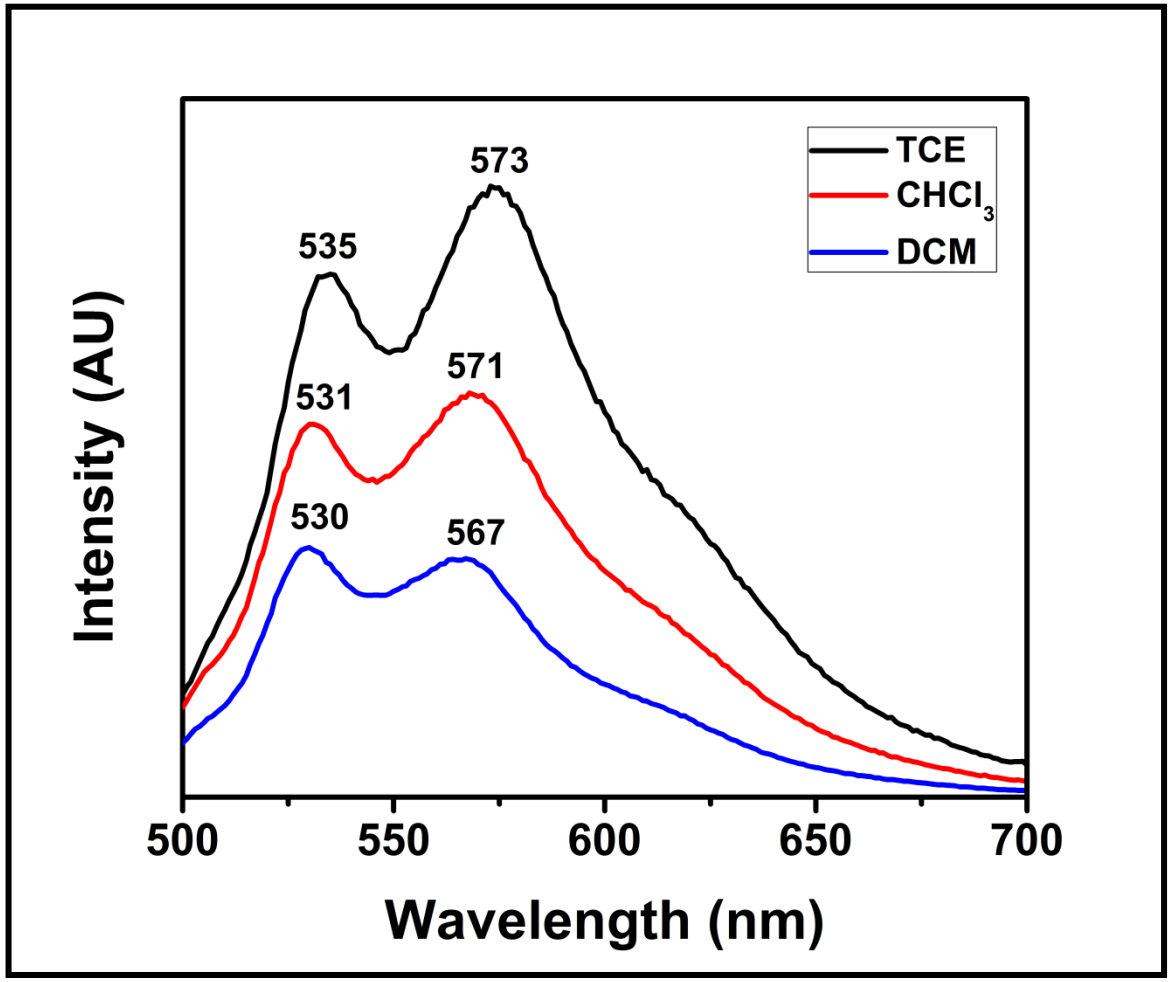

Figure 4.57: Emission Spectra of BP-PPD in Non-polar Solvents

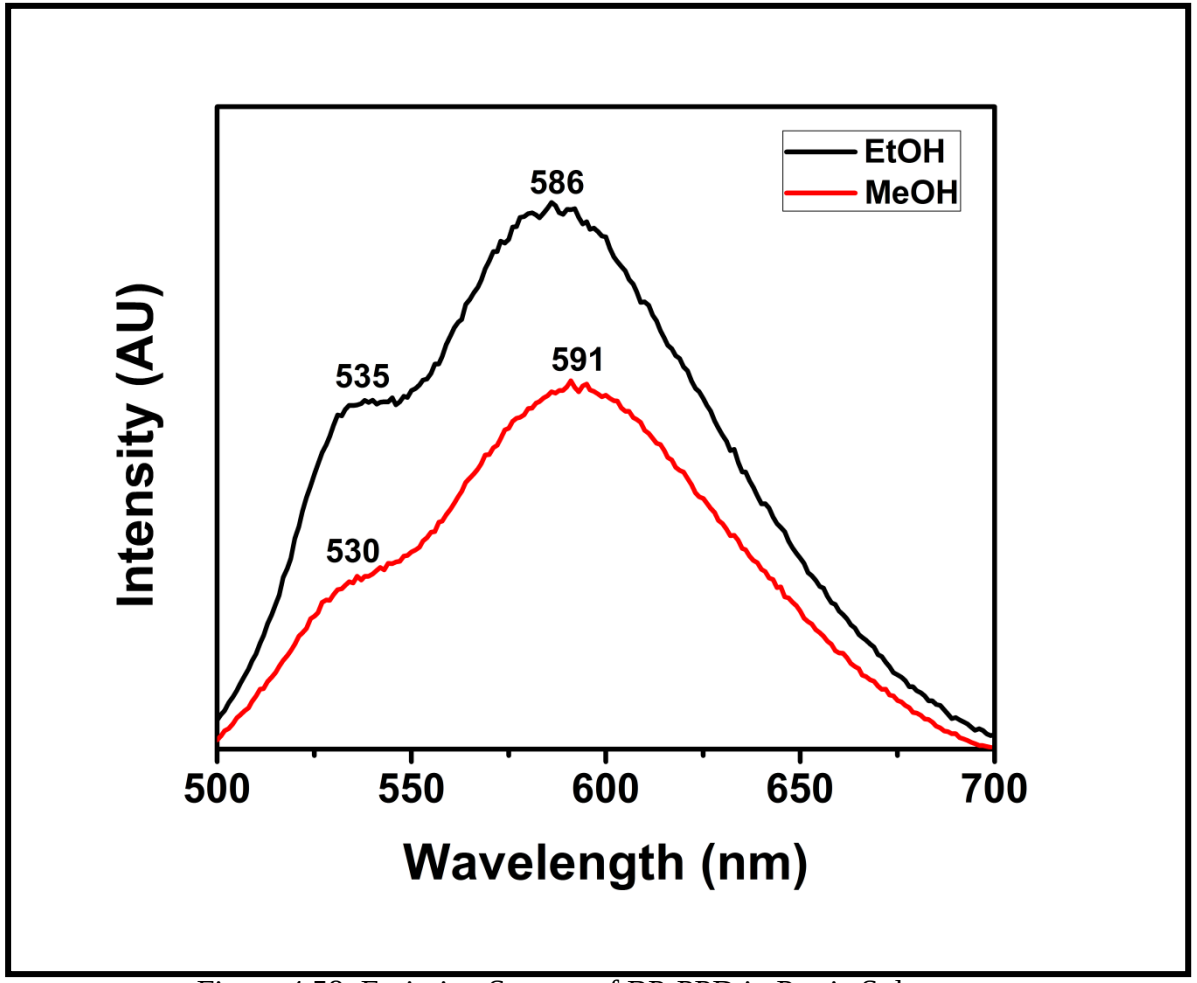

Figure 4.58: Emission Spectra of BP-PPD in Protic Solvents

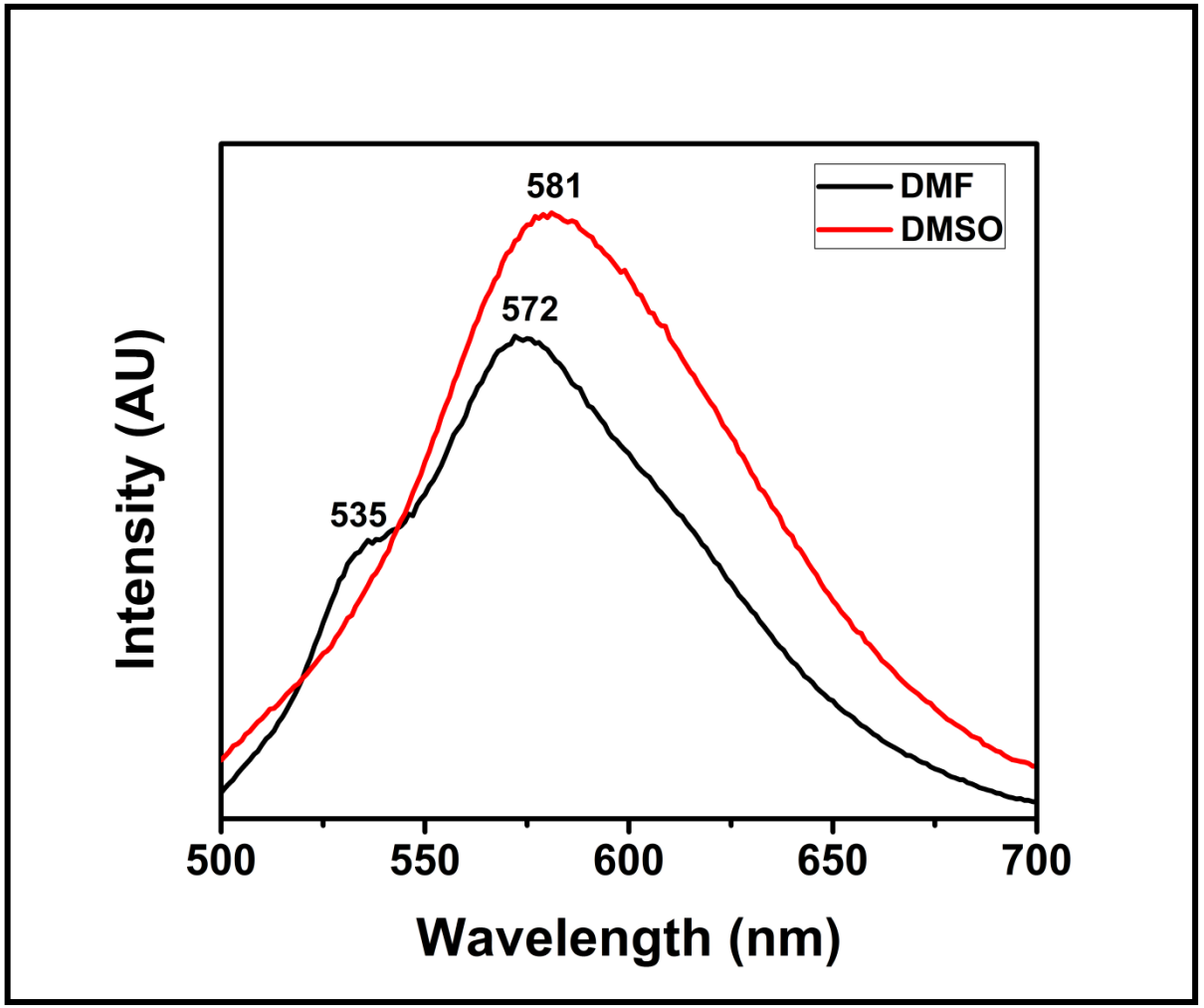

Figure 4.59: Emission Spectra of BP-PPD in Aprotic Solvents

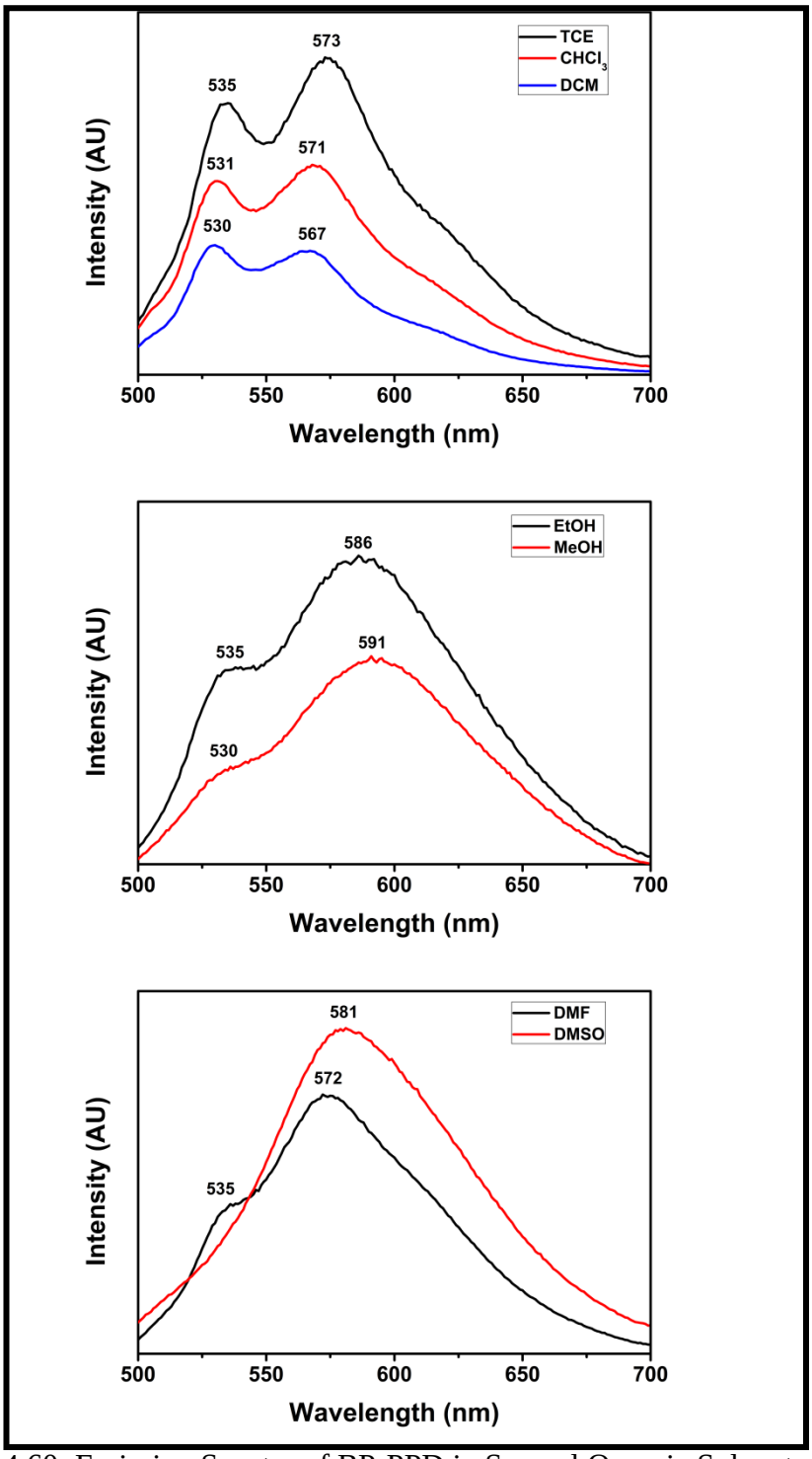

Figure 4.60: Emission Spectra of BP-PPD in Several Organic Solvents

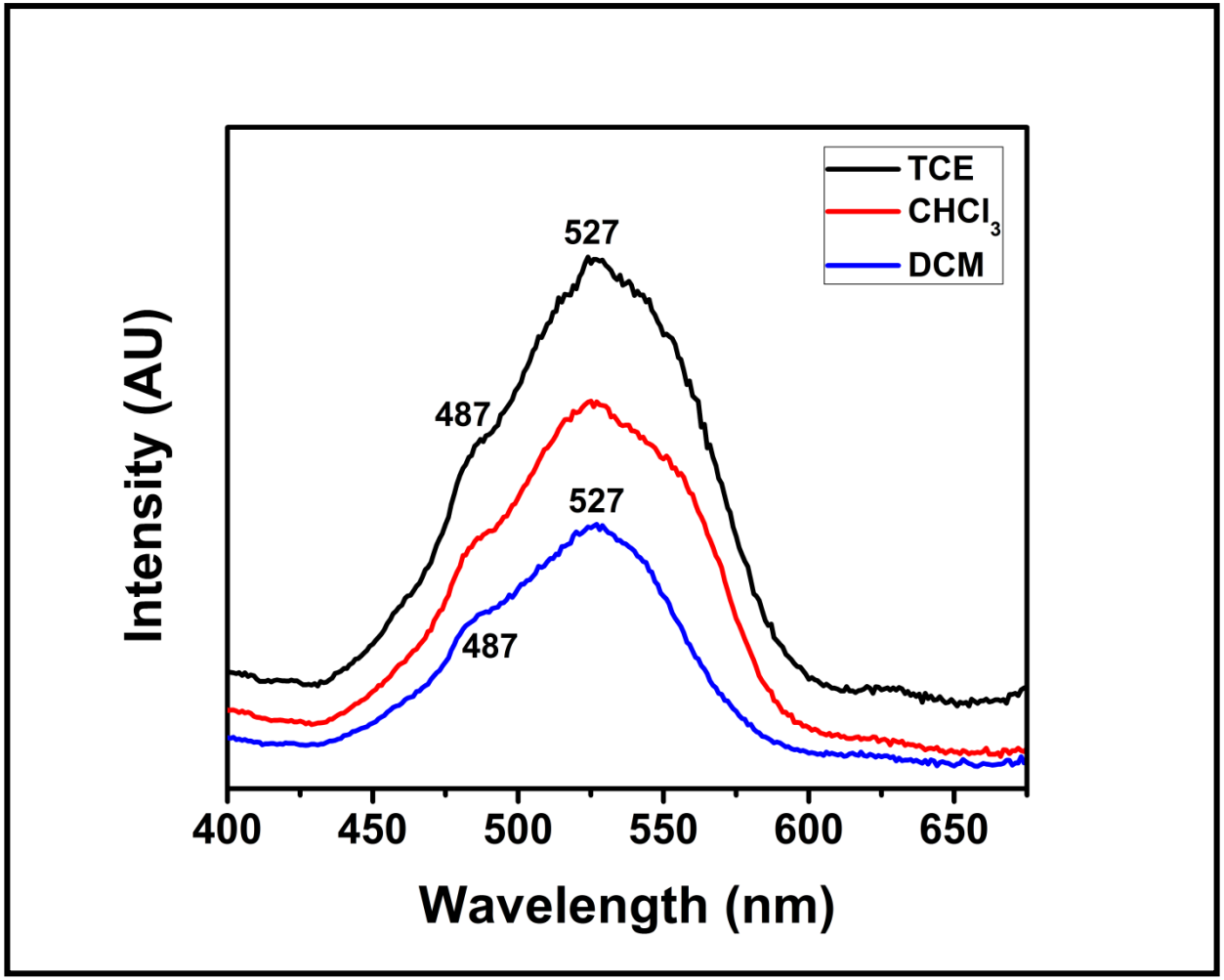

Figure 4.61: Excitation Spectra of BP-PPD in Non-polar Solvents

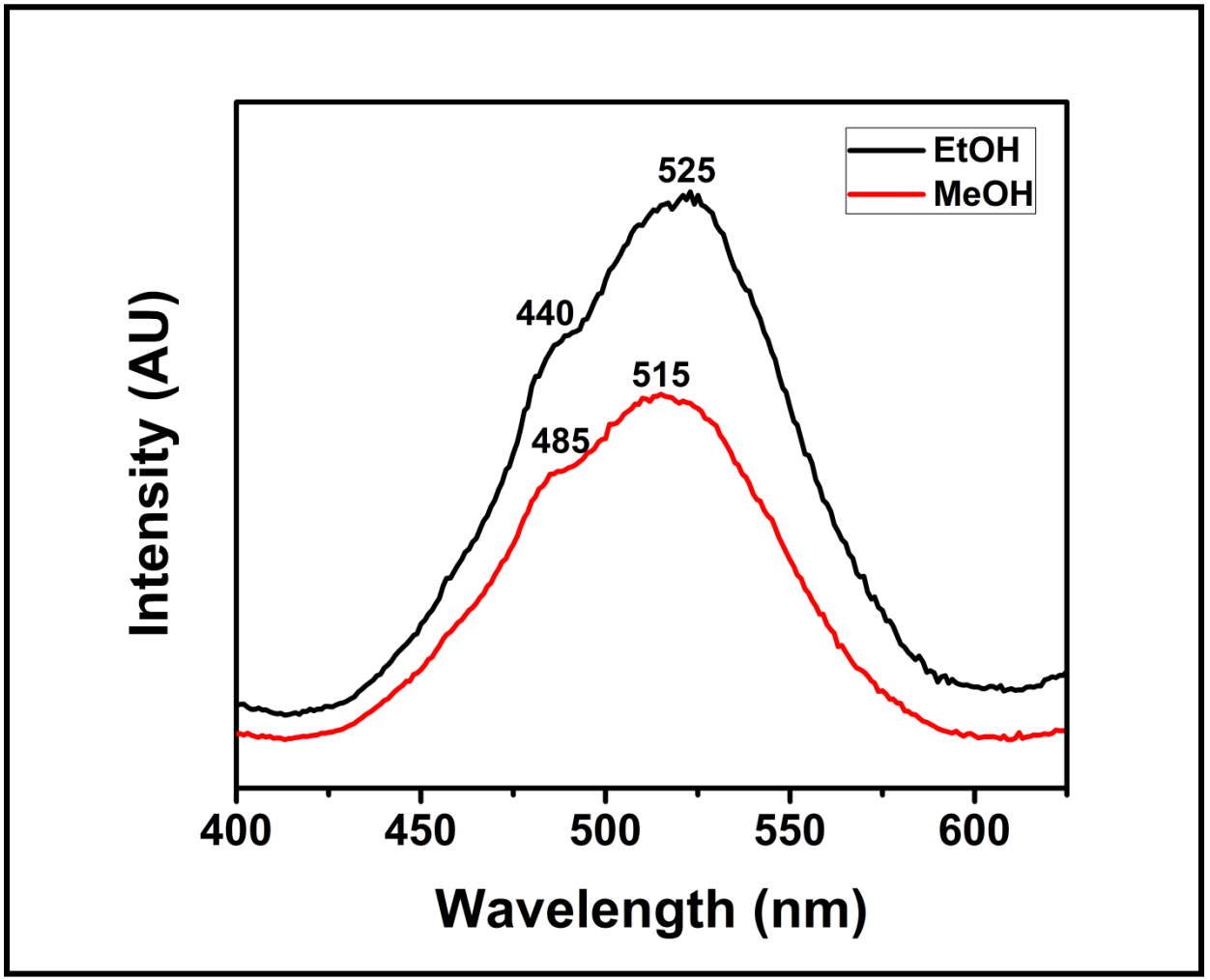

Figure 4.62: Excitation Spectra of BP-PPD in Protic Solvents

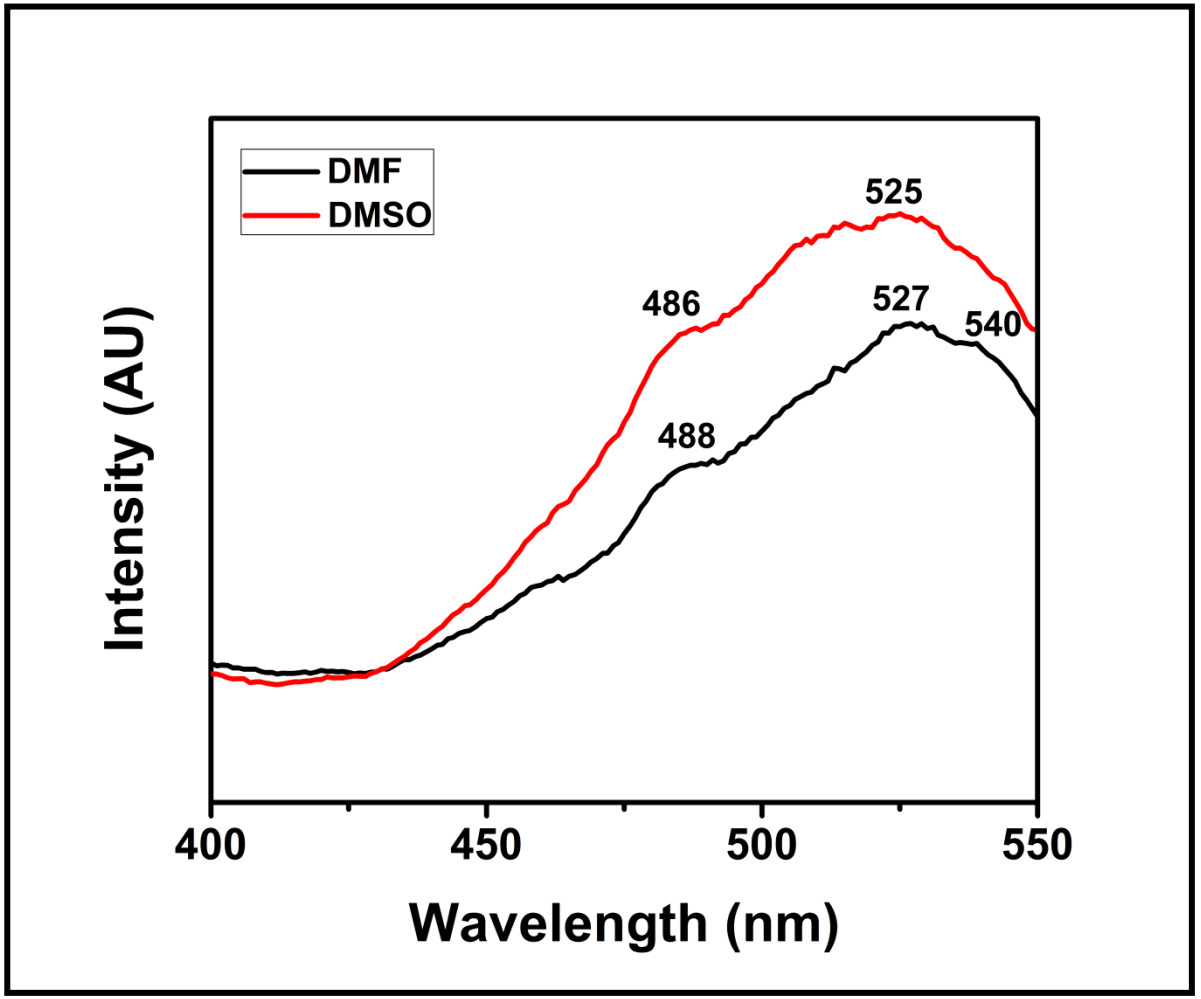

Figure 4.63: Excitation Spectra of BP-PPD in Aprotic Solvents

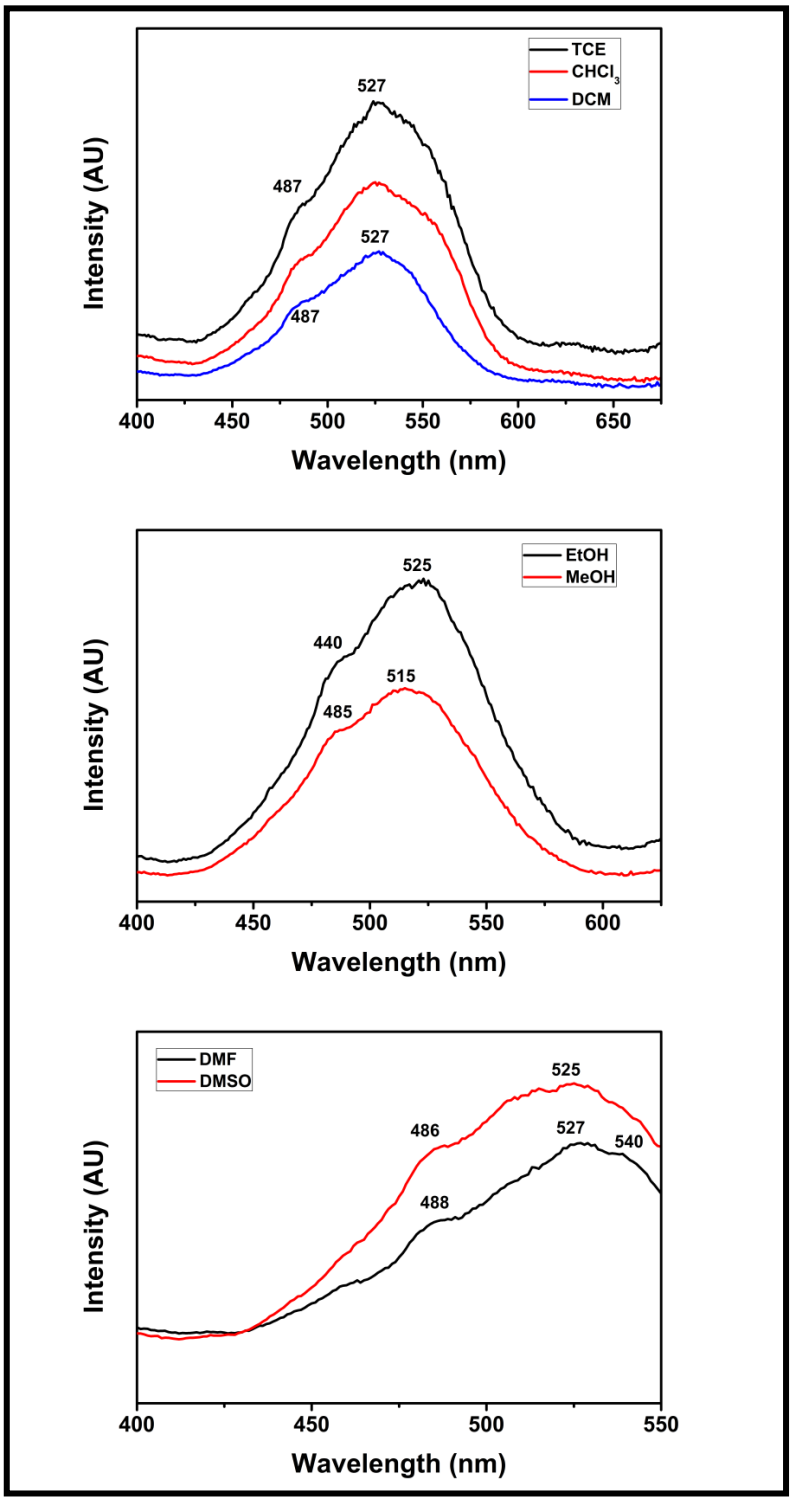

Figure 4.64: Excitation Spectra of BP-PPD in Several Organic Solvent

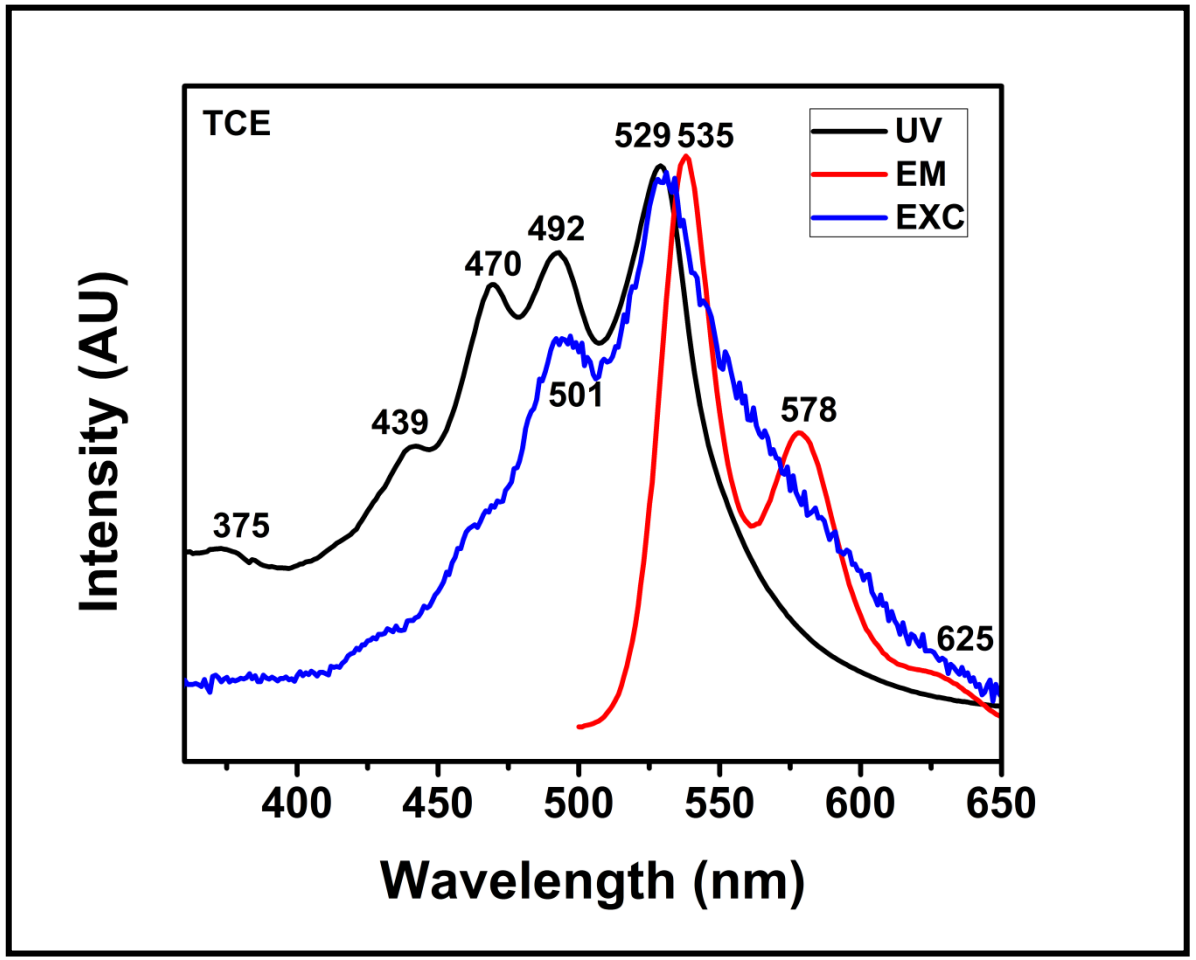

Figure 4.65: Absorption, Emission and Excitation Spectra of TPE-PDI in TCE

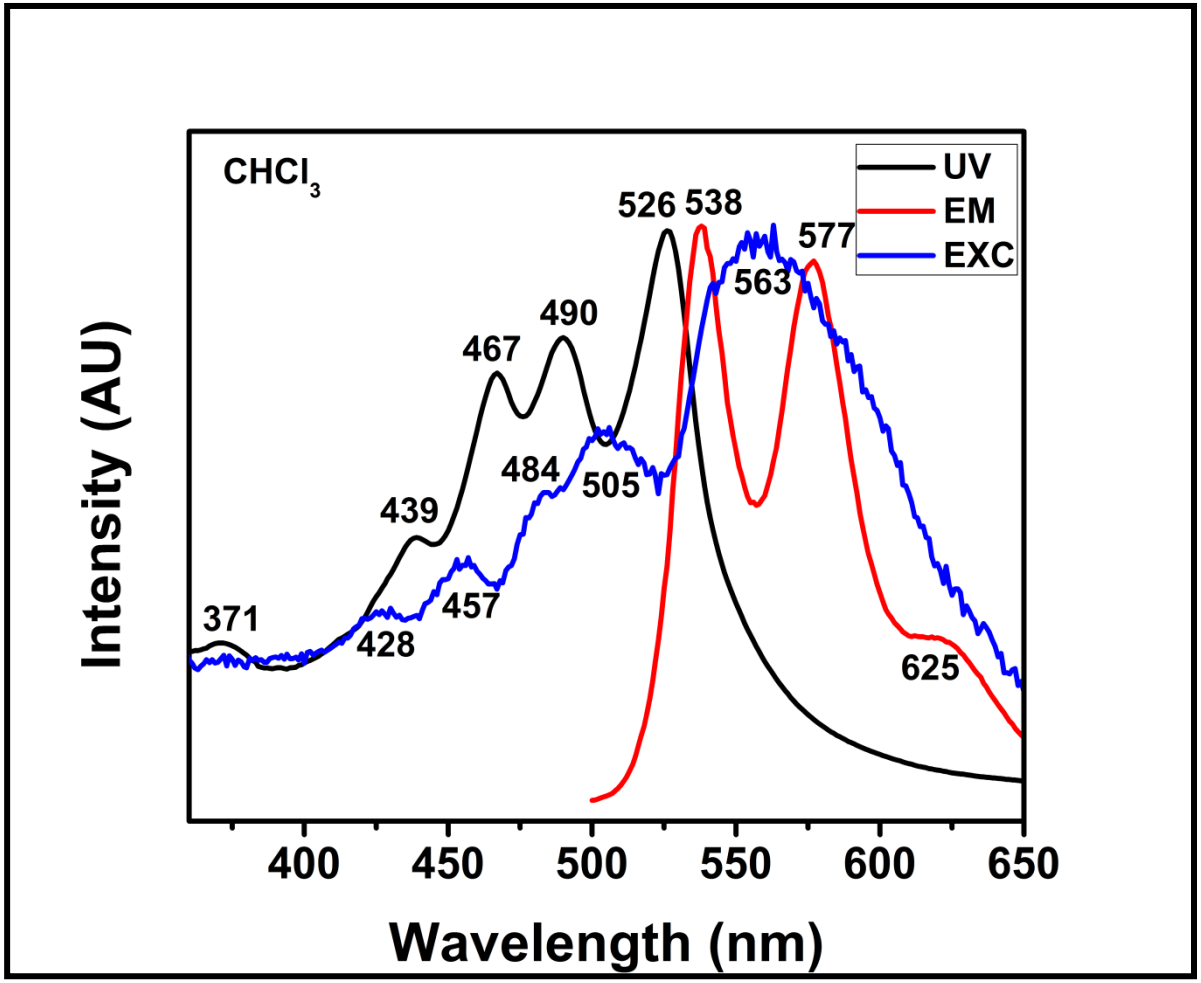

Figure 4.66: Absorption, Emission and Excitation Spectra of TPE-PDI in $CHCl_3$

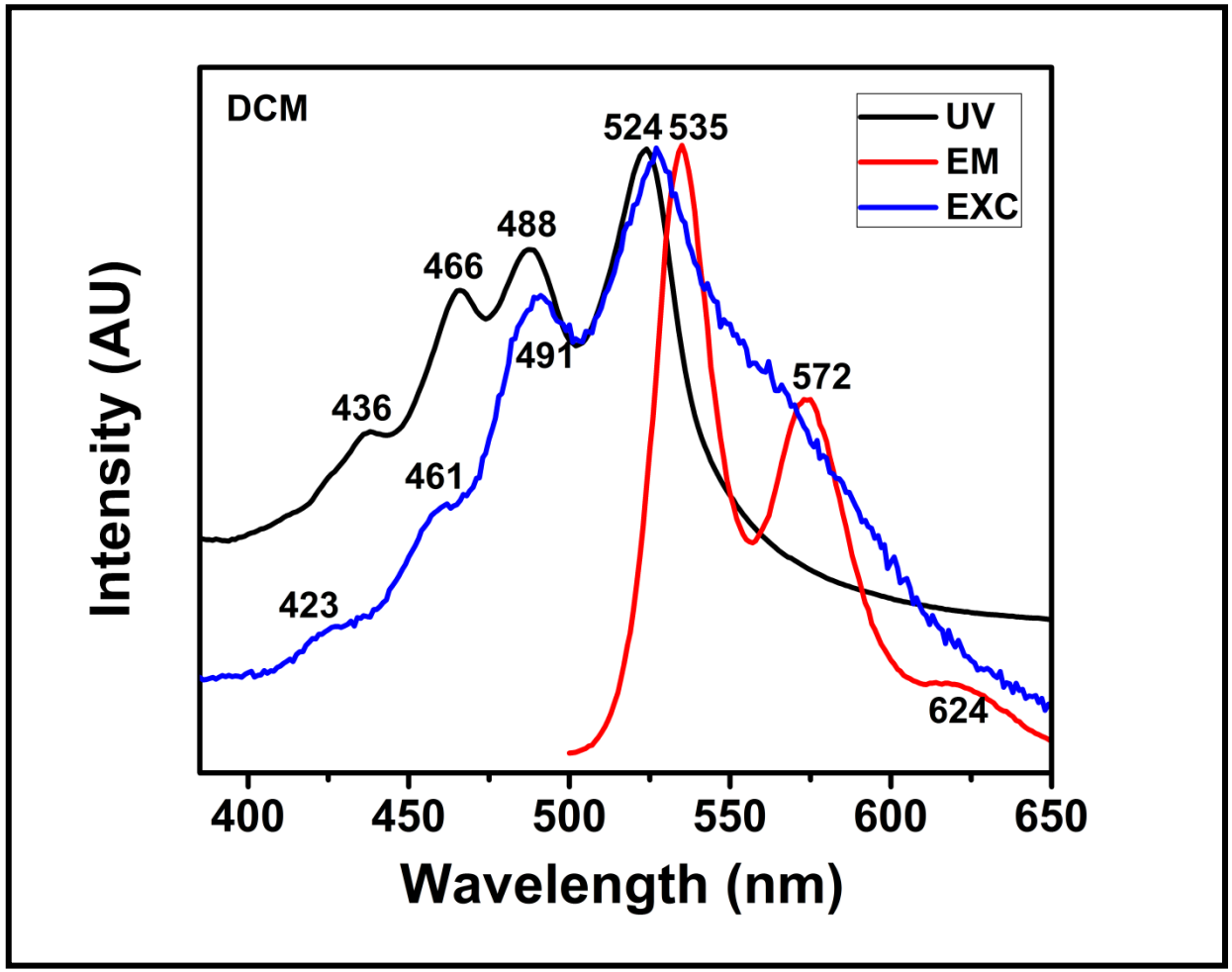

Figure 4.67: Absorption, Emission and Excitation Spectra of TPE-PDI in DCM

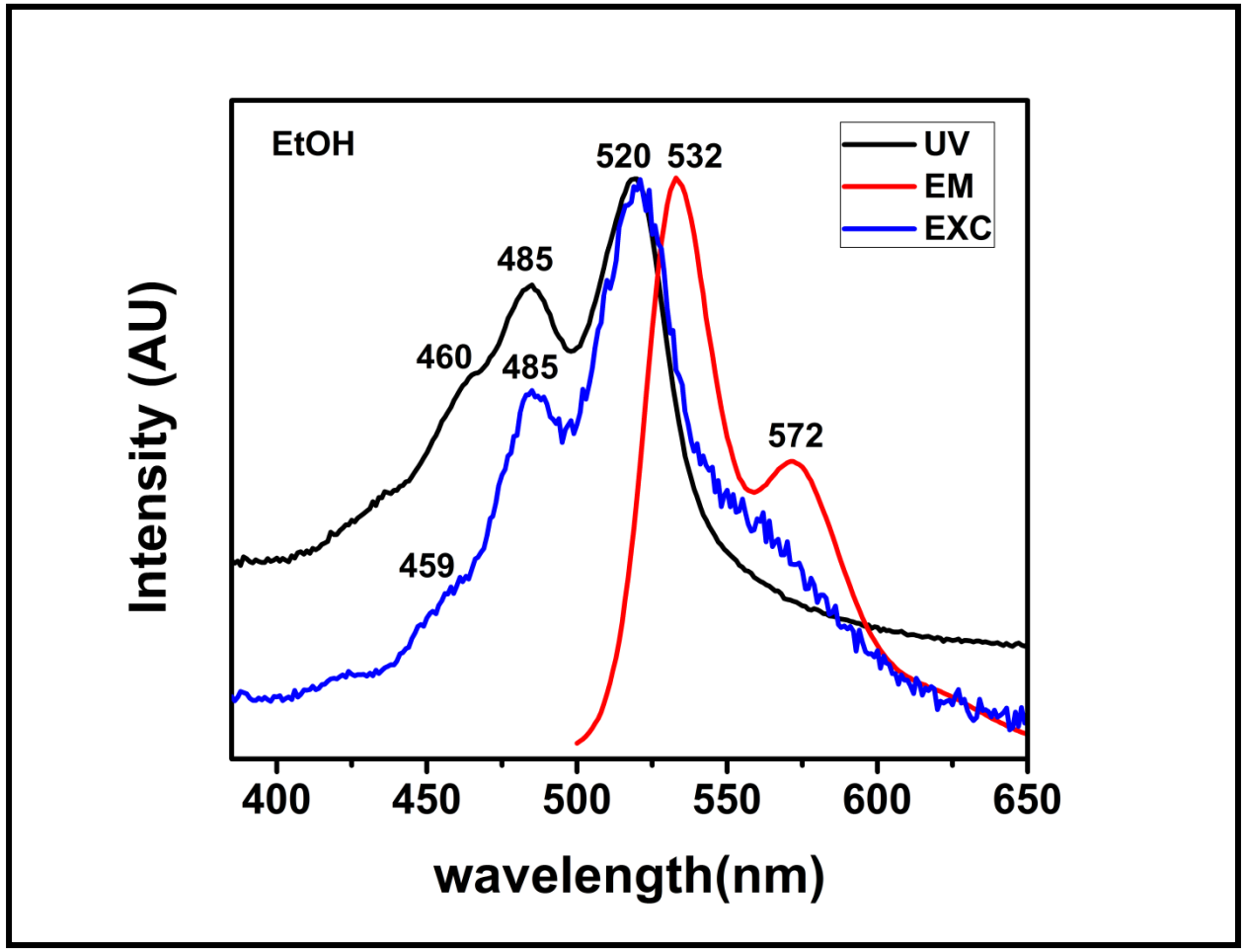

Figure 4.68: Absorption, Emission and Excitation Spectra of TPE-PDI in EtOH

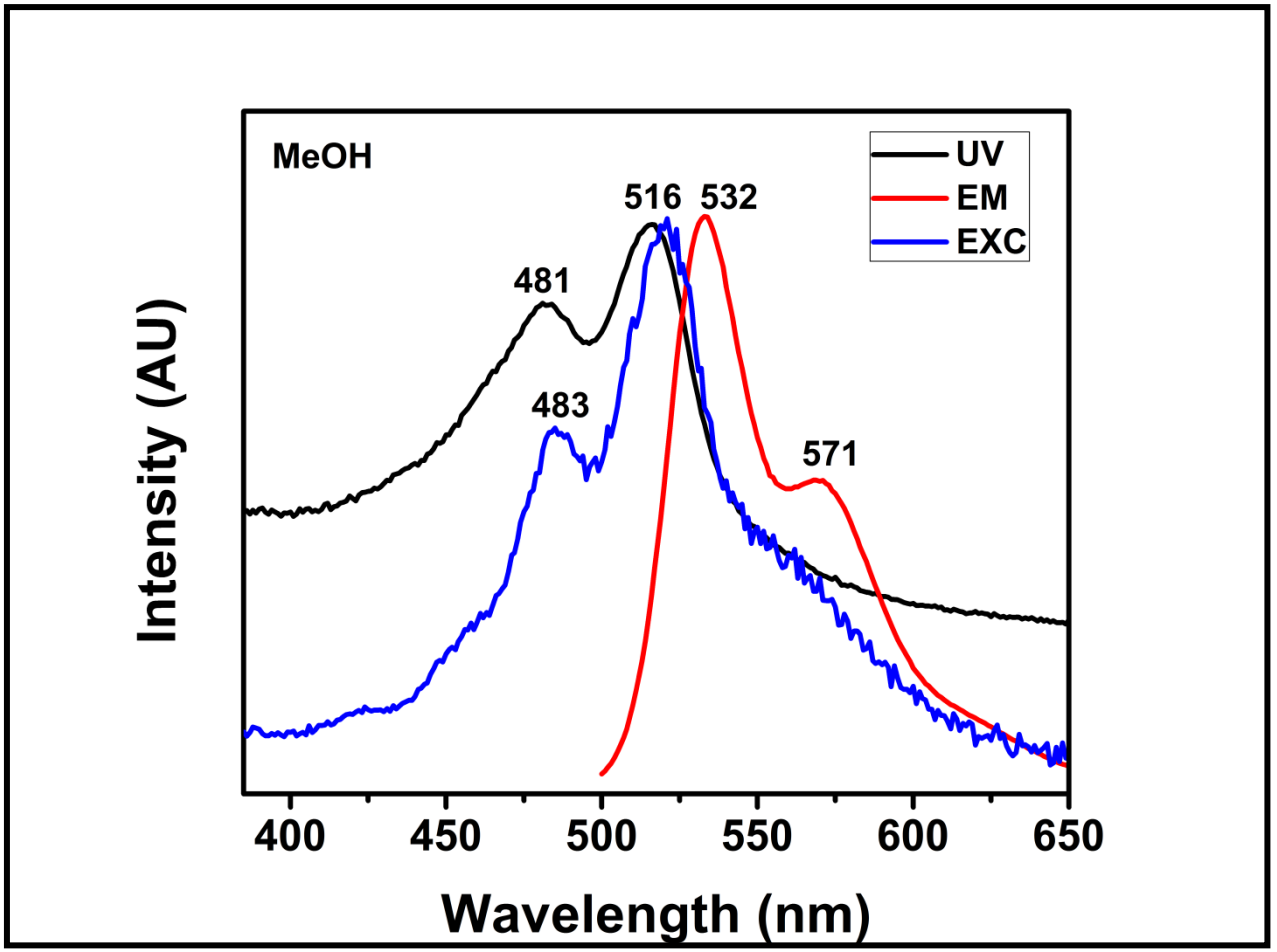

Figure 4.69: Absorption, Emission and Excitation Spectra of TPE-PDI in MeOH

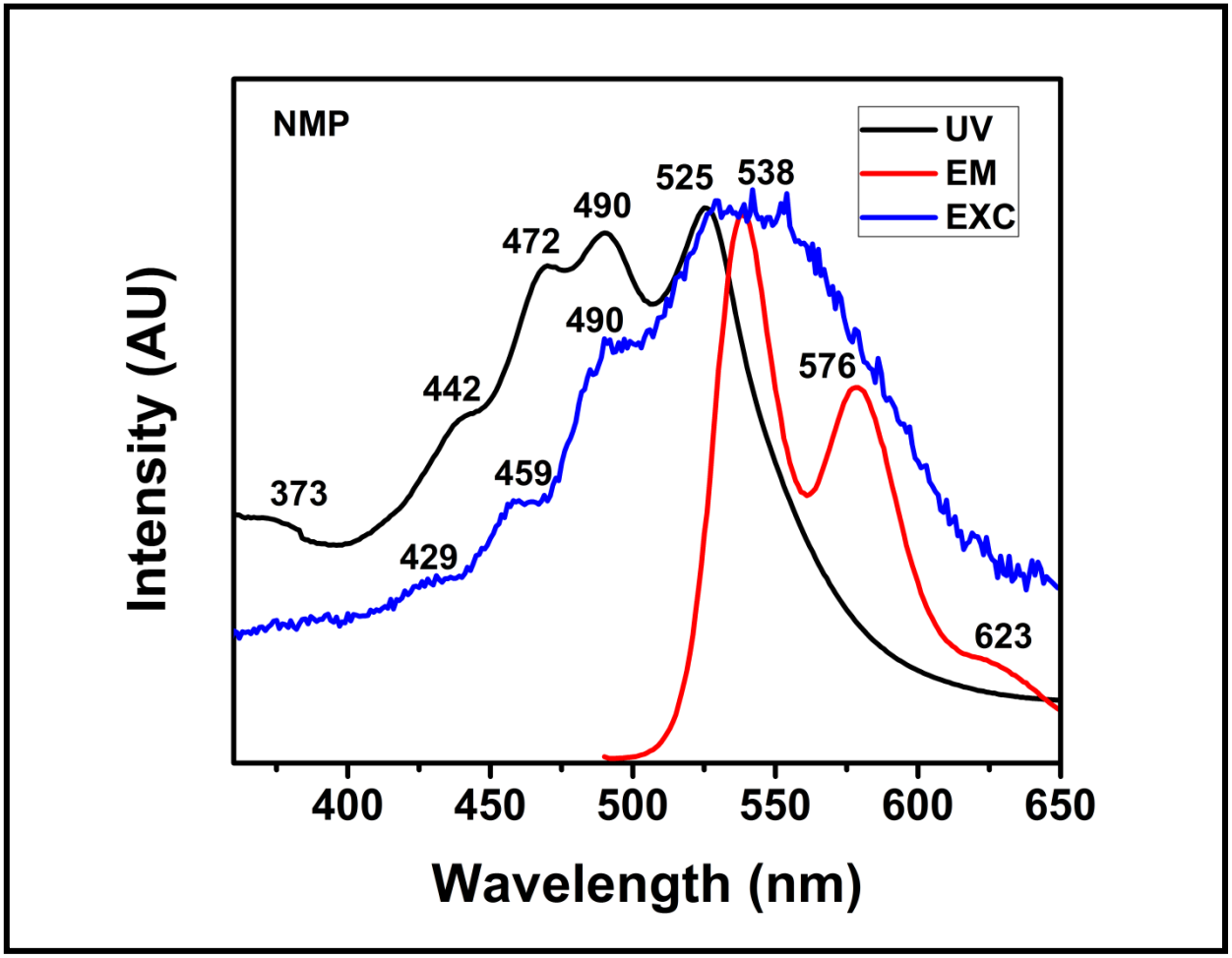

Figure 4.70: Absorption, Emission and Excitation Spectra of TPE-PDI in NMP

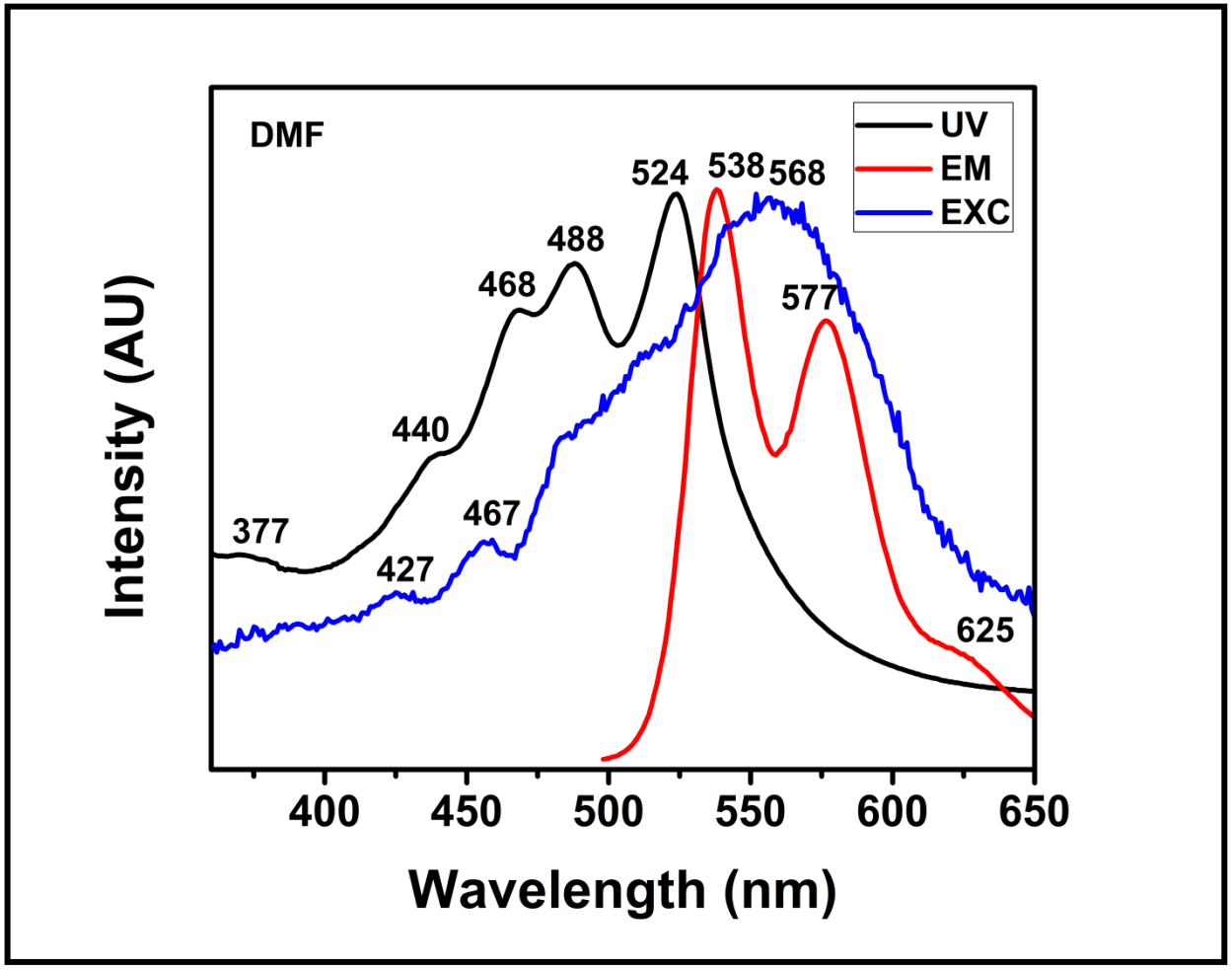

Figure 4.71: Absorption, Emission and Excitation Spectra of TPE-PDI in DMF

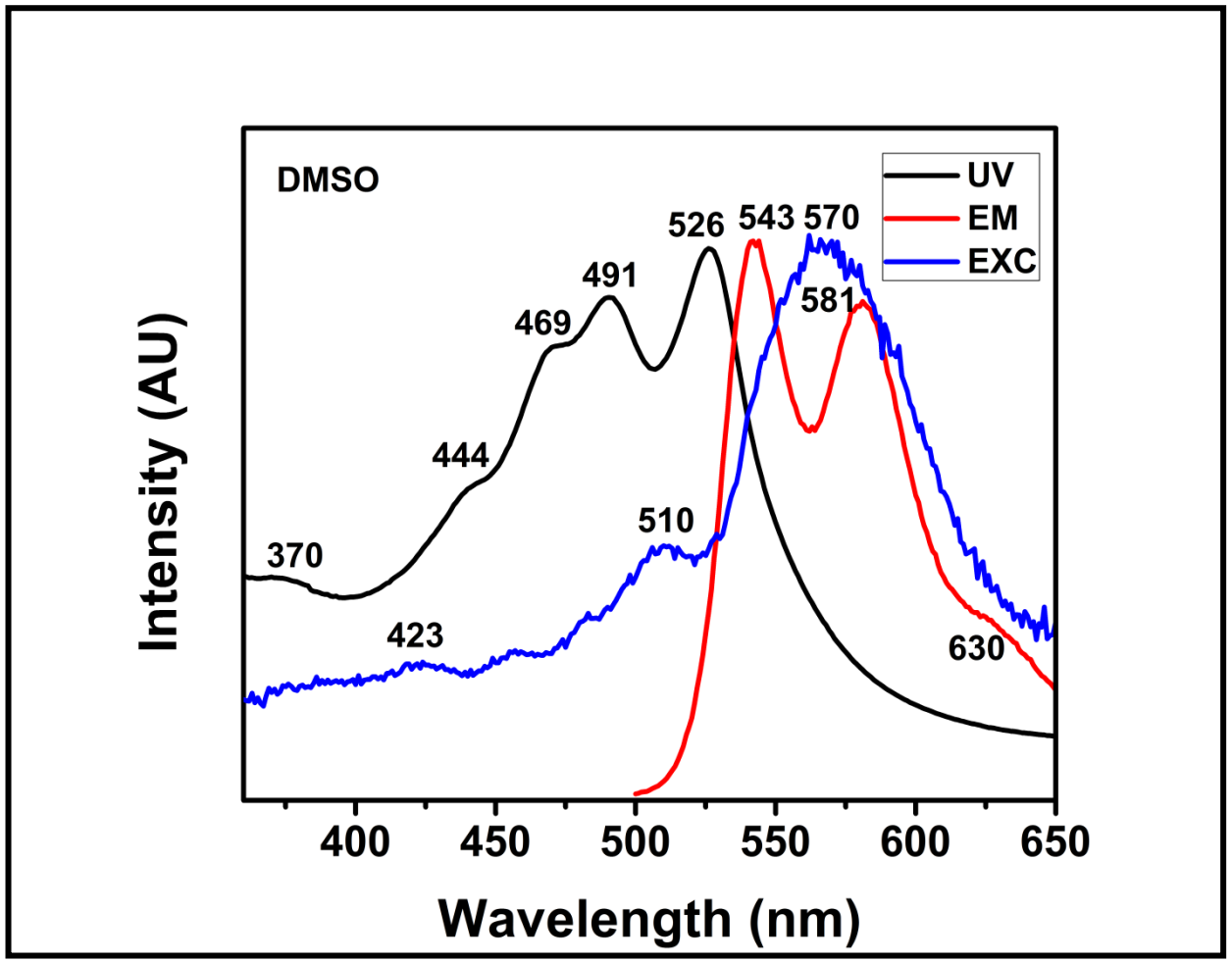

Figure 4.72: Absorption, Emission and Excitation Spectra of TPE-PDI in DMSO

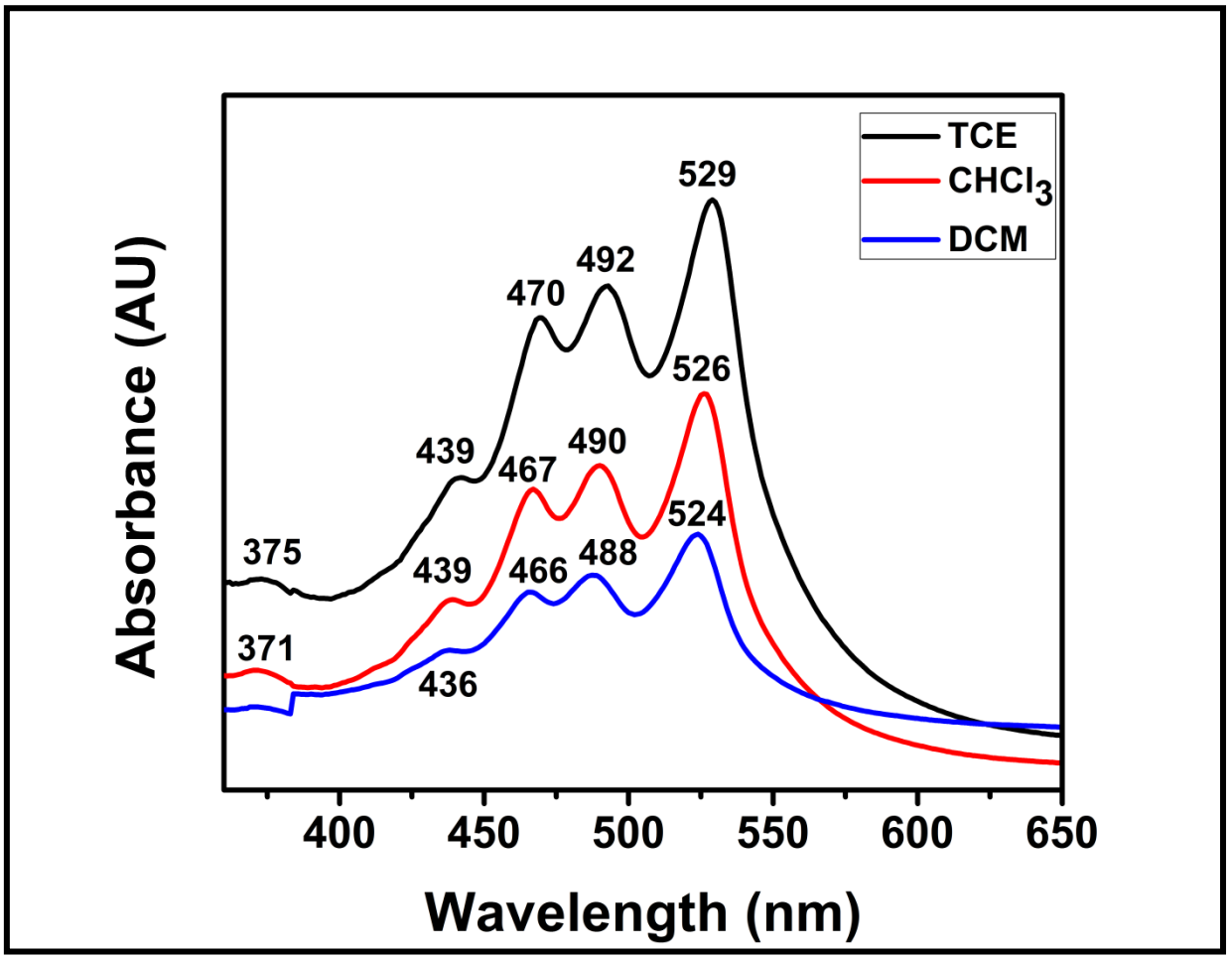

Figure 4.73: UV-visible Absorption Spectra of TPE-PDI in Non-polar Solvents

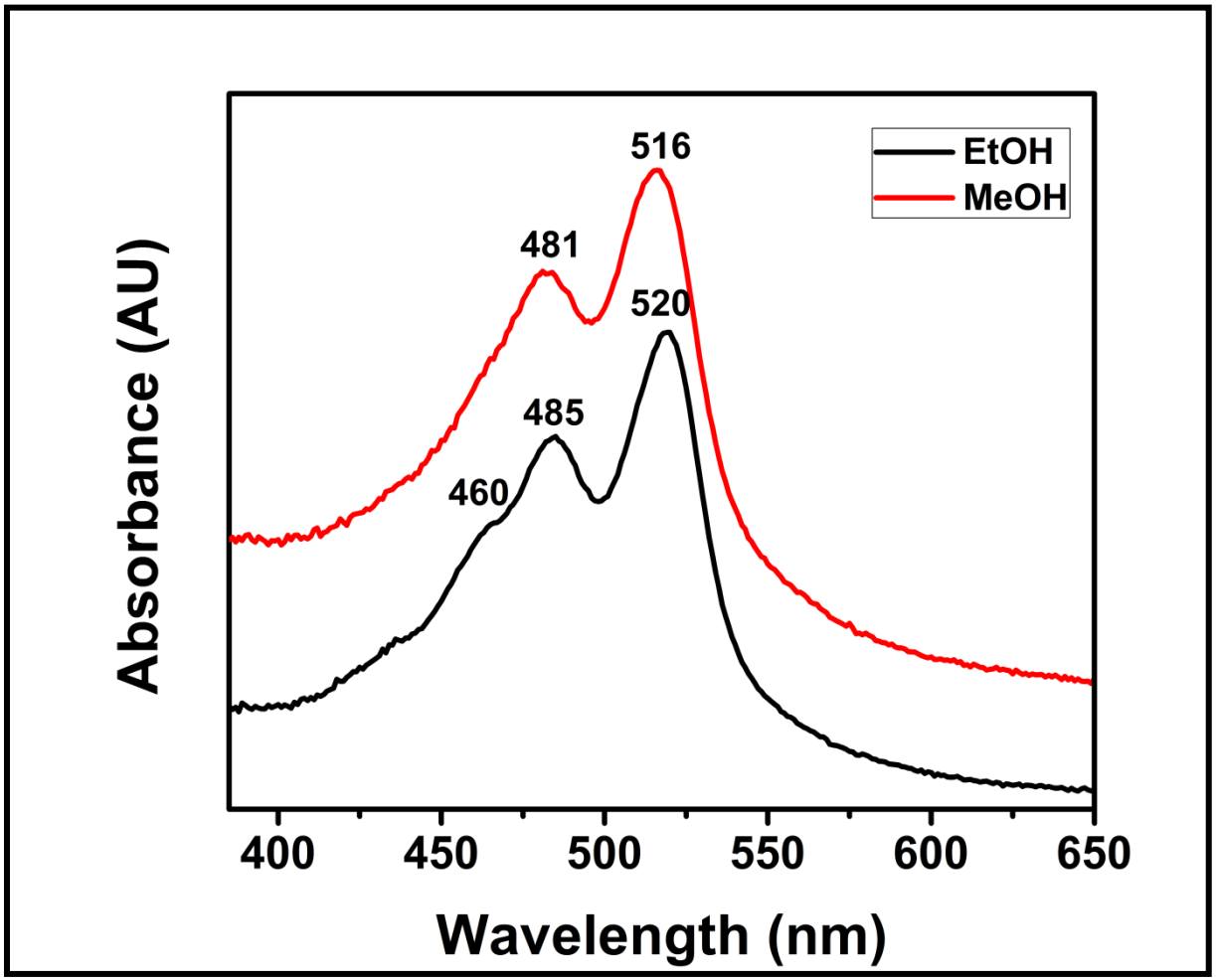

Figure 4.74: UV-visible Absorption Spectra of TPE-PDI in Protic Solvents

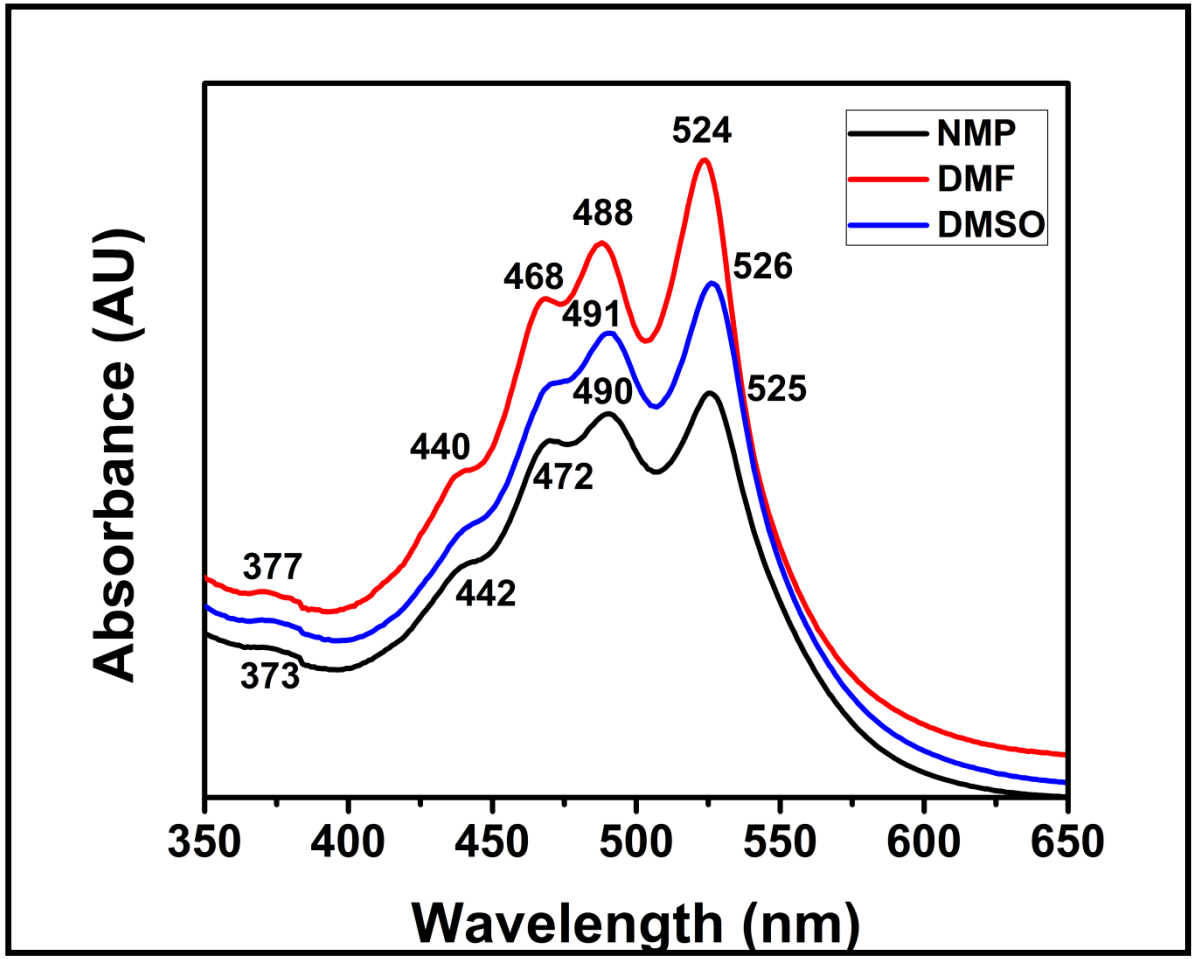

Figure 4.75: UV-visible Absorption Spectra of TPE-PDI in Aprotic Solvents

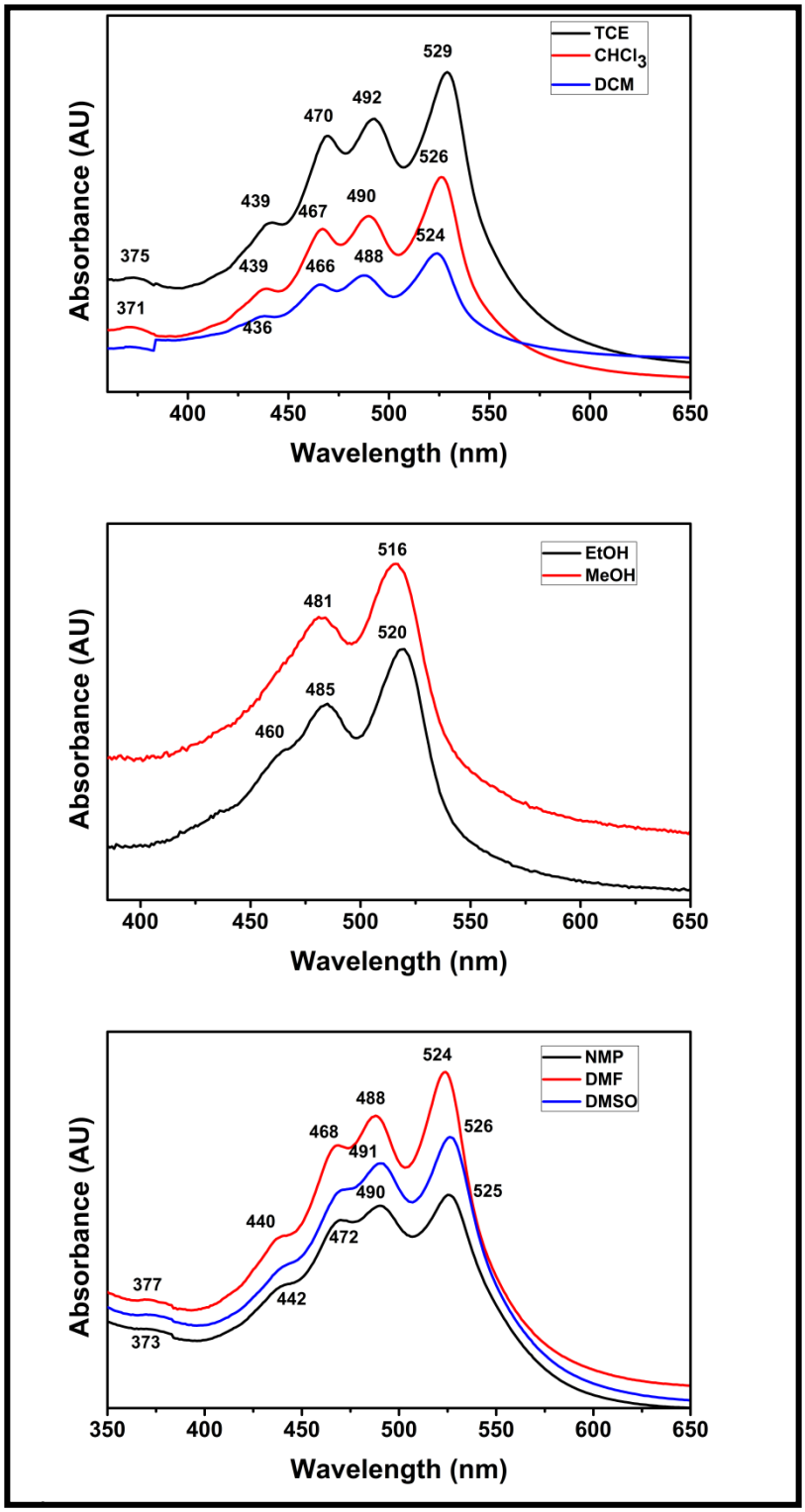

Figure 4.76: UV-visible Absorption Spectra of TPE-PDI in Several Organic Solvents

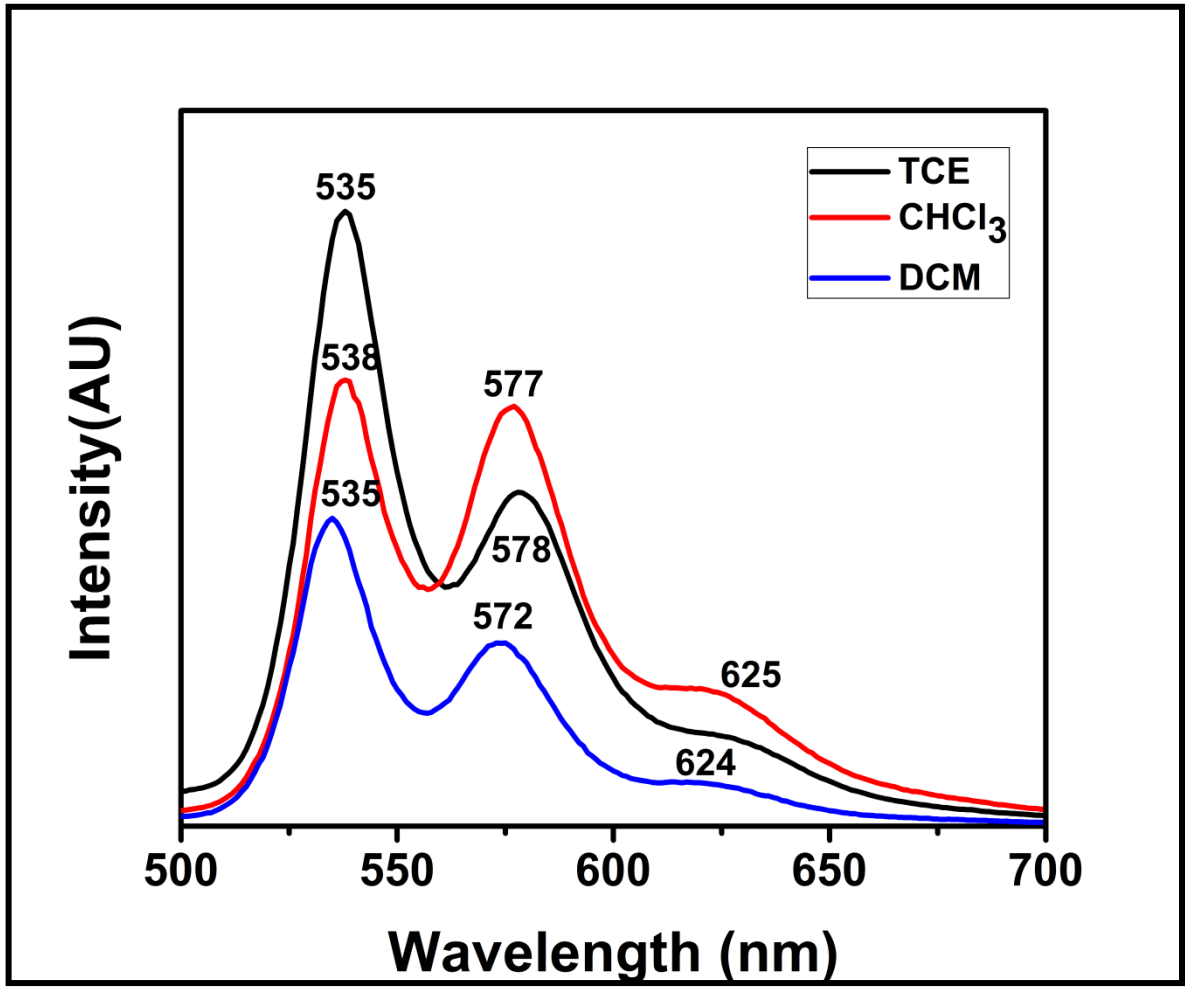

Figure 4.77: Emission Spectra of TPE-PDI in Non-polar Solvents

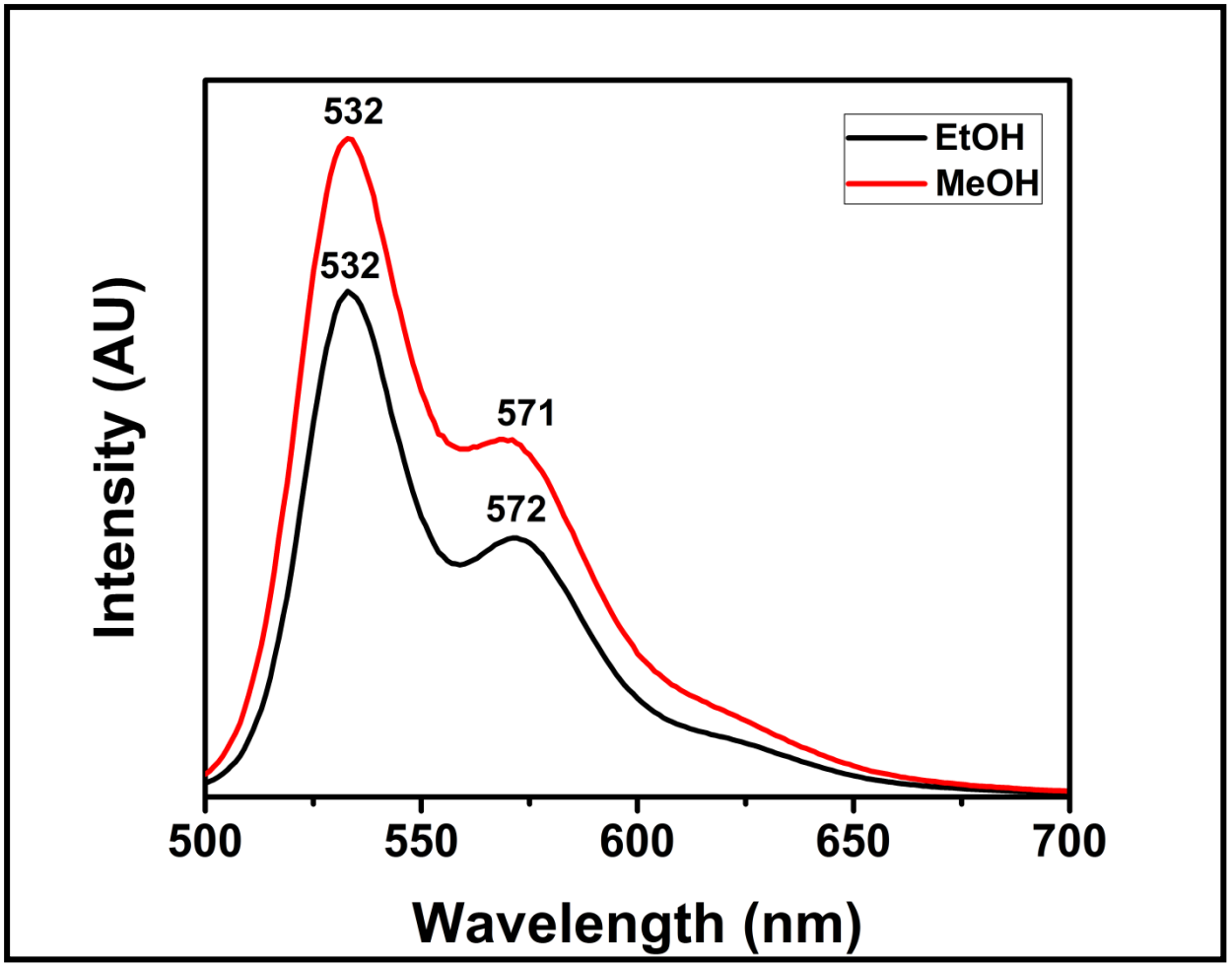

Figure 4.78: Emission Spectra of TPE-PDI in Protic Solvents

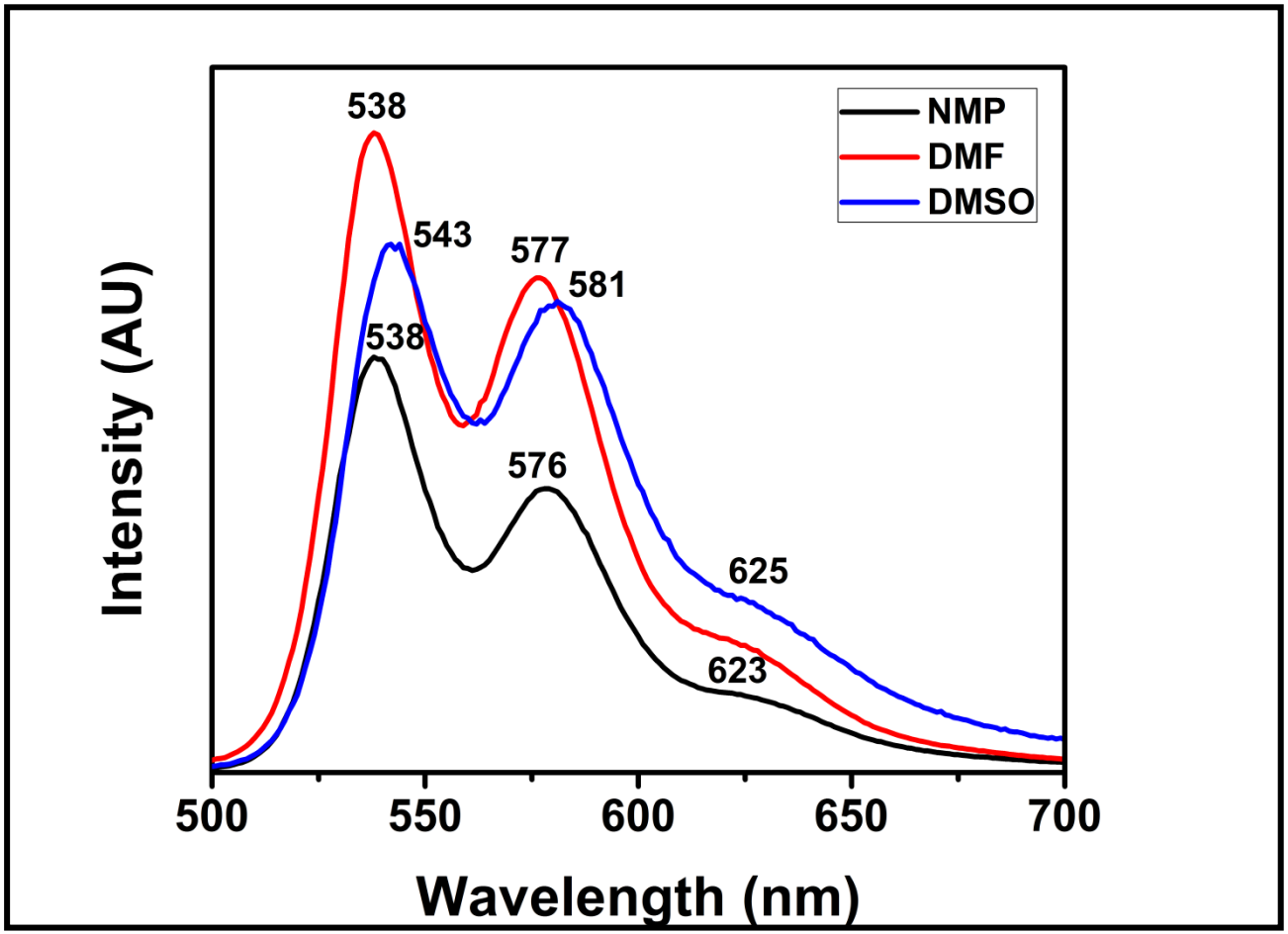

Figure 4.79: Emission Spectra of TPE-PDI in Aprotic Solvents

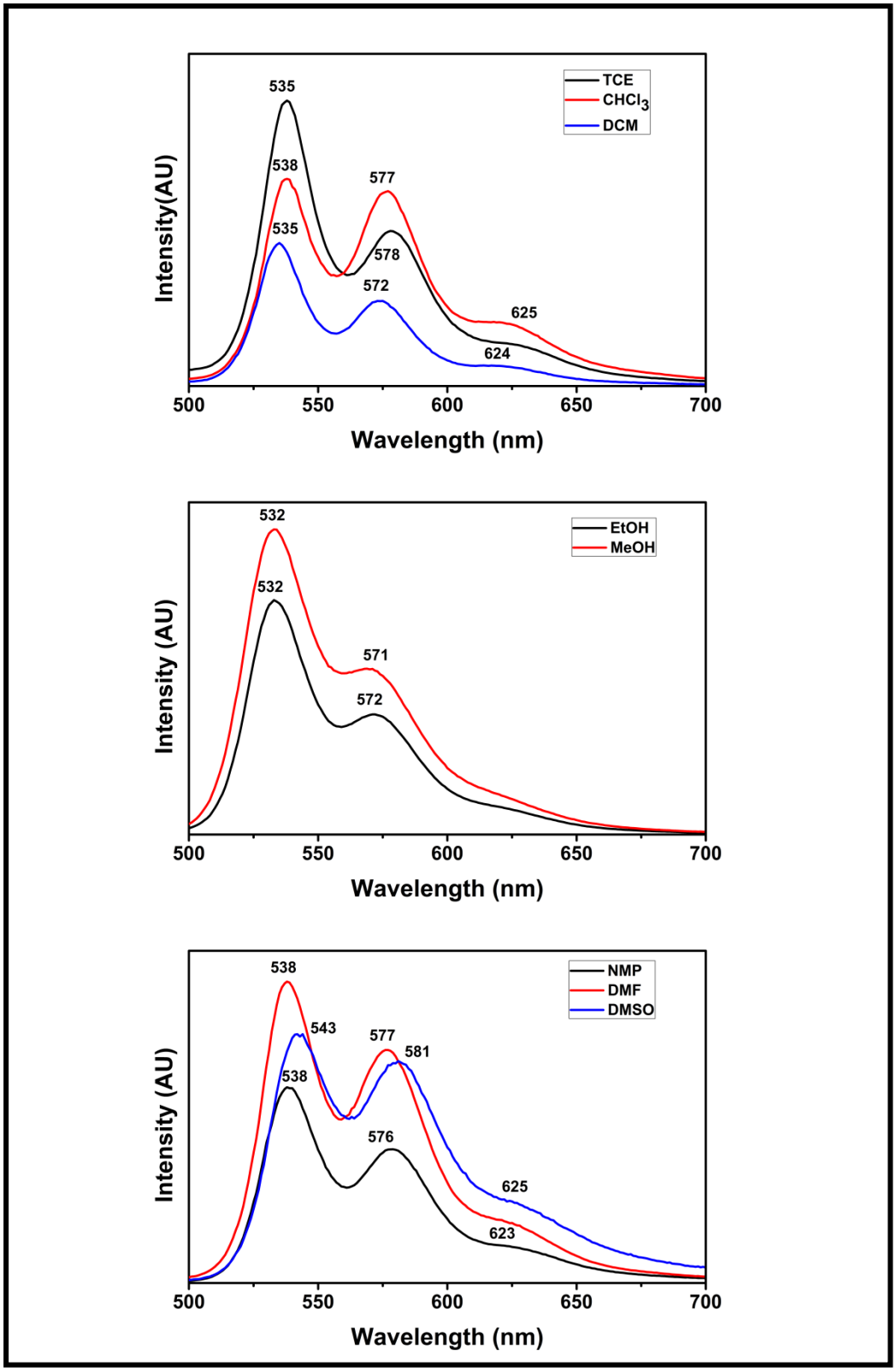

Figure 4.80: Emission Spectra of TPE-PDI in Several Organic Solvents

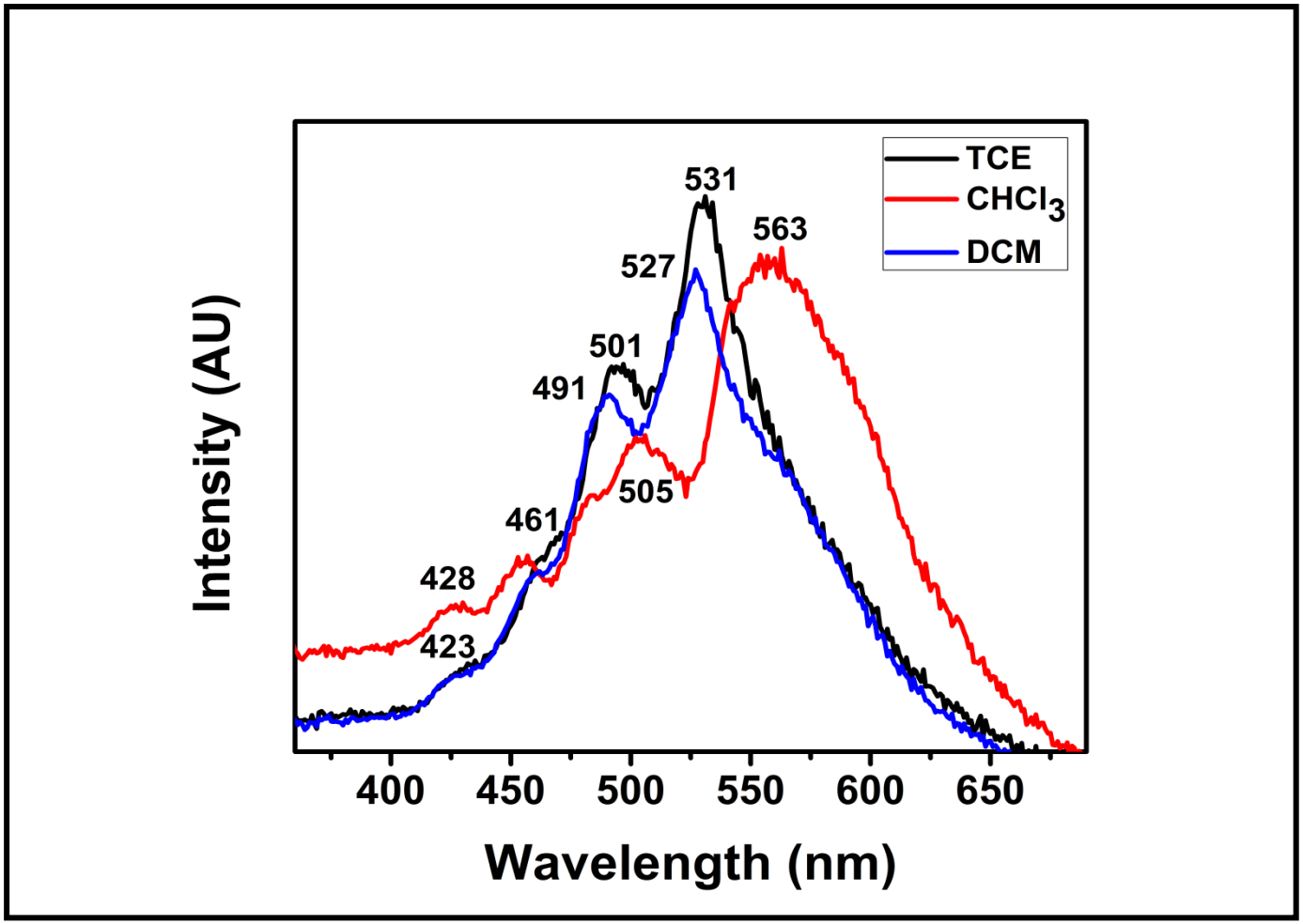

Figure 4.81: Excitation Spectra of TPE-PDI in Non-polar Solvents

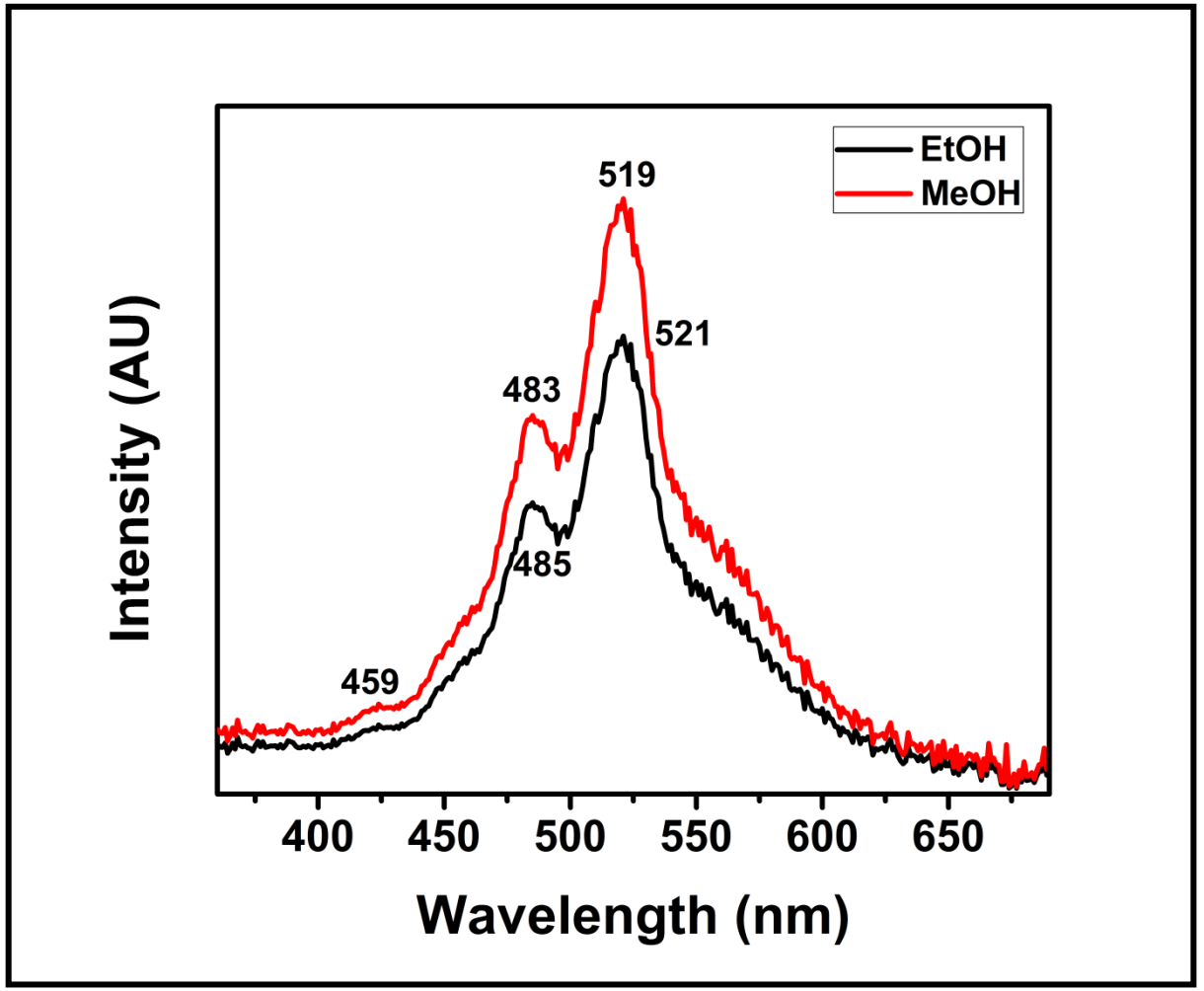

Figure 4.82: Excitation Spectra of TPE-PDI in Protic Solvents

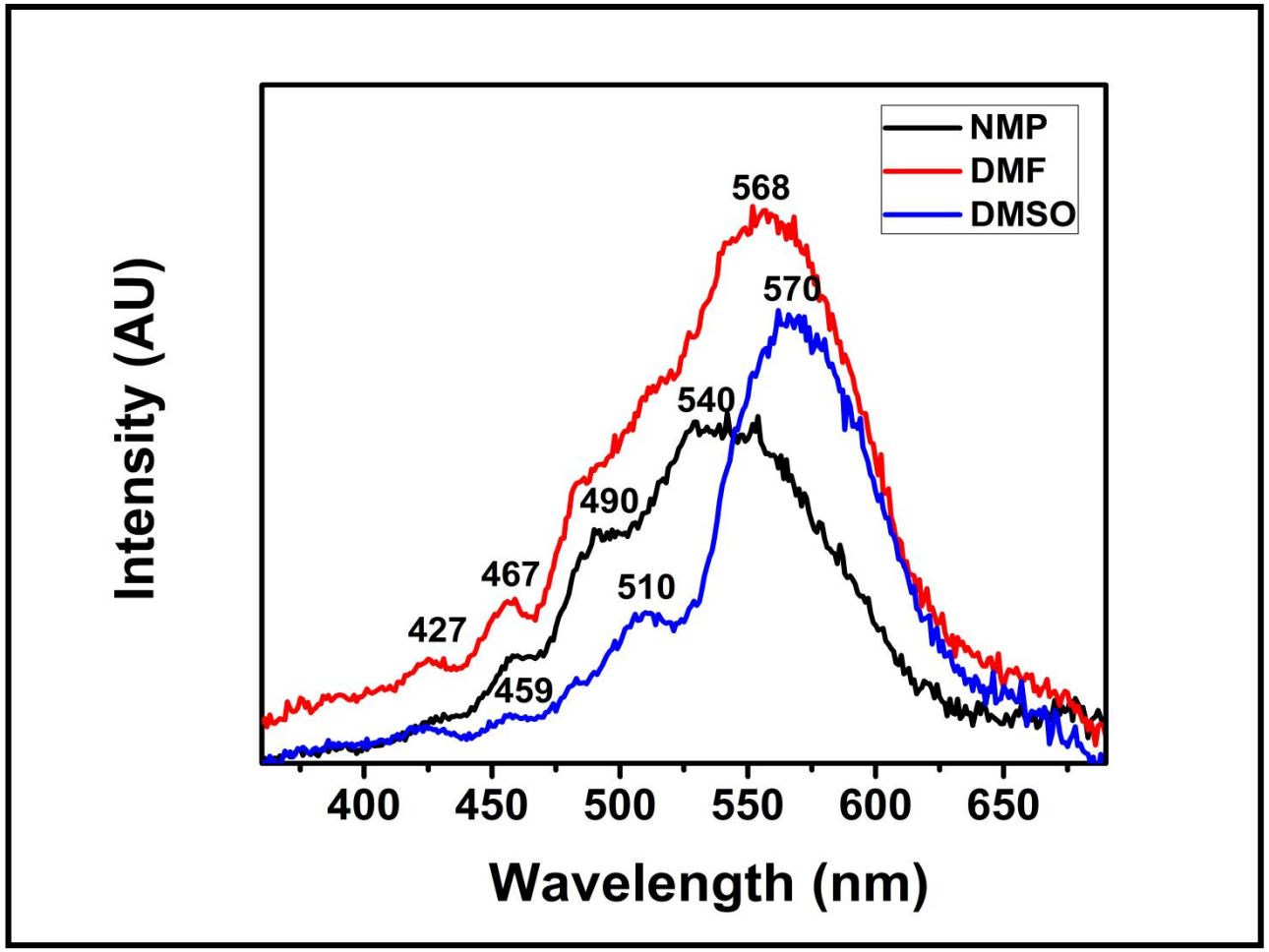

Figure 4.83: Excitation Spectra of TPE-PDI in Aprotic Solvents

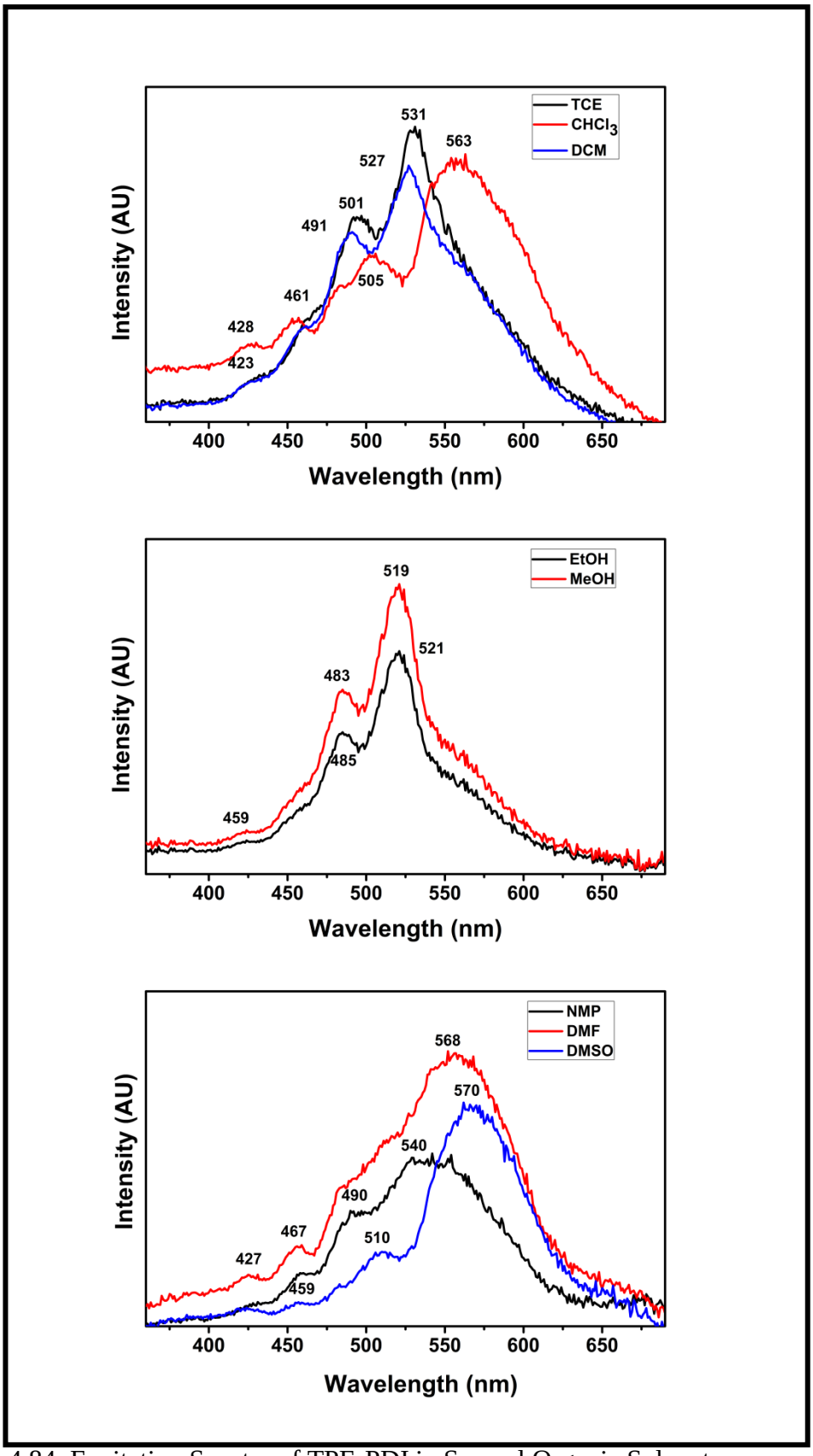

Figure 4.84: Excitation Spectra of TPE-PDI in Several Organic Solvents

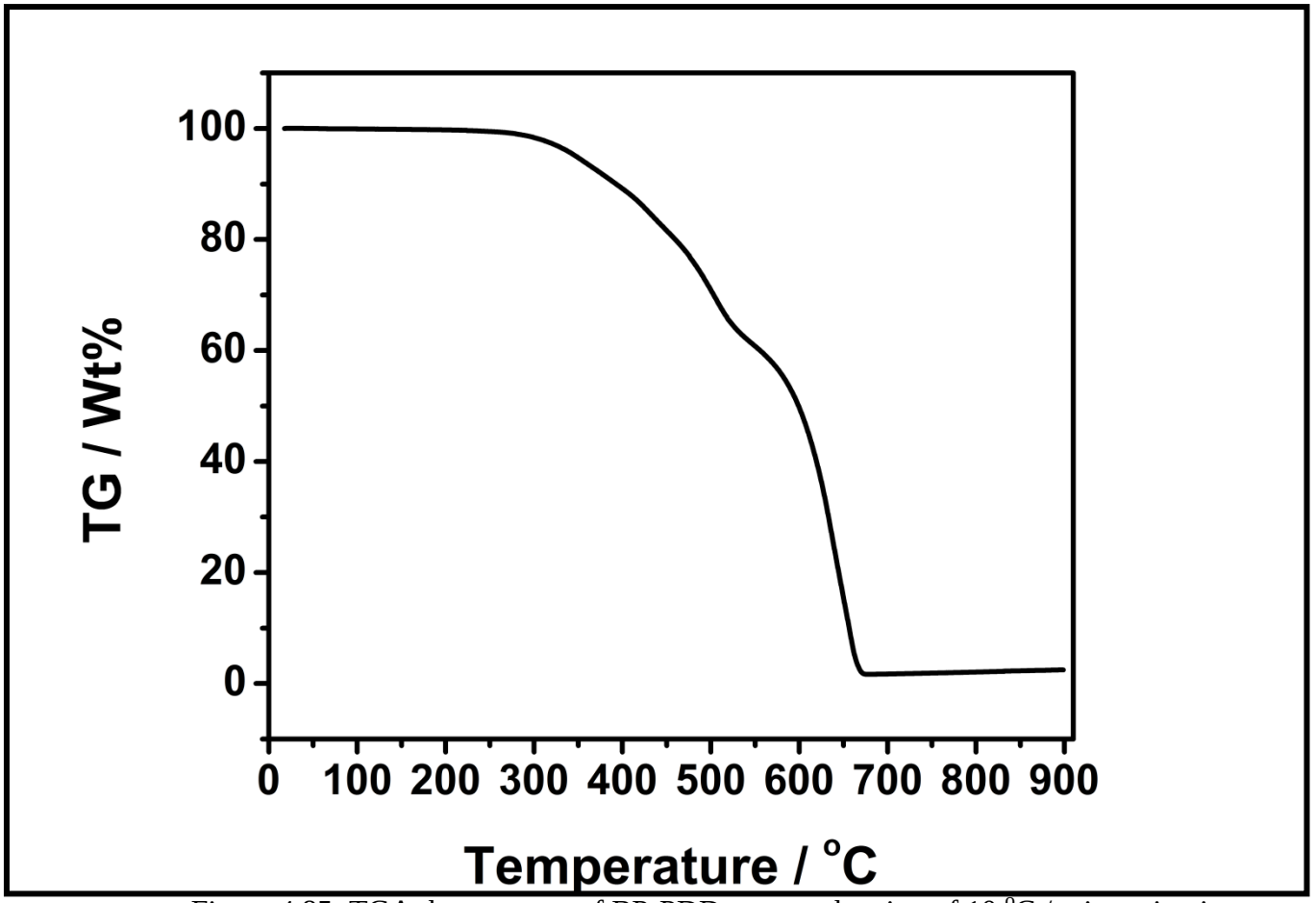

Figure 4.85: TGA thermogram of BP-PDD at space heating of 10 ^{o}C / minute in nitrogen

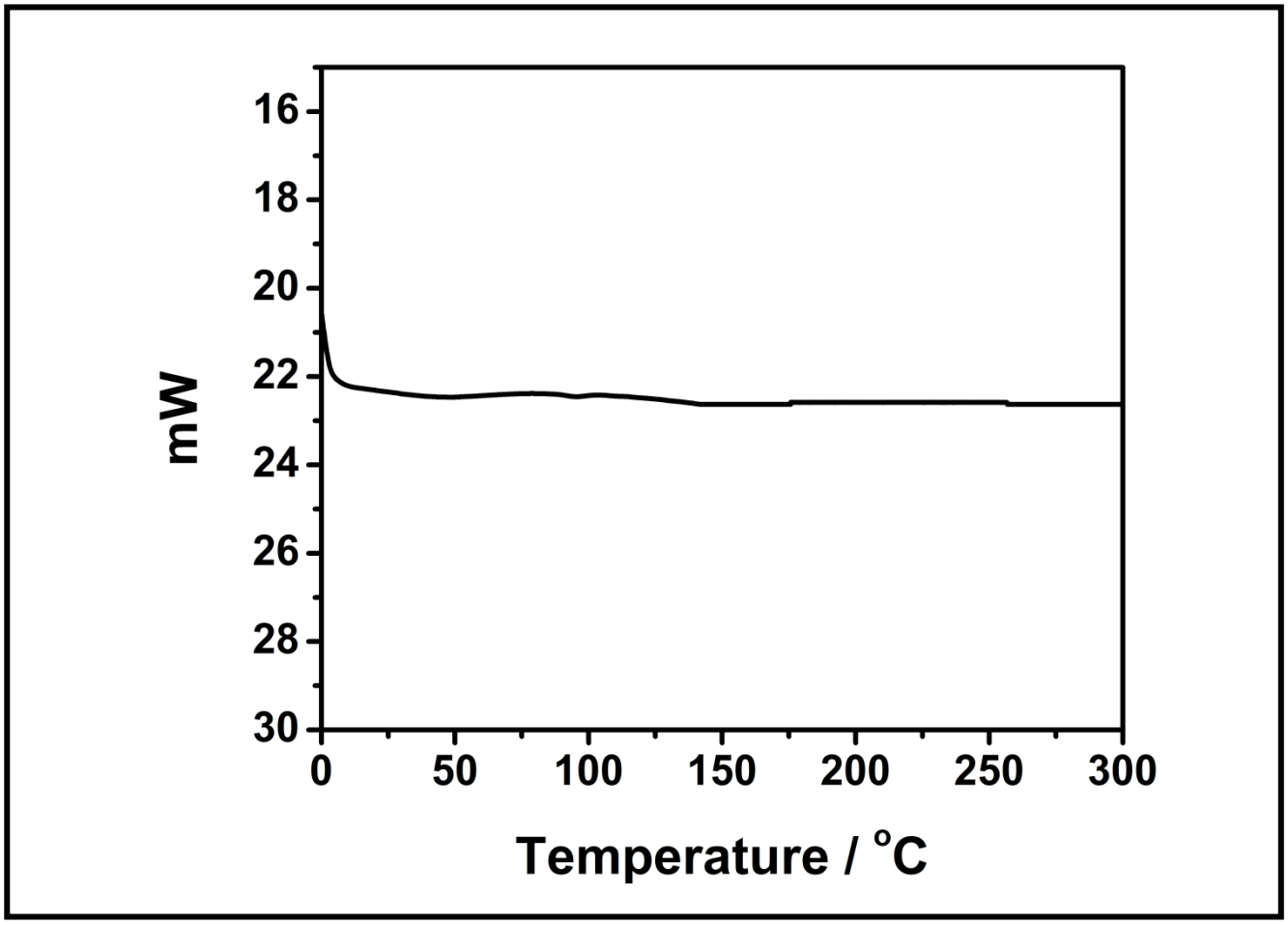

Figure 4.86: DSC diagram of BP-PDD at space heating of 10 ^{o}C / minute in nitrogen

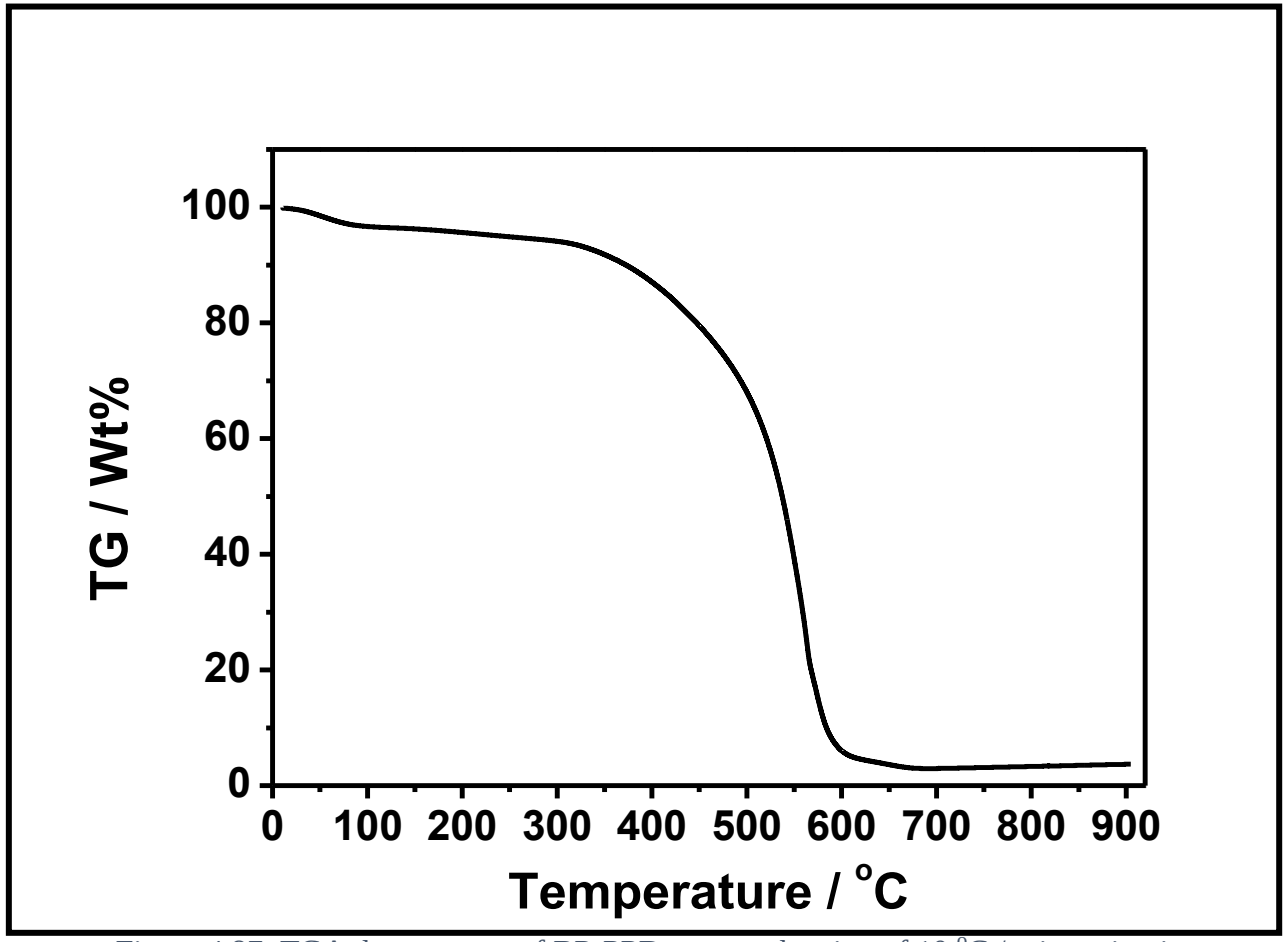

Figure 4.87: TGA thermogram of BP-PPD at space heating of 10 °C / minute in nitrogen

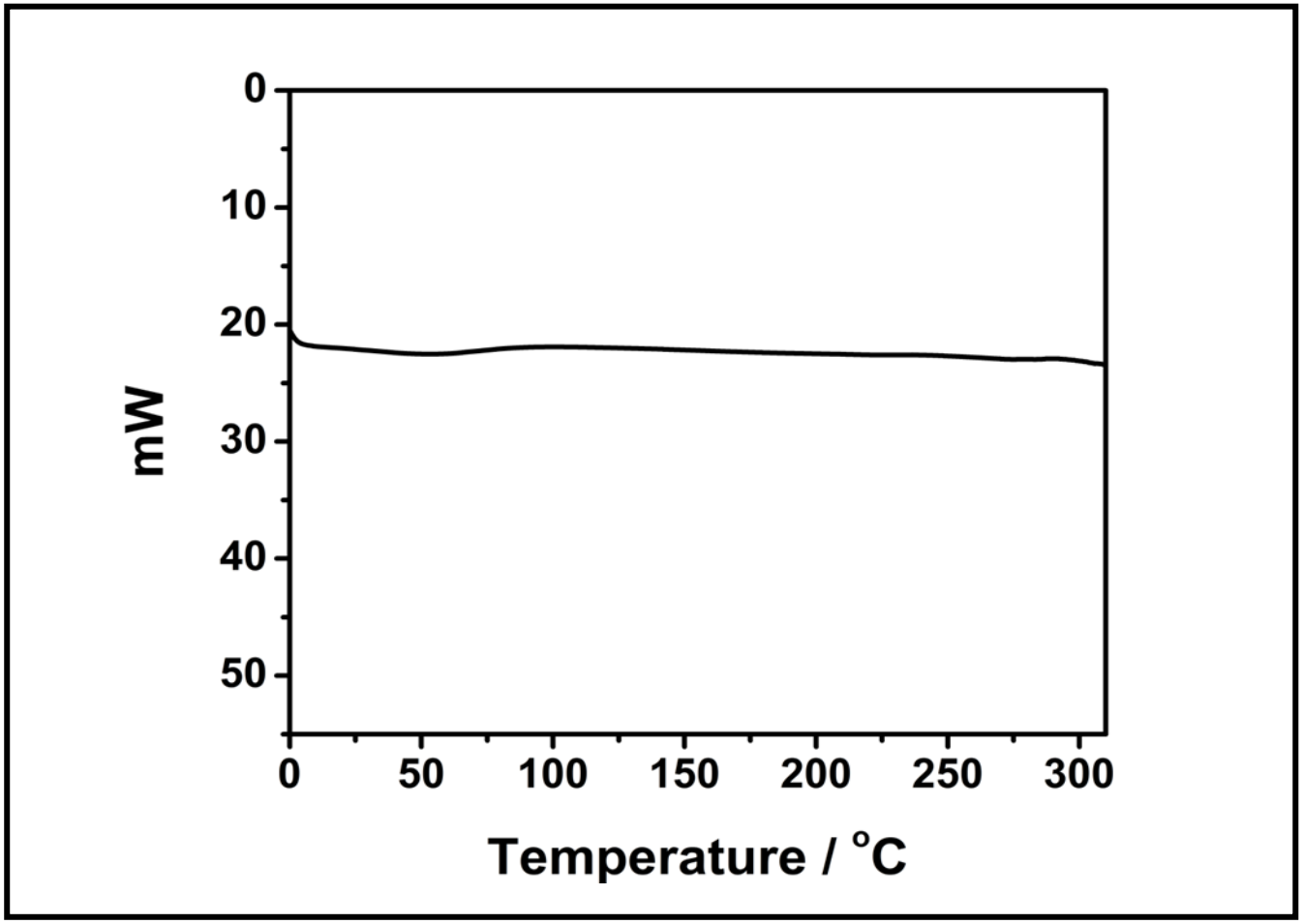

Figure 4.88: DSC diagram of BP-PPD at space heating of 10 ^{o}C / minute in nitrogen

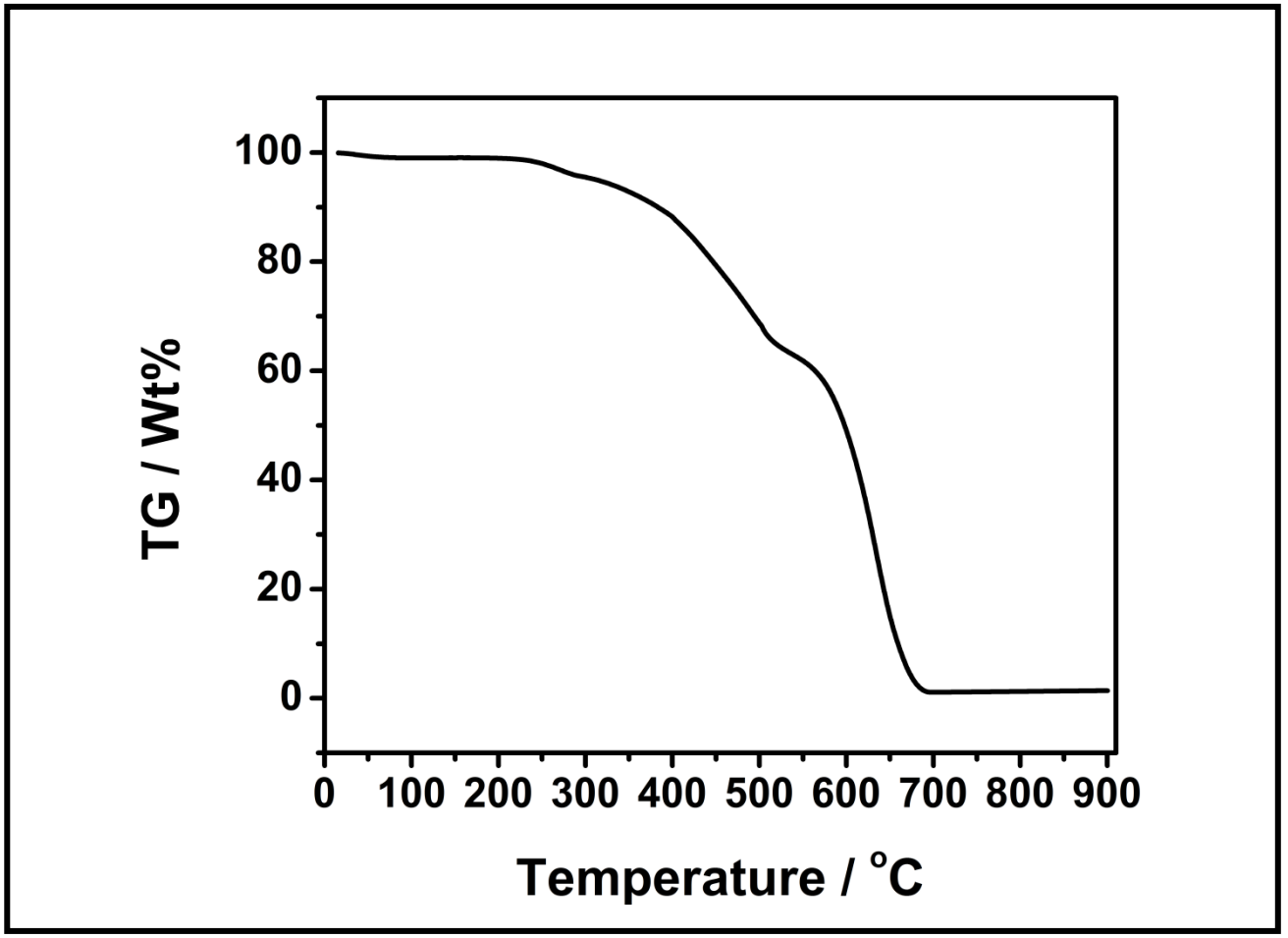

Figure 4.89: TGA thermogram of TPE-PDI at space heating of 10 ^{o}C / minute in nitrogen

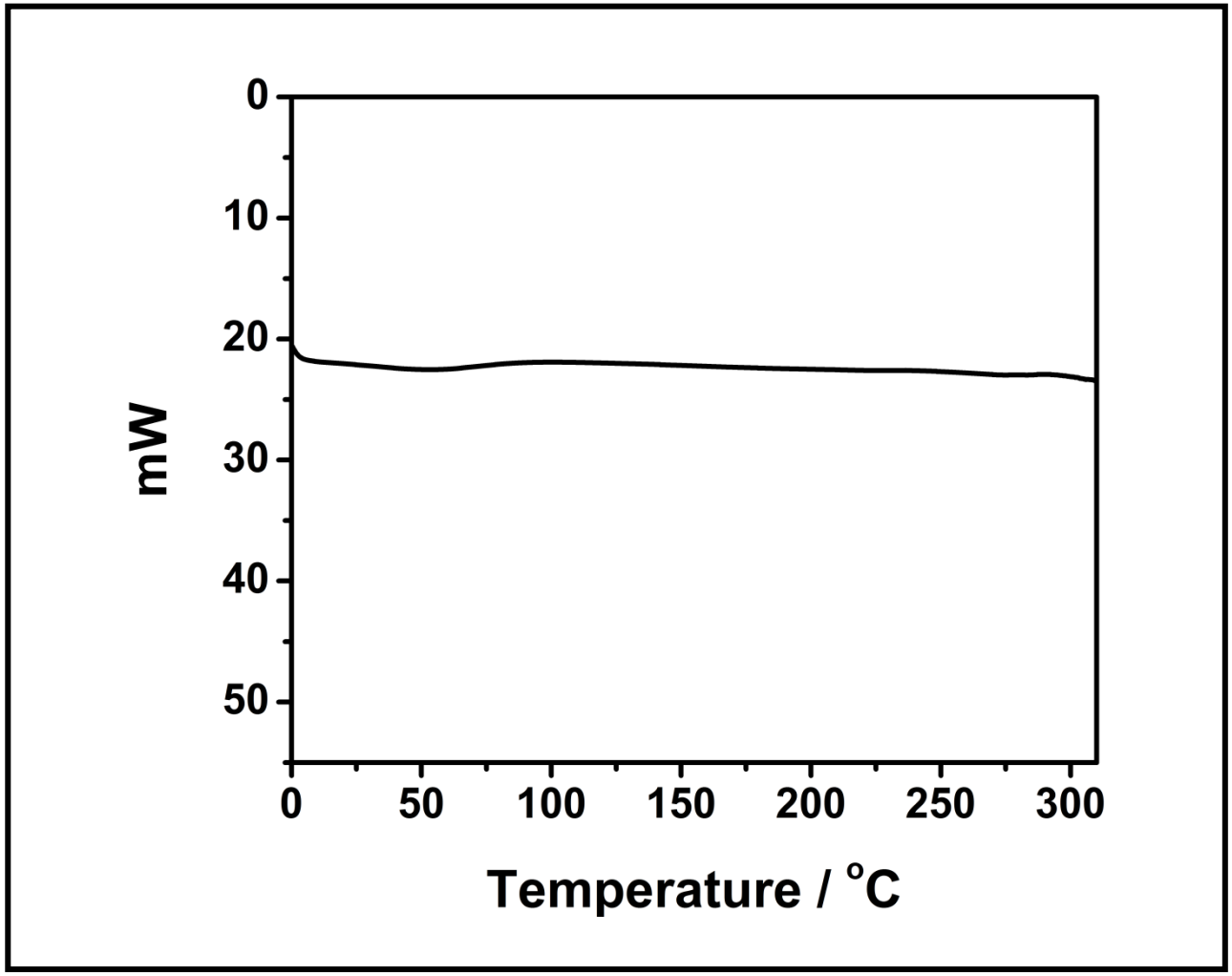

Figure 4.90: DSC diagram of TPE-PDI at space heating of 10 ^{o}C / minute in nitrogen

Chapter 5

RESULTS AND DISCUSSION

5.1 Electrochemistry of the N,N'-bis-{N-(3-[4-(3-amino-propyl)-piperazin-1-yl]-propyl)-N'-[1-dehdroabiety]-1,4,5,8-naphthalenetetracarboxydiimidly}-3,4,9,10-perylenebis(dicarboximide) (NPM)

Electrochemistry of the multichromophoric compound (NPM) was first well examined followed by the components that made up the macromolecule, PDI and NMI. Cyclic voltammetry in DMSO as solvent with 0.1 M $NaBF_4$ as a supporting electrolyte and in solid state were performed in different scan rates (Figures 4.4, 4.5, 4.7, 4.8, and 4.10). The redox potentials, calculated HOMO, LUMO energies and Eg values of the three compounds were tabulated and discussed below.

5.1.1 Electrochemical information of NPM

Tabulated below is the cyclic voltammetry data of NPM in DMSO solution and solid-state at different scan rates (Table 1.17). Also the redox potentials, LUMO, $E_{g,}$ and HOMO valued of NPM in DMSO solution and solid-state are tabulated in Table 1.18.

Table 1.17: Cyclic voltammetry data of NPM in DMSO solution and solid-state at different scan rates

NPM in DMSO Solution								
Scan Rate (mVs^{-1})	$E_{1/2,red}$ [c] *vs.* Fc	i_{pa}	i_{pc}	i_{pa}/i_{pc}				
	/ V		**/ µA**					
50	−1.100	437.74	287.38	1.52				
100	−1.094	386.98	264.62	1.46				
200	−1.107	338.57	233.93	1.45				
300	−1.100	316.59	218.72	1.45				
400	−1.100	281.78	188.69	1.49				
500	−1.107	243.75	164.04	1.49				
1000	−1.107	175.42	97.04	1.81				
NPM in solid-state								
Scan Rate (mVs^{-1})	$E_{1/2,red}$ *vs.* Fc	i_{pa}	i_{pc}	i_{pa}/i_{pc}	$E_{1/2,ox}$ [d] *vs.* Fc	i_{pa} [e]	i_{pc} [f]	i_{pa}/i_{pc}
	/ V		**/ µA**		**/ V**		**/ µA**	
50	−0.566	134.85	85.75	1.57	0.224	6.81	13.03	0.52
100	−0.546	146.80	108.15	1.36	0.253	9.33	30.21	0.31
200	−0.566	175.21	133.32	1.31	0.271	5.91	52.56	0.11
300	−0.562	195.72	143.07	1.37	0.267	11.78	72.31	0.16
400	−0.573	218.87	159.29	1.37	0.256	17.33	101.04	0.17
500	−0.573	248.77	175.39	1.42	0.264	26.72	130.82	0.20
1000	−0.577	264.35	184.64	1.43	0.263	41.20	152.10	0.27

Table 1.18: Redox potentials, LUMO, Eg,
and HOMO values of NPM in DMSO and in solid state

	NPM	
	DMSO	**Solid state**
E_{pc} (V)	–0.819	–0.399
		0.349
E_{pa} (V)	–0.289	–0.189
	0.718	0.709
ΔE_p (mV)	530	210
		360
$E_{1/2}$ (V)	–0.554	–0.294
vs. (Ag/AgCl)		0.523
E_{Fc} (V) vs.	0.534	0.270
(Ag/AgCl)		0.270
$E_{1/2}$ vs. Fc (V)	–1.088	–0.564
		0.253
LUMO (eV)	–3.711	–4.254
E_g (eV)	2.252	1.700
HOMO (eV)	–5.963	–5.954

Two reversible one-electron reductions was observed for NPM (versus ferrocene/ferrocenium couple, scan rate: 100 mV s^{-1}), first at –0.564 V and the second reduction at 0.253V in solid state with ΔE_p values at 210 mV and 360 mV

respectively. But in DMSO solution, the second reduction was not successful (–1.088, ΔE_p; 530 mV). This is due to weak oxidation potential PDI subunit that made up the macromolecule. Large ΔE_p value especially in solution showed low reversibility process. For every reversible reduction process, diffusion controlled one-electron transfer is specified which is in accordance to the standard reversibility criteria. Plots drawn for NPM in DMSO solution and in solid state showed that peak current against square root of scan rate were linear with R^2 = 0.982 and R^2 = 0.95 respectively (Figure 4.6). These results justify the criteria for diffusion controlled processes.

The LUMO energy was calculated to be –3.711 eV in DMSO and –4.254 eV in solid state. E_g values were calculated to be 2.252 eV and 1.700 eV in DMSO and solid state respectively. HOMO energy was calculated from LUMO energy and E_g values and the result in DMSO and in solid state were –5.963 eV and –5.954 eV respectively. Repetitive cycles of redox process were done to ascertain the electrochemical stability of the compound. NPM exhibited reversible reduction steps for the whole scanning rate from 50 to 1000 mV s^{-1} only in solid state (Figure 4.5).

5.1.2 Electrochemical information of PDI

Tabulated below is the cyclic voltammetry data of PDI in DMSO solution and solid-state at different scan rates (Table 1.19). Also the redox potentials, LUMO, E_g, and HOMO valued of PDI in DMSO solution and solid-state are tabulated in Table 1.20.

Table 1.19: Cyclic voltammetry data of PDI in DMSO solution and solid-state at different scan rates

PDI in DMSO Solution								
Scan Rate (mVs^{-1})	$E_{1/2,red(1)}$ *vs.* Fc	i_{pa}	i_{pc}	i_{pa}/i_{pc}	$E_{1/2,red(2)}$[a] *vs.* Fc	i_{pa}	i_{pc}	i_{pa}/i_{pc}
	/ V		**/ µA**		**/ V**		**/ µA**	
100	−1.113	15.04	9.04	1.66	–	–	–	–
200	−1.114	21.41	12.21	1.75	–	–	–	–
500	−1.120	36.19	19.17	1.89	−0.864	2.45	2.62	0.94
600	−1.127	39.93	20.82	1.92	−0.861	4.18	4.18	1.00
750	−1.123	44.82	22.39	2.00	−0.857	5.51	5.56	0.99
1000	−1.129	53.82	27.69	1.94	−0.864	7.14	7.23	0.99

PDI in solid-state								
Scan Rate (mVs^{-1})	$E_{1/2,red}$ *vs.* Fc	i_{pa}	i_{pc}	i_{pa}/i_{pc}	$E_{1/2,ox}$ *vs.* Fc	i_{pa}	i_{pc}	i_{pa}/i_{pc}
	/ V		**/ µA**		**/ V**		**/ µA**	
50	−0.518	66.36	39.17	1.69	0.260	11.37	4.66	2.44
100	−0.524	73.70	46.40	1.59	0.264	18.13	6.28	2.89
200	−0.530	85.09	51.46	1.65	0.260	28.35	12.17	2.33
500	−0.539	98.41	44.73	2.20	0.263	54.18	27.99	1.94
750	−0.546	99.13	37.55	2.64	0.273	73.23	33.64	2.18
1000	−0.546	108.83	39.67	2.74	0.275	90.42	43.50	2.08

[a] No reversible second reduction was noticed up to the scan rate 500 mVs^{-1}.

Table 1.20: Redox potentials, LUMO, Eg, and HOMO values of PDI in DMSO and in solid state

	PDI	
	DMSO	**Solid state**
E_{pc} (V)	–0.658	–0.369
		0.329
E_{pa} (V)	–0.499	–0.139
	0.651	0.739
ΔE_p (mV)	159	230
		410
$E_{1/2}$ (V) vs. (Ag/AgCl)	–0.578	–0.254
		0.534
E_{Fc} (V) vs. (Ag/AgCl)	0.534	0.270
		0.270
$E_{1/2}$ vs. Fc (V)	–1.112	–0.524
		0.264
LUMO (eV)	–3.687	–4.276
E_g (eV)	2.252	1.790
HOMO (eV)	–5.939	–6.066

[a] supporting electrolyte: 0.1 M $NaBF_4$.
[b] supporting electrolyte: 1 M HCl.
[c] $E_{1/2,red}$: half wave reduction potential.
[c] $E_{1/2,ox}$: half wave oxidation potential.
[e] i_{pa}: anodic current.
[f] i_{pc}: cathodic current.

Two reversible one-electron reductions was observed for PDI (versus ferrocene/ferrocenium couple, scan rate: 100 mV s^{-1}), first at –0.524 V and the second reduction at 0.264 V in solid state with ΔE_p values at 230 mV and 410 mV respectively But in DMSO solution, the second reduction was not successful in low scan rates (–1.112 V, ΔE_p; 159 mV). This could be due to symmetry of the diimide and its interaction with the aprotic solvent. Large ΔE_p values showed low reversibility process. For every reversible reduction process, diffusion controlled one-electron transfer is specified which is in accordance to the standard reversibility criteria. Plots drawn for PDI in DMSO solution and in solid state showed that peak current versus scan rate's square root were linear with R^2 = 0.991 and R^2 = 0.99 respectively (Figure 4.9). These results justify the criteria for diffusion controlled processes.

The LUMO energy was calculated to be –3.687 eV in DMSO and –4.276 eV in solid state. E_g values were calculated to be 2.252 eV and 1.790 eV in DMSO and solid state respectively. HOMO energy was calculated from LUMO energy and E_g values and the result in DMSO and in solid state were –5.939 eV and –6.066 eV respectively. Repetitive cycles of redox process were done to ascertain the electrochemical stability of the compound. PDI exhibited reversible reduction steps for the whole scanning rate from 50 to 1000 mV s^{-1} in solid state but reversible reduction steps were observed in solution at higher scan rates (Figure 4.8).

5.1.3 Electrochemical information of NMI

Tabulated below is the cyclic voltammetry data of NMI only in DMSO solution at different scan rates (Table 1.21). Its cyclic voltammetry data in solid state could not be observed. Also the redox potentials, LUMO, E_g, and HOMO valued of PDI in DMSO solution are tabulated in Table 1.22.

Table 1.21: Cyclic voltammetry data of NMI in DMSO solution at different scan rates

NMI in DMSO Solution					
Scan Rate (mVs^{-1})	$E_{1/2,red(1)}$ *vs.* Fc	i_{pa}	i_{pc}	i_{pa}/i_{pc}	$E_{1/2,red(2)}$[a] *vs.* Fc
	/ V		**/ µA**		**/ V**
50	−1.243	30.26	30.55	0.99	−0.844
100	−1.244	41.40	40.51	1.02	−0.840
200	−1.239	57.90	58.60	0.99	−0.837
500	−1.246	92.42	90.28	1.02	−0.830
600	−1.250	98.96	98.96	1.00	−0.830
750	−1.243	111.66	111.55	1.00	−0.824
1000	−1.247	128.79	131.64	0.98	−0.816

Table 1.22: Redox potentials, LUMO, Eg, and HOMO values of NMI in DMSO

	NMI
	DMSO
E_{pc} (V)	–0.370
	–0.769
E_{pa} (V)	–0.241
	–0.649
ΔE_p (mV)	129
	120
$E_{1/2}$ (V)	–0.306
vs. (Ag/AgCl)	–0.709
E_{Fc} (V) vs.	0.534
(Ag/AgCl)	0.534
$E_{1/2}$ vs. Fc (V)	–0.840
	–1.243
LUMO (eV)	–3.556
E_g (eV)	3.000
HOMO (eV)	–6.556

Two reversible reduction processes were observed for NMI in solution (versus ferrocene/ferrocenium couple, scan rate: 100 mV s^{-1}), first at –0.840 V and the second reduction at -1.243 V in DMSO with ΔE_p values at 129 mV and 120 mV. All efforts to determine its electrochemical potentials in solid state were futile. For every reversible reduction process, diffusion controlled one-electron transfer is specified which is in accordance to the standard reversibility criteria. Plot drawn for NMI in

DMSO showed that peak current versus scan rate's square root was a straight line with R^2 = 0.998 (Figure 4.11). These results justify the criteria for diffusion controlled processes.

The LUMO energy was calculated to be –3.556 eV in DMSO. E_g value was calculated to be 3.000 eV. HOMO energy was calculated from LUMO energy and E_g value in DMSO and the result was found to be -6.556 eV. Repetitive cycles of redox process were done to ascertain the electrochemical stability of the compound. NMI exhibited reversible reduction steps for the whole scanning rate from 50 to 1000 mV s^{-1} in solution (Figure 4.10).

The Diffusion constants (D) of the compounds in solution and solid state were calculated using Randles-Sevcik equation as stated in chapter 4 and the valves were tabulated in Table 1.2.

5.2 Syntheses of Bay-substituted Compounds and Characterization

The bay-substituted perylene compounds were synthesized using two different methods. The first method (Method A) started with the iodine catalyzed bromination of 3,4,9,10-perylenetetracarboxylic dianhydride (PDA) in about 98% concentrated sulfuric acid followed by substitution of bromine with phenol and finally, conversion of dianhydride to diimide.

The second method (Method B) started from condensation reaction of perylene dianhydride with an amine followed by bromination at the bay positions (1,7) and finally, substitution of bromine with piperidine compound.

The structural characteristics of the products were checked with solid state IR spectra (Fig.4.15, 4.16 and 4.19) of KBr pellets. The IR Spectrum of BP-PDD, showed four

main characteristic different bands from PDA at 2921 and 2850 (aliphatic C-H), 1697 and 1656 (imide C=O), 1345 (C-N str.) and at 1262 (C-O-C ether).

Similarly, the IR Spectrum of BP-PPD showed some main characteristic different bands from PDA at 3440, 3328 and 3200 (N-H str.), 2852 (S-H), 1703 and 1672 (imide C=O), 1622 (N-H bend), 1339 (C-N str.), 1252 (C-O-C ether) and at 1196 (C-N amine),

Likewise, the FT-IR Spectrum of TPE-PDI, exhibited different peak bands from its PDI at 3546 (OH), one more N-H and Aliphatic C-H peaks were observed. Also from its PDI-Br which showed the bromine peak at 1044 (aromatic C-Br), this aromatic C-Br stretching peak is found to has disappeared.

5.2.1 Solubility of Bay-substituted compounds

Bay-substituted compounds usually show better solubility compared to their perylene diimides/bisimides. Shown in Table 1.23, BP-PDD exhibited good solubility mostly in non-polar solvents followed by aprotic solvents then protic solvents.

Table 1.23: Solubility of BP-PDD

Solubility / Color	
Solvent	**BP-PDD**
TCE	(++) / reddish brown
$CHCl_3$	(++) / reddish brown
DCM	(++) / dark brown
EtOH	(- +) / pink
MeOH	(- +) / pink
NMP	(+) / brown
DMF	(+) / brown
DM_{AC}	(+) / brown
DMSO	(+) / pale brown

(++): soluble at r. temp., (+): partially soluble at r. temp.
(- +): slightly soluble on heating at $50^{o}C$ in sonicator.

Compared with BP-PDD, BP-PPD exhibited less solubility which could be due to no aliphatic chain in its structure. But in aprotic solvent like DMSO, it showed good solubility. Tabulated in Table 1.24 is the solubility and color detail of BP-PPD.

Table 1.24: Solubility of BP-PPD

Solubility / Color	
Solvent	**BP-PPD**
TCE	(- - +) / lilac
$CHCl_3$	(- - +) / lilac
DCM	(- - +) / lilac
EtOH	(- - +) / lilac
MeOH	(- - +) / lilac
NMP	(- +) / dark brown
DMF	(- +) / dark brown
DM_{AC}	(- +) / dark brown
DMSO	(+) / voilet

(++): soluble at r. temp., (+): partially soluble at r. temp.
(- +): slightly soluble on heating at 50^{o}C in sonicator, (- - +): less slightly soluble on heating at 50^{o}C in sonicator.

Finally, compound TPE-PDI showed excellent solubility in non-polar solvent which is not so when compared with its PDI. No complete solubility was observed for its PDI in all organic solvents used which could be due to the presence of the amino group at the end of its aliphatic chain. Upon drying, TPE-PDI showed good thin film forming property for ease processability in many applications. Table 1.25 is the solubility table for compound TPE-PDI.

Table 1.25: Solubility of TPE-PDI

Solubility / Color	
Solvent	**TPE-PDI**
TCE	(++) / orange
$CHCl_3$	(++) / orange
DCM	(++) / orange
EtOH	(- - +) / light orange
MeOH	(- - +) / light orange
NMP	(+) / orange
DMF	(- +) / orange
DMAC	(- +) / orange
DMSO	(- - +) / pink

(++): soluble at r. temp., (+): partially soluble at r. temp.
(- +): slightly soluble on heating at 50°C in sonicator, (- - +): less slightly soluble on heating at 50°C in sonicator.

5.2.2 NMR Spectra Analyses

The NMR analyses of the three compounds synthesized are stated below. First is compound BP-PDD followed by compound BP-PPD and finally compound TPE-PDI.

Compound BP-PDD:

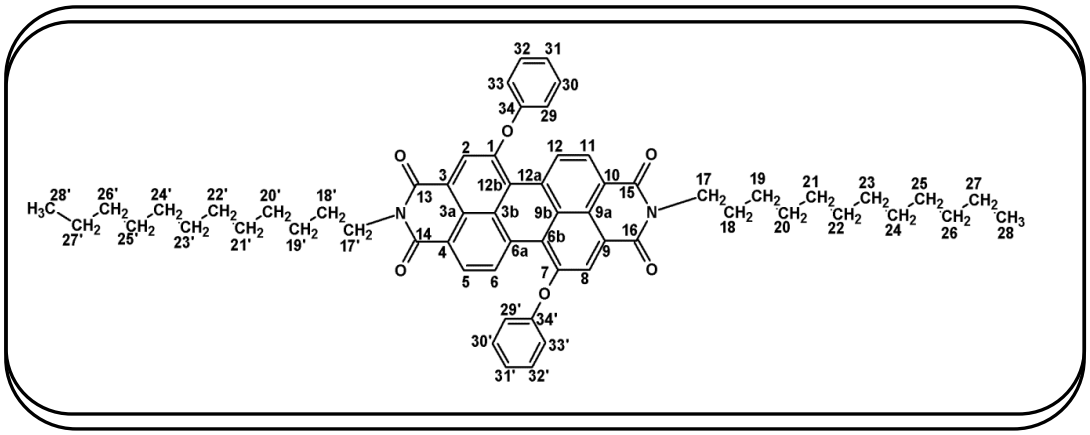

^{1}H NMR, δ_H (ppm) (500 MHz, DMSO + $CDCl_3$): 7.97 (d, *J* = 4.0 Hz, 4 Ar-H, H-C (5), H-C (6), H-C (11), H-C (12)), 7.32 (s, 2 Ar-H; H-C (2), H-C(8)), 7.12 (b, d, 10 Ar-H, H-C (29-33, 29'-33')), 3.75 (b, 2 CH_2, H-C (17), H-C (17')), 1.19 (d, *J* = 13.50 Hz, 20 CH_2, H-C (18-27, 18'-27')), 0.79 (s, 2 CH_3, H-C (28), H-C (28')).

Compound BP-PPD:

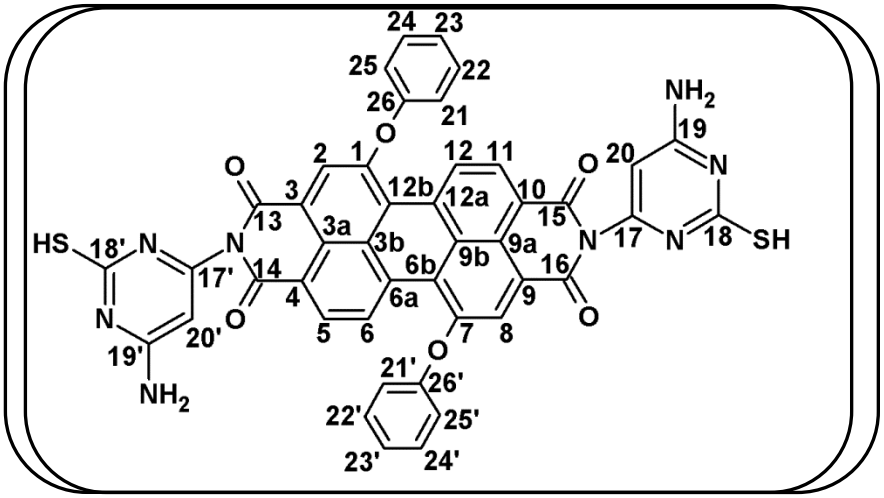

^{1}H NMR, δ_H (ppm) (400 MHz, DMSO): 8.27 - 7.96 (b, 8 Ar-H, H-C (5), H-C (6), H-C (11), H-C (12), H-C (2), H-C (8), H-C (20), H-C (20')), 7.62 - 7.27 (b, d, 12 Ar-H, H-C (21-26), H-C (21'-26')), 2.90 (s, 4H, SH-C(18,18')), 2.75 (s, NH_2-C s, 2H, (19, 19')).

^{13}C NMR, δ_C (ppm) (100 MHz, DMSO): 157.79-158.94 (4 C=O, 8 C, C(13-16), C(17-20), C(17'-20')), 119.28-110.69 (20 Ar–C, C(1-12), C(3a), C(3b), C(6a), C(6b), C(9a), C(9b), C(12a), C(12b))

Compound TPE-PDI:

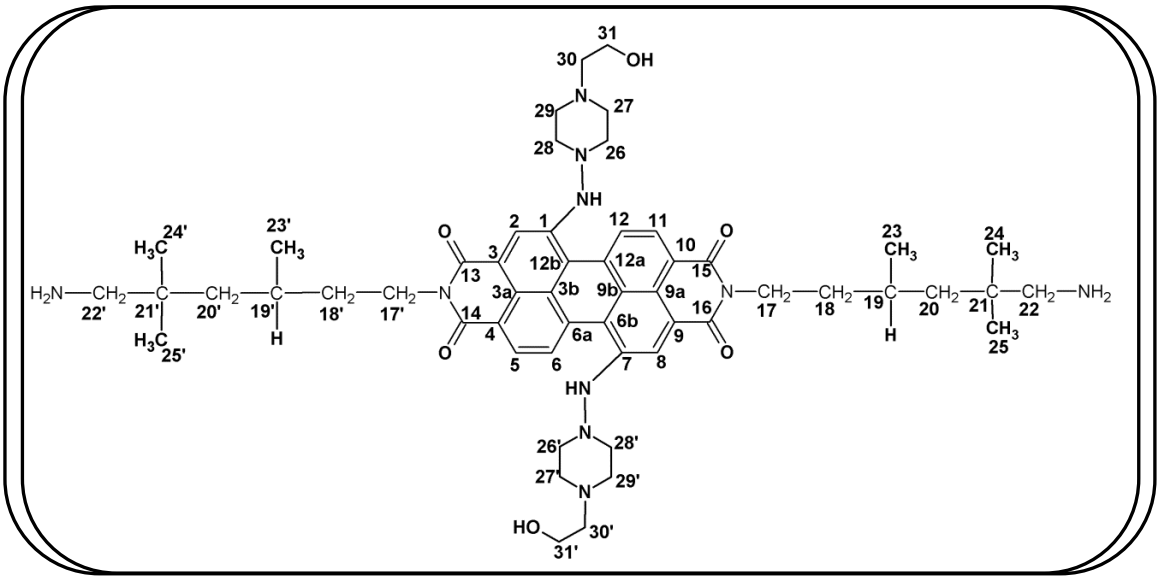

^{1}H NMR, δ_H (ppm) (400 MHz, $CDCl_3$): 8.49 (b, d, , *J*=36.0 Hz 6 Ar-H, H-C (2), H-C (5), H-C (6), H-C (8), H-C (11), H-C (12)), 4.14 (m, 2 CH_2, H-C (31), H-C (31')), 3.56 (t, 2 CH_2, H-C (17), H-C (17')), 3.23 (s, NH-C (7)), 2.78 (t, 2 CH_2, H-C (30), H-C (30')), 2.60 (s, 2 CH_2, H-C (22), H-C (22)'), 2.28 (t, J=8.0 Hz, 2 CH_2, H-C (18), H-C (18')), 1.97 (m, 2 CH, H-C (19), H-C (19')), 1.59 (s, 2 OH, HO-C (31), HO-C (31')), 1.35 (d, J=8.0 Hz, 2 CH_2, H-C (20), H-C (20')), 1.18 (s, 4 CH_3, H-C (24), H-C (25), H-C (24'), H-C (25')), 1.02 - 0.81 (m, 10 CH_2, H-C (26-29), H-C (26'-29'), NH_2-C(22), NH_2-C(22'), H-C (23), H-C (23')).

^{13}C NMR, δ_C (ppm) (100 MHz, $CDCl_3$): 166.66 (4C=O, C(13), C(14), C(15), C(16)), 147.01-118.56 (20 Ar–C, C(1-12), C(3a), C(3b), C(6a), C(6b), C(9a), C(9b), C(12a), C(12b)), 60.85 (2 OH–C, C(31), C(31'), 52.97 (2CH_2, C(22), C(22')), 46.97 (2CH_2, C(20), C(20')), 44.67 (2CH_2, C(17), C(17')), 38.50 (3CH_2, C(18), C(18')),

34.67 (2(C), C(21), C(21')), 28.69 (2CH, C(19), C(19')), 27.0 (4CH_3, C(24), C(25), C(24'), C(25')), 23.08 (8CH_2, C(26), C(27), C(28), C(29), C(26') C(27'), C(28'), C(29')), 21.06 (2CH_2, C(30), C(30')) 19.46 (2CH_3, C(23), C(23'))

5.2.3 Analyses of UV-vis Absorption Spectra

5.2.3.1 UV-visible Absorption Spectra of BP-PDD

The UV–vis absorption spectra of BP-PDD in several organic solvents ranging from non-polar to aprotic solvents (10^{-5} M) are shown in Figures 4.27-4.37. The values of the absorption wavelengths maxima in chloroform ($CHCl_3$) are 392, 503 and 538 nm. The strongest absorption is attributed to S_0-S_1 transitions and the shoulder band to S_0-S_2 electronic transitions. Unsubstituted perylene diimides/bisimides normally have an absorption maximum at 527 nm approximately with a sharp vibronic fine structure which belongs to S_0-S_1 electronic transition. By introducing phenoxy substituents (donor group) at the bay region of the perylene core leads to enlargement of π-conjugation and thereby a red shift of the absorption maximum to 538 nm in $CHCl_3$ and even more red shifted in 1,1,2,2-tetrachloroethane (TCE), 543 nm. This is assigned to the inductive effect enforced by the phenyl group on the diimide. According to the literature of related dyes, these phenoxy substitutes cause a twisting of the two naphthalene subunits in the perylene core by about 15^o for two substituents. The resulting planarity loss and firmness of the perylene diimide/bisimide chromophore causes considerable line broadening and a lesser definite vibronic fine structure [87].

As stated earlier, the absorption spectra of BP-PDD in TCE exhibited more red shifted wavelengths (515 and 543 nm) more than the other non-polar solvents. Notably, only one broad absorption peak was observed in MeOH which is a blue shifted absorption peak. This could be due to formation of hydrogen bonding

interaction and also could result from low solubility of the product in this solvent. But reverse is the case for EtOH which showed three weak absorption peaks. In aprotic solvents (DMF and DMSO), the spectra showed three absorption peak with their wavelength similar to unsubstituted PDI but exhibited weak vibronic structure which is due to the bay substitution.

5.2.3.2 UV-visible Absorption Spectra of BP-PPD

Figure 4.46-4.56 showed the absorption emission and excitation of BP-PDD in different solvents (10^{-4} M). The absorption wavelengths maxima in dimethyl formamide (DMF) values are 435, 503 and 525 nm. Unlike compound BP-PDD, this compound exhibited similar absorption maxima like the unsubstituted perylene diimides which normally possess an absorption maximum at 527 nm approximately but the vibronic fine structure is similar to the substituted PDI. In non-polar solvents, the compound showed rough vibronic structures which could be due to low solubility couple with intermolecular synergy in solution. In protic solvents, the compound exhibited one broad absorption peak which could be due to charge transfer characteristic and intermolecular interactions in protic solvents. Curiously, in these same protic solvents, it showed red shifting characteristics especially in MeOH with its absorption at 550 nm. This encourages for better study of this compound in protic solvents. Aprotic solvents DMF and DMSO showed different characteristic absorption peaks which could be due to their differences in solubility behavior and intermolecular interaction in solution. A weak peak shoulder was noticed in DMSO at a longer wavelength, 551 nm which could be attributed to disruption of planarity in the vibronic structure.

5.2.3.3 UV-visible Absorption Spectra of TPE-PDI

Compound TPE-PDI showed interesting characteristics in its absorption spectra in all the organic solvents used. The strong electron donating piperidine group substitutes led to its deviation from fundamental electronic structure of the perylene diimide core. The spectra exhibited five different absorption peaks in non-polar and aprotic solvents which are quite different from its PDI. Figure 4.65-4.76 showed the absorption emission and excitation of TPE-PDI in different solvents (10^{-5} M). In chloroform, the absorption maxima exhibited are 371, 439, 467, 490 and 526 nm. In protic solvents EtOH and MeOH, they showed three absorption peaks like the normal PDI and are blue shifted compared to other solvents which could be attributed to hydrogen bonding interaction with the polar solvents. The absorption spectra in aprotic solvents showed similar absorption peaks with those of non-polar solvents. This synthesis gave a low yield which could be attributed to the strong electron-donating effect of piperidine group which increased the electron cloud density on the perylene core making the active nucleophile to react strainly.

5.2.4 Analyses of Emission Spectra

5.2.4.1 Emission Spectra of BP-PDD

The emission spectra of BP-PDD which was taken at λ_{exc} = 485 nm showed one characteristic emission band each at 570 nm in DCM and 579 nm in TCE and $CHCl_3$ with a shoulder-like peak at 541 nm and big Stoke shift value around 40 nm. Excitation spectra in these solvents were also taken which showed similar spectra with their absorption spectra. In protic solvents, it showed one broad emission peak with the values almost the same as the non-polar solvents. This was also the same for the aprotic solvents. The Φ_f values were calculated in several solvents via the

standard stated above as referrence (Φ_f = 1). The (Φ_f) values were calculated and recorded in Table 1.8.

Surprisingly in $CHCl_3$ and DCM, it gave a higher yield Φ_f values when compared with similar synthesis in the literature. In protic solvents, it gave its lowest values which could be attributed to self-quenching because of the intra-intermolecular interactions. All the emission spectra exhibited an excimer-like emission.

5.2.4.2 Emission Spectra of BP-PPD

The emission spectra of BP-PPD which was taken at λ_{exc} = 485 nm showed two characteristic emission bands at 535 and 572 nm in DMF. But in DMSO it gave one broad peak at 581 nm. In protic solvents, it gave more red shifted excimer-like emission bands at 535, 586 nm in EtOH and 530, 591 nm in MeOH. This could be attributed to π-π stacked interactions with strong intermolecular interactions in solution and also the effect of hydrogen bonding interaction. For non-polar solvents, it gave two characteristic peaks around 530 and 573 nm and TCE having the largest values i.e. red shifted compared with it other non-polar solvents. The (Φ_f) values were calculated and recorded in Table 1.8 using the same reference as mentioned above. Remarkably, it gave its highest Φ_f value in TCE and its lowest in EtOH. The low yields in other solvents could be as a result of re-absorption of emitted photons and all spectra exhibited excimer-like emission. Its excitation spectra were quite similar to its absorption spectra.

5.2.4.3 Emission Spectra of TPE-PDI

The emission spectra, (Φ_f) values and fluorescence lifetime of TPE-PDI were discovered to rely on the polarity of surrounding environs because of the existence of electron donating piperidine derivatives attached at the perylene bay-regions. The emission spectra was taken at λ_{exc} = 485 nm showed three main characteristic

emission bands at 538, 577 and 625 nm in $CHCl_3$. The emission spectra are not exact mirror image of their absorption spectra with the stoke shift of 12 nm in $CHCl_3$. Unlike the emission spectra in non-polar solvents and aprotic solvents which showed three traditional peaks of PDI, only two peaks were observed in protic solvents with the values 532 and 572 nm. Their excitation spectra were quite similar to their absorption spectra. The (Φ_f) values were calculated and recorded in Table 1.8 using the same reference as mentioned above. It showed its highest Φ_f valve in DCM, 0.61 followed by EtOH with the value of 0.54. DMSO exhibited the lowest value of 0.08 which is attributed to polarity and self-quenching attributed to effective intersystem crossing in solution. Fluorescence lifetimes (τ_f) were calculated in several solvents which showed its highest values in protic solvents.

5.2.5 Analyses of Thermal Properties

Thermal studies of the compounds were done using differential scanning calorimetry (DSC) and thermogravimetry (TGA) techniques. The heating rate for TGA was 10 ^oC / min in nitrogen and exhibited its starting decomposition at 370 ^oC for compound BP-PDD (Figure 4.85). A prompt weight loss of 38.8 % of the original weight happened from 400 to 550 ^oC followed by weight loss of 58.7 %. When the compound was heated to 670 ^oC, 97.5 % of the compound's weight was gone given 2.5% as char yield. The DSC thermogram of this compound (Figure 4.86) exhibited no glass transition and no melting point in the DSC runs up to 300 ^oC in nitrogen atmosphere.

The same conditions were applied for the remaining two compounds. Found in compound BP-PPD, its starting decomposition was at 400 ^oC with a speedy loss of weight of 93.4 % of the original weight happened between 430 ^oC and 555 ^oC. At 700 ^oC, 96.4 % of the compound's weight was gone given and 3.6 % as char yield

was found (Figure 4.87). The DSC thermogram of this compound exhibited no glass transition and no melting point in the DSC runs up to 300 ^{o}C in nitrogen atmosphere (Figure 4.88). Also in compound TPE-PDI its starting decomposition was at 350 ^{o}C with a speedy loss of weight of 32.5 % of the original weight happened between 400 and 550 ^{o}C followed by weight loss of 61.6 %. At 690 ^{o}C, 98.6 % of the compound's weight was gone given 1.4% as char yield (Figure 4.89). The DSC thermogram of this compound exhibited no glass transition and no melting point in the DSC runs up to 300 ^{o}C in nitrogen atmosphere (Figure 4.90).

Chapter 6

CONCLUSION

In the course of this thesis work, the electrochemical properties of a chiral macromolecular compound with the syntheses and characterization of novel bay-substituted perylene macromolecules were presented.

The electrochemical analysis of the chiral macromolecule constituting one perylene chromophore and two naphthalene chromophoric units has been studied in details both in solution and in solid state. PDI and NPM exhibited similar redox properties both in solution and in solid state. The electrochemical data of NMI could only be studied in solution and not in solid state. The LUMO, HOMO energies and E_g of these compounds were determined from the reduction peak potentials.

The FT-IR and NMR spectra of three bay-substituted compounds proved the structure and purity of these compounds. Two different methods were used for the syntheses of the three bay-substituted compounds. As explained in chapter 3, method A was used to synthesize BP-PDD and BP-PPD while method B was used in the synthesis of TPE-PDI. The three bay-substituted perylene compounds with different electron donating substituents result in a loss in planarity of the aromatic scaffolds and exhibiting moderately low fluorescence quantum yield value when compared with their PDIs. The lowest energy band of compound BP-PDD which relates to S_0-S_1 electronic transitions exhibited bathochromic shift when compared with basic

unsubstituted PDI. This showed noticeable electronic synergy between the PDI center and the phenyl compounds attached to bay regions. Compound BP-PPD exhibited similar UV-vis absorption value with respect to the basic unsubstituted PDI but showed weak vibronic structure. The fluorescence quantum yields and extinction coefficients in different solvents of this compound is very low. The two compounds showed excimer-like emission properties in their emission spectra.

Using different method for the synthesis of TPE-PDI, it showed remarkable absorption spectra in most of the solvents used. It exhibited enlarged range of absorption with five absorption peaks in a finely vibronic structure which is different from the unsubstituted PDI which exhibited three absorption peaks. But its emission spectra exhibited similar characteristics as the normal PDI. Its also showed high extinction coefficient values. The thermochemical properties of these bay-substituted compounds were studied with TGA thermogram and DSC. Their starting decomposition temperatures were found to be from 350 ^{o}C with no glass temperature and melting point in their DSC run up to 300 ^{o}C.

With the results of these novel synthesized compounds, they could be made useful in different industrial areas like fabrication of systems for light harvesters, photovoltaic devices such as solar cells etc.

REFERENCES

[1] Nazeeruddin Md. K.; Baranoff E.; Gratzel M. Dye-sensitized solar cells: A brief overview. *Solar Energy* 85 (2011) 1172–1178.

[2] Lu J. F.; Bai J.; Xu X. B.; Li Z. H.; Cao K.; Cui J.; Wang M. K. Alternate redox electrolytes in dye-sensitized solar cells. *Chin Sci Bull* (2012) 57 4131-4142.

[3] Niu H.; Luo J.; Wu W.; Mu J.; Wang C.; Bai X.; Wen W. Linear and Star Branched Perylene-Containing Polyimides: Synthesis, Characterization, and Photovoltaic Properties of Novel Donor–Acceptor Dyes Used in Solar Cell. *Journal of Applied Polymer Science* 125 (2012) 200–211.

[4] Delcamp J. H.; Yella A.; Holcombe T. H.; Nazeeruddin M. K.; Gratzel M. The Molecular Engineering of Organic Sensitizers for Solar-Cell Applications. *Angew. Chem. Int. Ed.* 52 (2013) 376 –380.

[5] Chen S-L.; Yang L-N.; Li Z-S. How to Design More Efficient Organic Dyes for Dye-sensitized Solar Cells? Adding More sp2-Hybridized Nitrogen in the Triphenylamine Donor. *Journal of Power Sources* 223 (2013) 86-93.

[6] Hu X.; Zuo L.; Pan H.; Hao F.; Pan J.; Fu L.; Shi M.; Chen H. Synthesis and photovoltaic properties of n-type conjugated polymers alternating 2,7-carbazole and arylene diimides. *Solar Energy Materials & Solar Cells* 103 (2012) 157–163.

[7] Lin L.; Geng H.; Shuai Z.; Luo Y. Theoretical insights into the charge transport in perylene diimides based n-type organic semiconductors. *Organic Electronics* 13 (2012) 2763–2772.

[8] Gawrys P.; Damien Boudinet D.; Zagorskaa M. et al. Solution processible naphthalene and perylene bisimides: Synthesis, electrochemical characterization and application to organic field effect transistors (OFETs) fabrication. *Synthetic Metals* 159 (2009) 1478–1485.

[9] Kim J. Y.; Chung I. J.; Lee C.; Kim Y. C.; Kim J. K.; Yu J-W. Mobility of Electrons and Holes in an n-Type Organic Semiconductor Perylene Diimide Thin Film. *Current Applied Physics* 5 (2005) 615–618. [10] Lu G. Organic Semiconductor. University of Rochester, Rochester, NY 14627 USA.

[10] Bagui M.; Dutta T.; Zhong H. et al. Synthesis and optical properties of perylene diimide derivatives with triphenylene-based dendrons linked at the bay positions through a conjugated ethynyl linkage. *Tetrahedron* 68 (2012) 2806-2818.

[11] Pucci A.; Donati F.; Nazzi S.; Barretta G. U.; Pescitelli G.; Di Bari L.; Ruggeri G. Association phenomena of a chiral perylene derivative in solution and in poly(ethylene) dispersion. *Reactive & Functional Polymers* 70 (2010) 951–960.

[12] Thalacker C. and Würthner F. Chiral Perylene Bisimide±Melamine Assemblies: Hydrogen Bond-Directed Growth of Helically Stacked Dyes with Chiroptical Properties. *Adv. Funct. Mater*. 12 (2002) 209-218.

[13] Würthner F. Bay-substituted Perylene Bisimides: Twisted Fluorophores for Supramolecular Chemistry. *Pure Appl. Chem.* (2006) 2341–2349.

[14] Krygowski T. M.; Ejsmont K.; Stepien B. T.; Cyranski M. K.; Poater J. and Sola M. Relation between the Substituent Effect and Aromaticity. *J. Org. Chem.* (2004) 69, 6634-6640.

[15] Rajasingh P.; Cohen R.; Shirman E.; Shimon L. J.W.; Rybtchinski B. Selective Bromination of Perylene Diimides under Mild Conditions. J. Org. Chem. 72 (2007) 5973-5979.

[16] Chao C-C. and Leung M-k. Photophysical and Electrochemical Properties of 1,7-Diaryl-Substituted Perylene Diimides. *J. Org. Chem.* (2005) 70, 4323-4331.

[17] Dey S.; Efimov A. and Lemmetyinen H. Diaryl-Substituted Perylene Bis(imides): Synthesis, Seperation, Characterization ans Comparison of Electrochemical and Optical Properties of 1,7- and 1,6-Regioisomer. *Eur. J. Org. Chem.* (2012) 2367-2374.

[18] Raj M. R.; Ramkumar S. and Anandan S. Photovoltaic Studies on Perylene Diimide-Based Copolymers Containing Electronic Push-pull Chromophores. *RSC Adv.* (2013) 3, 5108-5120.

[19] Hoppea H. and Sariciftci N. S. Organic Solar Cells: An Overview. *J. Mater. Res.* (2004), 19, No. 7, 1924-1944.

[20] Osswald P.; Reichert M.; Bringmann G. and Wurthner F. Perylene Bisimide Atropisomers: Synthesis, Resolution, and Stereochemical Assignment *J. Org. Chem.* (2007), *72*, 3403-3411.

[21] Sivamurugan V.; Kazlauskas K.; Jursenas S.; Gruodis A.; Simokaitiene J.; Grazulevicius J. V. and Valiyaveettil S. Synthesis and Photophysical Properties of Glass-Forming Bay-Substituted Perylenediimide Derivatives. *J. Phys. Chem. B* (2010**),** *114*, 1782–1789.

[22] Patra D.; Ramesh M.; Sahu D.; Padhy H.; Chu C-W.; Wei K-H.; Lin H-C. Enhancement of photovoltaic properties in supramolecular polymer networks featuring a solar cell main-chain polymer H-bonded with conjugated cross-linkers. *Polymer* 53 (2012) 1219-1228.

[23] Abbel R.; Schenning A. P. H.; Meijer E.W. Fluorene-Based Materials and Their Supramolecular Properties. *Journal of Polymer Science: Part A: Polymer Chemistry* 47 (2009) 4215–4233.

[24] Zhao F. and Zhao M. Supramolecules: The Chemical Building Blocks of the Future. *Recent Res. Devel. Physics* 6 (2005) 1-12.

[25] Würthner F. Supramolecular Dye Chemistry. *Springer* (2005) 324 pages.

[26] Yu Y.; Li Y.; Qin Z.; Jiang R.; Liu H.; Li Y. Designed synthesis and supramolecular architectures of furan-substituted perylene diimide. *Journal of Colloid and Interface Science* 399 (2013) 13–18.

[27] Ryu J-H.; Tang L.; Lee E.; Kim H-J.; Lee M. Supramolecular Helical Columns from the Self-Assembly of Chiral Rods. *Chem. Eur. J.* (2008) 14 871 – 881.

[28] El-Batal H.; Guo K.; Li X.; Wesdemiotis C.; Moorefield C. N.; Newkome G. R. Perylene-Based Bis-, Tetrakis-, and Hexakis(terpyridine) Ligands and Their Ruthenium(II)–Bis(terpyridine) Complexes: Synthesis and Photophysical Properties. *Eur. J. Org. Chem.* (2013) 3640–3644.

[29] Lin X.; Hirono M.; Seki T.; Kurata H.; Karatsu T.; Kitamura A.; Kuzuhara D. et al. Covalent Modular Approach for Dimension-Controlled Self-Organization of Perylene Bisimide *Dyes. Chem. Eur. J.* 19 (2013) 6561 – 6565.

[30] Hu J.; Kuang W.; Deng K.; Zou W.; Huang Y.; Wei Z.; Faul C. F. J. Self-Assembled Sugar-Substituted Perylene Diimide Nanostructures with Homochirality and High Gas Sensitivity. *Adv. Funct. Mater.* 22 (2012) 4149–4158.

[31] Thalacker C. and Würthner F. Chiral Perylene Bisimide±Melamine Assemblies: Hydrogen Bond-Directed Growth of Helically Stacked Dyes with Chiroptical Properties. *Adv. Funct. Mater.* 12 (2002) 209-218.

[32] Savenije T. J. Organic Solar Cells, Opto-Electronic Materials Section DCT, TNW Delft (2008) University of Technology The Netherlands (Thesis).

[33] Brabec C. J. Organic Photovoltaics: Technology and Market. *Solar Energy Materials & Solar Cells* 83 (2004) 273–292.

[34] Lee S.; Koo B.; Park J-G.; Moon H.; Hahn J.; Kim J. M. Development of High-Performance Organic Thin-Film Transistors for Large-Area Displays. *Mrs Bulletin* 31 (2006) 455-459.

[35] Harris T. R. Review of Organic Light Emitting Diode Fabrication and Recent Progress. *Ece-592-S Soft Electronics* (2008) 1-6.

[36] Ryu G-S.; Choe K-B.; Song C-K. Array of Organic Thin Film Transistors Integrated with Organic Light Emitting Diodes on a Plastic Substrate. *Thin Solid Films 514* (2006) 302–305.

[37] Wiatrowski M,; Dobruchowska E.; Maniukiewicz W.; Pietsch U.; Kowalski J.;

Szamel Z.; Ulanski J. Self-assembly of Perylenediimide Based Semiconductor on Polymer Substrate. *Thin Solid Films* 518 (2010) 2266–2270.

[38] Vertsimakha Y.; Lutsyk P.; Palewska K.; Sworakowski J.; Lytvyn O. Optical and Photovoltaic Properties of Thin Films of N,N′-Dimethyl-3,4,9,10-perylenetetracarboxylic Acid Diimide. *Thin Solid Films* 515 (2007) 7950–7957.

[39] Coropceanu V.; Cornil J.; Filho D.A.; Olivier Y.; Silbey R.; Bredas J-C. Charge Transport in Organic Semiconductors. *Chem. Rev*. 107 (2007) 926-952.

[40] Ostroverkhova O.; Platt A. D.; Shepherd W. E. B. Optical, Photoluminescent, andPhotoconductive Properties of Novel High- Performance Organic Semiconductors. *Advances in Lasers and Electro Optics* (2010) 838.

[41] Acikbas Y.; Capan R.; Erdogan M.; Yukruk F. Thin Film Characterization and Vapor Sensing Properties of a Novel Perylenediimide Material. *Sensors and Actuators B* 160 (2011) 65– 71.

[42] Chen Y.; Feng Y.; Gao J.; Bouvet M. Self-assembled Aggregates of Amphiphilic Perylene Diimide–based Semiconductor Molecules: Effect of Morphology on Conductivity. *Journal of Colloid and Interface Science* 368 (2012) 387–394.

[43] Chen Y.; Bouvet M.; Sizun T.; Barochi G.; Rossignol J.; Lesniewska E. Enhanced Chemosensing of Ammonia Based on the Novel Molecular Semiconductor-doped Insulator (MSDI) Heterojunctions. *Sensors and Actuators B* 155 (2011) 165–173.

[44] Taguchi D.; Shino T.; Chen X.; Zhang L.; Lia J.; Weis M.; Manakaa T.; Iwamoto M. Determination of Lifetime of Double-Layer CuPc/C60 Organic Solar Cells by Optical Electric-Field-Induced Second-Harmonic. *Physics Procedia* 14 (2011) 167–171.

[45] Yonehara H.; Pat C. Photoelectrical Properties of Double-layer Organic Solar Cells using CeO and Phthalocyanines. *Thin Solid Films* 278 (1996) 108-l 13.

[46] KhodaSiddiki M.; Venkatesan S.; Wang M.; Qiao Q. Materials and Devices Design for Efficient Double Junction Polymer Solar Cells. *Solar Energy Materials & Solar Cells* 108 (2013) 225–229.

[47] Liu C.; Li Y.; Minari T.; Takimiya K.; Tsukagoshi K. Forming semiconductor/dielectric double layers by one-step spin-coating for enhancing the performance of organic field-effect transistors. *Organic Electronics* 13 (2012) 1146–1151.

[48] Kim S. M.; Yang Y. S.; Lee J. H.; Lee J-K.; Chu H. Y.; Lee H.; Oh J.; Do L-M.; Zyung T. Organic Field-effect Transistors using Perylene. *Optical Materials* 21 (2002) 439–443.

[49] Th.B. Singh Th. B.; Erten S.; Gunes S.; Zafer C.; Turkmen G.; Kuban B.; Teoman Y.; Sariciftci N. S.; Icli S. Soluble Derivatives of Perylene and Naphthalene Diimide for n-Channel Organic Field-effect Transistors. *Organic Electronics* 7 (2006) 480–489.

[50] Han S. H.; Lee K.J.; Lee S. H.; Jang J. N-type Organic Thin-film Transistor Using *N,N'*-dioctyl-3,4,9,10-perylenetetracarboxylic Diimides Grown by Organic Vapor Deposition. *Journal of Non-Crystalline Solids* 354 (2008) 2870–2874.

[51] Hamasaki T.; Morimune T.; Kajii H.; Minakata S.; Tsuruoka R.; Nagamachi T.; Ohmori Y. Fabrication and Characteristics of Polyfluorene Based Organic Photodetectors Using Fullerene Derivatives. *Thin Solid Films* 518 (2009) 548–550.

[52] Liu C.; Liu L.; Che G.; Cui Y.; Wang Q.; Li W.; Liu M. High Response Organic Ultraviolet Photodetectors Based on 4,7-Diphenyl-1,10-phenanthroline. *Solar Energy Materials & Solar Cells* 96 (2012) 29–32.

[53] Colle M. and Tsutsui T. Patterning of Organic Light-emitting Diodes Containing a Layer of Perylene Derivative Using an He–Ne Laser. *Synthetic Metals* 111–112 (2000) 95–97.

[54] Kufazvinei C.; Ruether M.; Wang J.; Blau W. A Blue Light Emitting Perylene Derivative with Improved Solubility and Aggregation Control: Synthesis, Characterisation and Optical Limiting Properties. *Organic Electronics* 10 (2009) 674–680.

[55] Erten-Ela S. and Turkmen G. Perylene Imide Dyes for Solid-state Dye-sensitized Solar cells: Spectroscopy, Energy Levels and Photovoltaic Performance. *Renewable Energy* 36 (2011) 1821-1825.

[56] Lu S.; Niu J.; Li W.; Mao J.; Jiang J. Photophysics and Morphology Investigation Based on Perylenetetracarboxylate/Polymer Photovoltaic Devices. *Solar Energy Materials & Solar Cells* 91 (2007) 261–265.

[57] Jacob M.V.; Easton C.D.; Woods G.S.; Berndt C.C. Fabrication of a novel organic polymer thin film. *Thin Solid Films* 516 (2008) 3884–3887.

[58] Puigdollers J.; Voz C.; Orpella A.; Quidant R.; Martın I.; Vetter M.; Alcubilla R. Pentacene Thin-film Transistors with Polymeric Gate Dielectric. *Organic Electronics* 5 (2004) 67–71.

[59] Du H.; Deng Z.; Lun J.; Zhou M.; YinY.; Zou Y.; Lü Z.; Chen Z.; Wang Y. Pentacene Doping for the Efficiency Improvement of Polymer Solar Cells. *Synthetic Metals* 161 (2011) 2083– 2086.

[60] Ryu K. K.; Nausieda I.; Da He D.; Akinwande A. I.; Bulovic V.; Sodini C. G. Bias-Stress Effect in Pentacene Organic Thin-Film Transistors. *IEEE Transactions on Electron Devices* 57 (2010) 1003-1008.

[61] Schon J. H.; Kloc Ch.; Batlogg B. Pentacene Based Photovoltaic Devices. *Synthetic Metal* 124 (2001) 95-97.

[62] Sadowski J.T. Pentacene Growth on 3-Aminopropyltrimethoxysilane Modified Silicon Dioxide. *Optical Materials* 34 (2012) 1635–1638.

[63] Kanazawa S.; Ichikawa M.; Fujita Y.; Koike R.; Koyama T.; Taniguchi Y. The Effect of Thiophene Sequence Separation on Air-stable Organic Thin-film Transistor Materials. *Organic Electronics* 9 (2008) 425–431.

[64] Chang G-P. and Hsieh K-H. High-performance Semiconductors Based on Oligocarbazole–thiophene Derivatives for Solution-fabricated Organic Field-effect Transistors. *Thin Solid Films* 527 (2013) 291–298.

[65] Lee J.; Keum C. M.; Choi H.; Park H.; Lee D.; Kim W.; Kim B.; Hong M.; Bae B. S. Proposal of Fast-Moving Ball Actuator Mode for Electronic-Paper Displays. *Jpn. J. Appl. Phys*. 50 (2011) 1-5.

[66] Dimitrakopoulos C. D. and Malenfant P. R. L. Organic Thin Film Transistorsfor Large Area Electronics. *Adv. Mater.* 14 (2002) 99-117.

[67] Chen Z.; Debije M. G.; Debaerdemaeker T.; Osswald P.; Wurthner F. Tetrachloro-substituted Perylene Bisimide Dyes as Promising n-Type Organic Semiconductors: Studies on Structural, Electrochemical and Charge Transport Properties. *ChemPhysChem* 5 (2004) 137-140.

[68] Lu G. Organic Semiconductor. *University of Rochester, Rochester, NY* (2006) 1-4.

[69] Chochos C. and Choulis S. A. How the Structural Deviations on the Backbone of Conjugated Polymers Influence their Optoelectronic Properties and

Photovoltaic Performance. *Progress in Polymer Science* 36 (2011) 1326–1414.

[70] Li Y. and Lagowski J. B. Electric Field Effects on Bipolaron Transport in Heterocyclic Conjugated Polymers with Application to Polythiophene. *Optical Materials* 32 (2010) 1177–1187.

[71] Nunzi J-M. Organic Photovoltaic Materials and Devices. *C. R. Physique* 3 (2002) 523–542.

[72] Zhang Z.; Zhan C.; Zhang X.; Zhang S.; Huang J.; Li A. D. Q.; Yao J. A Self-Assembly Phase Diagram from Amphiphilic Perylene Diimides. *Chem. Eur. J.* 18 (2012) 12305–12313.

[73] Pasaogullari N.; Icil H.; Demuth M. Symmetrical and Unsymmetrical Perylene Diimides: Their Synthesis, Photophysical and Electrochemical Properties. *Dyes and Pigments* 69 (2006) 118-127.

[74] Herrmann A.; Weil T.; Sinigersky V.; Wiesler U-M.; Vosch T.; Hofkens J.; De Schryver F.; Müllen K. Polyphenylene Dendrimers with Perylene Diimide as a Luminescent Core. *Chem. Eur. J.* 7 (2001) 4844-4854.

[75] Icil H. and Arslan E. Synthesis and Spectroscopic Properties of Highly Pure Perylene Fluorescent Dyes. *Spectroscopy Letters* 34 (2001) 355–363.

[76] Grätzel M. Conversion of sunlight to electric power by nanocrystalline dye-sensitized solar cells. *Journal of Photochemistry and Photobiology A: Chemistry* 164 (2004) 3–14.

[77] Ma W.; JiaoY. and Meng S. Predicting Energy Conversion Efficiency of Dye Solar Cells from First Principles. *J. Phys. Chem. C* 118 (2014), 16447−16457.

[78] Nozik A. J. and Miller J. Introduction to Solar Photon Conversion. *Chem. Rev.* 110 (2010), 6443–6445.

[79] Cappel U. B.; Karlsson M. A.; Pschirer N.G.; Eickemeyer F.; Schoneboom J.; Erk P.; Boschloo G. and Hagfeldt A. A Broadly Absorbing Perylene Dye for Solid-State Dye-Sensitized Solar Cells. *J. Phys. Chem. C*, 113 (2009), 14595-14597.

[80] Erten-Ela S. and Turkmen G. Perylene Imide Dyes for Solid-state Dye-sensitized Solar Cells: Spectroscopy, Energy Levels and Photovoltaic Performance. *Renewable Energy* 36 (2011), 1821-1825.

[81] Chen C.; Yang X.; Cheng M.; Zhang F.; Zhao J.and Sun L. Efficient Panchromatic Organic Sensitizers with Dihydrothiazole Derivative as π-Bridge for Dye-Sensitized Solar Cells. *ACS Appl. Mater. Interfaces* 5 (2013), 10960−10965.

[82] Mete E.; Uner D.; Cakmak M.; Gulseren O. and Ellialtoglu S. Effect of Molecular and Electronic Structure on the Light-Harvesting Properties of Dye Sensitizers. *J. Phys. Chem. C* 111 (2007), 7539-7547.

[83] Gibson E. A.; Pleux L. L. Fortage J. et al. Role of the Triiodide/Iodide Redox Couple in Dye Regeneration in p-Type Dye-Sensitized Solar Cells. *Langmuir* 28 (2012), 6485−6493.

[84] Zhang T.; Guan W.; Wen S.; et al. Theoretical Studies on Metalloporphyrin−Polyoxometalates Hybrid Complexes for Dye-Sensitized Solar Cells. *J.Phys.Chem.* (2014) A-F.

[85] Meng S. and Kaxiras E. Electron and Hole Dynamics in Dye-Sensitized Solar Cells: Influencing Factors and Systematic Trends. *Nano Lett*. 10 (2010), 1238–1247.

[86] Osswald P.; Reichert M.; Bringmann G. and Wurthner F. Perylene Bisimide Atropisomers: Synthesis, Resolution, and Stereochemical Assignment. *J. Org. Chem*.72 (2007), 3403-3411.

[87] Xie Z.; Stepanenko V.; Radacki K.; Wurthner F. Chiral J-Aggregates of Atropo-Enantiomeric Perylene Bisimides and Their Self-Sorting Behavior. *Chem. Eur. J.* 18 (2012), 7060–7070.

[88] Asir S.; Demir A. S.; Icil H. The synthesis of novel, unsymmetrically substituted, chiral naphthalene and perylene diimides: Photophysical,

electrochemical, chiroptical and intramolecular charge transfer properties. *Dyes and Pigments* 84 (2010), 1–13.

[89] Zheng J.; Qiao W.; Wan X.; Gao J.P.; Wang Z. Y. Near-Infrared Electrochromic and Chiroptical Switching Materials: Design, Synthesis, and Characterization of Chiral Organogels Containing Stacked Naphthalene Diimide Chromophores. *Chem. Mater.* 20 (2008), 6163–6168.

[90] Xue C.; Chen M.; Jin S. Synthesis and Characterization of the First Soluble Nonracemic Chiral Main-chain Perylene Tetracarboxylic Diimide Polymers. *Polymer* 49 (2008) 5314–5321.

[91] Wang W.; Shaller A. D. and Li A. D. Q. Twisted Perylene Stereodimers Reveal Chiral Molecular Assembly Codes. *J. AM. CHEM. SOC.* 130 (2008), 8271–8279.

[92] Safont-Sempere M. M.; Stepanenko V..; Lehmann M.; Wurthner F. Impact of Core Chirality on Mesophase Properties of Perylene Bisimides. *J. Mater. Chem.* 21 (2011) 7201.

[93] Guo P. and Liu M. Chiral Supramolecular Assemblies from Some Achiral Schiff Bases without Alkyl Chain through the Organization at the Air/Water Interface. *Colloids and Surfaces A: Physicochem. Eng. Aspects* 70–73 (2006) 284–285.

[94] Bui B. B. B.; Coles S. J.; Davies D.B.; Drake A. F.; Eaton R. J.; Hursthouse M. B.; Kilic A.; Shaw R. A.; Yesilot S. Chiral Separation and CD Characterisation of Enantiomeric Cyclotriphosphazene Derivatives. *CHIRALITY* 17 (2005) 438–443.

[95] Refiker H. and Icil H. Amphiphilic and Chiral Unsymmetrical Perylene Dye for Solid-state Dye-sensitized Solar Cells. *Turk J Chem* 35 (2011) 847–859.

[96] Nyanhongo G. S.; Steiner W.; Gubitz G. M. Biofunctionalization of Polymers and their Applications. *Advances in Biochemical Engineering Biotechnology* 125 (2011) 1-305.

[97] Bodapati J. B. Novel Donor-Acceptor Polymers for Solar Cells. (2011) Thesis.

[98] Wurthner F.; Stepanenko V.; Chen Z.; Saha-Moller C. R.; Kocher N.; Stalke D. Preparation and Characterization of Regiosomerically Pure 1,7-Disubstituted Perylene Bisimide Dyes. *J. Org. Chem*. 69 (2004) 7933-7939.

[99] Koyuncu S.; Kus M.; Demic S.; Kaya L.; Ozdemir E.; Icil S. Electrochemical and Optical Properties of Novel Donor-Acceptor Thiophene-Perylene-Thiophene Polymers. *Journal of Polymer Science: Part A: Polymer Chemistry* DOI 10. 1002/pola.

[100] Rajasingh P.; Cohen R.; Shirman E. et al. Selective Bromination of Perylene Diimides under Mild Conditions. *J. Org. Chem.*72 (2007) 5973-5979.

[101] Yuney K. and Icil H. Synthesis, photochemical, and electrochemical properties of naphthalene-1,4,5,8-tetracarboxylicacidbis-(N,N'-bis-(2,2,4(2,4,4) trimethylhexylpolyimide)) and poly(N,N'-bis-(2,2,4(2,4,4)-trimethyl-6-aminohexyl) 3,4,9,10-perylenetetracarboxdiimide). *European Polymer Journal* 43 (2007) 2308–2320.

[102] Zhang X.; Zhan C.; Zhang X. and Yao J. Orientation of bromination in bay-region of perylene diimides. *Tetrahedron* 69 (2013) 8155-8160.

[103] Sun B., Zhao Y., Qiu X., Han C., Yu Y. & Shi Z. Substitution Effect of 1,7-Asymmetrically Substituted 3,4:9,10-Perylenebis(dicarboximide) Dyes. *Supramolecular Chemistry,* 20 (2008) 537–544.

[104] Icil, H., & Icli, S. Synthesis and Properties of a New Photostable Polymer:Perylene-3,4,9,10-tetracarboxylic Acid-Bis-(N,N_-dodecylpolyimide). *J. Poly. Sci. A: Polym. Chem.* 35 (1997): 2137-2142.

[105] Bodapati, J. B., & Icil, H. Highly Soluble Perylene Diimide and Oligomeric Diimide Dyes Combining Perylene and Hexa(ethylene glycol) Units: Synthesis, Characterization, Optical and Electrochemical Properties. *Dyes and Pigments.* 79 (2008): 224-235.

[106] Bard, A. J., & Faulkner, L. R. (2001) Electrochemical Methods: Fundamentals and Applications, 2nd Ed, John Wiley & Sons, Inc. New York.